UNIVERSITY OF CALIFORNIA, SAN DIEGO

Biological Control of Vertical Carbon Flux in the California Current and Equatorial Pacific

A dissertation submitted in partial satisfaction of the
requirements for the degree Doctor of Philosophy

in

Oceanography

by

Michael Raymond Stukel

Committee in Charge:

Professor Michael R. Landry, Chair
Professor Mark Ohman, Co-chair
Professor Kathy Barbeau
Professor Peter J. S. Franks
Professor Andrew Scull

2011

The Dissertation of Michael Raymond Stukel is approved, and it is acceptable in quality and form for publication on microfilm and electronically:

_____

_____

_____

_____
Co-chair

_____
Chair

University of California, San Diego

2011

DEDICATION

This dissertation is dedicated to Fozzy, who has guarded the office for many years, and to Moira, Brendan, and Jenny, who are my friends.

TABLE OF CONTENTS

Signature Page……. iii

Dedication…… iv

Table of Contents……. v

List of Abbreviations…….. ix

List of Figures…… xi

List of Tables……. xiv

Acknowledgements……. xv

Vita and Publications…… xxi

Abstract…….. xxiii

Introduction…… 1

Carbon export, the ecological perspective……. 1
Measurement of carbon export rates…….. 3
Carbon flux in the California Current Ecosystem……. 4
Dissertation outline…… 6
References……. 9

Chapter 1 Contribution of picophytoplankton to carbon export in the equatorial Pacific: A re-assessment of food-web flux inferences from inverse models…… 14

1.1 Abstract……..... 14
1.2 Introduction…….. 16
1.3 Methods…… 19
1.3.1 Sampling and data…… 20
1.3.2 Model structure…… 23
1.3.3 Model solution and statistical analyses…… 25
1.3.4 Ecosystem parameters…….. 26
1.3.5 Alternative model structure with size-fractionated detritus……. 27
1.4 Results……... 28
1.4.1 Least minimum norm results and comparison to JGOFS EqPac……. 28
1.4.2 Model sensitivity…….. 30
1.4.3 Random-walk exploration of the solution space……. 31
1.4.4 Size-fractionated detritus model…… 33

1.5 Discussion…….. 34
1.5.1 Inverse model solutions and biases……... 34
1.5.2 Comparisons to EqPac…….. 35
1.5.3 Processes altering export rates…….. 40
1.6 Tables..…….. 44
1.7 Figures…….. 54
1.8 References……. 61

Chapter 2 Trophic cycling and carbon export relationships in the California Current Ecosystem…… 67

2.1 Abstract……. 67
2.2 Introduction……... 68
2.3 Methods……..... 70
2.3.1 Overview of Lagrangian design…….. 70
2.3.2 Trophic cycling relationships…….. 71
2.3.3 Biological rate parameters…….. 73
2.3.4 ^{234}Th derived carbon export…… 74
2.4 Results……. 76
2.4.1 Comparison of measured and net rates…….. 76
2.4.2 Offshore, oligotrophic water parcel……..... 77
2.4.3 California Current Proper water parcel…….. 79
2.4.4 Inshore water parcels……. 80
2.5 Discussion…… 83
2.5.1 Trophic cycling and carbon export……. 83
2.5.2 Export measurements……. 84
2.5.3 Timescales…….. 86
2.5.4 Microzooplankton shunt…… 88
2.5.5 Decoupling of new and export production……. 89
2.5.6 Changing zooplankton concentrations: implications…….. 92
2.6 Tables……... 95
2.7 Figures……. 97
2.8 References……..... 104

Chapter 3 Do inverse ecosystem models accurately reconstruct food web flows? A comparison of two solution methods using field data from the California Current Ecosystem……..…. 109

3.1 Abstract……. 109
3.2 Introduction……... 110
3.3 Methods…… 112
3.3.1 Model structure…… 112
3.3.2 Ecological measurements…… 114
3.3.3 Model solution……. 115

3.4 Results…….. 117
3.4.1 Comparison of L_2MN and MCMC: numerical experiments……... 117
3.4.2 Comparison of L_2MN and MCMC: ecosystem parameters…… 120
3.4.3 Effect of steady-state assumption……... 122
3.4.4 Inverse ecosystem modeling error sources……. 122
3.5 Discussion…… 123
3.5.1 Spring in the CCE…… 123
3.5.2 Inverse ecosystem modeling…… 125
3.6 Conclusion…… 131
3.7 Tables……... 134
3.8 Figures……. 140
3.9 Appendix 3.1. Model equalities and inequalities…… 152
3.10 Appendix 3.2. L_2 minimum norm solution method..…….. 155
3.11 Appendix 3.3. The Markov Chain Monte Carlo solution method……. 157
3.12. References…… 159

Chapter 4 Mesozooplankton contribution to vertical carbon export in a coastal Upwelling biome……... 163

4.1 Abstract…… 163
4.2 Introduction……..... 164
4.3 Methods…… 166
4.3.1 Cruises and sampling plans……. 166
4.3.2 ^{234}Th export measurements……. 167
4.3.3 Sediment trap deployment and analyses……. 168
4.3.4 Microscopic enumeration of sediment trap fecal pellets…… 170
4.3.5 Mesozooplankton community enumeration…… 171
4.3.6 Calculation of active carbon transport……. 171
4.3.7 Mesozooplankton gut pigment analyses……. 172
4.4 Results……. 174
4.4.1 Cruise conditions……. 174
4.4.2 Carbon export…….. 175
4.4.3 Sediment trap contents…… 177
4.4.4 Active transport by DVM mesozooplankton…….. 180
4.5 Discussion…… 182
4.5.1 Export flux measurements…….. 182
4.5.2 Contribution of fecal carbon to vertical flux…….. 184
4.5.3 Role of mesozooplankton in vertical carbon flux……... 187
4.6 Tables……... 191
4.7 Figures……. 196
4.8 References…… 217

Conclusions…….. 222

Assessing the biological pump…….. 222
Biological control of sinking POC in the CCE…….. 223
Going forward…… 225
References…….. 227

LIST OF ABBREVIATIONS

A_U – Activity of uranium-238

A_{Th} – Activity of thorium-234

BP – bacterial production

^{14}C-PP – ^{14}C primary production

CCE – California Current Ecosystem

CCP – California Current Proper

Chl *a* – chlorophyll *a*

DOC – dissolved organic carbon

e-ratio – ratio of export to total production

EE – egestion efficiency

EEP – eastern equatorial Pacific

f-ratio – ratio of new to total production

GGE – gross growth efficiency

GPP – gross primary production

HPLC – high pressure liquid chromatography

L2MN – L_1 minimum norm

LTER – Long Term Ecological Research

MCMC – Markov chain Monte Carlo

NPP – net primary production

NSS – non-steady state

POC – particulate organic carbon

PP – primary production

RW – random walk

SS – steady state

SVD – singular value decomposition

ThE – ratio of thorium-based export production to total production

LIST OF FIGURES

Chapter 1

Figure 1.1 Station locations for EB04 (December 2004) and EB05 (September 2005) cruises…… 54

Figure 1.2 Schematic representation of ECO model…….55

Figure 1.3 Random walk exploration of the solution space…….. 56

Figure 1.4 Grazer diets…….. 57

Figure 1.5 Sources of particulate flux out of the euphotic zone…….. 58

Figure 1.6 Grazing balance……. 59

Figure 1.7 Carbon fluxes supported by cyanobacterial and diatom production in the RW-solution to the SF-DET model……. 60

Chapter 2

Figure 2.1 Map of the study region…… 97

Figure 2.2 Vertical profiles of chlorophyll, primary productivity, phytoplankton growth rate, and microzooplankton grazing rate……... 98

Figure 2.3 Vertically integrated cycle averages…….. 99

Figure 2.4 ^{234}Th deficiency in Oligotrophic Offshore and California Current Proper water parcels…….. 100

Figure 2.5 Vertically averaged temperature and salinity for the upper 50 m of All CTD profiles of the four water parcels…… 101

Figure 2.6 ^{234}Th deficiency in inshore water parcels……. 102

Figure 2.7 Comparison of trophic cycling relationships to ^{234}Th deficiency steady-state model…… 103

Chapter 3

Figure 3.1 Model estimation of measured parameters……..... 140

Figure 3.2 Model predictions of gross growth efficiencies of heterotrophic nanoflagellates, microzooplankton, mesozooplankton, and bacteria….. 142

Figure 3.3 Comparisons of the relative strengths of the different food web components by the MCMC and L_2MN models…….. 143

Figure 3.4 Fraction of vertical carbon export derived from gravitational Sinking of detrital phytoplankton, as determined by the L_2MN and the MCMC methods…… 145

Figure 3.5 Comparison of steady state and non-steady state models…….. 146

Figure 3.6 Comparison of the uncertainties due to under-determinacy of the inverse model and to measurement errors……. 147

Figure 3.7 Comparison of food webs…….. 149

Figure 3.8 Mesozooplankton trophic levels predicted by the MCMC and the L_2MN solution approaches……. 150

Figure 3.9 Model predictions of bacterial production with assumed DOC Accumulation…… 151

Chapter 4

Figure 4.1 Bathymetry map of our study region……. 196

Figure 4.2 ^{234}Thorium export. A comparison of ^{234}Th export rates as estimated by a ^{238}U-^{234}Th deficiency with a one-dimensional steady-state equation that neglects upwelling and the amount of ^{234}Th collected in contemporaneous sediment traps…… 197

Figure 4.3 ^{234}Th deficiency profiles……. 198

Figure 4.4 C:^{234}Th ratios…… 199

Figure 4.5 Pigment flux…….. 200

Figure 4.6 Phaeopigment and fecal pellet mass flux…….. 201

Figure 4.7 Flux of recognizable fecal pellets into sediment traps…….. 202

Figure 4.8 Flux of fecal pellet mass into sediment traps…… 204

Figure 4.9 Relationship between cylindrical fecal pellets and total crustacean abundance…… 205

Figure 4.10 Relationship between fecal pellet mass flux and mesozooplankton biomass…….. 207

Figure 4.11 Vertical distribution of copepod biomass……. 209

Figure 4.12 Vertical distribution of euphausiid biomass…….. 210

Figure 4.13 Vertical distribution of chaetognath biomass…… 211

Figure 4.14 Vertical distribution of 'other' biomass…… 212

Figure 4.15 Active transport of carbon by DVM mesozooplankton……. 213

Figure 4.16 Contribution of each flux component to total carbon export……. 215

LIST OF TABLES

Chapter 1

Table 1.1 Experimental inputs to the base (ECO) model…… 44

Table 1.2 Steady-state equations for the base (ECO) model…….. 45

Table 1.3 Minimum and maximum biological constraints on the model solution.. 46

Table 1.4 Solutions to the base (ECO) model……. 48

Table 1.5 Correlations between model inputs (measured rate and standing stocks) and outputs (flows) that explain at least 30% of the variance in the modeled flow, as derived from the Monto Carlo error analysis… 50

Table 1.6 SF-Det model solutions…….. 52

Chapter 2

Table 2.1 Vertically integrated ecosystem values……... 95

Table 2.2 Calculated, vertically integrated estimates of *f*-ratios……. 96

Chapter 3

Table 3.1 Measured inputs to the model……. 134

Table 3.2 MCMC solutions to the inverse ecosystem model…….. 136

Table 3.3 L_2MN solutions to the inverse ecosystem model…… 138

Chapter 4

Table 4.1 Mesozooplankton length:carbon relationships…… 191

Table 4.2 ^{234}Th fluxes and C:^{234}Th ratios……... 192

Table 4.3 Sediment trap flux measurements…….. 193

Table 4.4 Active transport by diel vertically migrating mesozooplankton…… 194

Table 4.5 Contribution of phytoplankton and fecal pellets to vertical flux as assessed from pigment analyses…….. 195

ACKNOWLEDGMENTS

Finishing a dissertation is almost impossible without a good advisor – and I've had a great one. I'll always be indebted to Mike for all of his advice, encouragement, and willingness (not to mention patience) to let me grow as an oceanographer. He accepted me when I was an idiot undergraduate who knew nothing about the ocean, and never made me feel stupid when I came to him with less than intelligent questions. He trusted me and gave me the freedom to explore and choose my own project, and was amazingly able to advise me across the broad array of topics that my interests pulled me towards. When I found myself drawn to a topic that he didn't know as much about, he set up a meeting for me with one of the experts in the field. He's spent countless hours supporting my work at sea and even bled for me on the fantail. He gave me the space to grow as a scientist while always keeping his door always open, and for that I'll always be grateful.

The rest of my committee has been wonderful as well. Mark Ohman's enthusiasm for science is infectious (especially when playing 'Name that plankton' at 4am) and he's been a great help to me many times throughout my career. I can't count the amount of times that Mark has saved me when I went to him at the last minute to find a cruise supply I'd forgotten to order. He's always given insightful comments for my work and instilled in me a profound love of metazooplankton. Peter Franks is an amazingly caring teacher who always puts students first. He's always been helpful whenever I've needed advice with manuscripts or constructing models and I've learned a ton from classes with him. I'll always appreciate Kathy Barbeau for being

the one member of my committee who was perceptive enough to challenge some of the BS oversimplifications that tended to spew from my mouth during committee meetings. Andy Scull brought an outside perspective and was always amazingly attentive and able to point out aspects of my work that I might otherwise have taken for granted. It would also be remiss for me to forget to acknowledge Claudia Benitez-Nelson, who despite being in South Carolina, has been a de facto member of my committee. Claudia has taught me everything that I know about measuring and interpreting ^{234}Th distributions and has been more than willing to count all of the samples that I've sent her. My dissertation wouldn't have been possible without her advice and counsel and she's been an incredible joy to work with.

This dissertation relies heavily on the amazingly collaborative efforts of everyone involved with the CCE LTER Program. While the amount of volunteers, technicians, students, and professors who've contributed to the project are too numerous to list, some deserve special mention. I feel that Ralf Goericke's competence at sea forms the backbone of the CCE Process cruises and many of my favorite moments came while he, Landry, and I were all leaning against the starboard railing and chatting as we made our countless approaches on the drifter. From Ralf's lab, I should also mention Shonna Dovel and Megan Roadman who do a ton of the crucial, but thankless work, without making the frequent mistakes that us grad students make, and pitched in and helped me with my work more times than I can count. Lihini Aluwihare has given me a lot of advice about organic carbon cycling and also leant me her McLane pump on many cruises. Dave Checkley has been a good teacher and is fun to work with at sea.

Mati Kahru provided invaluable satellite support. E.T. (the wayward little drifter who phoned home at last) has been a stalwart companion through many cruises. Many of the CCE grad students have been wonderful friends and collaborators for years. I feel like we all own small pieces of each others' dissertations. Moira Decima, Darcy Taniguchi, Jesse Powell, Ally Pasulka, Alison Cawood, Ryan Rykaczewski, Roman Dejesus, Travis Meador, Brian Hopkinson, Andrew King, Ty Samo, Byron Pedler… I've loved working and sailing with all of them.

I owe a debt of gratitude to many other people and groups at Scripps, many of whom I'm probably forgetting to mention. The Scripps graduate office and IOD administration offices are amazing and actually make dealing with the administration a pleasure (and we all know how rare that is). Bruce Deck in the Analytical Facility is great at dealing with students and getting data to us in a timely and efficient manner. A multitude of wonderful teachers have done credit to SIO as a teaching institution. Paul Dayton has served as a role model as an ecologist, teacher, and environmentalist. John and John from the machine shop have taught me to use a wide variety of power tools necessary to build my equipment. Also Dan Wick, who might be the nicest person alive. Dave Skydel, Gary Lain, and the rest of the radiation safety group. And of course, our work wouldn't be possible without the captains, crews, and restechs from all of the cruises I've been on, particularly Jim Dorrance, Gene Picard, Meghan Donohue, Gus Aprans, and John (sorry I forgot your last name John).

And then there are others from around the country. Karen Selph has been a big sister to our lab, and has been an incredible help to me on the two cruises that

bookended my graduate career. Stephen Baines has likewise been a ton of fun to work with and learn from on cruises, as has Sasha Chekalyuk. Tammi Richardson was kind enough to give a lot of valuable advice for Chapter 1.

My funding has been provided by a National Science Foundation (NSF) Graduate Research Fellowship and NASA Earth and Space Science (NESSF) Fellowship as well as two fellowships through SIO (the Wyers Fellowship and the Henry L. and Grace Doherty Fellowship). The University of California ship funds program graciously funded our student cruise during April 2009 (CCE-P0904), which was an amazing learning experience for me. My research has been funded primarily by three NSF grants; the CCE LTER Program (OCE-04-17616), the Equatorial Biocomplexity grant (OCE-0322074), and the Arabian Sea / Pirates / Costa Rica Dome grant (OCE-0826626).

And now for all the friends and family who've been my support system through six and a half years of grad school. My entire family (parents, sister, grandparents, aunts and uncles (both biological and Maufolk) have encouraged me ever since I was a five-year old who wanted to save the whales. Even when they thought that marine biologists did nothing but clean fish tanks or swab the decks on navy ships, they never tried to squash my dreams. They fostered my love for nature from an early age with countless trips to the zoo, camping trips almost every weekend of the summer, museum and aquarium visits, and endless hours of reading "Fish do the Strangest Things" over and over and over… They've allowed me to head further and further

from home in pursuit of my education, with only the slightest bit of resistance, and even traveled en masse across country when I moved out to San Diego.

Finally, I've had an amazing group of friends while I've been out here. They've been family to me in every way possible. Moira is my office mate, lab mate, cruise mate, soccer teammate, and twin and I can't imagine what grad school would have been like without her. Brendan took me on my first backpacking trip, ate lunch with us almost every day for six years, acts as my proxy whenever I'm at sea, and functions as my chemist. He and Moira have even followed me up to Sequoia as I sit here finishing my dissertation. Jenny has taught courses with me repeatedly, taken endless classes with me, been my roommate, and owns a dog with me. And that dog… He's about as dumb as they come, but makes up for it by being so sweet and loyal. I really don't know what I'm going to do without those three. And I'd be remiss if I didn't mention the youngsters as well. Geoff has been the youngster who's always given me advice about grad school stuff. Darcy's always been a great friend to hang out and work with, and her pet funerals may qualify as the funniest recurring theme on any of our cruises (but don't tell her that). Jesse has been a huge help with all kinds of cruise related work, and may have spent more time helping other grad students than doing his own dissertation work. Alison has helped me unravel the ZooScan data many times. Suki has patiently and consistently tried to teach Fozzy how to have thoughts.

Chapter 1, in full, has been published in Limnology and Oceanography: Stukel, M. R., Landry, M.R., 2010. "Contribution of picophytoplankton to carbon export in the equatorial Pacific: A re-assessment of food-web flux inferences from inverse models."

Limnol. Oceanogr. **55**: 2669-2685. The dissertation author was the primary investigator and author of this paper.

Chapter 2, in full, has been submitted for publication in Limnology and Oceanography: Stukel, M. R., Landry, M.R., 2010, Benitez-Nelson, C. R., Goericke, R. "Trophic Cycling and carbon export relationships in the California Current Ecosystem." The dissertation author was the primary investigator and author of this paper.

Chapter 3, in full, is currently in preparation for submission: Stukel, M. R., Landry, M. R., Benitez-Nelson, C. R., Goericke, R. "Do inverse models accurately reconstruct food web flows? A comparison of two solution methods using field data from the California Current Ecosystem." The dissertation author was the primary investigator and author on this paper.

Chapter 4, in full, is currently in preparation for submission: Stukel, M. R., Landry, M. R., Ohman, M. D., Benitez-Nelson, C. R.. "Mesozooplankton and vertical carbon export in a coastal upwelling biome." The dissertation author was the primary investigator and author on this paper.

VITA AND PUBLICATIONS

EDUCATION

2011 Doctor of Philosophy, University of Californa, San Diego

2004 Bachelor of Arts, Northwestern University, Evanston, IL

CRUISE EXPERIENCE (158 days)

CRD-2010 - Measured carbon export, new production, and mesozooplankton gut phycoerythrin concentrations

CCE-P0904 - Chief scientist on a cruise addressing the ecological and biogeochemical role of fronts in the CCE

CCE-P0810 - Continued ^{234}Th & sediment trap measurements and added new production measurements

CCE-P0704 - Continued ^{234}Th measurements and added sediment trap deployments as independent confirmation of measured rates

CCE-P0605 - Measured carbon export in the CCE using ^{234}Th disequilibrium

EB05 - Investigated mixotrophic nano- and microflagellates in the eastern Equatoial Pacific

CONFERENCES

Ocean Sciences 2010	Talk	Carbon cycling in the equatorial Pacific: Export driven by large phytoplankton
LTER ASM 2009	Poster	Trophic cycling and vertical flux in the CCE
Ocean Sciences 2008	Talk	Carbon export and the fate of primary productivity in the California Current
LTER ASM 2006	Poster	Thorium export in the California Current Ecosystem
Ocean Sciences 2006	Poster	Mixotrophs are major grazers in the equatorial Pacific

TEACHING AND OUTREACH EXPERIENCE

2009 Reality Changers: Tutored under-privilege high school students

2006-2008 Academic Connections (UCSD): Co-designed and co-taught a three-week Biological oceanography course for advanced high school students each summer

2005 Aquatic Adventures: Helped teach 2-week marine biology course for underprivileged youth in San Diego

PUBLICATIONS

Stukel, M. R.; M. R. Landry; K. E. Selph. In press. "Nanoplankton mixotrophy in the eastern equatorial Pacific." Deep-Sea Res. II. doi:10.1016/j.dsr2.2010.08.016

Selph, K. E.; M. R. Landry; A. G. Taylor; E. J. Yang; C. I. Measures; J. J. Yang; M. R. Stukel; S. Christenson; R. R. Bidigare. In Press. "Spatially-resolved taxon-specific phytoplankton production and grazing dynamics in relation to iron distributions in the equatorial Pacific between 110 and 140°W. Deep-Sea Res. II. doi:10.1016/j.dsr2.2010.08.014

Stukel, M. R.; M. R. Landry. 2010. "Contribution of picophytoplankton to carbon export in the equatorial Pacific: A re-assessment of food-web flux inferences from inverse models." Limnol. Oceanogr. **55**: 2669-2685

Landry, M. R.; M. D. Ohman; M. R. Stukel; K. Tsyrklevich. 2009. "Lagrangian studies of phytoplankton growth and grazing relationships in a coastal upwelling ecosystem off Southern California." Prog. Oceanogr. **83**: 208-216

ABSTRACT OF THE DISSERTATION

Biological Control of Vertical Carbon Flux in the California Current and Equatorial Pacific

by

Michael Raymond Stukel

Doctor of Philosophy in Oceanography

University of California, San Diego, 2011

Professor Michael R. Landry, Chair

Professor Mark D. Ohman, Co-chair

The "biological pump" is a key component in the global biogeochemistry of carbon dioxide that is sensitive, through a multitude of ecological interactions of euphotic zone plankton, to climatic fluctuations. In this dissertation I address the biological control of vertical carbon flux out of the surface ocean in two regions of the Pacific Ocean. I begin by addressing the hypothesis that most export production in the

equatorial Pacific is derived from the primary production of picophytoplankton. Using inverse ecosystem modeling techniques to synthesize detailed rate measurements I show that eukaryotic phytoplankton are the dominant producers of eventually exported material and that export comes after processing by mesozooplankton, but that the results of inverse modeling studies are dependent upon subjective decisions about model structure, input data, and solution schemes. I then move on to studies in the California Current Ecosystem (CCE), where a combination of my own *in situ* measurements of vertical carbon export and collaborators' measurements of key planktonic rates allow me to address the question of what constitutes sinking flux in this coastal upwelling biome. I begin with simple trophic cycling relationships that use phytoplankton growth, micro- and mesozooplankton grazing, and simple assumptions about organismal efficiency, and show that fecal pellet production could account for the magnitude and variability in carbon export measured by ^{234}Th disequilibrium during a cruise in May 2006. I then utilize inverse modeling techniques to show that on two spring cruises the contribution of grazing products to export was substantially greater than that of gravitational sinking of phytoplankton, and also that Markov Chain Monte Carlo methods do an accurate job of solving inverse ecosystem models. Finally, I use sediment trap samples to directly assess the contribution of fecal pellets to vertical flux, finding that mesozooplankton pellets were the dominant component of flux during the spring, but that during a fall cruise their contribution was variable, with flux becoming increasingly dominated by non-pigmented small material and marine snow as productivity decreased.

INTRODUCTION

Carbon export, the ecological perspective - While marine phytoplankton are responsible for roughly half the world's photosynthesis (see Field et al. 1998 for a review), most of this fixed carbon is respired in the euphotic zone and hence retained in the upper ocean-atmosphere system. Marine carbon sequestration is dependent upon biological and physical processes that transport particulate organic carbon (POC) to depth, thus removing it from the atmosphere for timescales of up to a millennium. The "biological pump," which transports carbon against its concentration gradient, is mediated primarily by plankton ecological interactions that repackage POC into large particles and aggregates that sink into the deep ocean. Despite its vast importance in biogeochemical cycles, climate change, and the supply of energy to the benthos, the biological pump remains difficult to predict due to the complexity and variability inherent to marine ecosystems.

The classic ecological paradigm of marine carbon export emphasizes the crucial role of large phytoplankton, particularly diatoms, in vertical flux (Michaels and Silver 1988). These large autotrophs are believed to sink faster (Smayda 1970) and have shorter trophic pathways to large fecal pellet-producing mesozooplankton than their smaller competitors. These mechanistic explanations are further supported by the measurement of high new (Eppley and Peterson 1979) and export production (Buesseler 1998) during bloom conditions dominated by large plankton.

This paradigm has been challenged in a series of studies (Richardson et al. 2004,2006; Richardson and Jackson 2007) that utilized inverse ecosystem modeling techniques to reconstruct unmeasured fluxes. These inverse results, from the Joint Global Ocean Flux (JGOFS) Equatorial Pacific (EqPac) and Arabian Sea programs, suggest that exported carbon in the open ocean is derived primarily from the

production of picophytoplankton, particularly *Prochlorococcus*. This dominant role for picophytoplankton in export production follows from the assumption (based on size-fractionated chlorophyll and HPLC biomass proxies) that picophototrophs are responsible for the majority of primary production as well as model structures that allow significant direct flux of picophytoplankton to depth, presumably after particle aggregation.

The controversial results of these inverse modeling studies also highlight another dichotomy dealing with the nature of sinking material. While marine chemists (e. g. Dunne et al. 2005) and ecosystem modelers investigating the effects of inorganic ballasting (e. g. Armstrong et al. 2002) and aggregation (e. g. Jackson et al. 2005) emphasize the sinking rates of ungrazed phytoplankton, food web ecologists often underscore the importance of fecal pellets in rapidly transporting carbon to depth (e.g. Bruland and Silver 1981; Landry et al. 1994; Dam et al. 1995). These fecal pellets efficiently pack egested particulate matter within dense membrane-enclosed particles, which can greatly enhance the sinking rate with vertical velocities that range from meters to kilometers per day (see Turner 2002 for a review).

While the difference between flux of ungrazed carbon and minerals in organic aggregates or flux within mesozooplankton fecal pellets may seem semantic, it in fact implies distinctly different utilization scenarios for primary production. Dominance of fecal pellet flux suggests a system with a greater number of trophic steps, and hence higher respiration in the euphotic zone, and also possible control of primary production by grazing pressure. Furthermore, the relative importance of ungrazed phytoplankton and fecal pellets in flux would suggest opposite relationships between mesozooplankton concentration and carbon export rates; if flux is supported by fecal pellets we can expect a positive correlation between export and mesozooplankton, but

if it is dominated by ungrazed phytoplankton products increased mesozooplankton grazing pressure would lead to greater recycling and less export.

Measurement of carbon export rates – Sediment traps are a conceptually simple means of measuring carbon export in the ocean, and are particularly useful because they allow the collection of sinking material that can be analyzed to ascertain the nature of sinking particles. However, their efficacy in accurately assessing particle flux has frequently been questioned (e.g. Buesseler et al. 2007). Comparison studies that measure ^{234}Th based export during sediment trap deployments have shown biases that vary significantly between sites, with over one-third of the studies showing a factor of three difference between the two methods (Buesseler 1991).

Several sources of bias are inherent to moored and tethered sediment traps, notably dissolution of organic carbon (Knauer et al. 1984), 'swimmer' effects (Knauer et al. 1979), and hydrodynamic biases. These hydrodynamic biases tend to be magnified at high flow rates and low sinking rates, although many other factors can be important (Baker et al. 1988). An additional difficulty in interpreting sediment trap results derives from the long distances over which particles can be transported by lateral advection as they sink. The source for sediment trap material is thus not a point directly above the trap, but instead a statistical funnel that varies in size and location based on the speed, direction, and variability of flow fields above the traps and the sinking rates of the particles (Siegel et al. 1990; Siegel et al. 2008). The development of neutrally buoyant sediment traps alleviate many of the hydrodynamic issues, yielding more accurate flux estimates (Buesseler et al. 2000), but at the same time may increase the effect of the statistical funnel when vertical shear is high.

An alternative method of approximating carbon export from the euphotic zone has grown from studies of oceanic thorium distributions (see reviews by Savoye et al. 2006; Van Der Loeff et al. 2006; Waples et al. 2006). ^{234}Th is the first long-lived (half-life = 24.1 days) intermediary in the decay chain from ^{238}U (half-life = 4.5 * 10^9 yrs). The rapid decay of ^{234}Th relative to ^{238}U should lead to secular equilibrium between the two isotopes, with equal decay rates. However, while ^{238}U is conserved in the upper ocean and covaries with salinity, ^{234}Th scavenges onto particles and hence is removed from the system as particles sink, creating a disequilibrium between the parent and daughter isotopes. The assumption of a steady-state model allows calculation of rates of ^{234}Th removal from the upper ocean over a time scale similar to the half-life of ^{234}Th:

$$^{234}Th\ Export = \int_0^{depth} \left(A_{^{238}U} - A_{^{234}Th}\right) \lambda_{^{234}Th} \qquad (1)$$

where A_{238U} and A_{234Th} are the activities of ^{238}U and ^{234}Th, respectively, and λ_{234Th} is the decay rate of ^{234}Th. This equation calculates the rate of removal of ^{234}Th from the upper ocean, but it does not directly imply a rate of particle or carbon removal. To convert to carbon export rate it is necessary to measure the ratio of C:^{234}Th of sinking material at the depth horizon of interest. This ratio can vary greatly with depth, location, season, size of particles, and other parameters (Buesseler et al. 2006) thus it must be determined empirically from each measured water parcel.

Carbon flux in the California Current Ecosystem – The majority of this thesis is based on studies undertaken as a part of the CCE Long-Term Ecological Research (LTER) Program. The California Current Ecosystem (CCE) is an eastern boundary current biome that experiences strong equatorward winds in the spring and summer months, leading to strong flows out of the north and wind-stress induced coastal

upwelling (Lynn and Simpson 1987; Hickey 1993). This input of nutrients and concurrent increase in primary production leads to a spring bloom dominated by diatoms and other large phytoplankton in the coastal region near Point Conception. Offshore, the floral community exhibits less seasonal variability and is dominated by smaller taxa (Venrick 1998,2002).

The ocean-atmosphere system of the CCE is clearly highly coupled, and has been extensively sampled on routine CalCOFI (California Cooperative Oceanographic Fisheries Investigations) cruises since 1949. El Niño conditions often lead to a decrease in the spatial extent of eutrophic conditions (e.g. Kahru and Mitchell 2000) and cause a shift in dominant zooplankton taxa (e.g. Brinton and Townsend 2003; Lavaniegos and Ohman 2003; Hereu et al. 2006). The Pacific Decadal Oscillation (PDO) has also been shown to affect the biotic community with a period of 20-30 years (e.g. Mantua et al. 1997; McGowan et al. 2003). Meanwhile, a secular warming trend has been recorded throughout the region and may be responsible for a significant decline in zooplankton biovolume (Roemmich and McGowan 1995b; 1995a). This has been attributed to a decrease in pelagic tunicates (Lavaniegos and Ohman 2003,2007), which are known to have very high rates of grazing and efficient repackaging into large rapidly settling fecal pellets. Thus the decadal trend of declining mesozooplankton biovolume and shifting community composition may significantly alter the efficiency of particle export.

Despite the unparalleled ecological time-series of surface ocean dynamics, comparatively little work has been conducted on carbon export in the CCE, with the exception of a few areas in the Southern California Bight, such as the Santa Monica Basin (Nelson et al. 1987; Landry et al. 1992) and the Santa Barbara Basin (Shipe et

al. 2002). A long term study at Station M to the northwest of Point Conception, has also measured carbon flux to the deep sea, with time-series sediment traps near the seafloor (Baldwin et al. 1998; Smith et al. 2006). These studies have shown highly variable export rates, even within the same regions. Spring carbon fluxes as low 35 mg m^{-2} day^{-1} (Nelson et al. 1987) and over 400 mg m^{-2} day^{-1} (Landry et al. 1992) were found in 100 m sediment traps in the Santa Monica Basin. Time series of deeper sediment traps in the Santa Barbara Basin (Pilskaln et al. 1996), as well as seafloor traps near Station M (Baldwin et al. 1998), exhibited strong seasonality coupled to surface productivity.

Dissertation Outline – The primary goal of this dissertation is to elucidate biological mechanisms controlling the vertical flux of POC, with the eventual goal of allowing prediction of the feedbacks between marine carbon sequestration and climate. My approach assumes that experimentally determined carbon export rates can be understood within the context of contemporary autochthonous ecological processes. With this in mind, the core of the dissertation (Chapters 2-4) centers around three Process Cruises of the CCE LTER program during which Lagrangian drift experiments allowed simultaneous measurements of ecological processes (including phytoplankton growth and zooplankton grazing) and vertical carbon fluxes. In many ways, this dissertation involved a continual realization that *in situ* measurements are crucial to resolving the difference between alternate hypotheses, and hence is a progression towards more accurate direct measurement of ecological and biogeochemical processes.

In Chapter One, entitled "Contribution of picophytoplankton to carbon export in the equatorial Pacific: A re-assessment of food-web flux inferences from inverse

models," we addressed the controversial recent hypothesis that picophytoplankton-derived production dominates carbon export in the equatorial Pacific (Richardson et al. 2004; Richardson and Jackson 2007). Implicit in this ecosystem view is the assumption that picophytoplankton contribute to carbon export primarily through the gravitational sinking of ungrazed picophytoplankton, presumably after aggregation in marine snow particles. Using a new dataset from two equatorial cruises of the Equatorial Biocomplexity Program, we showed that picophytoplankton were not the dominant primary producers in the region and were almost completely grazed in the euphotic zone by protozoans. While they may have contributed to export in proportion to their role in primary production, this conclusion relied crucially on the assumption that all detrital particles (regardless of size) were equally likely to sink. A more nuanced portrayal of the detrital pool suggested instead that large phytoplankton contributed disproportionately to export and that sinking carbon existed primarily in the form of mesozooplankton fecal pellets. The paper based on this chapter has recently been published in Limnology and Oceanography (Stukel and Landry 2010).

Chapter Two, entitled "Trophic cycling and carbon export relationships in the California Current Ecosystem," builds on this idea that vertical carbon flux is largely dominated by mesozooplankton fecal pellets. To test the hypothesis that grazing processes largely determine carbon export within the region, we constructed simple trophic cycling relationships that predicted POC export, phytoplankton accumulation, and new production from phytoplankton growth and grazing measurements made on the 2006 CCE Process Cruise. These simple trophic cycling relationships were found to accurately predict simultaneously measured carbon export rates, suggesting that fecal production, rather than gravitational sinking of phytoplankton, was the dominant

ecological process controlling carbon export. The paper based on this chapter is presently in review at Limnology and Oceanography.

Chapter Three, entitled "Do inverse ecosystem models accurately reconstruct food web flows? A comparison of two solution methods using field data from the California Current Ecosystem," was primarily written to contrast two methods of solving under-constrained inverse ecosystem problems. In addition, it utilized ecological and biogeochemical data from two cruises of the CCE LTER Program to constrain an ecosystem model for eight different ecosystem states encountered during 2006 and 2997 spring cruises in the CCE. Sinking POC was estimated to be composed primarily of fecal material, with a smaller proportion of ungrazed phytoplankton sinking as well.

Chapter Four, entitled "Mesozooplankton and vertical carbon export in a coastal upwelling biome," addressed the same question of what constitutes sinking POC but more directly, using the results of sediment trap deployments on the 2007 and 2008 Process Cruises of the CCE LTER Program. Identifiable fecal pellets from sediment trap samples were enumerated and sized. Along with measurements of pigment sinking rates, the data suggest that fecal material was consistently a much greater proportion of the sinking material than ungrazed phytoplankton. While fecal pellets comprised the majority of flux in productive conditions, and particularly during the spring, sediment traps deployed during the fall contained a large proportion of unidentifiable marine snow aggregates. Mesozooplankton abundance profiles also showed that active transport by diel vertically migrating organisms was a significant portion of total carbon export.

REFERENCES

ARMSTRONG, R. A., C. LEE, J. I. HEDGES, S. HONJO, and S. G. WAKEHAM. 2002. A new, mechanistic model for organic carbon fluxes in the ocean based on the quantitative association of POC with ballast minerals. Deep-Sea Res. II **49:** 219-236.

BAKER, E. T., H. B. MILBURN, and D. A. TENNANT. 1988. Field assessment of sediment trap efficiency under varying flow conditions. J. Mar. Res. **46:** 573-592.

BALDWIN, R. J., R. C. GLATTS, and K. L. SMITH. 1998. Particulate matter fluxes into the benthic boundary layer at a long time-series station in the abyssal NE Pacific: composition and fluxes. Deep-Sea Res. II **45:** 643-665.

BRINTON, E., and A. TOWNSEND. 2003. Decadal variability in abundances of the dominant euphausiid species in southern sectors of the California Current. Deep-Sea Res. II **50:** 2449-2472.

BRULAND, K. W., and M. W. SILVER. 1981. Sinking rates of fecal pellets from gelatinous zooplankton (salps, pteropods, doliolids). Mar. Biol. **63:** 295-300.

BUESSELER, K. O. 1991. Do upper-ocean sediment traps provide an accurate record of particle flux? Nature **353:** 420-423.

BUESSELER, K. O. 1998. The decoupling of production and particulate export in the surface ocean. Glob. Biogeochem. Cycle **12:** 297-310.

BUESSELER, K. O., A. N. ANTIA, M. CHEN, S. W. FOWLER, W. D. GARDNER, O. GUSTAFSSON, K. HARADA, A. F. MICHAELS, M. R. VAN DER LOEFF'O, M. SARIN, D. K. STEINBERG, and T. TRULL. 2007. An assessment of the use of sediment traps for estimating upper ocean particle fluxes. J. Mar. Res. **65:** 345-416.

BUESSELER, K. O., C. R. BENITEZ-NELSON, S. B. MORAN, A. BURD, M. CHARETTE, J. K. COCHRAN, L. COPPOLA, N. S. FISHER, S. W. FOWLER, W. GARDNER, L. D. GUO, O. GUSTAFSSON, C. LAMBORG, P. MASQUE, J. C. MIQUEL, U. PASSOW, P. H. SANTSCHI, N. SAVOYE, G. STEWART, and T. TRULL. 2006. An assessment of particulate organic carbon to thorium-234 ratios in the ocean and their impact on the application of ^{234}Th as a POC flux proxy. Mar. Chem. **100:** 213-233.

BUESSELER, K. O., D. K. STEINBERG, A. F. MICHAELS, R. J. JOHNSON, J. E. ANDREWS, J. R. VALDES, and J. F. PRICE. 2000. A comparison of the quantity and

composition of material caught in a neutrally buoyant versus surface-tethered sediment trap. Deep-Sea Res. I **47:** 277-294.

DAM, H. G., X. S. ZHANG, M. BUTLER, and M. R. ROMAN. 1995. Mesozooplankton grazing and metabolism at the equator in the central Pacific: Implications for carbon and nitrogen fluxes. Deep-Sea Res. II **42:** 735-756.

DUNNE, J. P., R. A. ARMSTRONG, A. GNANADESIKAN, and J. L. SARMIENTO. 2005. Empirical and mechanistic models for the particle export ratio. Glob. Biogeochem. Cycle **19:** doi:10.1029/2004GB002390.

EPPLEY, R. W., and B. J. PETERSON. 1979. Particulate Organic-Matter Flux and Planktonic New Production in the Deep Ocean. Nature **282:** 677-680.

FIELD, C. B., M. J. BEHRENFELD, J. T. RANDERSON, and P. FALKOWSKI. 1998. Primary production of the biosphere: Integrating terrestrial and oceanic components. Science **281:** 237-240.

HEREU, C. M., B. E. LAVANIEGOS, G. GAXIOLA-CASTRO, and M. D. OHMAN. 2006. Composition and potential grazing impact of salp assemblages off Baja California during the 1997-1999 El Niño and La Niña. Mar. Ecol. Prog. Ser. **318:** 123-140.

HICKEY, B. M. 1993. Physical Oceanography, p. 19-70. *In* M. D. Dailey, D. J. Reish and J. W. Anderson [eds.], Ecology of the Southern California Bight: A Synthesis and Interpretation. University of California Press.

JACKSON, G. A., A. M. WAITE, and P. W. BOYD. 2005. Role of algal aggregation in vertical carbon export during SOIREE and in other low biomass environments. Geophys. Res. Lett. **32:** 4.

KAHRU, M., and B. G. MITCHELL. 2000. Influence of the 1997-98 El Niño on the surface chlorophyll in the California Current. Geophys. Res. Lett. **27:** 2937-2940.

KNAUER, G. A., D. M. KARL, J. H. MARTIN, and C. N. HUNTER. 1984. *In situ* effects of selected preservatives on total carbon, nitrogen and metals collected in sediment traps. J. Mar. Res. **42:** 445-462.

KNAUER, G. A., J. H. MARTIN, and K. W. BRULAND. 1979. Fluxes of particulate carbon, nitrogen, and phosphorus in the upper water column of the Northeast Pacific. Deep-Sea Res. **26:** 97-108.

LANDRY, M. R., C. J. LORENZEN, and W. K. PETERSON. 1994. Mesozooplankton grazing in the Southern California Bight .2. Grazing impact and particulate flux. Mar. Ecol. Prog. Ser. **115:** 73-85.

LANDRY, M. R., W. K. PETERSON, and C. C. ANDREWS. 1992. Particulate flux in the water column overlying Santa Monica Basin. Prog. Oceanogr. **30:** 167-195.

LAVANIEGOS, B. E., and M. D. OHMAN. 2003. Long-term changes in pelagic tunicates of the California Current. Deep-Sea Res. II **50:** 2473-2498.

LAVANIEGOS, B. E., and M. D. OHMAN. 2007. Coherence of long-term variations of zooplankton in two sectors of the California Current System. Prog. Oceanogr. **75:** 42-69.

LYNN, R. J., and J. J. SIMPSON. 1987. The California Current System: the seasonal variability of its physical characteristics. J. Geophys. Res. Oceans **92:** 12947-12966.

MANTUA, N. J., S. R. HARE, Y. ZHANG, J. M. WALLACE, and R. C. FRANCIS. 1997. A Pacific interdecadal climate oscillation with impacts on salmon production. Bulletin of the American Meteorological Society **78:** 1069-1079.

MCGOWAN, J. A., S. J. BOGRAD, R. J. LYNN, and A. J. MILLER. 2003. The biological response to the 1977 regime shift in the California Current. Deep-Sea Res. II **50:** 2567-2582.

MICHAELS, A. F., and M. W. SILVER. 1988. Primary production, sinking fluxes and the microbial food web. Deep-Sea Res. **35:** 473-490.

NELSON, J. R., J. R. BEERS, R. W. EPPLEY, G. A. JACKSON, J. J. MCCARTHY, and A. SOUTAR. 1987. A particle flux study in the Santa Monica-San Pedro Basin off Los Angeles: particle flux, primary production, and transmissometer survey. Cont. Shelf Res. **7:** 307-328.

PILSKALN, C. H., J. B. PADUAN, F. P. CHAVEZ, R. Y. ANDERSON, and W. M. BERELSON. 1996. Carbon export and regeneration in the coastal upwelling system of Monterey Bay, central California. J. Mar. Res. **54:** 1149-1178.

RICHARDSON, T. L., and G. A. JACKSON. 2007. Small phytoplankton and carbon export from the surface ocean. Science **315:** 838-840.

RICHARDSON, T. L., G. A. JACKSON, H. W. DUCKLOW, and M. R. ROMAN. 2004. Carbon fluxes through food webs of the eastern equatorial Pacific: an inverse approach. Deep-Sea Res. I **51:** 1245-1274.

RICHARDSON, T. L., G. A. JACKSON, H. W. DUCKLOW, and M. R. ROMAN. 2006. Spatial and seasonal patterns of carbon cycling through planktonic food webs of the Arabian Sea determined by inverse analysis. Deep-Sea Res. II **53:** 555-575.

ROEMMICH, D., and J. MCGOWAN. 1995a. Climatic warming and the decline of zooplankton in the California Current. Science **267:** 1324-1326.

ROEMMICH, D., and J. MCGOWAN. 1995b. Climatic warming and the decline of zooplankton in the California Current (Vol 267, Pg 1324, 1995). Science **268:** 352-353.

SAVOYE, N., C. BENITEZ-NELSON, A. B. BURD, J. K. COCHRAN, M. CHARETTE, K. O. BUESSELER, G. A. JACKSON, M. ROY-BARMAN, S. SCHMIDT, and M. ELSKENS. 2006. ^{234}Th sorption and export models in the water column: A review. Mar. Chem. **100:** 234-249.

SHIPE, R. F., U. PASSOW, M. A. BRZEZINSKI, W. M. GRAHAM, D. K. PAK, D. A. SIEGEL, and A. L. ALLDREDGE. 2002. Effects of the 1997-98 El Niño on seasonal variations in suspended and sinking particles in the Santa Barbara basin. Prog. Oceanogr. **54:** 105-127.

SIEGEL, D. A., E. FIELDS, and K. O. BUESSELER. 2008. A bottom-up view of the biological pump: Modeling source funnels above ocean sediment traps. Deep-Sea Res. I **55:** 108-127.

SIEGEL, D. A., T. C. GRANATA, A. F. MICHAELS, and T. D. DICKEY. 1990. Mesoscale eddy diffusion, particle sinking, and the interpretation of sediment trap data. J. Geophys. Res. Oceans **95:** 5305-5311.

SMAYDA, T. J. 1970. The suspension and sinking of phytoplankton in the sea. Oceanogr. Mar. Biol. Ann. Rev. **8:** 353-414.

SMITH, K. L., R. J. BALDWIN, H. A. RUHL, M. KAHRU, and B. G. MITCHELL. 2006. Climate effect on food supply to depths greater than 4,000 meters in the northeast Pacific. Limnol. Oceanogr. **51:** 166-176.

STUKEL, M. R., and M. R. LANDRY. 2010. Contribution of picophytoplankton to carbon export in the equatorial Pacific: A re-assessment of food-web flux inferences from inverse models. Limnol. Oceanogr. **55:** 2669-2685.

TURNER, J. T. 2002. Zooplankton fecal pellets, marine snow and sinking phytoplankton blooms. Aquat. Microb. Ecol. **27:** 57-102.

VAN DER LOEFF, M. R., M. M. SARIN, M. BASKARAN, C. BENITEZ-NELSON, K. O. BUESSELER, M. CHARETTE, M. DAI, O. GUSTAFSSON, P. MASQUE, P. J. MORRIS, K. ORLANDINI, A. R. Y. BAENA, N. SAVOYE, S. SCHMIDT, R. TURNEWITSCH, I. VOGE, and J. T. WAPLES. 2006. A review of present techniques and methodological advances in analyzing Th-234 in aquatic systems. Mar. Chem. **100:** 190-212.

VENRICK, E. L. 1998. Spring in the California current: the distribution of phytoplankton species, April 1993 and April 1995. Mar. Ecol. Prog. Ser. **167:** 73-88.

VENRICK, E. L. 2002. Floral patterns in the California Current System off southern California: 1990-1996. J. Mar. Res. **60:** 171-189.

WAPLES, J. T., C. BENITEZ-NELSON, N. SAVOYE, M. R. VAN DER LOEFF, M. BASKARAN, and O. GUSTAFSSON. 2006. An introduction to the application and future use of ^{234}Th in aquatic systems. Mar. Chem. **100:** 166-189.

CHAPTER 1

Contribution of picophytoplankton to carbon export in the equatorial Pacific: A re-assessment of food-web flux inferences from inverse models

By Michael R. Stukel and Michael R. Landry

Abstract

The paradigm that carbon export is derived almost exclusively from the primary production of large phytoplankton has been challenged by inverse ecosystem modeling studies that suggest that most carbon export in the open ocean is fueled by picophytoplankton. To re-address this hypothesis, we use an inverse model to synthesize the planktonic rate measurements from a pair of recent cruises in the equatorial Pacific. The analysis based on this new experimental data, which crucially include vertically-integrated taxon-specific production and grazing estimates, largely resolve the unexpected results of the previous inverse studies, including unbalanced growth and grazing processes and the dominance of production by picophytoplankton. While this very small size class does not produce the majority of phytoplankton carbon that is eventually exported to depth (only 23%, vs. 73% from a previous analysis of Joint Global Ocean Flux Study Equatorial Pacific data), our base

model supports the conclusion that the role of picophytoplankton in vertical carbon flux is largely proportional to their contribution to net primary productivity (though neither is proportional to biomass). We show, however, that export-production proportionality is sensitive to the model representation of the detrital pool, such that the relative export role of picophytoplankton declines substantially for an alternate model with size-structured detritus. A definitive assessment of the role of picoplankton in vertical carbon flux will thus require detailed experimental examination of the origin, composition, and fate of euphotic zone detrital material.

Introduction

Small photosynthetic organisms (*Prochlorococcus, Synechococcus,* and picoeukaryotes) with cell sizes <2-μm diameter, collectively called the picophytoplankton, are abundant and important primary producers, especially over the vast tropical and subtropical regions of the ocean (Li et al. 1983; Takahashi and Bienfang 1983). Conventional wisdom holds that these picophytoplankton are too small to sink individually or to be exploited efficiently by most metazooplankton, but rather are consumed and largely respired in the euphotic zone by protistan consumers. Indeed, a good deal of experimental evidence from the ocean points to a close balance between picophytoplankton production and grazing losses to protists (Brown et al. 1999; Landry et al. 2003; Hirose et al. 2008), analogous to the tightly coupled growth-grazing-recycling processes of the 'microbial loop' that are presumed to dissipate most of the matter and energy produced by heterotrophic bacteria (Azam et al. 1983). If this is the case, the amount of picophytoplankton production that ultimately leaves the euphotic zone as exported carbon should be disproportionately small compared to export that originates as larger phytoplankton, which have more direct pathways to aggregate sinking and utilization by large pellet-producing zooplankton.

This conventional paradigm has been challenged recently in a series of papers (Richardson et al. 2004, 2006; Richardson and Jackson 2007) that have applied inverse modeling techniques to datasets derived from intensive investigations by the US Joint Global Ocean Flux Study (JGOFS) in the equatorial Pacific and the Arabian Sea. As synthesized in Richardson and Jackson (2007), these inverse analyses support two general conclusions regarding the relationship between picophytoplankton and export in open-ocean systems. The first is that the picophytoplankton contribution to vertical carbon export by sinking particles from direct and indirect pathways is a high

fraction of the community total, averaging 73% of export (SD = 21%, their table 1) across a broad range of seasonal and environmental conditions in the two major ecosystems examined. The second is that the picophytoplankton contribution to export is proportional to their contribution to net primary production. The proportionality hypothesis implies that the large percentage contribution of picophytoplankton to total flux derives mainly from their dominance of primary production. Whether picophytoplankton dominate production or not emerges as a separate question, as does the relationship between biomass and production, since Richardson et al. (2004, 2006) use size-class contributions to total phytoplankton biomass as a proxy for their relative contributions to net production rate.

Methodological considerations limit our ability to assess directly the actual contributions of large and small phytoplankton to export flux. However, picophytoplankton have been found in sediments, transported there by phytodetrital aggregates (Lochte and Turley 1988) or salp fecal pellets (Pfannkuche and Lochte 1993). Picoplankton-containing aggregates (Waite et al. 2000) and zeaxanthin (Lamborg et al. 2008) have also been caught in sediment traps, although both may be derived from unassimilated grazing on picophytoplankton (Gorsky et al. 1999; Waite et al. 2000). Nonetheless, the few studies that directly compare the flux of large and small phytoplankton (Silver and Gowing 1991; Rodier and Le Borgne 1997), typically find intact picophytoplankton to be only a small proportion of total carbon flux.

In a recent synthesis of food web fluxes in the Arabian Sea, Landry (2009) found that the JGOFS data for that region were consistent with a more conventional analysis of process rates and relationships than suggested by inverse methods. In particular, Landry (2009) highlighted potential problems in the model inputs for primary production, which were partitioned proportionately among size classes according to

filter-fractioned chlorophyll, a method that could inflate the smallest (picophytoplankton) class due to the extrusion of larger cells (or chloroplasts from broken cells) through the 2-μm filter pores. Based on size-fractioned chlorophyll, picophytoplankton comprised 70%, on average, of primary production for the seasons and stations that were modeled. According to microscopic and flow cytometric assessments from the same Arabian Sea cruises and stations (Garrison et al. 2000), however, picophytoplankton only comprised 35% of the total phytoplankton carbon biomass. Therefore, if production had been assumed to scale with carbon rather than size-fractioned chlorophyll, the ratio of modeled carbon flows originating from small and large cells would have decreased by a factor of four, likely affecting the behaviors of many pathways in the trophic network. In addition, the concept of proportionality in small cell contribution to export was enhanced in the Richardson et al. (2004, 2006) inverse models by an uncoupled growth-grazing condition that drove a large ungrazed fraction of picophytoplankton production directly to detritus. This growth-grazing imbalance was not, in fact, evident in the experimental data (Verity et al. 1996*b*), but arose rather from a decision to scale up computed taxon-specific phytoplankton growth rates to match ^{14}C-primary production (^{14}C-PP), without adjusting the corresponding estimates of microzooplankton grazing rates.

Here, we use an inverse ecosystem modeling approach to re-examine the question of picophytoplankton contribution to export flux in the equatorial Pacific. One important aspect of our analysis is the use of recent data from a pair of cruises in the eastern equatorial Pacific in December 2004 and September 2005. Whereas the JGOFS Equatorial Pacific (EqPac) results available to Richardson et al. (2004) were an assortment of independent rates lacking vertical resolution and with virtually no microscopy for estimating carbon biomass values of phytoplankton and protozoans,

the new data provides contemporaneous production, growth, and grazing rates and microscopical biomass estimates, all integrated for the full euphotic zone at a large number (31) of stations. This unprecedented assemblage of biomass and rate data allows us to rigorously constrain the net production (biomass growth) contributions of major phytoplankton taxa as model input. We further improve the analysis using variability in the field-measured ratio of gross primary production (GPP) to ^{14}C-PP to bound the GPP term, by using a random-walk technique to explore all possible solutions to the model terms and their statistics, and by comparing results to an alternative model structure that accounts for different fates in a size-structured detrital pool. We illustrate that picophytoplankton production is an important, but clearly not dominant source of carbon export in the equatorial Pacific, and that conclusions about the direct and indirect contributions of picophytoplankton to export vary substantially, depending on whether the model considers size-structured detritus or not. We also show that the generally used minimum norm solution significantly underestimates the flows of carbon to bacteria, and that an unstructured detrital pool significantly understates the export role of mesozooplankton. Further advances will require experimental studies that explicitly address the source, composition, and fate of detritus in the euphotic zone.

Methods

To best compare our results to those of Richardson et al. (2004), we used a similar construction and physiological constraints (explained in detail below) for our base ecological model (ECO), while incorporating the data (including group-specific growth and grazing) from the new cruises. As noted above, we expanded the analysis of the model results beyond Richardson et al. (2004) by generating confidence

intervals for all model outputs (using a Monte-Carlo technique) and by using a random walk technique to explore the solution space. In addition, we formatted and ran an alternative size-fractionated detritus (SF-Det) model construct that incorporates a size-structured detrital pool.

Sampling and data - Model inputs and constraints on biomass structure, primary production, nitrate uptake, phytoplankton growth, and micro- and mesozooplankton grazing came from data collected on Equatorial Biocomplexity cruises EB04 (December 2004) and EB05 (September 2005) in the eastern equatorial Pacific (Table 1). Each cruise included an east-west and a north-south transect of sampling stations within the region of 110-140°W and 4°N-4°S (Fig. 1). Transit times between stations were set to allow for collecting a coherent set of plankton biomass and daily rate measurements at each station on the same schedule each day. Analyses of the resulting euphotic-zone integrated data demonstrated remarkably low variability, with coefficients of variation of only 31%, 33%, 43%, and 32% of the mean estimates for ^{14}C-PP, phytoplankton specific growth rate, microzooplankton grazing, and mesozooplankton grazing, respectively (Balch et al. in press; Décima et al. in press; Landry et al. in press). We therefore pooled measured rates and standing stocks from all stations on both cruises to compute composite averages for the region (n = 31 stations, Table 1) over a significantly broader spatiotemporal scale than that of Richardson et al. (2004).

Phytoplankton growth and microzooplankton grazing rates were determined from pairs of two-point dilution experiments conducted for 8 sampling depths spanning the euphotic zone (to 0.1% of surface irradiance) at each station (Selph et al. in press). These experiments were incubated for 24 hours in seawater-cooled deck incubators at light levels representing 0.1%, 0.8%, 5%, 8%, 13%, 31%, 52% and 100% of incident

solar irradiance, corresponding to light levels at the depth of sample collection. Taxon-specific rates were determined by either high pressure liquid chromatography (HPLC) pigment analysis (divinyl chlorophyll *a* (Chl *a*) was considered representative of *Prochlorococcus*, fucoxanthin of diatoms, and monovinyl Chl *a* of total eukaryotic phytoplankton) or flow cytometry samples (*Prochlorococcus* and *Synechococcus*) (Selph et al. in press). Pigment-derived rates were corrected for systematic changes in cellular pigment content during incubation using the initial and final experimental samples to assess the changes in the mean ratios of accessory pigment to microscopical assessments of phytoplankton biomass (e.g., fucoxanthin:diatom C). Taxon-specific estimates of production rates were determined from specific growth rates and carbon biomass according to Landry et al. (2000) and integrated for the full euphotic zone (Landry et al. in press) Carbon biomass estimates of nano- and microphytoplankton were determined from the biovolumes of cells measured by epifluorescence microscopy (Taylor et al. in press) and biovolume:carbon ratios (Menden-Deuer and Lessard 2000). Carbon biomass estimates of picophototrophs were determined from flow cytometric analyses of cell abundances and cellular carbon content estimates (Garrison et al. 2000; Brown et al. 2008; Taylor et al. in press). For the sake of the present analysis, we divide the phytoplankton community into cyanobacteria, diatoms, and other eukaryotic phytoplankton, the three groups that could be differentiated most easily both in epifluorescence microscopy (flow cytometry for picoplankton) and pigment analysis. For simplicity, we do not distinguish eukaryotic picophytoplankton from other eukaryotes in this analysis, although we did microscopically and experimentally in results from the shipboard studies. True <2-μm pico-eukaryotes comprised a small fraction of the autotrophic carbon pools (2% of total eukaryotes and 7% of the total <2-μm size class; Taylor et

al. in press) and were therefore deemed to be inconsequential to the major pathways of carbon flux. Pico-eukaryotes were also determined experimentally to have the same dynamics as the cyanobacteria (i.e., a close balance between production and grazing by protistan consumers; Landry et al. in press); therefore, the flux behaviors of *Synechococcus* and *Prochlorococcus* were representative of this group.

Rates of ^{14}C-PP were measured in shipboard incubations of triplicate 250 mL samples from 6 discrete light levels spanning the euphotic zone (Balch et al. in press). The *f*-ratio (ratio of new to total production) was determined by Parker et al. (in press) from measured uptake rates of $^{15}NO_3^-$ and $^{15}NH_4^+$. Landry et al. (in press) determined that the depth pattern and magnitudes of primary production rates from ^{14}C-PP measurements and dilution growth rates were strongly related, with euphotic-integrated dilution calculations exceeding ^{14}C-PP by 29%, approximately the percentage difference observed when 12-h daytime incubations were compared to full 24-h incubations by the ^{14}C method (mean = 21%, SD = 6%, Dickson et al. 2001).

Mean daily estimates of mesozooplankton grazing rates on the bulk phytoplankton community were determined by Décima et al. (in press) from gut pigment analyses of the animals caught in paired day-night oblique plankton tows (202-μm mesh) at each station and the gut throughput estimates of Zhang et al. (1995). Mesozooplankton biomass was determined from size-fractioned dry weights (dry wt) from the same net tows, converted to carbon equivalents using the C:dry wt conversion factors in Landry et al. (2001). In synthesizing the production, growth, and grazing results of the EB cruises, Landry et al. (in press) demonstrated that euphotic zone averaged growth rates of the phytoplankton community were balanced by the combined grazing effects of micro- and mesozooplankton, resulting in a -0.01 ± 0.11 d^{-1} net residual growth rate for the 31 stations sampled. The community rate dynamics therefore conform to

expectations that the system largely functions as a steady-state chemostat (Frost and Franzen 1992; Dugdale and Wilkerson 1998). The EB cruise results therefore provide a well-integrated and strongly constrained data set for the equatorial Pacific system that includes plankton standing stocks, production, and grazing rates for the full euphotic zone.

Bacterial production (BP) and GPP were not measured on the EB04 and EB05 cruises. However, both rates showed strong correlations with ^{14}C-PP during the JGOFS EqPac cruises. BP was a relatively low proportion of primary productivity (cruise averages of 10-22%, Ducklow et al. 1995; Kirchman et al. 1995). Using the ^{18}O isotope method, Bender et al. (1999) showed that GPP varied from 1.9 to 2.6 times the concurrently measured rate of ^{14}C-PP. We used these field-derived relationships to set upper and lower bounds on the ratios of BP: ^{14}C-PP and GPP: ^{14}C-PP. For export, we chose not to constrain the rate of particulate organic carbon (POC) flux with EqPac data since a goal of our model was to compare POC cycling estimates to those from the EqPac study (Richardson et al. 2004); hence, we did not want to force similarities between the two models in this specific area.

Model structure – To accommodate differences in data collection between EqPac and EB cruises but staying as close as we could to the Richardson et al. (2004) structure, we divided the phytoplankton community into three taxonomic groups (diatoms, other eukaryotic autotrophs, and cyanobacteria – *Synechococcus and Prochlorococcus*) and included four size classes of grazers (pico- and nanoflagellates, microzooplankton, and mesozooplankton), as shown in Fig. 2. Grazers were allowed to graze on all equal or smaller size classes of organisms (and detritus) with the exception of the mesozooplankton, which were assumed unable to feed efficiently on picoplankton (<2 μm) including cyanobacteria, heterotrophic picoflagellates, and

heterotrophic bacteria. All biological compartments contributed to the dissolved organic carbon (DOC) pool through excretion and to the detrital pool via non-grazer related death (for phytoplankton and bacteria) and egestion of fecal matter (for grazer groups).

As in Richardson et al. (2004), standing stocks of the eight biological compartments in the model, as well as the two non-living compartments (detritus and DOC), were constrained to steady-state conditions (Table 2). This assumption is supported by the demonstrated balance between growth and grazing processes in the region (Landry et al. in press). Phytoplankton group-specific rates of growth and grazing from dilution experiments and the grazing rates of mesozooplankton were used as model constraints (Table 1). Since vertical fluxes were not measured on the cruises, we also required that combined export processes (vertical flux of detrital carbon, horizontal export of DOC away from the equator, and consumption of mesozooplankton by higher trophic levels) match the level of new production within the system, assuming similar N:C ratios for phytoplankton, mesozooplankton, detritus, and labile DOC. While shallow water nitrification has called into question the use of nitrate uptake as a proxy for new production in low-nitrate systems (Yool et al. 2007), it is probably insignificant in the high nitrate, upwelling region of the equatorial Pacific.

We further constrained the solution by requiring that the flows obey the same suite of biological inequalities (Table 3) used in the EqPac model (Richardson et al. 2004). Respiration for phytoplankton groups was allowed to vary from 5-30% of group GPP, while bacteria and grazers were required to respire a minimum of 20% of ingested carbon and a maximum set by an allometrically scaled specific respiration rate (*see* Table 3 for all biological constraints). DOC excretion was set to 2-55% of net primary

production (NPP) for phytoplankton groups, and between 10% of ingestion and 100% of respiration for grazers. Assimilation efficiencies for grazers were allowed to vary between 50-90% and gross growth efficiencies (GGE) between 10-40% (10-50% GGE for bacteria). As noted above, we used experimentally determined relationships from EqPac cruises to constrain BP to 10-22% of ^{14}C-PP (Ducklow et al. 1995; Kirchman et al. 1995) and GPP to 190-260% of ^{14}C-PP (Bender et al. 1999).

Model solution and statistical analyses - Even with the many biological constraints on the solution space described above, there remain an infinite number of possible solutions. To choose among these possibilities, we used the minimum norm technique of Vézina and Platt (1988) and a modified version of the MATLAB code of Jackson et al. (2001). Briefly, the method uses the singular value decomposition (SVD) to solve explicitly for the equalities ($Ax=b$). The SVD decomposes the A matrix into three matrices ($A=U \bullet L \bullet V^T$). The rank of the problem (less than or equal to the number of equalities) determines the number of vectors from the V matrix that are necessary to satisfy the equalities, while the remaining vectors form an orthonormal basis that can be added or subtracted to the solution while still satisfying the equality. These remaining vectors are used to find a solution that minimizes the L_2-norm while satisfying the inequality constraints ($Gx \geq h$). While this minimization scheme can be seen as a mathematically parsimonious approach, there is no a priori reason that it should approximate the ways in which ecosystems are constructed. Hence other minimization schemes may be equally valid.

To determine model sensitivity to cruise measurements (rates and standing stocks), we used the measurement means and their 95% confidence intervals to generate normal distributions for each variable. We then ran 100,000 simulations during which we allowed the inputs to vary simultaneously by drawing them randomly from their

respective distributions to generate confidence intervals for all model outputs. When possible, we utilized the full-rank inverse solution; where not, we followed the method of Olsen et al. (2006) selecting the highest-rank solution that satisfied the constraints.

The confidence intervals derived from the above method only address errors associated with the measurements, not with the model construction or the minimization scheme. To assess errors associated with our choice of minimization scheme, we used a random walk (RW) algorithm, inspired by Kones et al. (2009), to sample the solution space of our inverse problem. We drew random samples from a uniform distribution of the orthonormal set of vectors created by the SVD and added them to our minimum norm solution. By definition, this produces solutions that satisfy the equality constraints ($Ax=b$). After each solution jump, we checked that the new solution also satisfied the inequality constraints ($Gx \geq h$). If true, the new solution was used as a starting point for the next iteration, thus allowing a random walk sampling of the entire solution space (the ensemble of solution vectors that satisfy both equality and inequality constraints).

Ecosystem parameters - One of the great powers of constructing flux networks using inverse techniques is the ability to quantify indirect flows through the ecosystem. If G is the normalized production matrix, depicting the percentage of a compartment's carbon flow that originates from each of the other compartments, and I is the identity matrix, then the matrix $(I-G)^{-1}$ gives the normalized amount of energy (direct and indirect) that a compartment derives from any other compartment. Multiplying the rows of this matrix by the total energy of the compartments gives the amount of energy a compartment derives indirectly or directly from any other compartment (Hannon 1973). This technique, as applied in the Network Analysis approach (Ulanowicz and Kay 1991) used by Richardson et al. (2004), allowed us to

compare the relative importance of different biological groups to export of carbon out of the ecosystem. We also calculated the equivalent trophic level of each group, using the convention that detritus, DOC, and phytoplankton have a trophic level of 1 and that all other groups have a trophic level equal to one plus the sum of the trophic levels of their prey multiplied by the proportion of their diet comprised by that nutritional resource (following Christensen and Pauly 1992).

Alternative model structure with size-fractionated detritus - Assessing biases in calculated flows that result from the choice of model structure is difficult because ecosystems can be described in many ways. For evaluating the origins of system export, however, one obvious oversimplification of the base (ECO) model is the uniform treatment of detrital carbon, implicitly assuming complete and immediate aggregation and disaggregation of all detritus. While it is reasonable to assume that all carbon entering a biological compartment will be treated similarly when utilized by a metabolic pathway, the detrital pool contains no such averaging effect. Rather, one intuitively expects that the carbon associated with a dead cyanobacterium should behave very differently than a fecal pellet with regard to its probability of contributing to export. To address how such differences affect model outputs, we created an alternative model structure with size-fractionated detritus (hereafter referred to as model SF-Det), that did not allow detrital aggregation.

In SF-Det, the detrital pool is split into pico-, nano-, and micro-detritus pools. The cyanobacteria and bacteria that die as individual cells can only contribute to the picodetritus, while the other phytoplankton can flow to either the nano- or microdetritus compartments. Grazers contribute fecal pellets to the detrital pool smaller than themselves (e.g., heterotrophic nanoflagellates produce picodetritus) with the exception of the heterotrophic picoflagellates, which produce picodetritus.

Grazers were allowed to feed upon detrital size classes their own size or smaller, with the exception of the mesozooplankton which again could not feed upon pico-sized particles. We allowed vertical export of both nano- and microdetritus, but not picodetritus as 0.2-2 μm particles are generally considered to be non-sinking colloids.

Results

Our results are presented in four subsections. In the first, we use the least minimum norm (MN) solution to directly compare our model results to the EqPac model of Richardson et al. (2004). We then consider the uncertainties introduced into the model by errors in the measured ecological data, which raise some issues with the MN solution. In the third subsection, we use a random-walk assessment of the solution space to demonstrate the range of values allowed by the model and to show that the MN norm is not representative of the wider solution space. We then use the alternative model structure with size-fractionated detritus to show that a slightly more complex model does not significantly change the structure of the biological components of the ecosystem, but does give a more realistic assessment of the flux of sinking detritus to depth.

Least minimum norm (MN) results and comparison to JGOFS EqPac - To compare with the JGOFS EqPac results of Richardson et al. (2004), we determined the model solution that minimized the L_2-norm. This MN solution minimizes the summed squares of all the flows but tends to simultaneously set minor flows to zero and minimize the largest flows in the model.

The use of average rate and biomass measurements from the EB cruises allows us to model composite averages of the flows in the eastern equatorial Pacific (EEP) (Table 4). Production is dominated by the non-diatom eukaryotic phytoplankton of

our ‘AUT’ category (Fig. 3). Diatoms and cyanobacteria account for 27% and 28% of GPP, respectively. Net primary productivity is largely balanced by the direct utilization of phytoplankton by zooplankton grazers. In the MN solution, only the ‘AUT’ group produces excess ungrazed biomass that passes directly to a detrital pool, and this flux is only 9% of group NPP. While cyanobacteria net production is grazed completely by protozoans, mesozooplankton exert a significant proportion of the grazing pressure on eukaryotic phytoplankton (47% of total grazing on diatoms and 31% on other autotrophs). Protozoan losses to respiration are high, accounting for more than half (55%, 70%, and 52% for pico-, nano-, and microzooplankton, respectively) of total carbon ingested. Larger zooplankton rely proportionally more on carnivory. Mesozooplankton, for example, derive 31% of their carbon requirements from other heterotrophs and occupy a mean trophic level of 2.29. Bacteria constitute a relatively small portion of protozoan diets (25%, 9%, and 1% for pico-, nano-, and microzooplankton), yet play a significant role in carbon flux, respiring 10% of GPP.

Export out of the ecosystem is split between horizontal advection of DOC, vertical sinking of POC, and energy transport through mesozooplankton to higher trophic levels. The *e*-ratio (ratio of vertical carbon flux to net primary productivity) predicted by the model is a moderate 10%. Some detritus comes directly from phytoplankton (27%), but most is formed as fecal carbon after digestive processing by the various zooplankton size classes. System flows indicate that the carbon export derives primarily from non-diatom eukaryotic phytoplankton (65%), with diatoms and cyanobacteria contributing 16% and 19%, respectively.

Our results depict an ecosystem that is strikingly different from that of the similarly structured model of Richardson et al. (2004). While this previous model predicted a phytoplankton community with production dominated by

picophytoplankton, the present analysis is constrained by field data that establishes that most production comes from eukaryotes. Cyanobacteria were completely grazed by protozoan grazers in our experimental data (Landry et al. in press), while the Richardson et al. (2004) model suggested that over a quarter of picoplankton productivity was ungrazed and passed directly into the detrital pool (Table 4). Nonetheless, the two models produce similar estimates of the utilization of heterotrophic protists in the diets of mesozooplankton, and both suggest that carbon is exported from the system by DOC advection and by higher trophic levels in relatively similar amounts. Both models also suggest that detritus must form a significant portion of mesozooplankton diets, although the contribution is significantly higher for the EqPac model. Unlike the present results, however, the EqPac model required significant remineralization of detritus to DOC both to support the bacterioplankton community and as a sink for the large amount of detritus produced by ungrazed picophytoplankton. The EqPac model also produced lower vertical fluxes, as a result of measurement constraints placed on the EqPac model that were absent in the present analysis.

Model sensitivity - We tested the sensitivity of our ECO model to measurement inaccuracies using the Monte Carlo approach of simultaneously varying all measured values based on normal distributions created from their known means and standard errors (Table 4). To test the role of each measured input (taxon-specific net primary productivity, taxon-specific protozoan grazing, mesozooplankton grazing, *f*-ratio, size-fractionated protozoan biomass, bacterial biomass and ^{14}C-PP) on the model outputs, we regressed each pair of inputs and outputs (Table 5). Many of the resulting relationships were trivial dependencies, such as the relationship of diatom GPP to measured diatom NPP. The strongest correlations, relating pico- and

microzooplankton respiration to their respective biomasses, follow from the tendency of the MN algorithm to maximize the respiration of these groups. Likewise, the strong correlations among ^{14}C-PP and GPP, respiration, and excretion of all phytoplankton groups came from the model's tendency to minimize GPP. The most significant negative relationship was a surprising correlation between net primary productivity and respiration of the 'other autotrophs'. This pattern did not occur for other phytoplankton taxa, and probably resulted from minimization of the largest model flow (gross production of other autotrophs; gAUtoAUT) when NPP of this group was significantly larger than NPP of diatoms and cyanobacteria. Dividing phytoplankton gross primary production as equitably as possible among groups led to an inequitable distribution of respiration, particularly when NPP of the dominant taxa was high. Many of these correlations thus tell us less about the actual behavior of the ecosystem than they do about the behavior of the MN model solution. Several of these relationships, for example, highlight the tendency of the MN solution to set biological constraints (e.g., GGE) to either the maximum or minimum values allowed by the model (Table 3). Rather than settling on representative values that we might expect in the middle of any biologically possible range, the L_2-norm was minimized at the less likely extreme values; thus the choice of constraint ranges had a large (and undesirable) effect on the solution (e.g., 5-50% GGE would produce significantly different results than 10-40%). In particular, the MN solution appeared to maximize respiration from the zooplankton groups in order to shunt energy out of the system as rapidly as possible (Fig. 3, Table 3).

Random-walk (RW) exploration of the solution space - To explore the ensemble of solution vectors (the solution space) of our ECO model beyond the single MN result, we used a random-walk approach to sample the solutions that satisfied the biological

constraints. We applied the random-walk algorithm until the average of the random-walk solutions converged on a value. The entire solution space was then used to calculate means and 95% confidence intervals for all flows (Table 4, Fig. 3), allowing us to compare with the MN solution, which was shown to be a biased representative of the greater solution space. Several of the most unconstrained flows in the model were pairs of flows allowing bi-directional fluxes of carbon between compartments (e.g., DOC to bacteria and bacteria to DOC). These paired flows were strongly related, with statistical correlations of 0.90, 0.78, and 0.67 for bi-directional flows of bacteria to DOC, heterotrophic nanoflagellates to detritus, and mesozooplankton to detritus (flows between detritus and pico- or microzooplankton were better constrained due to the lower biomass of these grazers). The high correlations imply that the net uptakes or losses of carbon for each compartment were relatively well constrained and hence only weakly affected the other modeled flows, with the exception of increased ingestion leading to a concomitant increase in respiration.

As noted previously with regard to the biological constraints, the MN solution consistently used extreme values of the parameters (Fig. 3). To minimize the sum of squares, for example, the MN solution minimized the largest flow in the model (gAUtoAUT). Since NPP of the AUT group (non-diatom eukaryotic autotrophs) was a measured input to the model, this model behavior also minimized DOC excretion, which limited, in turn, the DOC uptake and the respiration of bacteria, leading to a relatively high bacterial GGE (36%).

The RW solution (Table 4) gave significantly higher GPP for the AUT group and lower for the DIA and CYA groups in comparison to the MN solution (Fig. 3). It allowed greater DOC exudation by the phytoplankton community, which was consumed by a less efficient assemblage of heterotrophic bacteria, which in turn

contributed more to total community respiration. Grazing efficiently regulated the phytoplankton community with only 5% of NPP passing ungrazed into the detrital pool. Cyanobacteria were particularly well constrained in the experimental field data and were completely grazed by the protozoan community in the inverse analysis. Despite their lower NPP, diatoms contributed the largest ungrazed proportion of their production (15%) directly to detritus. Grazing on the total phytoplankton community was dominated by the heterotrophic protists (Fig. 4), although mesozooplankton contributed 38% and 35% of the total grazing pressure on diatoms and other eukaryotic phytoplankton, respectively. Omnivory or carnivory comprised a significant fraction of the feeding of microzooplankton and especially mesozooplankton, while bacteria were a minor prey source for the zooplankton community. Detritus, however, was an important food source, especially for heterotrophic nanoflagellates. Vertical export of detritus out of the ecosystem came primarily from grazer-derived detritus and was indirectly derived from the phytoplankton groups in rough proportion to their NPP, with eukaryotic phytoplankton dominating the signal (Fig. 5a). Less carbon was exported than in the MN-solution, while more was transferred to higher trophic levels than allowed by the high respiratory losses imposed by the MN-solution.

Size-fractionated detritus (SF-Det) model - Our alternative SF-Det inverse model differs mainly from the base ECO model in defining size-based trophic interaction for three size classes of detritus, and by not allowing the smallest size class, the pico-detritus pool of colloidal-sized (0.2-2 μm) particles, to sink. Overall, most results of the SF-Det model were very similar to those of the original ECO model (Table 6). However, the SF-Det modifications significantly affected utilization of detritus and its export from the system. SF-Det gave higher export than the base ECO model (Fig.

5b) because the abundant nanoflagellates were no longer allowed to graze large (>20-μm) detrital particles. The proportion of export derived indirectly from diatoms also increased at the expense of that derived from cyanobacteria. The direct contribution to sinking detritus was also significantly altered by the SF-Det model structure with the flux coming primarily from fecal pellets of micro- and mesozooplankton at the expense of the fecal debris (egested vacuole contents) produced by smaller protozoans (Fig. 5c,d).

Discussion

As applied to the analysis of ocean food webs, the great strength of inverse models is their use of objective techniques to resolve the flows in complex networks where many of the rate terms are undetermined by data. This does not mean, however, that inverse analyses necessarily produce reliable or even realistic portrayals of system flows under all circumstances. Here we show that applying a new and more constrained dataset to an inverse model that was structurally-similar to Richardson et al. (2004), led to substantially different solutions with regard to the role of picophytoplankton in the equatorial Pacific food web, the balance of phytoplankton growth by grazing processes, the pathways and flows of production to DOC and detritus, and the efficiency of bacterial growth. In the sections below, we consider how the results of these models can be influenced by several factors including: different solution schemes, subjective assumptions about critical model input terms, and alternate structures for export-relevant processes.

Inverse model solutions and biases – Studies based on inverse ecosystem analyses often neglect errors associated with the minimization scheme (Fig. 3; Table 4). While a solution set that minimizes the L_2-norm may be parsimonious in a mathematical

sense, from an ecological perspective it imposes an additional structure on the solution that is not explicit in the applied equality and inequality constraints. In particular, the MN solution is achieved by maximizing respiratory losses of lower level grazers (Table 3) and minimizing the number of trophic links. In the Richardson et al. (2004, 2006) models, for example, this behavior contributed to low rates of DOC production by phytoplankton and hence the unrealistically high bacterial gross growth efficiencies noted by Landry (2009). The mean solution set, by averaging each flow from a random compilation of all vectors that solve both the equality and inequality constraints, may consequently provide a simpler and perhaps more ecologically relevant answer to the under-constrained ecosystem model.

Model structure also has a large and overlooked effect on inverse ecosystem analysis. However, it is often difficult to assess a priori the level of complexity that is necessary to accurately depict the ecology of the system, and, in fact, the necessary complexity depends on the questions addressed. In the present example, for instance, the added complexity of size-fractionated detritus did not seem to matter very much for assessing the major flows among most biological components of the equatorial Pacific ecosystem. However, it did significantly alter conclusions that can be made about the origins of carbon export from the euphotic zone (Fig. 5). Thus, when commonalities are found in the behaviors of disparate food webs, and especially when those results differ greatly from conventional understanding, it is important to assess the role that the model structure and assumptions may have played in forcing the solutions.

Comparison to EqPac – Based on inverse analysis of data from the US JGOFS EqPac Program as well as similar findings for the Arabian Sea (Richardson et al. 2004, 2006), Richardson and Jackson (2007) reported that picophytoplankton

production was directly and indirectly responsible for most (73%) of the carbon export in these two open-ocean ecosystems. In retrospect, this conclusion hangs critically on the assumption that production can be assigned to different size fractions based on their contributions to size-fractionated Chl *a*. For the EqPac program, which lacked a coherent database on plankton carbon biomass from microscopy, the assumed chlorophyll-production relationship led to picophytoplankton comprising an average of 73% (SD = 9%) of the total community primary production (PP) in the four cruise scenarios that were modeled. In contrast, our new data for the equatorial Pacific, based on robust microscopical analyses and carbon-based estimates of growth rates puts total picophytoplankton production at 27% of PP, with 23% originating as the production of cyanobacteria (Table 1), *Prochlorococcus* and *Synechococcus*, the two components that we have explicitly considered here. Our new model based on this data consequently shows a large decline in the export flux that can be attributed to picophytoplankton populations, but the difference principally reflects the former assumption vs. the new field-estimated rates that determine the input terms for size-structured production. In other respects, data from the EqPac and EB cruises do not show substantial differences. For example, a large fraction, 75-80%, of Chl *a* passed through 3-μm filters on the EB cruises (Balch et al. in press). The mean estimate of phytoplankton production consumed directly by protists on the EqPac cruises (88% of PP, Landry et al. 1997) was even higher than the 70% determined for EB cruises (Landry et al. in press). As noted above, the uncoupled growth and grazing in the Richardson et al. (2004) model was artificially imposed, in contradiction to direct field measurements from the EqPac study (Verity et al. 1996*b*). It appears therefore that the strongly different behaviors of the EqPac and our base ECO inverse models with regard to picophytoplankton flows to detritus and DOC arise not from major changes

in the equatorial Pacific between EqPac and EB studies, but from the carbon cycling challenges of the former model in meeting system steady-state model constraints when an unrealistic amount of production is assigned to the smallest size fraction.

Although the magnitude of the export flux contribution of picophytoplankton was exaggerated in the Richardson et al. (2004) model, according to new data on taxon-specific contributions to primary production in the equatorial Pacific, our revised model provides support for a central finding of the previous results. The RW-solution of our base ECO model indicates, for example, that cyanobacteria production accounted for 23% of C export (Fig. 5a), the same as their percentage contribution to production, as predicted by the *proportionality* tenet of Richardson and Jackson (2007). Thus, an important part of their challenge to conventional expectations of phytoplankton size-export relationships is retained in the results of the new model with well-constrained biomass and rate data. Nonetheless, since picophytoplankton production in the Richardson et al. (2004; 2006) models was assigned according to a biomass proxy, size-fractioned chlorophyll, it needs to be noted that the 23% cyanobacteria contribution to export in the present study falls far short of their contribution to phytoplankton biomass (36%). Thus, picophytoplankton contribution to biomass does not substitute for contribution to net production in the proportionality finding. The inclusion of size-structured detritus in our SF-Det model also led to a greater export role for larger cells like diatoms at the expense of picophytoplankton (Fig. 5b). Even under this model construction that did not allow direct sinking of picodetritus, however, picophytoplankton were responsible for producing 18% of the exported carbon (3/4 of the percentage predicted by the proportionality argument and half of their contribution to carbon biomass).

A strong growth-grazing balance for picophytoplankton populations, with protists applying essentially all of the grazing pressure, follows directly from the experimental measurements (Landry et al. in press; Selph et al. in press) and is a consistent feature of both forms of our model and minimization schemes. Thus, unlike the Richardson et al. (2004, 2006) analyses, the export of picophytoplankton-based production cannot be said to be unrealistically enhanced by a large fraction escaping consumption in the microbial food web and passing directly to detritus. As an output, our estimates of the *e*-ratio (export of 5.7% of ^{14}C-PP with the base ECO-model and 7.9% with the SF-Det model), which was left unconstrained by data in the present analyses, agree well with the region-wide EqPac estimates of <5-10% from Buesseler et al. (1995).

Complete grazing of cyanobacteria by protists may seem at odds with model results that show picophytoplankton contributing to export in proportion to their production. In both the EqPac and our base (ECO) models, however, this proportionality derives from the implicit assumption that there is complete and immediate homogenization of everything that enters the detrital pool, essentially allowing protozoan egesta to sink as rapidly as mesozooplankton fecal pellets. The maintenance of semi-proportionality after inclusion of detrital size-classes (picophytoplankton contribute 18% of export compared to 23% of NPP) in our SF-Det model is a more intriguing result, especially since mesozooplankton, which provide the dominant mechanism for producing sinking particles, are not allowed to graze on picoplankton. The relevant insight from field measured rates is that protists also consume most (60%) eukaryotic phytoplankton production (Fig. 6). Thus, the primary fates of pico- and larger phototrophs are not nearly as distinct as the traditional dichotomy between the 'classical food chain' and the 'microbial loop'. In fact, mesozooplankton derive only 44% of their ingestion from phytoplankton in the RW-

solution of our SF-Det model, with an additional 34% derived from grazing on protozoans and the remainder comprised of detrital material (Fig. 4). Thus, the contribution of cyanobacteria to export is derived from ecosystem linkages not readily assessed by traditional techniques (Fig. 7). It is also important to note that proportionality is only found for the RW-solution to the SF-Det model. The unrealistically high respiratory demands of the MN solution do not allow efficient energy transfer up the food chain.

While sediment traps cannot trace the primary source of exported carbon, their contents provide a glimpse of the nature of sinking particles. Rodier and Le Borgne (1997) utilized flow cytometry, microscopy and pigment analyses to assess the contents of drifting sediment traps deployed for a week on the equator at 150°W, finding that intact picophytoplankton comprised only a tiny fraction of the carbon flux. The dominant signal was from marine snow and fecal pellets, which were numerically dominated by particles in the 20-100 μm size class. Pigment analyses suggested that only 4% of POC flux came from intact phytoplankton while 12% came from recent herbivory. Similarly, sediment traps deployed at 140°W during EqPac had very low ratios of chlorophyll to phaeopigment (Newton and Murray 1994), indicative of a low export percentage of intact cells. These values compare favorably with our model predictions of direct flux from phytoplankton (7% for the RW solution of the base ECO-model and 11% for the SF-Det model) and from the fecal pellets of herbivorous zooplankters (41% for ECO and 36% for SF-Det), with the caveat that the percent pigmented ratio of detritus should decrease through microbial activity and coprophagy as particles sink to the depths of the traps.

Dam et al. (1995) determined that mesozooplankton fecal carbon production alone could have supported all the vertical flux measured during JGOFS EqPac cruises.

Consistent with this, our model suggests that fecal matter comprises the dominant pathway by which carbon leaves the system (Fig. 5c,d), as a by-product of the growth-grazing balance of the euphotic zone (Fig. 6), but that most is re-worked or degraded through coprophagy or dissolution to DOC. The SF-Det model indicated that food chain length to larger zooplankton was a major determinant of the efficiency of carbon export from the system, unlike the base ECO model, which, by treating all detrital particles equally, unrealistically allowed protozoan egesta to sink as rapidly as mesozooplankton pellets.

Processes altering export rates – Like all models, ours oversimplifies complex ecology and excludes processes deemed to be of lesser importance or poorly assessed by field measurements. The absence of phytoplankton density measurements means, for example, that we could not consider the inorganic ballasting effect of siliceous and calcareous planktonic taxa (Armstrong et al. 2002), which can significantly increase flux2es, thereby enhancing the export roles of diatoms and coccolithophores (both directly and by adding density to zooplankton egesta). We have likewise not explicitly accounted for particle aggregation (Alldredge and Gotschalk 1989; Walsh and Gardner 1992; Jackson 2001), which involves both phytoplankton and bacterial interactions (Passow et al. 1994, 2001) and provides an alternate pathway for flux of smaller particles to depth. In addition, the model does not expressly consider pelagic tunicates, like salps that can efficiently pack cyanobacteria into rapidly sinking fecal pellets (Pfannkuche and Lochte 1993) or appendicularians that concentrate picophytoplankton in the mucus web feeding nets of their discarded houses (Robison et al. 2005). By the same token, however, the model does not consider active diel vertical migrations of mesozooplankton, which transport to depth substantial amounts of carbon derived primarily from large prey (Dam et al. 1995; Zhang and Dam 1997).

All of these represent poorly constrained mechanisms that can alter the relative contributions of small and large phytoplankton to total system organic export.

The SF-Det model illustrates, however, the importance of including size-fractionated detritus when assessing the origin of sinking detritus, although its equivalent treatment of nano- and microdetritus with respect to sinking is still simplistic. Micro-sized fecal pellets produced by mesozooplankton are likely to sink much faster than smaller detrital particles, suggesting that these large fecal pellets may comprise an even greater proportion of exported material than the 49% suggested by the SF-Det model. In fact, 20-100 μm particles (equivalent to a portion of our microdetrital group) were the primary fecal material in the equatorial sediment traps examined by Rodier and Le Borgne (1997). Our model's microdetritus was composed primarily of mesozooplankton fecal pellets and supported by the production of eukaryotic phytoplankton with only minor contribution from cyanobacteria (Fig. 5). While this highlights the importance of an accurate treatment of detritus, better constraints on this non-living fraction will depend on experimental measurement by techniques such as detrital stains (Verity et al. 1996*a*) and sediment traps paired with polyacrylamide gels (Lundsgaard 1995).

In summary, we found that many of the unexpected results of the Richardson et al. (2004) inverse model of the equatorial Pacific – namely, the picophytoplankton dominance of export, the imbalance of phytoplankton growth and grazing processes, the unusual pathways and flows of production to DOC and detritus, and the high efficiency of bacterial growth – were largely resolved by better data constraints on biomass and rates for the full euphotic zone and the taxonomic and size-class origins of primary production, and by solution schemes that avoided the extremes of the minimal L_2-norm. Proportionality of net production and export contributions among

phytoplankton size classes, a central conclusion of Richardson and Jackson (2007), remained a robust feature of the base model despite the above refinements. We have shown, however, that this conclusion is sensitive to the treatment of detrital size classes; thus, this is an area where insights from direct field measurements and model development would be useful. Future progress in understanding the roles of different taxa in export processes also clearly requires data sets that more directly and quantitatively link the growth and trophic dynamics of different functional groups in the euphotic zone to their incorporation into exported material, so that we might usefully compare model predictions to measurements and highlight potentially important missing processes.

Acknowledgments

We thank the captains and crews of the R/V *Revelle* for their role in making our work possible. We are grateful to Chief Scientist Dave Nelson and all of our colleagues on the cruises for their support and collaboration. We give special thanks to Barney Balch, Alex Parker, Karen Selph, Moira Décima, and Andrew Taylor and their respective labs for making their data available to us. We are also grateful to Tammi Richardson, Mikhail Zubkov, and two anonymous reviewers, who provided insightful comments on various versions of the manuscript. This project was supported by Ocean Sciences Grants 0322074 and 0826626 from the National Science Foundation (NSF), and by NSF and National Aeronautics and Space Administration Earth and Space Science Graduate Research Fellowships to M. Stukel.

Chapter 1, in full, has been published in Limnology and Oceanography: Stukel, M. R., Landry, M.R., 2010. "Contribution of picophytoplankton to carbon export in the equatorial Pacific: A re-assessment of food-web flux inferences from inverse models." Limnol. Oceanogr. **55**: 2669-2685. The dissertation author was the primary investigator and author of this paper.

Table 1.1. Experimental inputs to the base (ECO) model. Table gives the measured mean rates and biomasses (± 95% confidence limits) from the EB04 and EB05 cruises. Equations relate the measured rates to the model compartments: diatoms (DIA), other eukaryotic autotrophs (AUT), cyanobacteria (CYA), heterotrophic picoflagellates (HPF), heterotrophic nanoflagellates (HNF), heterotrophic microzooplankton (MIC), mesozooplankton (MES), bacteria (BAC), detritus (DET), and dissolved organic carbon (DOC). Flows are written as SOURCEtoSINK, from the first carbon pool to the second. gDI, gAU, and gCY are gross primary production of the three phytoplankton groups. [1]Balch et al. in press; [2]Décima et al. in press; [3]Landry et al. in press; [4]Parker et al. in press; [5]Taylor et al. in press.

Rates	Equation	Value	Source
DiaNPP	gDItoDIA – DIAtoRES - DIAtoDOC	156 ± 54 mg C m^{-2} d^{-1}	3
AutNPP	gAUtoAUT – AUTtoRES – AUTtoDOC	505 ± 95 mg C m^{-2} d^{-1}	3
CyaNPP	gCYtoCYA – CYAtoRES – CYAtoDOC	203 ± 38 mg C m^{-2} d^{-1}	3
Diamzoogr	DIAtoHNF + DIAtoMIC	83 ± 28 mg C m^{-2} d^{-1}	3
Autmzoogr	AUTtoHNF + AUTtoMIC	316 ± 67 mg C m^{-2} d^{-1}	3
Cyamzoogr	CYAtoHPF + CYAtoHNF + CYAtoMIC	203 ± 36 mg C m^{-2} d^{-1}	3
Mzoogr	DIAtoMES + AUTtoMES	217 ± 41 mg C m^{-2} d^{-1}	2
NewProd	DOCtoEXT + DETtoEXT + MEStoEXT	F-rat•NPP	
Other parameters			
C-14PP		672 ± 73 mg C m^{-2} d^{-1}	1
F-Rat		0.22 ± 0.05	4
BioHpf		12 ± 3.9 mg C m^{-2}	5
BioHnf		242 ± 39.7 mg C m^{-2}	5
BioMic		78.6 ± 17.8 mg C m^{-2}	4
BioMes		994 ± 77 mg C m^{-2}	2
BioBac		679 ± 53.5 mg C m^{-2}	4

Table 1.2. Steady-state equations for the base (ECO) model. Flows and model conventions are the same as in Table 1.1.

Parameter	Steady-state equation
DIA	gDItoDIA – DIAtoRES – DIAtoHNF – DIAtoMIC – DIAtoMES – DIAtoDET - DIAtoDOC
AUT	gAUtoAUT – AUTtoRES – AUTtoHNF – AUTtoMIC – AUTtoMES – AUTtoDET – AUTtoDOC
CYA	gCYtoCYA – CYAtoRES – CYAtoHPF – CYAtoHNF – CYAtoMIC – CYAtoDET - CYAtoDOC
HPF	CYAtoHPF + BACtoHPF + DETtoHPF – HPFtoHNF – HPFtoMIC – HPFtoRES – HPFtoDET - HPFtoDOC
HNF	DIAtoHNF + AUTtoHNF + CYAtoHNF + HPFtoHNF + BACtoHNF + DETtoHNF – HNFtoMIC – HNFtoMES – HNFtoRES – HNFtoDET - HNFtoDOC
MIC	DIAtoMIC + AUTtoMIC + CYAtoMIC + HPFtoMIC + HNFtoMIC + BACtoMIC + DETtoMIC – MICtoMES – MICtoRES – MICtoDET - MICtoDOC
MES	DIAtoMES + AUTtoMES + HNFtoMES + MICtoMES + DETtoMES – MEStoRES - MEStoDET - MEStoDOC - MEStoEXT
BAC	DOCtoBAC – BACtoHPF – BACtoHNF – BACtoMIC – BACtoRES – BACtoDET - BACtoDOC
DET	DIAtoDET + AUTtoDET + CYAtoDET + HPFtoDET + HNFtoDET + MICtoDET + MEStoDET + BACtoDET – DETtoHPF – DETtoHNF – DETtoMIC – DETtoMES – DETtoDOC - DETtoEXT
DOC	DIAtoDOC + AUTtoDOC + CYAtoDOC + HPFtoDOC + HNFtoDOC + MICtoDOC + MEStoDOC + BACtoDOC + DETtoDOC – DOCtoBAC - DOCtoEXT

Table 1.3. Minimum and maximum biological constraints on the model solution. All units are mg C m^{-2} d^{-1}. MN and RW are constraint values for the minimal L_2-Norm (MN) solution and the mean of the random-walk exploration of the solution space (RW). Values in bold indicate that the model chose either a maximum or minimum allowable value for the parameter. * indicates percent of ingestion. ** indicates percent of respiration. *W* is the characteristic size of each group of organisms and is used for allometric determination of respiration rates. For consistency, *W*'s of 0.02, 7.5, 2047, and 3,800,000 pg C $cell^{-1}$ were taken from Richardson et al. (2004) for heterotrophic bacteria, heterotrophic nanoflagellates, microzooplankton, and mesozooplankton, respectively. For heterotrophic picoflagellates, a *W* of 0.17 pg C $cell^{-1}$ was obtained from Taylor et al. (in press).

Rate	Pop	Minimum	Maximum	MN	RW
GGE	HPF	10%	40%	24%	28%
	HNF	10%	40%	**10%**	24%
	MIC	10%	40%	27%	25%
	MES	10%	40%	**10%**	17%
	BAC	10%	50%	36%	16%
Assim. Eff.	HPF	50%	90%	**90%**	69%
	HNF	50%	90%	**90%**	68%
	MIC	50%	90%	**90%**	66%
	MES	50%	90%	**90%**	66%
Respiration	DIA	5% GPP	30% GPP	**30%**	20%
	AUT	5% GPP	30% GPP	11%	20%
	CYA	5% GPP	30% GPP	**30%**	20%
	HPF	20% ingestion	$1.7W^{-0.25} \bullet e^{(0.0693(T-20))} \bullet$biomass = 45	55%* = **45**	25%* = 38
	HNF	20% ingestion	$1.7W^{-0.25} \bullet e^{(0.0693(T-20))} \bullet$biomass = 352	70%* = 280	29%* = 197
	MIC	20% ingestion	$1.7W^{-0.25} \bullet e^{(0.0693(T-20))} \bullet$biomass = 114	52%* = **114**	25%* = 96
	MES	20% ingestion	$14W^{-0.25} \bullet e^{(0.0693(T-20))} \bullet$biomass = 446	70%* = 253	32%* = 179
	BAC	20% ingestion	$1.7W^{-0.25} \bullet e^{(0.0693(T-20))} \bullet$biomass = 4838	64%* = 121	51%* = 423
Excretion	DIA	2% NPP	55% NPP	52%	31%

Table 1.3. Cont.

Rate Pop		Minimum	Maximum	MN	RW
AUT		2% NPP	55% NPP	**2%**	29%
C	YA	2% NPP	55% NPP	24%	31%
	HPF	10% ingestion	100% respiration	11%* = 20%**	17%* = 68%**
	HNF	10% ingestion	100% respiration	**10%*** = 14%**	16%* = 54%**
	MIC	10% ingestion	100% respiration	11%* = 9%**	16%* = 36%**
	MES	10% ingestion	100% respiration	**10%*** = 14%	17%* = 52%**
Ingestion MES		-	$3.6W^{-0.25} \bullet e^{(0.0693(T-20))}$ •biomass = 2006	361	556
BAC		-	$63W^{-0.25} \bullet e^{(0.0693(T-20))}$ •biomass = 10246	189	829

Table 1.4. Solutions to the base ECO-model. Flows are, by convention, from the first carbon pool to the second. Carbon pools are GPP of diatoms (gDI), GPP of other eukaryotic phytoplankton (gAU), GPP of cyanobacteria (gCY), diatoms (DIA), other eukaryotic autotrophs (AUT), cyanobacteria (CYA), heterotrophic picoflagellates (HPF), heterotrophic nanoflagellates (HNF), microzooplankton (MIC), mesozooplankton (MES), bacteria (BAC), detritus (DET), dissolved organic carbon (DOC), respiration (RES), and export from the ecosystem (EXT). EqPac is the equivalent solutions of the Richardson et al. (2004) model. ECO MN is the solution that minimizes the L_2-norm of our base ECO model. Monte Carlo mean and 95% confidence intervals (conf inter) are derived from randomly drawing possible combinations of the measured inputs to the model. RW mean and 95% conf inter are drawn from a random walk exploration of the possible solution space. [1]Solutions are the minimum and maximum of the four time-series assessed by Richardson and Jackson (2004). [2]The EqPac model did not allow (na) flow from diatoms to nano-sized protists. [3]Combined values for the two non-diatom eukaryotic phytoplankton in the EqPac model. [4]The EqPac model's group of picophytoplankton includes picoeukaryotes but is functionally similar to our cyanobacteria compartment. [5]The EqPac model had no heterotrophic picoflagellate (HPF) group. [6]Since the EqPac model had no HPF group their protozoan group was equivalent to the sum of our HPF and HNF compartments.

	Variable	EqPac[1]	ECO MN	ECO Monte Carlo		ECO random walk	
				Mean	Conf inter	Mean	Conf inter
1	gDItoDIA	7.2-192	338	318	(228-381)	255	(188-325)
2	DIAtoRES	0.4-9.6	102	95.3	(67-114)	50.5	(13-92)
3	DIAtoHNF	na[2]	59.1	56.5	(41-72)	46.9	(4-81)
4	DIAtoMIC	2.4-61.2	23.9	21.0	(4-36)	36.1	(2-79)
5	DIAtoMES	0-42	73.0	70.2	(24-115)	50.3	(29-72)
6	DIAtoDET	4.0-75.6	0.0	20.6	(0-95)	22.7	(1-44)
7	DIAtoDOC	0.1-3.6	81.0	61.1	(4-88)	48.4	(6-84)
8	gAUtoAUT	155-431[3]	579	596	(521-681)	816	(655-1023)
9	AUTtoRES	7.8-21.6[3]	63.8	74.3	(28-168)	164	(46-286)
10	AUTtoHNF	23.2-140[3]	176	173	(139-207)	228	(64-313)
11	AUTtoMIC	0-77.3[3]	140	137	(103-170)	87.6	(3-252)
12	AUTtoMES	45.6-82.4[3]	144	141	(93-198)	167	(145-188)
13	AUTtoDET	64.2-219.8[3]	45.0	65.3	(0-176)	22.3	(1-44)
14	AUTtoDOC	2.9-5.0[3]	10.1	10.3	(8-12)	147	(23-269)
15	gCYtoCYA	997-1181[4]	359	363	(291-441)	333	(245-424)
16	CYAtoRES	49.9-59.0[4]	108	108	(85-132)	66.8	(17-121)
17	CYAtoHPF	na[5]	65.3	62.0	(50-74)	59.5	(3-143)
18	CYAtoHNF	445-1034[4,6]	86.5	86.4	(73-101)	83.7	(5-176)

Table 1.4. Cont.

Variable	EqPac[1]	ECO MN	ECO Monte Carlo		ECO random walk	
			Mean	Conf inter	Mean	Conf inter
19 C YAtoMIC	2.0-106[4] 51	.2	50.8	(39-62)	59.8	(3-157)
20 C YAtoDET	51.7-463[4] 0	.0	13.0	(0-60)	0.0	(0-0)
21 CYAto DOC	18.6-22.0[4] 48	.6	47.0	(4-101)	63.2	(8-109)
22 HPFt oHNF	na[5] 20	.0	21.7	(10-36)	22.4	(1-58)
23 HPFt oMIC	na[5] 0.	0	0.0	(0-0)	19.7	(1-54)
24 HPFt oRES	na[5] 45	.0	45.0	(30-60)	37.8	(24-44)
25 HPFt oDET	na[5] 8	.2	8.9	(7-11)	47.1	(14-88)
26 HPFt oDOC	na[5] 9.	0	14.0	(7-31)	25.6	(12-40)
27 HN FtoMIC	0.0	0.0	0.0	(0-0)	68.9	(3-196)
28 H NFtoMES	106-235	40.0	42.3	(36-52)	93.6	(6-238)
29 HNFtoRES	369-543	280	289 (	250-335)	198	(107-310)
30 H NFtoDET	68.3-112	40.0	41.2	(36-48)	220	(61-476)
31 H NFtoDOC	159-272	40.0	41.2	(36-48)	107	(53-186)
32 MICtoRES	4.3-30.6	114	114 (	104-123)	95.8	(63-113)
33 M ICtoMES	8.6-61.2	58.1	58.0	(41-78)	95.7	(35-177)
34 M ICtoDET	4.3-30.6	21.7	22.0	(20-25)	134	(40-234)
35 M ICtoDOC	4.3-30.6	23.2	26.7	(20-46)	63.9	(32-101)
36 MEStoRES	124-266	253	259 (	226-299)	179	(97-294)
37 M EStoDET	41.0-66.6	36.2	37.2	(33-43)	189	(54-381)
38 M EStoDOC	57.1-94.7	36.2	37.2	(33-43)	93.8	(47-166)
39 BA CtoRES	180-265	121	129	(97-172)	423	(256-596)
40 B ACtoHPF	na[5] 15	.4	15.6	(10-20)	33.1	(2-90)
41 B ACtoHNF	88.6-127[6] 36	.6	40.0	(28-53)	42.7	(2-104)
42 B ACtoMIC	0.0	1.3	4.9	(0-11)	33.7	(2-93)
43 B ACtoDET	3.8-91.6	13.9	7.8	(0-21)	20.8	(1-61)
44 B ACtoDOC	0-5.3	0.0	0.0	(0-0)	276	(11-709)
45 DETt oHPF	na[5] 1	.5	10.7	(0-34)	60.0	(3-150)
46 DETt oHNF	0-112[6] 2	2.6	34.7	(9-73)	263	(16-650)
47 DETt oMIC	0.0	0.0	5.3	(0-32)	83.7	(3-248)
48 D ETtoMES	236-288	46.5	60.3	(32-108)	148	(6-446)
49 D ETtoDOC	293-318	11.6	22.0	(0-59)	62.2	(2-199)
50 DOCtoBAC	300-450	189	196 (	158-243)	829	(492-1251)
51 D OCtoEXT	206-304	71.2	64.0	(35-89)	58.2	(4-123)
52 D ETtoEXT	22.8-42.0	82.8	85.0	(50-120)	38.4	(2-109)
53 MESto EXT	164-266	36.2	39.4	(34-50)	93.5	(47-161)

Table 1.5. Correlations between model inputs (measured rates and standing stocks) and outputs (flows) that explain at least 30% of the variance in the modeled flow, as derived from the Monte Carlo error analysis. Signs show whether the relationship was positive or negative. Model inputs are biomass of heterotrophic picoflagellates (BioHPF), biomass of heterotrophic nanoflagellates (BioHNF), biomass of microzooplankton (BioMIC), biomass of mesozooplankton (BioMES), biomass of bacteria (BioBAC), ^{14}C primary productivity (^{14}C-PP), *f*-ratio (F-rat), NPP of diatoms (DiaNPP), NPP of other eukaryotic autotrophs (AutNPP), NPP of cyanobacteria (CyaNPP), protozoan grazing on diatoms, other eukaryotic autotrophs, and cyanobacteria (Diamzoogr, Autmzoogr, Cyamzoogr, respectively), and mesozooplankton grazing (Mesgr).

Input	Output	R^2	Sign
BioHPF	HPFtoRES	1.00	+
BioMIC	MICtoRES	1.00	+
Autmzoogr	AUTtoHNF	0.97	+
Autmzoogr	AUTtoMIC	0.92	+
Diamzoogr	DIAtoHNF	0.84	+
Cyamzoogr	CYAtoMIC	0.83	+
Cyamzoogr	CYAtoHNF	0.82	+
Diamzoogr	DIAtoMIC	0.67	+
F-rat	DOCtoEXT	0.61	+
C-14PP	gCYtoCYA	0.55	+
C-14PP	CYAtoRES	0.52	+
C-14PP	CYAtoDOC	0.51	+
C-14PP	DOCtoBAC	0.50	+
DiaNPP	gDItoDIA	0.50	+
C-14PP	AUTtoRES	0.42	+
DiaNPP	DIAtoRES	0.41	+
F-rat	DETtoEXT	0.41	+
C-14PP	gAUtoAUT	0.40	+
Autmzoogr	MICtoDET	0.40	+
Cyamzoogr	CYAtoHPF	0.40	+
AutNPP	AUTtoDET	0.39	+
BioHPF	BACtoHPF	0.37	+
AutNPP	AUTtoRES	0.36	-
C-14PP	BACtoRES	0.36	+
CyaNPP	CYAtoDET	0.36	+
DiaNPP	DIAtoMES	0.33	+
AutNPP	gAUtoAUT	0.33	+
Cyamzoogr	CYAtoDET	0.32	-

Table 1.5. Cont.

Input	Output	R^2	Sign
C-14PP DI	AtoDOC	0.32	+
Autmzoogr B	ACtoMIC	0.31	-
C-14PP BACto	HNF	0.31	+
AutNPP DETto	EXT	0.31	+

Table 1.6. SF-Det Model Solutions. Variables are the same as in Table 3, but calculated for the size-fractionated detritus (SF-Det) model. PDT, NDT, and MDT are picodetritus, nanodetritus, and microdetritus, respectively. Equivalent solutions for the base ECO-model are shown for comparison. Note that all flows not involving detritus were similar between the two models.

		Min norm solutions		Random walk solutions		
	Variable	SF-Det	Base ECO	SF-Det Mean	95% CI	Base ECO
1	gDItoDIA	338	339	256	189-325	255
2	DIAtoRES	101	102	51.0	13-93	50
3	DIAtoHNF	55.8	59	47.0	4-81	47
4	DIAtoMIC	27.2	24	36.0	2-79	36
5	DIAtoMES	73.0	73	51.2	33-68	50
6	DIAtoNDT	0.0		11.2	1-31	
7	DIAtoMDT	0.0		10.6	1-30	
8	DIAtoDOC	80.5	81	48.9	6-84	48
9	gAUtoAUT	580	579	836	664-1045	816
10	AUTtoRES	65.2	64	178	50-297	164
11	AUTtoHNF	172	176	239	91-313	228
12	AUTtoMIC	144	140	76.8	3-225	88
13	AUTtoMES	144	144	166	149-184	167
14	AUTtoNDT	21.6		12.1	1-32	
15	AUTtoMDT	23.4		11.1	1-31	
16	AUTtoDOC	10.1	10	153	24-270	147
17	gCYtoCYA	359	359	331	245-422	333
18	CYAtoRES	108	108	65.8	17-120	67
19	CYAtoHPF	61.7	65	56.9	3-140	60
20	CYAtoHNF	85.0	86	90.6	7-180	84
21	CYAtoMIC	56.3	51	55.5	2-151	60
22	CYAtoPDT	0.0		0.0	0	
23	CYAtoDOC	48.0	49	62.5	8-109	63
24	HPFtoHNF	21.4	20	21.7	1-56	22
25	HPFtoMIC	0.0	0	19.1	1-53	20
26	HPFtoRES	45.0	45	37.4	23-44	38
27	HPFtoPDT	8.3		46.4	13-88	
28	HPFtoDOC	8.3	9	24.9	12-40	26
29	HNFtoMIC	0.0	0	65.2	3-180	69
30	HNFtoMES	40.3	40	77.5	5-185	94
31	HNFtoRES	282	280	172	103-266	197
32	HNFtoPDT	40.3		211	68-402	
33	HNFtoDOC	40.3	40	94.2	52-157	107

Table 1.6. Cont.

	Min norm solutions		Random walk solutions		
Variable	SF-Det	Base ECO	SF-Det Mean	95% CI	Base ECO
34 M ICtoRES	114	114	99.9	73-113	96
35 M ICtoMES	59.8	58	97.5	42-178	96
36 M ICtoNDT	40.5		173	84-251	
37 M ICtoDOC	23.8	23	67.1	38-102	64
38 MESto RES	248	253	162	95-256	179
39 M EStoMDT	35.4		194	68-346	
40 M EStoDOC	35.4	36	85.9	46-146	94
41 BA CtoRES	124	121	468	300-635	423
42 B ACtoHPF	14.1	15	35.4	2-93	33
43 B ACtoHNF	37.4	37	41.7	2-103	43
44 B ACtoMIC	8.8	1	33.2	2-92	34
45 B ACtoPDT	6.9		21.1	1-60	
46 BA CtoDOC	0.0	0	253	10-661	276
47 PDTt oHPF	7.2		57.3	3-145	
48 PDTt oHNF	30.6		122	5-347	
49 NDTt oHNF	0.0		56.5	2-158	
50 PDTt oMIC	1.9		56.1	2-169	
51 NDTt oMIC	0.0		40.1	2-127	
52 M DTtoMIC	0.0		55.6	2-160	
53 NDTt oMES	19.3		44.0	2-134	
54 M DTtoMES	17.6		90.8	3-274	
55 PDTt oDOC	15.8		42.6	2-134	
56 NDTt oDOC	0.0		31.5	1-103	
57 M DTtoDOC	0.0		40.8	2-126	
58 D OCtoBAC	192	189	852	533-1260	829
59 DOC toEXT	70.6	71	52.4	3-114	58
60 NDTt oEXT	42.9		24.2	1-77	
61 M DTtoEXT	41.2		28.9	1-87	
62 M EStoEXT	35.4	36	84.6	46-145	93

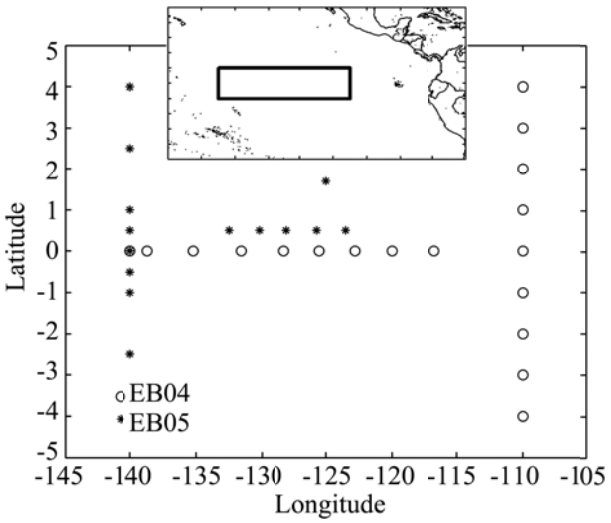

Figure 1.1 – Station locations for EB04 (December 2004) and EB05 (September 2005) cruises. Inset shows the study region within the greater eastern tropical Pacific from 160°W to 70°W and 25°S to 25°N.

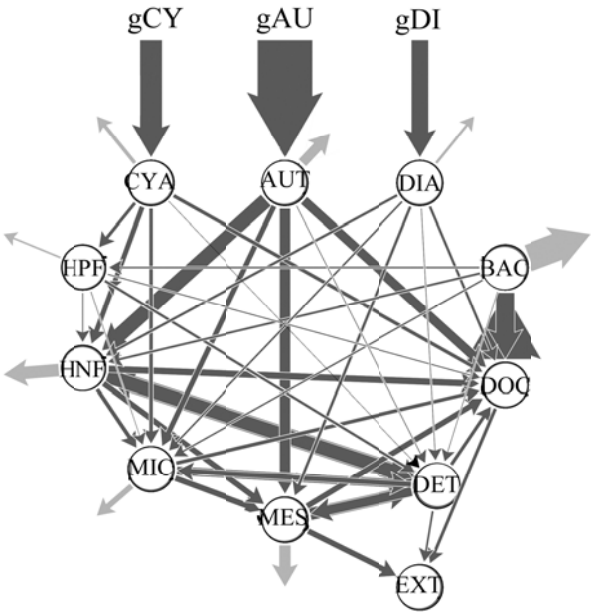

Figure 1.2 – Schematic representation of our model. Arrow widths are proportional to the carbon flows between any two compartments. Light gray arrows that do not end at any compartment represent respiration. Results are the mean values of a random walk exploration of the solution space. gCY, gDI, and gAU are gross primary production of cyanobacteria, diatoms, and other eukaryotic autotrophs, respectively. Compartments are cyanobacteria (CYA), diatoms (DIA), other eukaryotic autotrophs (AUT), bacteria (BAC), dissolved organic carbon (DOC), detritus (DET), mesozooplankton (MES), microzooplankton (MIC), heterotrophic nanoflagellates (HNF), heterotrophic picoflagellates (HPF). Ext is flux of carbon out of the ecosystem through consumption by higher predators, vertical flux of detritus, or lateral advection of DOC.

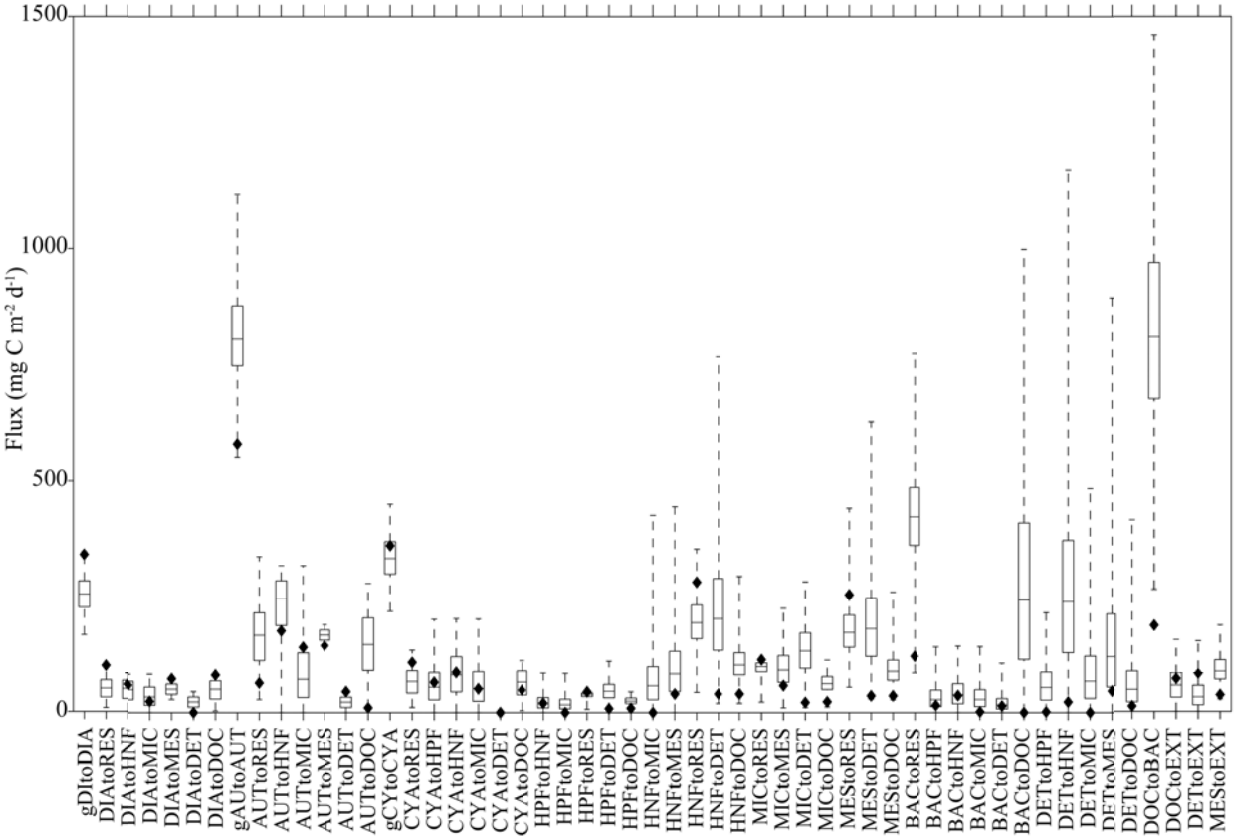

Figure 1.3 – Random Walk Exploration of the Solution Space. Boxes depict the middle two quartiles of a random-walk exploration of all the possible solutions that are consistent with the measured ecological rates and biological constraints imposed on the model. Dashed lines show the extreme values possible for each variable. Filled diamonds are the solutions obtained by using the common minimum norm technique. Note that for most variables the MN solution is an extreme value that is poorly representative of the entire solution space.

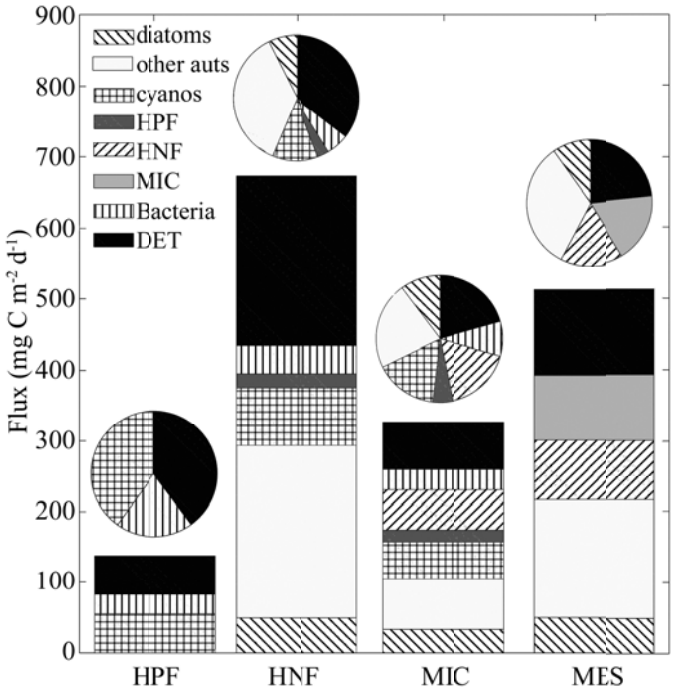

Figure 1.4 – Grazer Diets. Bars show the RW-solutions for the flux of carbon to each grazer from each of its prey groups. Pie charts show the composition of each grazer's diet for easier comparison.

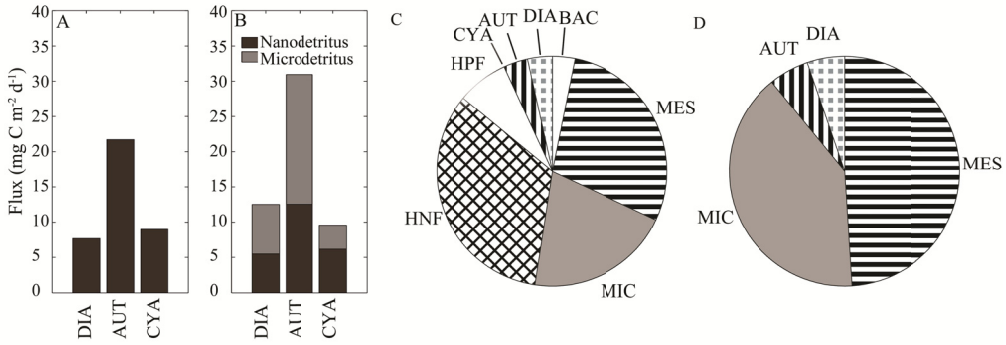

Figure 1.5 – Sources of particulate flux out of the euphotic zone. (A,B) show the amount of sinking carbon export supported indirectly by each of the three primary producers based on (A) the base ECO-model and (B) the SF-Det model. In (B) the carbon flux is broken into flux through nano- and microdetritus. (C,D) show direct contributions to sinking carbon export according to the (C) ECO- and (D) SF-Det models.

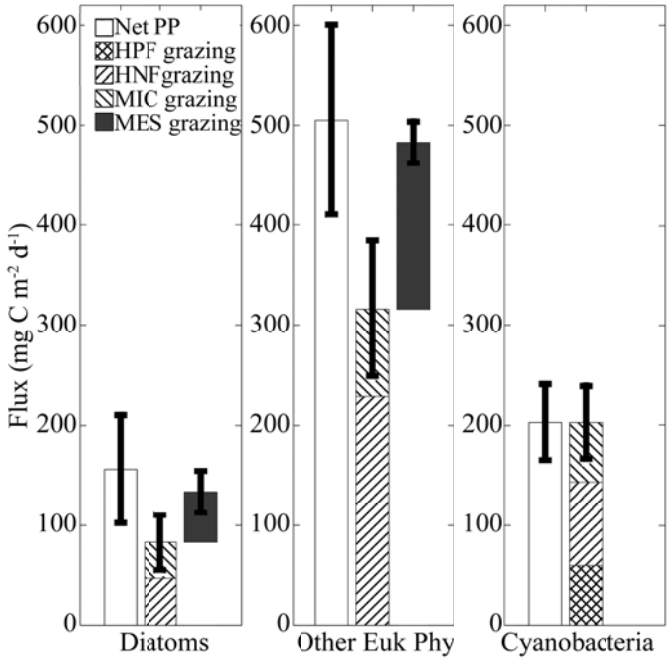

Figure 1.6 – Grazing Balance. Figure shows the balance between growth and grazing for diatoms, other eukaryotic phytoplankton, and cyanobacteria. Error bars for net primary productivity and protozoan grazing are the 95% confidence limits for the measured rates, while error bars for the mesozooplankton grazing were derived from the 95% confidence limits of the random-walk exploration of the solution space. Note the strong correlation between growth and community grazing for each phytoplankton group. Results are all from the base ECO-model, and were very similar to the equivalent results from the SF-Det model.

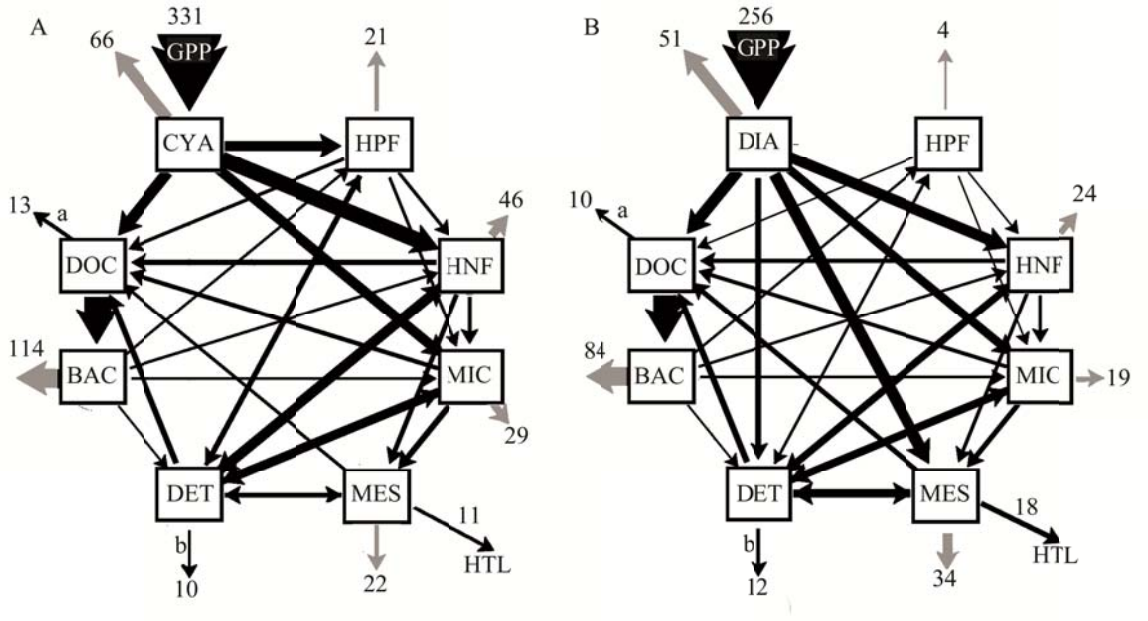

Figure 1.7 – Carbon fluxes supported by (A) cyanobacterial and (B) diatom production in the RW-solution to the SF-Det model. Widths are proportional to magnitude. Flows into (GPP) and out of (respiration (gray), flux to higher trophic levels (HTL), lateral advection of DOC (a), and vertical flux (b)) the model are given in units of mg C m^{-2} d^{-1}. For ease of visualization, all detrital size-classes are combined in the figure and only the net flow of DOC to bacteria is depicted. Note the similarity in the ecosystem structure supported by cyanobacteria and diatoms with most energy dissipated by respiration of the 'microbial loop' regardless of the primary carbon source. Fluxes were calculated using the indirect flow methods of Hannon (1973).

REFERENCES

ALLDREDGE, A. L., and C. C. GOTSCHALK. 1989. Direct observations of the mass flocculation of diatom blooms: characteristics, settling velocities and formation of diatom aggregates. Deep-Sea Res. **36:** 159-171.

ARMSTRONG, R. A., C. LEE, J. I. HEDGES, S. HONJO, and S. G. WAKEHAM. 2002. A new, mechanistic model for organic carbon fluxes in the ocean based on the quantitative association of POC with ballast minerals. Deep-Sea Res. II **49:** 219-236.

AZAM, F., T. FENCHEL, J. G. FIELD, J. S. GRAY, L. A. MEYER-REIL, and F. THINGSTAD. 1983. The ecological role of water-column microbes in the sea. Mar. Ecol. Prog. Ser. **10:** 257-263.

BALCH, W. M., A. J. POULTON, D. T. DRAPEAU, B. C. BOWLER, L. A. WINDECKER, and E. S. BOOTH. in press. Zonal and meridional patterns of phytoplankton biomass and carbon fixation in the equatorial Pacific Ocean, between 110°W and 140°W. Deep-Sea Res. II **57:** doi: 10.1016/j.dsr2.2010.08.004

BENDER, M., J. ORCHARDO, M. L. DICKSON, R. BARBER, and S. LINDLEY. 1999. In vitro O_2 fluxes compared with ^{14}C production and other rate terms during the JGOFS Equatorial Pacific experiment. Deep-Sea Res. I **46:** 637-654.

BROWN, S. L., M. R. LANDRY, R. T. BARBER, L. CAMPBELL, D. L. GARRISON, and M. M. GOWING. 1999. Picophytoplankton dynamics and production in the Arabian Sea during the 1995 Southwest Monsoon. Deep-Sea Res. II **46:** 1745-1768.

BROWN, S. L., M. R. LANDRY, K. E. SELPH, E. J. YANG, Y. M. RII, and R. R. BIDIGARE. 2008. Diatoms in the desert: Plankton community response to a mesoscale eddy in the subtropical North Pacific. Deep-Sea Res. II **55:** 1321-1333.

BUESSELER, K. O., J. A. ANDREWS, M. C. HARTMAN, R. BELASTOCK, and F. CHAI. 1995. Regional estimates of the export flux of particulate organic carbon derived from thorium-234 during the JGOFS EqPac Program. Deep-Sea Res. II **42:** 777-804.

CHRISTENSEN, V., and D. PAULY. 1992. ECOPATH II: a software for balancing steady-state ecosystem models and calculating network characteristics. Ecol. Model. **61:** 169-185.

DAM, H. G., X. S. ZHANG, M. BUTLER, and M. R. ROMAN. 1995. Mesozooplankton grazing and metabolism at the equator in the central Pacific: Implications for carbon and nitrogen fluxes. Deep-Sea Res. II **42:** 735-756.

DÉCIMA, M., M. R. LANDRY, and R. R. RYKACZEWSKI. in press. Broad-scale patterns in mesozooplankton biomass and grazing in the eastern equatorial Pacific. Deep-Sea Res. II **57**: doi: 10.1016/j.dsr2.2010.08.006

DICKSON, M. L., J. ORCHARDO, R. T. BARBER, J. MARRA, J. J. MCCARTHY, and R. N. SAMBROTTO. 2001. Production and respiration rates in the Arabian Sea during the 1995 Northeast and Southwest Monsoons. Deep-Sea Res. II **48:** 1199-1230.

DUCKLOW, H. W., H. L. QUINBY, and C. A. CARLSON. 1995. Bacterioplankton dynamics in the equatorial Pacific during the 1992 El-Niño. Deep-Sea Res. II **42:** 621-638.

DUGDALE, R. C., and F. P. WILKERSON. 1998. Silicate regulation of new production in the equatorial Pacific upwelling. Nature **391:** 270-273.

FROST, B. W., and N. C. FRANZEN. 1992. Grazing and iron limitation in the control of phytoplankton stock and nutrient concentration: A chemostat analog of the Pacific equatorial upwelling zone. Mar. Ecol. Prog. Ser. **83:** 291-303.

GARRISON, D. L., M. M. GOWING, M. P. HUGHES, L. CAMPBELL, D. A. CARON, M. R. DENNETT, A. SHALAPYONOK, R. J. OLSON, M. R. LANDRY, S. L. BROWN, H. B. LIU, F. AZAM, G. F. STEWARD, H. W. DUCKLOW, and D. C. SMITH. 2000. Microbial food web structure in the Arabian Sea: a US JGOFS study. Deep-Sea Res. II **47:** 1387-1422.

GORSKY, G., M. J. CHRETIENNOT-DINET, J. BLANCHOT, and I. PALAZZOLI. 1999. Picoplankton and nanoplankton aggregation by appendicularians: Fecal pellet contents of Megalocercus huxleyi in the equatorial Pacific. J. Geophys. Res. Oceans **104:** 3381-3390.

HANNON, B. 1973. Structure of ecosystems. J. Theor. Biol. **41:** 535-546.

HIROSE, M., T. KATANO, and S. I. NAKANO. 2008. Growth and grazing mortality rates of Prochlorococcus, Synechococcus and eukaryotic picophytoplankton in a bay of the Uwa Sea, Japan. J. Plankton Res. **30:** 241-250.

JACKSON, G. A. 2001. Effect of coagulation on a model planktonic food web. Deep-Sea Res. I **48:** 95-123.

JACKSON, G. A., N. NIQUIL, A. BURD, and T. L. RICHARDSON. 2001. Ecosystem Modeling Group Software, Inverse model code. Texas A&M Univ. http://oceanz.tamu.edu/~ecomodel/Software/invmodel/invmodel.html.

KIRCHMAN, D. L., J. H. RICH, and R. T. BARBER. 1995. Biomass and biomass production of heterotrophic bacteria along 140°W in the equatorial Pacific - effect of temperature on the microbial loop. Deep-Sea Res. II **42:** 603-619.

KONES, J. K., K. SOETAERT, D. VAN OEVELEN, and J. O. OWINO. 2009. Are network indices robust indicators of food web functioning? A Monte Carlo approach. Ecol. Model. **220:** 370-382.

LAMBORG, C. H., K. O. BUESSELER, J. VALDES, C. H. BERTRAND, R. BIDIGARE, S. MANGANINI, S. PIKE, D. STEINBERG, T. TRULL, and S. WILSON. 2008. The flux of bio- and lithogenic material associated with sinking particles in the mesopelagic "twilight zone" of the northwest and North Central Pacific Ocean. Deep-Sea Res. II **55:** 1540-1563.

LANDRY, M. R. 2009. Grazing processes and secondary production in the Arabian Sea: A simple food web synthesis with measurement constraints, p. 133-146. *In* J. D. Wiggert, R. R. Hood, S. W. A. Naqvi, K. H. Brink and S. L. Smith [eds.], Indian Ocean biogeochemical processes and ecological variability. AGU Monograph. American Geophysical Union.

LANDRY, M. R., H. AL-MUTAIRI, K. E. SELPH, S. CHRISTENSEN, and S. NUNNERY. 2001. Seasonal patterns of mesozooplankton abundance and biomass at Station ALOHA. Deep-Sea Res. II **48:** 2037-2061.

LANDRY, M. R., R. T. BARBER, R. R. BIDIGARE, F. CHAI, K. H. COALE, H. G. DAM, M. R. LEWIS, S. T. LINDLEY, J. J. MCCARTHY, M. R. ROMAN, D. K. STOECKER, P. G. VERITY, and J. R. WHITE. 1997. Iron and grazing constraints on primary production in the central equatorial Pacific: An EqPac synthesis. Limnol. Oceanogr. **42:** 405-418.

LANDRY, M. R., S. L. BROWN, J. NEVEUX, C. DUPOUY, J. BLANCHOT, S. CHRISTENSEN, and R. R. BIDIGARE. 2003. Phytoplankton growth and microzooplankton grazing in high-nutrient, low-chlorophyll waters of the equatorial Pacific: Community and taxon-specific rate assessments from pigment and flow cytometric analyses. J. Geophys. Res. Oceans **108:** 8142, doi: 8110.1029/2000jc000744

LANDRY, M. R., J. CONSTANTINOU, M. LATASA, S. L. BROWN, R. R. BIDIGARE, and M. E. ONDRUSEK. 2000. Biological response to iron fertilization in the eastern

equatorial Pacific (IronEx II). III. Dynamics of phytoplankton growth and microzooplankton grazing. Mar. Ecol. Prog. Ser. **201:** 57-72.

LANDRY, M. R., K. E. SELPH, A. G. TAYLOR, M. DÉCIMA, W. M. BALCH, and R. R. BIDIGARE. in press. Phytoplankton growth, grazing and production balances in the HNLC equatorial Pacific. Deep-Sea Res. II **57:** doi: 10.1016/j.dsr2.2010.08.011

LI, W. K. W., D. V. S. RAO, W. G. HARRISON, J. C. SMITH, J. J. CULLEN, B. IRWIN, and T. PLATT. 1983. Autotrophic picoplankton in the tropical ocean. Science **219:** 292-295.

LOCHTE, K., and C. M. TURLEY. 1988. Bacteria and cyanobacteria associated with phytodetritus in the deep sea. Nature **333:** 67-69.

LUNDSGAARD, C. 1995. Use of a high viscosity medium in studies of aggregates, p. 141-152. *In* S. Floderus, A.-S. Heisakanen, M. Oleson and P. Wassmann [eds.], Sediment trap studies in the Nordic countries 3. Proceedings of the Symposium on Seasonal Dynamics of Planktonic Ecosystem and Sedimentation in Coastal Nordic Waters.

MENDEN-DEUER, S., and E. J. LESSARD. 2000. Carbon to volume relationships for dinoflagellates, diatoms, and other protist plankton. Limnol. Oceanogr. **45:** 569-579.

NEWTON, J., and J. MURRAY. 1994. Comparison of sinking particulate material in the central equatorial Pacific measured during the EqPac US-JGOFS field year. EOS, Transactions, American Geophysical Union **75:** 82.

OLSEN, Y., S. AGUSTI, T. ANDERSEN, C. M. DUARTE, J. M. GASOL, I. GISMERVIK, A. S. HEISKANEN, E. HOELL, P. KUUPPO, R. LIGNELL, H. REINERTSEN, U. SOMMER, H. STIBOR, T. TAMMINEN, O. VADSTEIN, O. VAQUE, and M. VIDAL. 2006. A comparative study of responses in planktonic food web structure and function in contrasting European coastal waters exposed to experimental nutrient addition. Limnol. Oceanogr. **51:** 488-503.

PARKER, A. E., F. P. WILKERSON, R. C. DUGDALE, A. MARCHI, V. HOGUE, M. R. LANDRY, AND A. G. TAYLOR. in press. Spatial patterns of nitrogen uptake and phytoplankton in the equatorial upwelling zone (110°W - 140°W) during 2004 and 2005. Deep-Sea Res. II **57**: doi: 10.1016/j.dsr2.2010.08.013

PASSOW, U., A. L. ALLDREDGE, and B. E. LOGAN. 1994. The role of particulate carbohydrate exudates in the flocculation of diatom blooms. Deep-Sea Res. I **41:** 335-357.

PASSOW, U., R. F. SHIPE, A. MURRAY, D. K. PAK, M. A. BRZEZINSKI, and A. L. ALLDREDGE. 2001. The origin of transparent exopolymer particles (TEP) and their role in the sedimentation of particulate matter. Cont. Shelf Res. **21:** 327-346.

PFANNKUCHE, O., and K. LOCHTE. 1993. Open ocean pelago-benthic coupling: cyanobacteria as tracers of sedimenting salp feces. Deep-Sea Res. I **40:** 727-737.

RICHARDSON, T. L., and G. A. JACKSON. 2007. Small phytoplankton and carbon export from the surface ocean. Science **315:** 838-840.

RICHARDSON, T. L., G. A. JACKSON, H. W. DUCKLOW, and M. R. ROMAN. 2004. Carbon fluxes through food webs of the eastern equatorial Pacific: an inverse approach. Deep-Sea Res. I **51:** 1245-1274.

RICHARDSON, T. L., G. A. JACKSON, H. W. DUCKLOW, and M. R. ROMAN. 2006. Spatial and seasonal patterns of carbon cycling through planktonic food webs of the Arabian Sea determined by inverse analysis. Deep-Sea Res. II **53:** 555-575.

ROBISON, B. H., K. R. REISENBICHLER, and R. E. SHERLOCK. 2005. Giant larvacean houses: Rapid carbon transport to the deep sea floor. Science **308:** 1609-1611.

RODIER, M., and R. LE BORGNE. 1997. Export flux of particles at the equator in the western and central Pacific Ocean. Deep-Sea Res. II **44:** 2085-2113.

SELPH, K. E., M. R. LANDRY, A. G. TAYLOR, E. J. YANG, C. I. MEASURES, J. J. YANG, M. R. STUKEL, S. CHRISTENSON, and R. R. BIDIGARE. in press. Spatially-resolved taxon-specific phytoplankton production and grazing dynamics in relation to iron distributions in the equatorial Pacific between 110 and 140°W. Deep-Sea Res. II **57**: doi: 10.1016/j.dsr2.2010.08.014

SILVER, M. W., and M. M. GOWING. 1991. The "particle" flux: Origins and biological components. Prog. Oceanogr. **26:** 75-113.

TAKAHASHI, M., and P. K. BIENFANG. 1983. Size structure of phytoplankton biomass and photosynthesis in subtropical Hawaiian Waters. Mar. Biol. **76:** 203-211.

TAYLOR, A. G., M. R. LANDRY, K. E. SELPH, and E. J. YANG. in press. Biomass, size structure and depth distributions of the microbial community in the eastern equatorial Pacific. Deep-Sea Res. II **57**: doi: 10.1016/j.dsr2.2010.08.017

ULANOWICZ, R. E., and J. J. KAY. 1991. A package for the analysis of ecosystem flow networks. Environmental Software **6:** 131-142.

VERITY, P. G., T. M. BEATTY, and S. C. WILLIAMS. 1996*a*. Visualization and quantification of plankton and detritus using digital confocal microscopy. Aquat. Microb. Ecol. **10:** 55-67.

VERITY, P. G., D. K. STOECKER, M. E. SIERACKI, and J. R. NELSON. 1996*b*. Microzooplankton grazing of primary production at 140°W in the equatorial Pacific. Deep-Sea Res. II **43:** 1227-1255.

VÉZINA, A. F., and T. PLATT. 1988. Food web dynamics in the ocean .1. Best estimates of flow networks using inverse methods. Mar. Ecol. Prog. Ser. **42:** 269-287.

WAITE, A. M., K. A. SAFI, J. A. HALL, and S. D. NODDER. 2000. Mass sedimentation of picoplankton embedded in organic aggregates. Limnol. Oceanogr. **45:** 87-97.

WALSH, I. D., and W. D. GARDNER. 1992. A comparison of aggregate profiles with sediment trap fluxes. Deep-Sea Res. **39:** 1817-1834.

YOOL, A., A. P. MARTIN, C. FERNANDEZ, and D. R. CLARK. 2007. The significance of nitrification for oceanic new production. Nature **447:** 999-1002.

ZHANG, X., H. G. DAM, J. R. WHITE, and M. R. ROMAN. 1995. Latitudinal variations in mesozooplankton grazing and metabolism in the central tropical Pacific during the US JGOFS EqPac Study. Deep-Sea Res. II **42:** 695-714.

ZHANG, X. S., and H. G. DAM. 1997. Downward export of carbon by diel migrant mesozooplankton in the central equatorial Pacific. Deep-Sea Res. II **44:** 2191-2202.

CHAPTER 2

Trophic cycling and carbon export relationships in the California Current Ecosystem

By Michael R. Stukel, Michael R. Landry, Claudia R. Benitez-Nelson, and Ralf Goericke

Abstract

The vertical flux of carbon from the surface ocean is a critical component of the global carbon cycle that remains poorly understood in dynamic coastal regions. To better understand the relationships between export, plankton rate processes and plankton community variability in the California Current Ecosystem (CCE), we constructed a simple model of trophic cycling relationships and tested its predictions about export of mesozooplankton fecal material against export flux measurements by the ^{234}Th method. For modeled trophic processes, we used ^{14}C-primary production and chlorophyll-based rate estimates of phytoplankton growth, microzooplankton grazing, mesozooplankton grazing, and net phytoplankton growth of the phytoplankton from Lagrangian experiments conducted in May 2006 over a range of environmental conditions, from inshore coastal upwelling to offshore oligotrophic conditions. *E*-ratios (carbon export/^{14}C-primary production) predicted by the model ranged from 0.08 - 0.14, in good agreement with both the magnitude and the variability found in contemporaneous measurements of ^{234}Th export and C: ^{234}Th ratios of sinking particles. *E*-ratios were strongly decoupled from new production estimates, with the lowest measured and predicted *e*-ratios associated with richer water

parcels with net accumulating phytoplankton in the inshore region. For the range of conditions studied, variability in export efficiency was determined by the local net balance of growth and grazing and the relative strengths of grazing pathways to microzooplankton and mesozooplankton. Despite very different plankton assemblages studied, the good agreement between independently measured production-grazing processes and biogeochemical rates suggest that zooplankton are the major drivers of vertical carbon flux in this system during springtime. If that is generally the case, significant decadal-scale oscillations in large zooplankton, well documented for the region, may have substantial implications for carbon cycling and export.

Introduction

The vertical export of particulate carbon from the surface to the deep ocean is a critical component of the ocean's carbon cycle. While much is known about the general patterns of export and their relationships to ecosystem properties over large regions of the open ocean (e.g. Buesseler 1998), our understanding of fluxes and regulatory mechanisms in coastal regions is sparse by comparison. Because coastal regions typically have high rates of new and primary production on an areal basis, they likely play disproportionate roles in carbon cycling and export (Eppley and Peterson 1979). However, they are temporally and spatially complex and difficult to study. The biologically mediated mechanisms that drive export may also vary among and within coastal regions, from sinking phytodetritus (Green and Sambrotto 2006) to fecal pellet flux (e.g. Landry et al. 1994; Umani et al. 2002), with varying additional effects of the physiological state of phytoplankton, inorganic ballasting (Armstrong et al. 2002), and aggregation processes (Alldredge and Gotschalk 1989; Walsh and

Gardner 1992; Jackson 2001) involving both phytoplankton and bacteria (Passow et al. 1994; 2001). Studies are thus needed that link explicitly measured ecological rates to vertical carbon flux measurements across the range of conditions that define coastal ecosystems.

Because coastal regions can be strongly advective systems with uncoupled production and export processes, Lagrangian sampling schemes that allow simultaneous measurement of ecosystem processes, net community changes, and biogeochemical fluxes may be well suited to their study. Landry et al. (2009), for instance, used a Lagrangian strategy to investigate phytoplankton rate relationships across a spectrum of ecological conditions and biotic communities in the California Current Ecosystem (CCE), finding that measured depth-integrated growth and grazing rates explained >90% of the variability in the observed net growth rates of ambient phytoplankton over the duration of 3-5 day experiments. This good agreement between observed and predicted net changes based only on growth rate estimates and grazing losses to micro- and mesozooplankton suggested that direct sinking of phytoplankton out of the euphotic zone contributed surprisingly little, on average, to the temporal dynamics of phytoplankton. Here, we use data from four widely varying water parcels sampled in May 2006 of that study to ask the question in a different way -- are experimental measurements of growth and grazing rates sufficient to explain the magnitude and pattern of export flux in this coastal system, without consideration of direct cell sinking? To answer this question, we develop a simple trophic relationship model for computing carbon export estimates from experimental process rates, which we test against independent measurements of export flux based on the ^{234}Th method. The underlying hypothesis in this comparison is that variability in vertical carbon flux in the CCE can be largely explained by the fluxes along trophic pathways that lead to

fecal pellet production of metazooplankton. Alternatively, significant underprediction of export rates from the trophic model would be a strong indication that direct sinking of unconsumed phytoplankton, or other unmeasured processes, contribute substantially to the signal. Since direct cell sinking and grazing losses to micro- and mesozooplankton are each coupled to export with very different efficiencies, our results highlight the importance of including a mechanistic understanding of ecological process rates and interactions in biogeochemical flux models. They also illustrate the strongly advective and unbalanced nature of the CCE upwelling ecosystem, where contemporaneous export is significantly lower than the expected rate of new production.

Methods

Overview of Lagrangian design - The study area (Fig. 1) was principally along historical time-series sampling Line 80 of the CalCOFI Program (California Cooperative Oceanic Fisheries Investigations), extending from the physically dynamic coastal upwelling region off of Point Conception, California to nutrient-depleted offshore waters. For water parcels chosen to exploit the onshore-offshore range of ecosystem variability, a Lagrangian experimental approach was used to investigate relationships between measured rates of trophic interactions and vertical carbon flux. As described by Landry et al. (2009), individual experiments were initiated in homogenous surface water parcels, identified and surveyed with a combination of satellite imagery and underway surveys with a Moving Vessel Profiler system (MVP, M. D. Ohman, unpubl.). Water parcels were tagged with a drift array that included a 3x1 m holey-sock drogue centered at 15-m depth, a surface float equipped with Globalstar satellite communications, and a line below with attachments for in situ bottle incubations to assess growth, production and grazing rates of the phytoplankton

community. Sampling and experimental studies were conducted daily while tracking the water parcels for the duration of an experimental cycle (typically 4 days). This strategy provided estimates of the net observed changes in the ambient phytoplankton community concurrently with the experimentally determined rates of production and grazing processes, which we use below for trophic modeling. To estimate vertical carbon flux, we measured ^{234}Th deficiency and C: ^{234}Th ratios on either 35-75 μm or 20-75 μm particles at specific depth horizons within the same water parcels.

Four experimental cycles were conducted, including two inshore parcels of recent and aged upwelled water (inshore Cycles 1 and 2, respectively), one in the low-salinity core of the California Current proper, and one in offshore oligotrophic waters (Fig. 1). Initial surface chlorophyll *a* (Chl *a*) concentrations at these sites varied from 0.10 to 2.87 μg Chl *a* L^{-1}. Regions containing strong gradients were intentionally avoided when choosing experimental sites to minimize the possibility that the drogued drift array would cross a frontal feature if it slipped relative to the net mixed-layer currents. Surface-layer temperature and salinity characteristics of water parcels were assessed with MVP surveys to ensure coherency of water parcels over the duration of the experimental cycles.

Trophic cycling relationships - Our experiments provided rate estimates for phytoplankton growth and production, grazing processes and export flux over the range of conditions sampled in the marked water parcels. Since growth and grazing measurements explained >90% of the observed net rate of change in ambient phytoplankton chlorophyll (Landry et al. 2009), we formulate this net rate of change as the difference between biomass production and the combined grazing losses to micro- and mesozooplankton. We describe this relationship below in the format that is most commonly used in NPZ (nutrient-phytoplankton-zooplankton) models. In Eq. 1,

phytoplankton production is the product of biomass (P) and specific growth rate (μ_P, units of d^{-1}), and grazing losses are determined by the respective biomass-specific grazing rates (m_P and M_P, units of d^{-1} grazer biomass^{-1}) and biomasses (z and Z) of micro- and mesozooplankton.

$$\frac{dP}{dt} = \mu_P \times P - m_P \times z \times P - M_P \times Z \times P \qquad (1)$$

Accordingly, the combined terms $m_P z$ and $M_P Z$ in Equ. 1 are the instantaneous grazing rates of the micro- and mesozooplankton assemblages, respectively, feeding on phytoplankton.

We assume that microzooplankton standing stock grows with a gross growth efficiency (GGE_1) of 30% (Straile 1997) and is grazed upon by mesozooplankton at the biomass-specific rate of M_z. Thus:

$$\frac{dz}{dt} = GGE_1 \times m_P \times z \times P - M_z \times Z \times z \qquad (2)$$

Mesozooplankton likewise grow with a gross growth rate of GGE_2, yielding:

$$\frac{dZ}{dt} = GGE_2(M_P \times Z \times P + M_z \times Z \times z) \qquad (3)$$

As discussed further below, but consistent with the results of Landry et al. (2009), we assume that direct sinking of phytoplankton from the euphotic zone did not account for significant loss of biomass during our experiments. Potential export as fecal matter produced by the feeding of mesozooplankton (dF/dt) can therefore be estimated from the trophic relationships described above, assuming an egestion efficiency (EE) of 30% (Conover 1966):

$$\text{Export} = \frac{dF}{dt} = EE(M_P \times Z \times PP + M_z \times Z \times z) \qquad (4)$$

Assuming steady-state conditions of microzooplankton standing stock over the few days of each experimental cycle, Equ. 2 simplifies to:

$$GGE_1 \times m_P \times z \times P = M_z \times Z \times z \quad (5)$$

and equation 4 becomes:

$$Export = EE \times (M_P \times Z \times P + GGE_1 \times m_P \times z \times P) \quad (6)$$

Dividing the entire equation by the gross growth rate of the phytoplankton community ($\mu_P P$), allows us to rewrite the equation in terms of the *e*-ratio:

$$e\text{-ratio} = \frac{export}{\mu_P P} = EE \times \left(\frac{M_P Z}{\mu} + \frac{GGE_1 \times m_P z}{\mu}\right) \quad (7)$$

According to Eq. 7, the *e*-ratio therefore becomes a function of the egestion efficiency of mesozooplankton, the gross growth efficiency of the microzooplankton, and the ratios of micro- and mesozooplankton community grazing to phytoplankton specific growth rate. While canonical values of 0.30 are used for both efficiency terms, the model results are relatively insensitive to ±10% change in either of these parameters, due to the inherent variability in our repeated biological rate measurements.

Biological rate parameters – As presented in Landry et al. (2009), daily instantaneous rates (d^{-1}) of phytoplankton growth (μ_p in our model) and microzooplankton community grazing (m_{comm}, equivalent to $m_P z$ in our model) were determined by two-point dilution experiments conducted in 2.7-L bottle samples incubated at in situ temperature and light conditions on a line attached below our surface drifter. Eight sampling depths were chosen to span the euphotic zone with the deepest bottle pair at a depth corresponding to roughly the 0.4% light level, which

varied from 50 m inshore to 100 m offshore. The paired bottles represented whole (100%) seawater and 33% whole seawater, diluted with 0.1-µm filtered seawater. Water bottles were incubated for a 24-h period beginning and ending at ~04:00 PST each day. Rate assessments were based on initial and final 250-mL subsamples for chlorophyll *a* (Chl *a*). For consistency, all biological rates and standing stocks were vertically integrated to the depth of the deepest ^{14}C primary productivity (^{14}C-PP) incubation (35 to 40-m inshore and 70-m offshore).

Daily instantaneous rates of mesozooplankton community grazing on phytoplankton (M_{comm}, equivalent to M_PZ in our model) were determined from twice daily (mid-day and mid-night) net tows using 202-µm mesh, 0.71-m diameter bongo nets with attached flow meter towed to a maximum depth of 210 m (Landry et al. 2009 and M. D. Ohman, unpubl.). Daily community ingestion rates were calculated from the sum of the day-night means of Chl *a* and phaeopigment.

^{14}C-PP was measured from 4-L samples incubated in polycarbonate bottles at six depths (Fig. 2a) on the in situ array. Triplicate 250-mL subsamples were filtered through GF/F filters, which were then fumed with HCl to remove inorganic ^{14}C. After addition of scintillation cocktail, beta decays were detected with a Beckman-Coulter scintillation counter.

^{234}Th derived carbon export - ^{234}Th deficiencies were calculated using the 4-L method (Benitez-Nelson et al. 2001; Buesseler et al. 2001; Pike et al. 2005). Samples (4 L) were taken from 8 depths per cast of a Niskin rosette (typically to a depth of approximately twice the euphotic zone). HNO_3 was added to the samples to acidify to a pH of ~2, and the samples were immediately spiked with a known aliquot of ^{230}Th (1 mL at 10 dpm mL^{-1}) and allowed to sit for >4 h. NH_4OH was then added to adjust pH

to ~9, after which 100 µL each of 7.5 g L^{-1} $KMnO_4$ and 33 g L^{-1} $MnCl_2$ were added. Samples were shaken and let sit for >8 h to allow Th to co-precipitate with MnO_2. The precipitates were vacuum filtered onto a 25-mm quartz microfiber filter and allowed to air dry prior to mounting in a RISO cup. They were counted on land with a low-level RISO beta counter, followed >6 half-lives later by a second count to establish background beta emission levels. To calculate the yield of the Th-MnO_2 co-precipitation, all samples were dissolved in 8 M HNO_3/10% H_2O_2 solution and spiked with a gravimetrically measured aliquot of ^{229}Th (typically 1 g at 99.5 dpm g^{-1}). They were purified on a Poly-Prep chromatography column (Bio-Rad Laboratories) containing AG 1-X8 100-200 mesh chloride form resin (Bio-Rad Laboratories) and eluted with HCl. The HCl was subsequently evaporated off so that the residue could be reconstituted in a solution of 10% HNO_3/1% HF for Inductively Coupled Plasma Mass Spectrometric Analysis of the $^{229:230}$Th ratio at the WHOI Analytical Lab. Recoveries averaged 80 ± 8% (mean ± standard deviation). ^{234}Th deficiency was calculated as the difference between the measured activity and the expected activity if ^{234}Th was in equilibrium with ^{238}U, the latter being calculated from salinity as: ^{238}U (dpm L^{-1}) = 0.0686 • salinity • density (Chen et al. 1986). ^{234}Th export estimates for the three furthest offshore experimental cycles depicted in Fig. 1 were determined using a one-dimensional steady state model ($E = \lambda_{Th} (A_U - A_{Th})$) and trapezoidal vertical integration. While this steady-state approximation is an oversimplification of the complex cycling of particulate and dissolved thorium in the water column, it can provide a reasonable estimate of flux if ^{234}Th concentrations are near steady-state and upwelling terms are negligible. It is the only feasible method of estimating carbon export from water parcels when repeat occupations over long (>2-week) time periods

are not possible. The potential errors associated with this steady-state approximation are addressed in our discussion.

Samples for particulate C: ^{234}Th ratio were collected from beneath the euphotic zone, typically at 100 m (150 m for the furthest offshore cycle). A McLane WTS-LV large-volume in situ pump was used to filter 200 to 300-L of water through size-fractionated filters. We used a 75-µm pre-filter to screen out swimming mesozooplankton which could significantly alter the measured C: ^{234}Th ratio (Buesseler et al. 2006; Rodriguez Y Baena et al. 2006). Samples representative of sinking material were collected on 20- or 35-µm Nitex filters and then washed onto 25-mm quartz microfiber filters, which were dried and mounted on RISO cups for beta counting. Samples were beta counted as with the ^{234}Th deficiency samples, including background count following decay of ^{234}Th. The samples were then combusted for carbon and nitrogen contents using a Costech 4010 Elemental combustion analyzer (SIO Analytical Facility).

Results

Comparison of measured and net rates – From the Lagrangian experimental approach, we measured trophic process rates and carbon export in the CCE over conditions spanning a 30-fold range in sea-surface chlorophyll concentration. Despite widely differing characteristics of the plankton communities, some generalities emerged. Microzooplankton grazing was the primary loss term for phytoplankton for all experiments, accounting for 61 ± 15 to 92 ± 23% (mean ± standard error) of the measured total grazing impact. Phytoplankton growth rates typically exceeded microzooplankton grazing pressure near the surface, but decreased more rapidly with depth relative to grazing rates (Fig. 2). This led to excess grazing over growth at depth,

which was likely supported by phytoplankton from the upper layer that either sunk slowly or were mixed deeper. ^{14}C-PP estimates of production were similar to the growth-based estimates derived from the growth rates from dilution experiments and microscopically determined phytoplankton biomass. Both patterns exhibited high surface productivity nearshore with a distinct subsurface maximum in productivity in the furthest offshore region.

Despite the relative constancy of microzooplankton grazing as a phytoplankton loss term, the percentage of phytoplankton growth consumed by microzooplankton differed appreciably in the experimental water parcels, varying from only 41 ± 9% inshore to 119 ± 34% of phytoplankton μ offshore. This stark difference drives the overall pattern in the calculated instantaneous net rates of phytoplankton growth ($\mu_P - m_P z - M_P Z$), which varied from a net decrease of 0.04 ± 0.04 d^{-1} offshore to a net increase of 0.20 ± 0.07 d^{-1} inshore. Calculated net growth rates for the phytoplankton community were within the error of the net measured rates of change of chlorophyll in the euphotic zone calculated from daily CTD casts at the drifter locations (Fig. 3). The ability to predict reasonably well the in situ rate of change of the ambient community from process rate measurements is a common feature of all four cycles, supporting the view that direct sinking of phytoplankton was not a major loss term during the study. Otherwise, we would expect the observed rate of change to be significantly lower than that predicted solely from growth and grazing terms.

Offshore, oligotrophic water parcel (OOP)- Two of the water parcels studied are representative of the low productivity waters found offshore in the CCE. The furthest offshore experiment was initiated 350 km from the coast in water far beyond the low-salinity core of the California Current, with the marked parcel moving further seaward for the duration of our 4-d experimental cycle. The phytoplankton community was

comprised of relatively small cells (Taylor, A. G., pers. comm.), similar to those of the relatively stable offshore community commonly found throughout the oligotrophic subtropical Pacific (Venrick 1998,2002). ^{234}Th profiles taken on the first and final day of the cycle (Fig. 4a) show little difference (although the final profile was missing several samples that were lost during filtration). They thus support the assumption of a general steady state. The profiles exhibit a strong subsurface maximum in deficiency at the top of the strong deep chlorophyll maximum, which corresponds to the depth of a subsurface maximum of production measured by the ^{14}C-PP incubations. The particulate C: ^{234}Th sample (65 ± 9 µg C dpm^{-1}, mean ± measurement error) was collected on a 20-µm filter at a depth of 150 m to include flux out of the deep euphotic zone. Inspection of the ^{234}Th deficiency profile shows that remineralization probably began near 100 m. A comparison of the vertically integrated deficiencies between 100 and 150-m (47,400 and 40,500 dpm m^{-2}, respectively) suggests that as much as 15% of the ^{234}Th that sank out of the euphotic zone was remineralized before reaching the 150-m depth horizon, with likely a higher percentage of carbon remineralized, due to preferential carbon remineralization of many microorganisms (Buesseler et al. 2006). The ThE-ratio (ratio of ^{234}Th derived carbon export to primary productivity), calculated from carbon export across the 150-m depth horizon and ^{14}C-PP integrated over the euphotic zone, was 0.15 ± 0.08 (mean ± standard error is reported unless otherwise specified) for this water parcel.

The biological community for this experimental cycle was comprised of a small standing stock that exhibited relatively low mean growth rates for the euphotic zone, of only 0.13 ± 0.02 d^{-1}, and microzooplankton community grazing was an order of magnitude higher than that for mesozooplankton (Table 1). Grazing exceeded growth of the phytoplankton, and hence our predicted rate of change for the community was

slightly negative. As shown in Figure 3, the net predicted rate of change from experimental rate measurements closely matched the net observed change of chlorophyll concentration in the water column; the slight overestimate in the calculated net growth rate is likely attributable to our choice to only integrate growth and grazing to the depth of the primary productivity cast. Utilizing the measured community values for μ_p, m_{comm}, and M_{comm}, calculations from the trophic cycling model suggest an *e*-ratio of:

$$e\text{-ratio} = EE * \left(\frac{M_P Z}{\mu} + GGE * \frac{m_P z}{\mu}\right) = 0.14 \pm 0.03 \qquad (8)$$

which is similar to the observed ThE-ratio of 0.15 ± 0.08.

California Current Proper (CCP) water parcel - The other experiment that sampled a water parcel characterized by relatively small phytoplankton cells, low chlorophyll concentration and low primary productivity was initiated 170-km offshore and associated with the low-salinity core of the California Current, which transports water southward. Our initial parcel for this experiment drifted into a restricted area after 2 days; so the experiment was reinitiated for another 2 days by moving to a location substantially upstream of the first. These differences may explain the noisy replicate ^{234}Th deficiency profiles of Fig. 4b. The complex vertical structure of the CCP (e.g. Lynn and Simpson 1987) may also contribute to the depth variability of these ^{234}Th deficiency profiles. In the mixed layer where our drifter was drogued, for example, the profiles were not too different, while the deeper samples showed greater variability, perhaps reflecting different shears and lateral inputs at depth. Vertically integrated deficiency (integrated to 100 m = 36,200 ±11,100 dpm m^{-2}) and C: ^{234}Th ratio (100 m, 35-μm filter, 70 ± 8 μg C dpm^{-1}, mean ± measurement error) were very

similar to those found in the offshore oligotrophic region, but the higher rates of primary productivity led to a slightly lower ThE-ratio of 0.12 ± 0.04.

The phytoplankton community of the CCP was largely at steady state during the time of our sampling, with a net growth rate of -0.04 ± 0.05 d^{-1}. Chlorophyll concentrations were comparable to that of the oligotrophic offshore water, but specific growth rates were significantly higher and balanced by losses to grazing, dominated by microzooplankton but with mesozooplankton accounting for a substantial (>20%) portion. The net calculated rate of change of phytoplankton in the CCP parcels was again close to the observed net growth rate of the ambient community (0.01 ± 0.08). Our trophic cycling model also predicted an *e*-ratio of 0.13 ± 0.03, which was close to the measured ThE-ratio.

Inshore water parcels - The two water parcels studied inshore of the CCP were dominated by larger phytoplankton (Taylor, A. G., pers. comm.) and had higher chlorophyll concentrations characteristic of the coastal area impacted by seasonally variable upwelling (Venrick 1998,2002). The cold temperatures and high salinities of these parcels are indicative of recently upwelled water, and we believe they had similar origins near Point Conception. Our sampling for inshore Cycle 1 (IC1) began roughly 30 km from the coast, and the drifter tracked almost directly offshore (west) for 4 days with an average velocity of 11 km d^{-1}. Inshore Cycle 2 (IC2) began 15 days later 80 km from the coast and also drifted west at an even higher speed. The drifter was lost after providing 3 days of data (IC2a), but an additional day of rate measurements (IC2b) was added by initiating a new experiment at a location close to where the first drifter was lost. Additional evidence for similar histories of Inshore Cycles 1 and 2 can be seen in Fig. 5, which plots temperature-salinity values averaged over the euphotic zone for each water parcel. Both inshore cycles show similar

trajectories of warming and freshening as the water parcels advect offshore, and in fact, the continued evolution of IC1 would result in conditions similar to the start of IC2. While IC1 still retained significant concentrations of upwelled nitrate in the euphotic zone (initial surface concentrations >13 μM, decreasing with time), IC2 was depleted in nitrate at the surface (<1μM) with a strong nitracline near 40 m.

The simple steady-state model predicts a ^{234}Th export rate of 920 ± 170 dpm m^{-2} d^{-1} for IC1. However, the dynamic nature of this region led us to question the applicability of the steady-state assumption in this case. A full account of ^{234}Th for IC1 should involve both a non-steady state term and terms for horizontal and vertical advection and diffusion (Savoye et al. 2006):

$$\frac{\partial A_{Th}}{\partial t} = \lambda_{Th}(A_U - A_{Th}) - E + V \qquad (9)$$

whereas before A_U and A_{Th} are the activities of ^{238}U and ^{234}Th, respectively, λ_{Th} is the decay constant of ^{234}Th, E is the export of ^{234}Th on vertically sinking particles, and V is the sum of vertical and horizontal advective and diffusive water movements. While we can tentatively neglect horizontal advection due to our Lagrangian sampling strategy, we cannot reasonably neglect the non-steady state term since the recently upwelled water of IC1 had probably not reached a steady state with regard to ^{234}Th concentration. Since vertical upwelling may also reasonably have played a significant role in creating the measured deficiency, we chose not to assume a steady-state model of export for this cycle. Although synoptic wind conditions suggested that our cruise coincided with a period of relaxation of upwelling (Rykaczewski and Checkley 2008), assuming a typical upwelling rate of 1 m d^{-1} prior to our occupation of the cycle, combined with the vertical ^{234}Th gradient of 0.015 dpm L^{-1} m^{-1}, would add an additional 1500 dpm m^{-2} d^{-1} to the ^{234}Th:^{238}U deficiency export term of 920 ± 170 dpm

m^{-2} d^{-1}. Thus, the total export of ^{234}Th for this upwelling affected cycle may be over 150% higher than that derived from the steady-state assumption. However, a technical failure prevented us from measuring the C:^{234}Th ratio of exported particulates for this cycle; hence, we cannot reliably convert the ^{234}Th export measurement to its C export equivalent.

IC2 is a better fit to the assumptions required for steady state. Slightly decreasing density of the surface water, combined with the aforementioned synoptic wind measurements, suggest that upwelling was not significant. A comparison of the vertically integrated deficiencies for the final day of IC1 (37,900 dpm m^{-2}) and the first day of IC2 (37,500 dpm m^{-2}) suggest also that the inclusion of a non-steady state term would have negligible impact on the export calculation (see Discussion). Repeat profiles suggest that differences within IC2a were due to a deepening of the thermocline and nitracline from 38 to 42 m, perhaps driven by some combination of downwelling and/or internal waves and tides. Further support for a steady-state interpretation comes from the rapid switch from net deficiency to net remineralization at the base of the (~50 m) euphotic zone for IC2a. IC2b (a separate one-day experiment) was in a slightly different water mass that showed a higher deficiency (65,300 ± 20,000 versus 39,700 ± 2,200 dpm m^{-2} for IC2b and IC2a, respectively) and lower C:^{234}Th ratio (50 ± 5 versus 133 ± 16 μmolC dpm^{-1} and for IC2b and IC2a, respectively). We therefore use separate C: ^{234}Th ratios for the two segments of IC2 to calculate carbon export across the 100-m depth horizon.

Although IC1 had a significantly higher biomass than IC2, the biological community behaved similarly in both inshore cycles. For both cycles (including both sections of IC2), growth exceeded grazing, and the ambient phytoplankton grew at net rates similar to those predicted experimentally (Fig. 2, Table 1). Mesozooplankton

grazing was slightly higher during IC1 than IC2, contributing 39 ± 29% of grazing compared to 23 ± 25%. Our trophic relationships suggested an *e*-ratio of 0.08 ± 0.01 for IC2a compared to a ThE-ratio of 0.09 ± 0.01, and an *e*-ratio of 0.08 ± 0.03 compared to a ThE of 0.07 ± 0.03 for IC2b. For IC1, the trophic relationships predicted an *e*-ratio of 0.12 ± 0.02, but, as mentioned previously, the lack of a C:^{234}Th ratio did not allow us to calculate a corresponding ThE-ratio.

Discussion

Trophic cycling and carbon export – The suite of measurements from each experimental cycle in the present study allow us to assess the biological regulation of two biogeochemically relevant processes, autotrophic biomass accumulation and vertical carbon flux. By making process rate measurements while monitoring the temporal evolution of the phytoplankton community, Landry et al. (2009) demonstrated that phytoplankton growth and grazing losses determine to first order the observed net growth rates of the phytoplankton in the CCE. Fig. 3b clearly shows the strong correlation between the calculated and observed net rates of change. For all cycles, the two measurements fall within the margin of error. Although there is a slight (0.04 d^{-1} average) overestimate in the calculated rates of change relative to the observed rates, this discrepancy reflects, in part, our choice (for consistency) to integrate all rates to the depth of the deepest primary productivity sample incubations, as growth typically decreases more rapidly with depth than grazing.

Our simple trophic model builds on these previous findings to explain the variability of *e*-ratios (and hence vertical carbon flux) determined on the May 2006 cruise (Fig. 7). In fact, ^{234}Th steady-state estimates of export were in good agreement with those predicted from measured growth and grazing rates and the trophic model,

well within margins of error for all cycles for which carbon export could be assessed (Cycles 2-4). This agreement, despite major differences in the planktonic communities investigated, suggests that the underlying processes regulating export are relatively similar throughout the system. Net phytoplankton growth rate was highly variable and driven by the balance between growth and grazing processes dominated by microzooplankton. Export rates, however, were consistent in all cases with the sum of direct and indirect trophic linkages between phytoplankton and mesozooplankton.

It is important to note that the rates utilized for *e*-ratio calculations (specific growth rate, micro- and mesozooplankton grazing rates) were entirely distinct from the parameters used to calculate ThE-ratios (^{234}Th deficiency, C:^{234}Th ratio, ^{14}C-PP). Furthermore, the independent parameters in the calculations (egestion efficiency and gross growth efficiency) were not tuned to the data; canonical mean values of 0.30 were used for each. Thus, the ability to explain the general low magnitude and two-fold variability in ThE-ratio is a striking result suggesting that we may have reasonably represented the processes that regulate carbon export in this system. At worst, it indicates that the Th-derived export estimates are consistent with reasonable inferences about the plankton trophic interactions leading to fecal pellet production by mesozooplankton.

Export Measurements – All carbon export methods have limitations and sources of error. Surface-tethered sediment traps, for instance, collect sinking material for specific depths and time periods of deployment, but those measurements can be biased by complex flows around the collector mouth (Buesseler et al. 2007) that may be exacerbated in a dynamic region like the CCE. Additionally, sediment traps measure carbon flux not of the water column directly above their deployment, but rather from a

statistical funnel determined by the ratio of horizontal diffusivities and current velocities to vertical sinking rates of particulate material (Siegel et al. 1990).

Radionuclide disequilibrium methods (including ^{238}U-^{234}Th, ^{210}Pb-^{210}Po, and ^{90}Y-^{90}Sr) overcome this difficulty by explicitly approximating export from specific patches of water; however, they also have their own associated errors. Each method must approximate the ratio of C:radionuclide, a value with significant spatiotemporal and methodological variability (see Buesseler et al. 2006). Additionally, the impracticality of obtaining fully resolved deficiency profiles requires that assumptions be made about the relative importance of terms in the full accounting of radionuclide activities (see Equ. 9). These include vertical and horizontal water movements, advection as well as diffusion, although the latter parameter is typically neglected assuming that horizontal gradients and vertical diffusivity are both minimal. For our Lagrangian sampling plan, we also neglect horizontal processes. Vertical velocities can be a significant term in coastal regions when strong upwelling transports subsurface sufficiencies of ^{234}Th into the mixed layer. However, synoptic wind measurements suggest that upwelling was minimal during our cruise (Rykaczewski and Checkley 2008).

The assumption of temporal steady state is a major issue within our study region, particularly at inshore sites where high springtime productivity and biomass accumulation may lead to episodic export events. An ideal study would track a parcel of water for an extended period to measure the temporal evolution of water-column deficiency. However, truly effective tracking is methodologically difficult at best and more likely impossible in regions with vertical shear and horizontal heterogeneity. Thus, tradeoffs must be made between errors associated with inaccurate assessment of changing deficiencies and with slip relative to an in situ water parcel. Savoye et al. (2006) evaluated the uncertainty associated with the non-steady state (NSS)

approximation and suggested that water parcels be revisited after a period of >1-2 weeks, as shorter duration studies will have high uncertainties. Tracking a water parcel unambiguously in a heterogeneous a region like the CCE for weeks would be very difficult.

Figure 5 is a starting point for addressing the role that a non-steady state term might play in the inshore region since IC2a seems to have sampled similar water to IC1 that had aged as it moved offshore. From the mean deficiencies for IC1 and IC2a (31,800 ± 6000 and 39,700 ± 2200 dpm m^{-2}, respectively) and the time difference between the ^{234}Th measurements (12.7 days), we can calculate a NSS export of 1790 ± 488 dpm m^{-2} d^{-1} (mean ± S.E.) for the period between the two cycles. By this calculation, the steady-state export estimate of 1140 ± 70 dpm m^{-2} d^{-1} for IC2a may be low by ~36%, although 95% confidence intervals for the two determinations are not statistically different. The origins of the two water parcels may also not have been identical, accounting for some of their deficiency difference. Nonetheless, this comparison helps to put some constraints on the magnitude of the errors associated with the steady-state assumption.

Timescales - When the ThE-ratio is used to compute the fraction of phytoplankton production exported to depth, it is important to consider the relevant timescales of the measurements involved. ^{234}Th disequilibrium averages export over the mean lifetime of ^{234}Th (35 days). ^{234}Th-derived export values and C:^{234}Th ratio at depth should therefore not change substantially over a few days. ^{14}C-PP, meanwhile, considers phytoplankton production only over the duration of the incubation (usually 24 h). Thus, for a water parcel with high daily variability in primary productivity about a central mean, the ThE-ratio (^{234}Th derived carbon export / ^{14}C-PP) measured over

several days might well show a spurious inverse correlation of primary productivity with ThE-ratio, driven by variability of the ^{14}C-PP denominator.

With the Lagrangian experimental design, we were able to average several days of daily euphotic-zone integrated rate measurements for primary productivity, phytoplankton growth and grazing in each water parcel, thereby minimizing spurious results that might have arisen from process experiments conducted with more typical fixed-station sampling and allowing for measurements on the timescale of our experimental cycles (~4 days). Mesozooplankton grazing, however, is a rate with two intrinsic time-scales. While grazer-specific grazing rate can vary rapidly due to changes in both behavior (e.g. diel vertical migration or selective grazing) and prey field, mesozooplankton biomass itself has a longer time-scale on the order of weeks. The longer generation times of mesozooplankton may thus serve to dampen changes in export on short time periods (days to weeks) when fecal carbon flux dominates over direct sinking of phytoplankton.

For the four water parcels for which we have carbon export measurements (OOP, CCP, IC2a and IC2b), ThE-ratios are inversely correlated with net rates of change of the phytoplankton community (Table 1). In the OOP cycle, phytoplankton biomass declined over the 4-day cycle, and we measured a relatively high ThE-ratio. Conversely, in the inshore region of accumulating phytoplankton biomass, the ThE-ratio was lower. Over longer time periods than the experimental cycles, we would expect phytoplankton to reach a quasi-steady state, with growth balanced by grazing and other loss processes. Mechanistically, we could hypothesize that zooplankton grazing had temporarily outpaced phytoplankton growth in the offshore region and hence was reducing community biomass and primary production. Reduced food resources for microzooplankton grazers and perhaps mesozooplankton switching

predation pressure from phytoplankton to microzooplankton would presumably resolve this imbalance in time, allowing phytoplankton to increase. Nutrient decline and increasing grazing capacity would serve similarly as negative feedbacks to bring the accumulating phytoplankton biomass of the inshore area back into balance. These patterns are suggestive of a system in which contemporaneous imbalances of growth and grazing lead to autotrophic biomass accumulation (rather than sinking) or net heterotrophy on short timescales, while export measurements and the drivers of export reflect longer (weekly) timescales. Thus, temporal decoupling of the fast phytoplankton dynamics and the slower timescales of mesozooplankton population change implies that utilizing a constant *e*-ratio to estimate export capacity from primary production alone will have limited efficacy. Instead, rate measurements that explicitly partition this primary productivity into different utilization pathways may be necessary.

Microzooplankton shunt - Traditional formulations of the microbial loop (Azam et al. 1983) assume multiple trophic transfers within the microzooplankton, which greatly diminish transfer to mesozooplankton. The microbial food web is therefore considered to function largely as a remineralization pathway. Meanwhile, the prevalence of mesozooplankton fecal pellets and aggregates of larger cells, like diatoms, in sediment traps has led to an emphasis on the classical food chain in vertical carbon flux (Michaels and Silver 1988; Fasham et al. 2001). Contrary to this simple dichotomy, our rate relationships for the CCE suggest that microzooplankton can provide an important shunt of production from phytoplankton to mesozooplankton, with a single trophic step on average. To allow for additional trophic transfers within the microzooplankton, we need only add an exponent *n* to the microzooplankton GGE.

$$e\text{-ratio} = EE * \left(\frac{M}{\mu} + GGE^{n} * \frac{m}{\mu}\right) \quad (10)$$

Functionally, *n* represents the mean number of microzooplankton trophic steps that separate phytoplankton from mesozooplankton. The need to vary this parameter would obviously be greater in biological communities dominated by very small phytoplankton and with high grazing impact of microzooplankton, as is generally the case in the open ocean (Calbet and Landry 2004). Nonetheless, a meta-analysis of dilution experiments has shown that the percentage of primary productivity consumed on average by microzooplankton in coastal regions (60%) is not greatly different from the 70% consumed in oceanic systems (Landry and Calbet 2004). Although our coastal-offshore differences in microzooplankton grazing (42-44% vs 77-123%, respectively) were more extreme than the global averages, there was adequate food chain transfer for the OOP to support a moderate rate of export via the mesozooplankton, in fact the highest export ratio that we measured. Thus, the efficiency of transfer from micro- to mesozooplankton becomes an important determinant of the amount of primary productivity that can be exported. If we assume only a single trophic step within the microzooplankton in our experiments, then the relative proportion of mesozooplankton nutrition derived from microzooplankton ranges from 32 to 79% for our four cycles, which agrees well with the C:phaeopigment measurements of Small and Ellis (1992). Our relationships thus suggest that far from being strictly a remineralization pathway, the microzooplankton in the CCE shunt a significant amount of carbon into the export pathway.

Decoupling of new and export production - With typical *f*-ratios ranging from 0.2 to 0.8 in the Southern California Bight (Eppley et al. 1979), new production generally exceeds export production inshore of the CCP (e.g. Nelson et al. 1987). An estimate of the *f*-ratio can be gleaned from our relationships if we assume that the rate of uptake of recycled nitrogen is equal to its rate of production, which follows from the

preferential utilization of NH_4^+ over NO_3^- by phytoplankton. If we assume that phytoplankton do not exude nutrients, the rate of production of autochthonous material is simply the difference between the gross phytoplankton growth rate ($\mu_P P$) and the rate of export and biomass accumulation. Thus:

$$\text{Recycled Production} = \mu_p P - \frac{dF}{dt} - \frac{dP}{dt} - \frac{dZ}{dt} \qquad (11)$$

Since new production is the difference between total and recycled production, we can divide by total production ($\mu_P P$) to calculate an *f*-ratio:

$$f\text{-ratio} = \frac{\text{new}}{\text{total}} = \text{e-ratio} + \frac{dP/dt}{\mu_P P} + \frac{dZ/dt}{\mu_P P} \qquad (12)$$

By substituting in Equations (1), (3) and (7) and rearranging, we can see that the *f*-ratio is dependent on the rates of phytoplankton growth and micro- and mesozooplankton community grazing:

$$f\text{-ratio} = \frac{\mu_P - m_P z - M_P Z}{\mu_P} + \frac{(EE + GGE_2)(M_P Z + GGE_1 \times m_P z)}{\mu_P} \qquad (13)$$

However, this formulation is valid only if autochthonous production (Eq. 11) is less than total production, which may not be true if the phytoplankton community is declining (as for our offshore cycle). In addition, this calculated *f*-ratio neglects nitrogen excretion by phytoplankton, which would decrease the ratio by a factor of 1/(1+*%NPP excreted*). Given the uncertainties in our biological rate measurements, a relatively large excretion rate of 30% would still produce an *f*-ratio estimate within one standard error of the results of Eq. 13.

The above model calculations can be compared to regression estimates of new production by Harrison et al. (1987) that show a linear relationship (slope = 0.77 ± 0.10; intercept = 0.06 ± 0.02) between new production and the nutrient ratio of $[NO_3^-]$ to combined $[NO_3^-] + [NH_4^+]$ in the CCE based on measurements from Eppley et al.

(1979). *f*-ratios were calculated at each of our ^{14}C-PP sampling depths and then vertically integrated to calculate new production and hence the average *f*-ratio of the euphotic zone. This approach produces results in close agreement with our trophic calculations (Table 2), both predicting *f*-ratios of 0.6 to 0.8 for the nearshore cycles and ~0.3 for the CCP. For the OOP cycle, the assumption that autochthonous nutrient uptake matched production was violated, resulting in a negative ratio. Nevertheless, both calculations clearly predict significantly higher *f*-ratios in the inshore region, in contrast to the low measured and modeled *e*-ratios in this region.

Olivieri and Chavez (2000) and Plattner et al. (2005) have hypothesized that offshore transport of water upwelled near the California coast leads to a spatiotemporal decoupling of new and export production. The obvious disparity between our *e*- and *f*-ratios supports this view, and our Lagrangian sampling provides a unique perspective on the underlying processes. All of our inshore water parcels drifted rapidly offshore (net speeds of 13, 20 and 18 cm s^{-1} for IC1, IC2a and IC2b, respectively) as we measured net positive growth rates for the phytoplankton. In addition, we observed that particulate organic carbon and chlorophyll accumulated during offshore transport of each inshore cycle, with average rates of chlorophyll increase of 0.10, 0.14 and 0.28 d^{-1} for IC1, IC2a and IC2b, respectively.

The calculated excess of new production to export in the offshore region may be due to several factors. Carbon export could have been temporally decoupled from new production, with net production during spring conditions. Active transport of organic matter from the surface to depth by vertically migrating animals may also have been a relatively important component of export in these waters (e.g. Steinberg et al. 2000). Additionally, synoptic wind conditions (Rykaczewski and Checkley 2008) as well as the net changes in temperature and salinity observed along our drifter tracks were

consistent with the possibility of slow subduction of surface water as it moved offshore. However, we scrupulously avoided areas with strong gradients when we initiated our experiments and therefore avoided major subduction fronts that can occur where the offshore advection of cold saline upwelled water reaches the lower salinity CCP (Kadko et al. 1991; Washburn et al. 1991).

Changing zooplankton concentrations: implications - The discrepancies between our estimates of *e*- and *f*-ratios based on trophic interactions suggest that particulate flux of sinking phytoplankton and/or subduction may be important export processes in the CCE at some times and places. Nonetheless, on the daily timescales at which parcels of water generally move in the system, our relationships suggest that vertical flux can be reasonably explained by contemporaneous food-web processes leading to mesozooplankton consumption and fecal pellet production. The central role of zooplankton as flux mediators in these model calculations suggests a potential coupling between climate-associated community changes and carbon export in the CCE. The secular warming trend evident in CalCOFI data (Roemmich 1992) has been linked, for example, to a 70% decline in the biovolume of large zooplankton (Roemmich and Mcgowan 1995b,a), notably a decrease in salps (Lavaniegos and Ohman 2007). Because of their high filtration rates and dense, rapidly sinking fecal pellets, such organisms contribute disproportionately to the flux of organic matter to the deep sea (Bruland and Silver 1981; Silver and Bruland 1981; Pfannkuche and Lochte 1993). This decadal decline in mesozooplankton therefore suggests a substantial decrease in the efficiency of coupling of primary productivity to export in the CCE region.

In summary, we found that calculations based on simple trophic relationships and experimental process rate measurements in the CCE were consistent with measured

variations in the *e*-ratios of water parcels representing a range of conditions from recently upwelled coastal water to oligotrophic offshore regions. The good agreement between independently measured ecological and biogeochemical rates in these very different plankton assemblages suggest that zooplankton dynamics are an important, though often neglected, primary driver of vertical carbon flux in this system. For the range of conditions studied, variability in export efficiency was determined by the local net balance of growth and grazing processes and the relative strengths of grazing pathways through microzooplankton versus directly to mesozooplankton. This study was limited however to a few water parcels believed to be representative of the region during springtime. Therefore, further work is necessary to assess biological controls of carbon export under different seasonal conditions as well as to quantify and compare results to purely physical mechanisms of export, such as along subduction fronts. In this regard, the Lagrangian design that we used to obtain the rate measurements for this study appears to be a workable approach for constraining ecological and biogeochemical relationships in complex coastal regions, with the eventual goal of extending these relationships into mechanistic models with predictive power.

Acknowledgments

We thank the captain and crew of the R/V *Knorr* for their professionalism and contributions to conducting these experiments at sea. We are grateful to all of our colleagues in the California Current Ecosystem, Long-Term Ecological Research (CCE LTER) program for their support and collaboration, and particularly to M. D. Ohman for providing the mesozooplankton grazing results. We give special thanks to

M. Décima, S. Dovel, M. Roadman, R. Rykaczewski, J. Powell, D. Taniguchi, and K. Tsyrklevich for their assistance at sea and in laboratory analyses, and to M.D. Ohman and P.J.S. Franks for insightful discussions and suggestions on earlier versions of the paper. This work was supported by National Science Foundation (NSF) funding (OCE-04-17616) for the CCE LTER site, and by graduate research fellowships (NSF and NASA Earth and Space Science) to M. Stukel.

Chapter 2, in full, has been submitted for publication in Limnology and Oceanography: Stukel, M. R., Landry, M.R., 2010, Benitez-Nelson, C. R., Goericke, R. "Trophic Cycling and carbon export relationships in the California Current Ecosystem." The dissertation author was the primary investigator and author of this paper.

Table 2.1. Vertically integrated values. "μ" is the specific growth rate of the phytoplankton (d^{-1}). "m_{comm}" is the specific grazing rate of the microzooplankton (d^{-1}). "M_{comm}" is the specific grazing rate of the mesozooplankton (d^{-1}). "μ-m-M" is the calculated net growth rate of the phytoplankton (d^{-1}). "Net obs" is the observed net growth rate of the ambient phytoplankton community (d^{-1}). "PP" is ^{14}C-derived primary productivity (mg C m^{-2} d^{-1}). "^{234}Th Export" is the vertical flux of ^{234}Th across the 100-m (150-m for the offshore cycle) depth horizon (dpm m^{-2} d^{-1}) as calculated with a one-dimensional steady state model. "C:Th" is the carbon:^{234}Th ratio collected from beneath the euphotic zone (μg C dpm^{-1}) with a large volume (200-300 L) in situ pump. "Export" is carbon export calculated with a one-dimensional steady state model (mg C m^{-2} d^{-1}). "ThE" is the ratio of export to primary productivity. "Trophic e" is the *e*-ratio determined from our trophic relationships. All biological variables were integrated to the depth of the deepest primary productivity incubation (except mesozooplankton grazing, which was an average over the upper 200-m) and averaged over the length of the cycle, while ^{234}Th variables were integrated down to 100 m (150 m for the offshore cycle) and averaged over the cycle duration. Values are mean ± standard error of the repeat measurements for all measurements except C:Th ratio, which reports mean ± error associated with carbon and ^{234}Th measurements.

Cycle	μ	m_{comm}	M_{comm}	$\mu - m - M$	Net Obs	PP	^{234}Th Export	C:Th	C Export	Th-E	Trophic e
Offshore	0.13±0.02	0.16±0.04	0.013±0.002	-0.04±0.04	-0.12±0.15	520±100	1170±560	65±9	76±38	0.15±0.08	0.14±0.03
Cal Current	0.26±005	0.20±0.06	0.050±0.015	0.01±0.08	-0.04±0.05	610±10	1040±320	70±8	72±23	0.12±0.04	0.13±0.03
Inshore 1	0.33±0.02	0.14±0.03	0.088±0.024	0.11±0.04	0.10±0.11	4940±830	920±170				0.12±0.02
Inshore 2a	0.48±0.08	0.21±0.05	0.066±0.006	0.20±0.09	0.14±0.09	1760±160	1140±60	133±16	151±15	0.09±0.01	0.08±0.01
Inshore 2b	0.54±0.14	0.24±0.11	0.064±0.023	0.23±0.18	0.28±0.53	1420±330	1880±560	50±5	94±30	0.07±0.03	0.08±0.03

Table 2.2. Calculated, vertically integrated estimates of *f*-ratios. $f_{Harrison}$ uses ambient NO_3 and NH_4 concentrations, ^{14}C-PP, and the *f*-ratio relationship developed by Harrison et al. (1987): *f*-ratio = m * (NO_3 / (NO_3+NH_4)) + b, with m = 0.77 ± 0.10, b = 0.06 ± 0.02 (representative of the Southern California Bight). $f_{trophic}$ is calculated from our trophic relationships and is not applicable for the offshore cycle as the relationships predict that production of autochthonous nitrogen exceeds total nitrogen assimilation. For $f_{Harrison}$, errors include standard error of repeat measurements as well as the error in their measurement parameters. Error on $f_{trophic}$ is propagation of standard errors from repeat measurements.

	$f_{Harrison}$	$f_{trophic}$
Offshore	0.34 ± 0.13	NA
Cal. Current	0.31 ± 0.08	0.30 ± 0.31
Inshore 1	0.79 ± 0.27	0.56 ± 0.13
Inshore 2	0.57 ± 0.11	0.58 ± 0.10

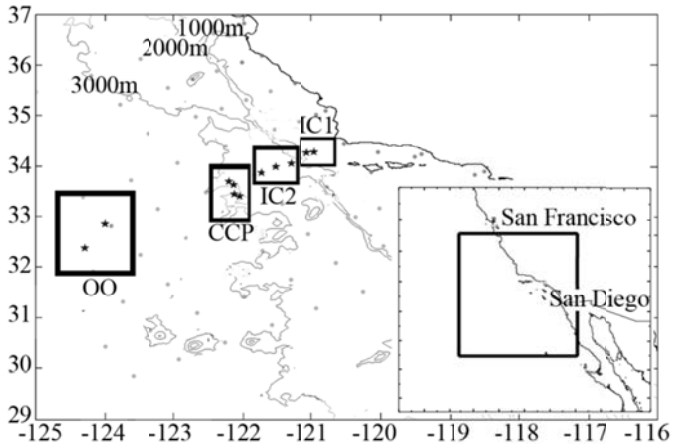

Figure 2.1 - Map of the study region. The stars show the locations of all ^{234}Th profiles, while the rectangles represent the four locations at which experimental cycles were conducted. Light gray dots show standard CalCOFI sampling stations in the area. Contour lines for seafloor depths of 1000, 2000 and 3000 m are in gray. Inset at bottom right shows the study area (black rectangle) within the context of the southwestern coast of North America.

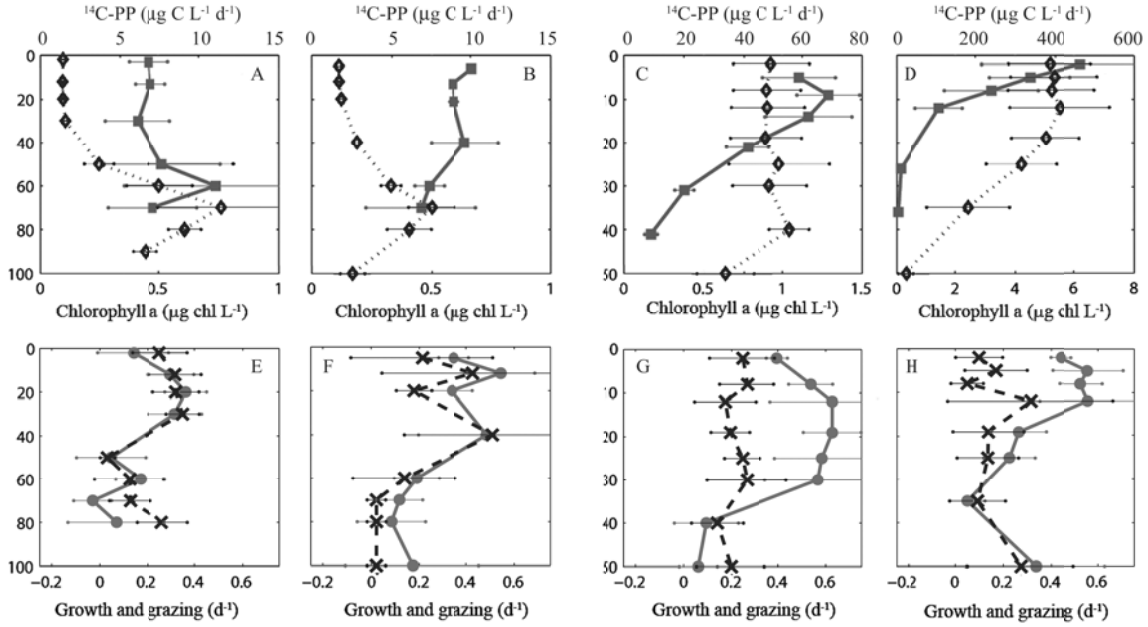

Figure 2.2 - Vertical profiles of chlorophyll, primary productivity, phytoplankton growth rate, and microzooplankton grazing rate. Plots A/E, B/F, C/G, and D/H are for cycles Oligotrophic Offshore, California Current Proper, Inshore 2, and Inshore 1, respectively. In plots A, B, C and D, squares and solid gray lines depict ^{14}C-PP and diamonds with dotted lines are extracted Chl *a* concentrations. In plots E, F, G and H, circles and gray line are phytoplankton specific growth rates from dilution experiments while x's and dashed lines are microzooplankton grazing rates. Error bars are +/- one standard deviation of the repeat measurements taken over the course of the cycle.

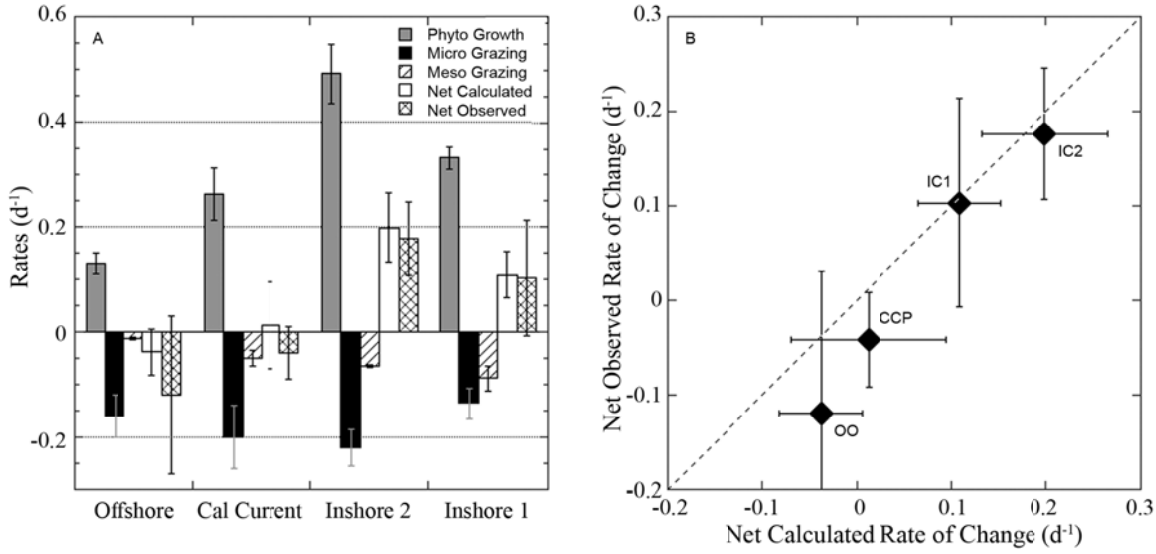

Figure 2.3 - Vertically integrated cycle averages. Panel a – growth and grazing rates. Phytoplankton (Phyto) growth is the instantaneous growth rate as determined from Chl *a* analyses of our dilution treatments. Microzooplankton (Micro) grazing is determined from the dilution experiments. Mesozooplankton (Meso) grazing rates were measured from gut pigment measurements taken on oblique net tows. Net calculated growth rate is the difference between growth and grazing and matches well with the rates of change of chlorophyll measured over the course of each cycle as the water parcels evolved. Rates were vertically integrated to the depth of the deepest ^{14}C-PP incubation. The standard error of each measurement is shown. Panel b – Calculated and observed rate of change of the phytoplankton community. OO, CCP, IC1, IC2 are the Offshore Oligotrophic, California Current Proper, Inshore 1, and Inshore 2 cycles, respectively.

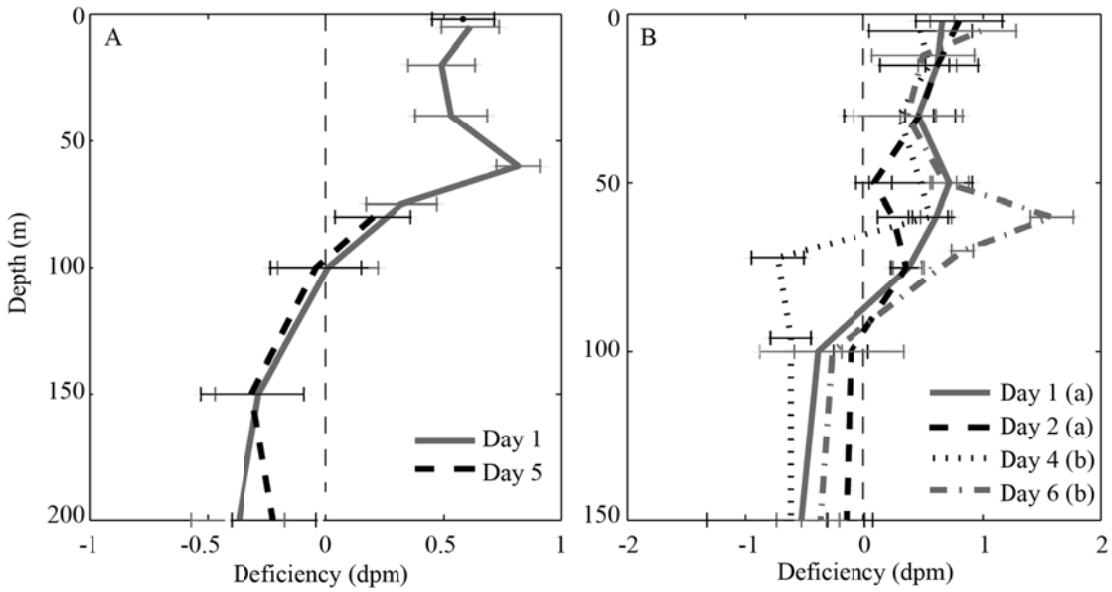

Figure 2.4 - ^{234}Th deficiency in Oligotrophic Offshore (panel A) and California Current Proper (panel B) water parcels. Error bars were determined by propagating errors from volume measurements, counting statistics, and the errors in yield calibrations. When yield analyses were not possible (because samples were lost during column chromatography), yield was assumed to be the average yield (80%) of each individual measurement with a larger error derived from the standard deviation of the yield measurements.

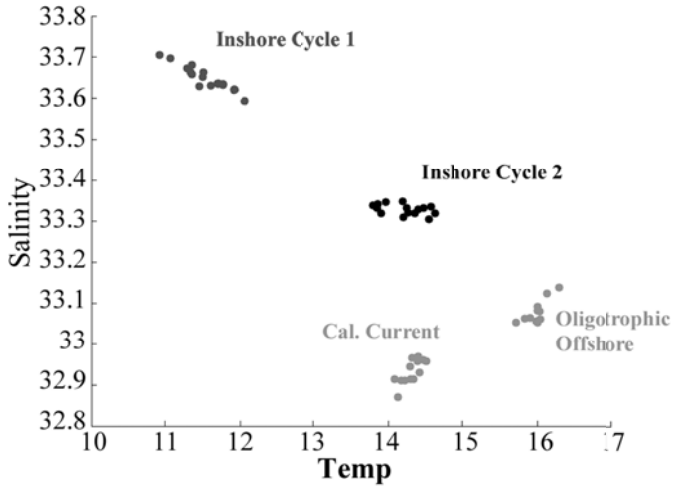

Figure 2.5 - Vertically averaged temperature and salinity for the upper 50 m of all CTD profiles of the four water parcels. Both Inshore Cycle 1 & 2 became warmer and less saline over the time period of our cycles.

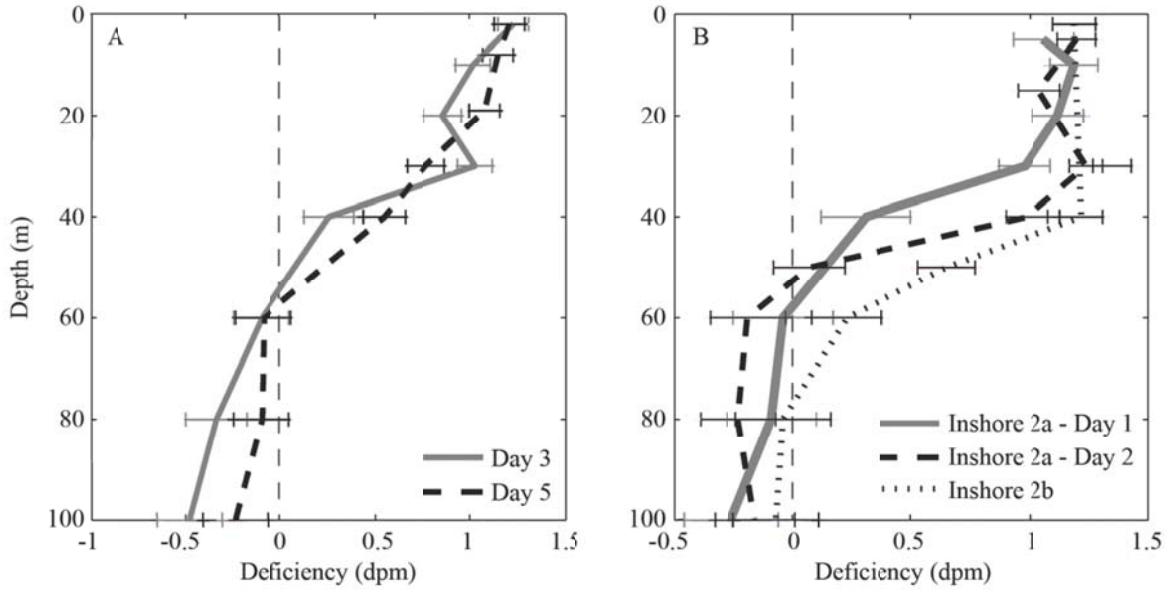

Figure 2.6 - ^{234}Th deficiency in inshore water parcels. A – Inshore Cycle 1, B – Inshore Cycles 2a & 2b. Error bands were determined by propagating errors from volume measurements, counting statistics, and the errors in yield calibrations. When yield analyses were not possible yield was assumed to be the average yield of each individual measurement with a larger error derived from the standard deviation of the yield measurements.

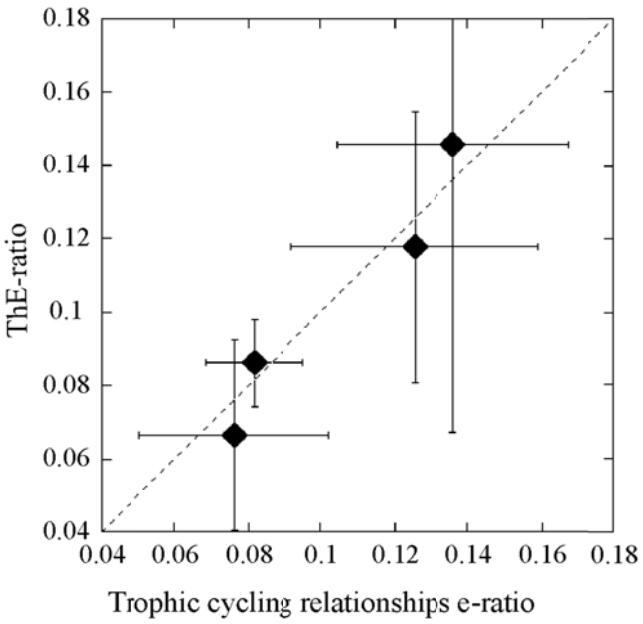

Figure 2.7 - Comparison of trophic cycling relationships to ^{234}Th deficiency steady-state model. OO, CCP, IC2a, IC2b are the Offshore Oligotrophic, California Current Proper, Inshore 2a, and Inshore 2b cycles, respectively.

References

ALLDREDGE, A. L., and C. C. GOTSCHALK. 1989. Direct observations of the mass flocculation of diatom blooms: characteristics, settling velocities and formation of diatom aggregates. Deep-Sea Res. **36:** 159-171.

ARMSTRONG, R. A., C. LEE, J. I. HEDGES, S. HONJO, and S. G. WAKEHAM. 2002. A new, mechanistic model for organic carbon fluxes in the ocean based on the quantitative association of POC with ballast minerals. Deep-Sea Res. II **49:** 219-236.

AZAM, F., T. FENCHEL, J. G. FIELD, J. S. GRAY, L. A. MEYER-REIL, and F. THINGSTAD. 1983. The ecological role of water-column microbes in the sea. Mar. Ecol. Prog. Ser. **10:** 257-263.

BENITEZ-NELSON, C. R., K. O. BUESSELER, M. R. VAN DER LOEFF, J. ANDREWS, L. BALL, G. CROSSIN, and M. A. CHARETTE. 2001. Testing a new small-volume technique for determining Th-234 in seawater. J. Radioanal. Nucl. Chem. **248:** 795-799.

BRULAND, K. W., and M. W. SILVER. 1981. Sinking rates of fecal pellets from gelatinous zooplankton (salps, pteropods, doliolids). Mar. Biol. **63:** 295-300.

BUESSELER, K. O. 1998. The decoupling of production and particulate export in the surface ocean. Glob. Biogeochem. Cycle **12:** 297-310.

BUESSELER, K. O., A. N. ANTIA, M. CHEN, S. W. FOWLER, W. D. GARDNER, O. GUSTAFSSON, K. HARADA, A. F. MICHAELS, M. R. VAN DER LOEFF'O, M. SARIN, D. K. STEINBERG, and T. TRULL. 2007. An assessment of the use of sediment traps for estimating upper ocean particle fluxes. J. Mar. Res. **65:** 345-416.

BUESSELER, K. O., C. BENITEZ-NELSON, M. R. VAN DER LOEFF, J. ANDREWS, L. BALL, G. CROSSIN, and M. A. CHARETTE. 2001. An intercomparison of small- and large-volume techniques for thorium-234 in seawater. Mar. Chem. **74:** 15-28.

BUESSELER, K. O., C. R. BENITEZ-NELSON, S. B. MORAN, A. BURD, M. CHARETTE, J. K. COCHRAN, L. COPPOLA, N. S. FISHER, S. W. FOWLER, W. GARDNER, L. D. GUO, O. GUSTAFSSON, C. LAMBORG, P. MASQUE, J. C. MIQUEL, U. PASSOW, P. H. SANTSCHI, N. SAVOYE, G. STEWART, and T. TRULL. 2006. An assessment of particulate organic carbon to thorium-234 ratios in the ocean and their impact on the application of ^{234}Th as a POC flux proxy. Mar. Chem. **100:** 213-233.

CALBET, A., and M. R. LANDRY. 2004. Phytoplankton growth, microzooplankton grazing, and carbon cycling in marine systems. Limnol. Oceanogr. **49:** 51-57.

CHEN, J. H., R. L. EDWARDS, and G. J. WASSERBURG. 1986. ^{238}U, ^{234}U and ^{232}Th in seawater. Earth Planet. Sci. Lett. **80:** 241-251.

CONOVER, R. J. 1966. Assimilation of organic matter by zooplankton. Limnol. Oceanogr. **11:** 338-345.

EPPLEY, R. W., and B. J. PETERSON. 1979. Particulate Organic-Matter Flux and Planktonic New Production in the Deep Ocean. Nature **282:** 677-680.

EPPLEY, R. W., E. H. RENGER, and W. G. HARRISON. 1979. Nitrate and phytoplankton production in southern California coastal waters. Limnol. Oceanogr. **24:** 483-494.

FASHAM, M. J. R., B. M. BALINO, M. C. BOWLES, R. ANDERSON, D. ARCHER, U. BATHMANN, P. BOYD, K. BUESSELER, P. BURKILL, A. BYCHKOV, C. CARLSON, C. T. A. CHEN, S. DONEY, H. DUCKLOW, S. EMERSON, R. FEELY, G. FELDMAN, V. GARCON, D. HANSELL, R. HANSON, P. HARRISON, S. HONJO, C. JEANDEL, D. KARL, R. LE BORGNE, K. K. LIU, K. LOCHTE, F. LOUANCHI, R. LOWRY, A. MICHAELS, P. MONFRAY, J. MURRAY, A. OSCHLIES, T. PLATT, J. PRIDDLE, R. QUINONES, D. RUIZ-PINO, T. SAINO, E. SAKSHAUG, G. SHIMMIELD, S. SMITH, W. SMITH, T. TAKAHASHI, P. TREGUER, D. WALLACE, R. WANNINKHOF, A. WATSON, J. WILLEBRAND, and C. S. WONG. 2001. A new vision of ocean biogeochemistry after a decade of the Joint Global Ocean Flux Study (JGOFS). Ambio **10:** 4-31.

GREEN, S. E., and R. N. SAMBROTTO. 2006. Plankton community structure and export of C, N, P and Si in the Antarctic Circumpolar Current. Deep-Sea Res. II **53:** 620-643.

HARRISON, W. G., T. PLATT, and M. R. LEWIS. 1987. F-ratio and its relationship to ambient nitrate concentration in coastal waters. J. Plankton Res. **9:** 235-248.

JACKSON, G. A. 2001. Effect of coagulation on a model planktonic food web. Deep-Sea Res. I **48:** 95-123.

KADKO, D. C., L. WASHBURN, and B. JONES. 1991. Evidence of Subduction within Cold Filaments of the Northern California Coastal Transition Zone. J. Geophys. Res. Oceans **96:** 14909-14926.

LANDRY, M. R., and A. CALBET. 2004. Microzooplankton production in the oceans. ICES J. Mar. Sci. **61:** 501-507.

LANDRY, M. R., C. J. LORENZEN, and W. K. PETERSON. 1994. Mesozooplankton grazing in the Southern California Bight .2. Grazing impact and particulate flux. Mar. Ecol. Prog. Ser. **115:** 73-85.

LANDRY, M. R., M. D. OHMAN, M. R. STUKEL, and K. TSYRKLEVICH. 2009. Lagrangian studies of phytoplankton growth and grazing relationships in a coastal upwelling ecosystem off Southern California. Prog. Oceanogr. **83:** 208-216.

LAVANIEGOS, B. E., and M. D. OHMAN. 2007. Coherence of long-term variations of zooplankton in two sectors of the California Current System. Prog. Oceanogr. **75:** 42-69.

LYNN, R. J., and J. J. SIMPSON. 1987. The California Current System: the seasonal variability of its physical characteristics. J. Geophys. Res. Oceans **92:** 12947-&.

MICHAELS, A. F., and M. W. SILVER. 1988. Primary production, sinking fluxes and the microbial food web. Deep-Sea Res. **35:** 473-490.

NELSON, J. R., J. R. BEERS, R. W. EPPLEY, G. A. JACKSON, J. J. MCCARTHY, and A. SOUTAR. 1987. A particle flux study in the Santa Monica-San Pedro Basin off Los Angeles: particleflux, primary production, and transmissometer survey. Cont. Shelf Res. **7:** 307-328.

OLIVIERI, R. A., and F. P. CHAVEZ. 2000. A model of plankton dynamics for the coastal upwelling system of Monterey Bay, California. Deep-Sea Res. II **47:** 1077-1106.

PASSOW, U., A. L. ALLDREDGE, and B. E. LOGAN. 1994. The role of particulate carbohydrate exudates in the flocculation of diatom blooms. Deep-Sea Res. I **41:** 335-357.

PASSOW, U., R. F. SHIPE, A. MURRAY, D. K. PAK, M. A. BRZEZINSKI, and A. L. ALLDREDGE. 2001. The origin of transparent exopolymer particles (TEP) and their role in the sedimentation of particulate matter. Cont. Shelf Res. **21:** 327-346.

PFANNKUCHE, O., and K. LOCHTE. 1993. Open ocean pelago-benthic coupling: cyanobacteria as tracers of sedimenting salp feces. Deep-Sea Res. I **40:** 727-737.

PIKE, S. M., K. O. BUESSELER, J. ANDREWS, and N. SAVOYE. 2005. Quantification of ^{234}Th recovery in small volume sea water samples by inductively coupled plasma-mass spectrometry. J. Radioanal. Nucl. Chem. **263:** 355-360.

PLATTNER, G. K., N. GRUBER, H. FRENZEL, and J. C. MCWILLIAMS. 2005. Decoupling marine export production from new production. Geophys. Res. Lett. **32:** 4.

RODRIGUEZ Y BAENA, A. M., M. METIAN, J. L. TEYSSIE, C. DE BROYER, and M. WARNAU. 2006. Experimental evidence for Th-234 bioaccumulation in three Antarctic crustaceans: Potential implications for particle flux studies. Mar. Chem. **100:** 354-365.

ROEMMICH, D. 1992. Ocean warming and sea-level rise along the Southwest U.S. Coast. Science **257:** 373-375.

ROEMMICH, D., and J. MCGOWAN. 1995a. Climatic warming and the decline of zooplankton in the California Current. Science **267:** 1324-1326.

ROEMMICH, D., and J. MCGOWAN. 1995b. Climatic warming and the decline of zooplankton in the California Current (Vol 267, Pg 1324, 1995). Science **268:** 352-353.

RYKACZEWSKI, R. R., and D. M. CHECKLEY. 2008. Influence of ocean winds on the pelagic ecosystem in upwelling regions. Proc. Natl. Acad. Sci. U. S. A. **105:** 1965-1970.

SAVOYE, N., C. BENITEZ-NELSON, A. B. BURD, J. K. COCHRAN, M. CHARETTE, K. O. BUESSELER, G. A. JACKSON, M. ROY-BARMAN, S. SCHMIDT, and M. ELSKENS. 2006. ^{234}Th sorption and export models in the water column: A review. Mar. Chem. **100:** 234-249.

SIEGEL, D. A., T. C. GRANATA, A. F. MICHAELS, and T. D. DICKEY. 1990. Mesoscale eddy diffusion, particle sinking, and the interpretation of sediment trap data. J. Geophys. Res. Oceans **95:** 5305-5311.

SILVER, M. W., and K. W. BRULAND. 1981. Differential feeding and fecal pellet composition of salps and pteropods, and the possible origin of the deep-water flora and olive-green cells. Mar. Biol. **62:** 263-273.

SMALL, L. F., and S. G. ELLIS. 1992. Fecal carbon production by zooplankton in Santa-Monica Basin: The effects of body size and carnivorous feeding. Prog. Oceanogr. **30:** 197-221.

STEINBERG, D. K., C. A. CARLSON, N. R. BATES, S. A. GOLDTHWAIT, L. P. MADIN, and A. F. MICHAELS. 2000. Zooplankton vertical migration and the active transport of dissolved organic and inorganic carbon in the Sargasso Sea. Deep-Sea Res. I **47:** 137-158.

STRAILE, D. 1997. Gross growth efficiencies of protozoan and metazoan zooplankton and their dependence on food concentration, predator-prey weight ratio, and taxonomic group. Limnol. Oceanogr. **42:** 1375-1385.

UMANI, S. F., A. ACCORNERO, G. BUDILLON, M. CAPELLO, S. TUCCI, M. CABRINI, P. DEL NEGRO, M. MONTI, and C. DE VITTOR. 2002. Particulate matter and plankton dynamics in the Ross Sea Polynya of Terra Nova Bay during the Austral Summer 1997/98. J. Mar. Syst. **36:** 29-49.

VENRICK, E. L. 1998. Spring in the California current: the distribution of phytoplankton species, April 1993 and April 1995. Mar. Ecol. Prog. Ser. **167:** 73-88.

VENRICK, E. L. 2002. Floral patterns in the California Current System off southern California: 1990-1996. J. Mar. Res. **60:** 171-189.

WALSH, I. D., and W. D. GARDNER. 1992. A comparison of aggregate profiles with sediment trap fluxes. Deep-Sea Res. **39:** 1817-1834.

WASHBURN, L., D. C. KADKO, B. H. JONES, T. HAYWARD, P. M. KOSRO, T. P. STANTON, S. RAMP, and T. COWLES. 1991. Water Mass Subduction and the Transport of Phytoplankton in a Coastal Upwelling System. J. Geophys. Res. Oceans **96:** 14927-14945.

CHAPTER 3

Do inverse ecosystem models accurately reconstruct food web flows? A comparison of two solution methods using field data from the California Current Ecosystem

ABSTRACT

Inverse methods have often been used to elucidate ecosystem dynamics when only a few basic measurements have been made. Despite their increasing use, the only studies that have directly assessed the efficacy of inverse ecosystem modeling techniques in recovering system flows have been restricted to simulated datasets. Meanwhile, new Markov Chain Monte Carlo (MCMC) methods have called into question the commonly used L_2 minimum norm (L_2MN) technique and provided an alternative to cost function minimization schemes. In the present study we test the MCMC and L_2MN methods' ability to recover measured ecosystem rates that were sequentially excluded from the input datasets. We utilized data from two cruises of the CCE LTER program on which Lagrangian tracking of 8 distinct water parcels (varying from rich upwelling to offshore oligotrophic communities) allowed repeat measurements of ecosystem rates and simultaneous determination of net phytoplankton rates of change. Both the MCMC and L_2MN methods were able to accurately determine the well-constrained rates of protozoan and mesozooplankton grazing rates, although the MCMC method significantly overestimated primary production. The MCMC method was a much more accurate predictor of the poorly

constrained rate of vertical carbon export than the L_2MN method, which consistently overestimated export. Results involving DOC and bacterial production were equivocal, because labile DOC concentrations were not determined on the cruise. We suggest that, when primary production is a measured input, MCMC methods provide a more accurate depiction of ecosystem processes. We show that most uncertainty in inverse ecosystem models stems not from measurement uncertainty, but from the under-determinacy of the solution, which can only be calculated by MCMC methods. We also suggest that the commonly used steady-state assumption can significantly bias inverse modeling results, both in bloom and non-bloom situations.

INTRODUCTION

Inverse ecosystem models are a powerful data assimilation tool that allow synthesis of *in situ* measurements and *a priori* assumptions about ecosystem structure. Pioneering work in inverse ecosystem modeling (Vézina and Platt 1988; Jackson and Eldridge 1992) was limited by computational power and a dearth of planktonic rate measurements for setting constraints on the system. While these early studies allowed comparisons of different ecosystems, the absence of objective methods for assessing system constraint (analogous to model error) confounded attempts to infer accurate rates.

The paucity of ecological measurements relative to variables leads invariably to an under-determined system, and hence an infinite number of inverse solutions that

can fit the sparse data. To choose from among these solutions, investigators have typically used the L_2 minimum norm (L_2MN), which selects the least mathematically complex of all possible solution vectors, but in so doing, biases the results in ways that are dependent on both the model structure and measured parameters. In particular, the L_2MN consistently inflates the respiration of basal consumers to minimize the sum of squared flows in the ecosystem by shunting energy out as rapidly as possible (Stukel and Landry 2010).

An alternative method for solving the under-constrained inverse ecosystem problem involves the use of Markov Chain Monte Carlo (MCMC) techniques to fully sample the possible solution space and choose the maximal likelihood solution (Kones et al. 2006; Soetaert and Van Oevelen 2009; Van Oevelen et al. 2010). Unlike the L_2MN, this method makes no assumption about underlying ecosystem structure, but instead assumes that a set of ecosystem states fit the available data and chooses the most likely mean value of any particular ecosystem parameter as its mean from within the greater solution space. It thus avoids the L_2MN's tendency to choose extreme parameter values (Stukel and Landry 2010), while simultaneously allowing a calculation of the underdeterminacy of the solution with regard to each parameter of interest (Kones et al. 2009).

While the complete sampling of the solution space offered by the MCMC offers advantages relative to the L_2MN, no studies have shown that it provides a better approximation of the ecosystem. To date, most studies addressing the efficacy of inverse ecosystem modeling techniques have used simulated ecosystems in which the

ecologically relevant ecosystem components were assumed (Vézina and Pahlow 2003; Vézina et al. 2004). However, simulated ecosystems, by their very nature, behave in an easily predictable manner, while the underlying structure of *in situ* ecosystems is unknown and hence less apt to be accurately described by the model.

To compare the results of inverse ecosystem models solved using alternately the L_2MN and the MCMC method, we employ data from two cruises of the California Current Ecosystem (CCE) Long Term Ecological Research (LTER) Program. On these cruises in May 2006 (P0605) and April 2007 (P0704), a total of eight water parcels were tracked for an average period of 4 days each. During this period, ecosystem rates including phytoplankton growth rate, protozoan and mesozooplankton grazing, net phytoplankton accumulation, vertical carbon flux, and bacterial growth rates were assessed. By simultaneously running an inverse model using the L_2MN and the MCMC method while sequentially withholding measurements, we were able to assess each minimization scheme's ability to predict the measured data. By comparing a steady-state version of the model to one which allowed the phytoplankton to accumulate (or decrease) as measured, we also tested the steady-state assumption commonly used in inverse ecosystem studies.

METHODS

Model structure – The construction of an inverse ecosystem model structure involves inevitable tradeoffs between constraints (fewer compartments, less complexity) and broad depiction of ecosystem processes (more compartments, greater

complexity). Determining the correct level of complexity is a matter of judgment, but has been shown to influence model results (Stukel and Landry 2010). Since the primary goal of this study is to compare methodologies (with elucidation of flows within the California Current Ecosystem a secondary goal), we chose to err on the side of greater constraint and hence fewer compartments. We thus constructed a simple ecosystem with one phytoplankton group (Phy), three size-structured grazing groups (Hnf, Mic, Mes), bacteria (Bac), detritus (Det), and dissolved organic carbon (DOC). Each grazing group was allowed to graze upon phytoplankton and smaller consumers. Bacterivory was allowed only for nanoflagellates and microzooplankton. Egestion was incorporated as a flux from grazers to detritus, while phytoplankton contributed to detritus through cell death. Grazers and phytoplankton were also both allowed to contribute to DOC production through exudation (phytoplankton) and excretion and sloppy feeding (grazers). Energy could be dissipated through the respiration of each group, vertical flux of detritus sinking out of the euphotic zone, or mesozooplankton consumed by higher trophic levels. The model thus had a total of 29 variables (Tables 1,2). The model was constrained with experimental measurements of net primary production, herbivorous grazing by the total protistan community, mesozooplankton grazing, bacterial production, and particulate flux of sinking detritus (although some measurements were not made for each experimental cycle). The addition of seven mass-balance constraints (discussed below) led to a maximum of 12 constraints on the ecosystem.

Ecological Measurements - Model data (Table 3) comes from two spring cruises of the CCE-LTER Program in May 2006 (P0605) and April 2007 (P0704). During these cruises, homogeneous water parcels were located using a Moving Vessel Profiler (MVP, Ohman, unpub.data) and marked with a drift array drogued at 15 m in the surface mixed layer (Landry et al. 2009). Water parcels were typically followed for four days while ecological rates were measured simultaneously with net changes in the euphotic zone phytoplankton community. Landry et al. (2009) showed that (to first order) changes in the net phytoplankton community could be predicted by the difference between measured rates of phytoplankton growth and combined grazing pressure of the protozoan and metazoan communities, thus suggesting that the experimental measurements accurately assessed the processes controlling ecosystem changes. For the present study, we assess phytoplankton growth using ^{14}C primary productivity measurements (^{14}C-PP, Goericke, unpub. data). Protozoan community grazing pressure on phytoplankton was measured using the dilution technique (Landry and Hassett 1982; Landry et al. 2009). To ensure that the ratio of protozoan grazing to phytoplankton production was maintained, protozoan grazing was calculated (in carbon units) as the product of ^{14}C-PP and the ratio of protozoan grazing to phytoplankton specific growth rate calculated by the dilution technique. Mesozooplankton grazing was determined from the gut pigments (chlorophyll *a* and phaeopigments) in organisms collected in paired day-night oblique bongo tows with 200-μm mesh (Landry et al. 2009 and Ohman, unpub. data). As for protozoa, mesozooplankton grazing rates were scaled by ^{14}C-PP to convert to carbon units while

maintaining the measured ratios of grazing to production. Vertical carbon flux from the 2006 cruise was measured from ^{234}Th-^{238}U disequilibrium integrated over the upper 100-m and C:^{234}Th ratio on particles collected at 100-m depth (Stukel et al. submitted). For P0605 Cycle 1 (IC1 in Stukel et al. submitted), we followed the authors' assumption of 1 m d^{-1} upwelling, but used variability of upwelling rates ranging from negligible to 2 m d^{-1}. No export rate was measured for the furthest inshore cycle (P0605 Cycle 3). For the 2007 cruise, POC flux rates were determined from ^{234}Th-^{238}U disequilibrium and the average C:^{234}Th on particles collected with sediment traps and in situ pumps at 100-m depth. Bacterial production was measured on the P0704 cruise by the leucine incorporation technique (Samo, unpub. data). Net rates of change in phytoplankton community biomass were assessed by daily changes in vertically integrated chlorophyll concentrations at the drifter location multiplied by the ratio of chlorophyll to phytoplankton biomass calculated from epifluorescence microscopy samples.

Model Solution - The model solutions were further limited by a set of biological constraints (see Appendix 2). These included bounds on respiration, gross growth efficiency, and excretion for each group, as well as assimilation, maximum ingestion, and maximum clearance rates for the grazers. Except for phytoplankton, for which we measured the net rates of change,, we assumed that net accumulation rates of other biological components were 0±10% of their average biomass d^{-1}.

Despite these constraints, the model remained under-determined. To choose between the possible solutions, we utilized two different minimization schemes, the

L_2MN and the MCMC. The L_2MN procedure (Vézina and Platt 1988; Jackson et al. 2001) begins by using the singular value decomposition to solve the exact system of equations Ax=b. The solution, x is composed of a minimum exact solution x_0 of rank k, and a series of vectors (x_i) that can be added or subtracted to x_0 while still solving Ax=b. If the system of equations is consistent, k = the number of equations (e.g. the number of measurements plus the number of mass balance equations). At times, measurement inaccuracies led to an inconsistent system of equations (e.g., if phytoplankton growth minus grazing was less than the measured net change in phytoplankton biomass), and we followed the method of Olsen et al. (2006) decreasing the rank of the solution until we found a solution that fulfilled the inequalities ($Gx \geq h$). The remaining vectors from the singular value decomposition are then used to find the linear combination that minimizes the L_2 norm while also satisfying the inequality constraints (for greater detail, see Appendix 2).

The MCMC method (Kones et al. 2009) similarly utilizes the singular value decomposition to determine x_0 and x_i. Rather than calculate a single answer, however, the MCMC method uses the total set of solutions to the equality constraints (Ax=b) to conduct a random walk through the entire solution space, thus creating a random subset of the infinite number of solutions that satisfy the inverse problem. The MCMC method chooses the maximum likelihood solution as the mean value of each unknown in this subset, but from this subset it can also calculate standard deviations for all variables, which thus indicate the extent of under-determinacy of the solution (for full details, see Appendix 3).

In addition to error associated with the under-constrained nature of all inverse ecosystem models, we also accounted for measurement error with both the L_2MN and MCMC methods. We used a Monte Carlo method of simultaneously varying the input parameters (measurements and steady-state equations for all biological compartments), assuming a normal distribution for all measurements. For the L_2MN, we calculated a total of 10,000 solutions based on varied input parameters to calculate standard deviations for all estimated ecosystem flows. For the MCMC method, we used a minimum of 100 different sets of input parameters and calculated a subset of 100 solutions for each. These generated at least 10,000 solutions that account for measurement errors as well as errors associated with under-determinacy.

RESULTS

Comparison of L_2MN and MCMC: numerical experiments – To test the ability of the L_2MN and MCMC methods to accurately predict ecosystem flows, we conducted a series of numerical experiments in which we withheld a particular *in situ* rate measurement (^{14}C-PP, microzooplankton grazing, mesozooplankton grazing, vertical POC flux, or bacterial production) from the dataset and solved the inverse problem with both the L_2MN and MCMC as described above. By varying the input parameters based on the assumption of a normal distribution, we were able to generate means and 95% confidence intervals that could then be compared to the experimental measurements (Figure 1).

We can break these numerical experiments into two sets, one set including the relatively well-constrained growth and grazing relationships and the other including POC export and bacterial production. In the full dataset, the measured rate of change in phytoplankton concentration (ΔP) is equal to the difference between net production (^{14}C-PP) and the sum of protozoan grazing, mesozooplankton grazing, and phytoplankton loss to detritus (PHYtoDET). Thus the unconstrained flow, PHYtoDET, is fixed by the other measurements. This relationship can explain the relative responses of both the L_2MN and the MCMC to the exclusion of the first three rate measurements. When the ^{14}C-PP measurement is withheld, the difference between phytoplankton net growth and loss to detritus is fixed by the phytoplankton rate of change and grazing measurements. Individually, however, there is very little constraint on the net growth of phytoplankton (since we allowed phytoplankton to grow at a maximal rate of up to two doublings per day) and there are no constraints on phytoplankton mortality. To minimize total system flow, the L_2MN consistently sets a low PHYtoDET rate of essentially zero, thus setting ^{14}C-PP roughly equal to the sum of ΔP and grazing. The MCMC method, by contrast, samples all the possible combinations, leading to high rates of both primary production and PHYtoDET, which are highly correlated when the ^{14}C-PP measurement is withheld. Figures 1a,b clearly show that the L_2MN does a better job of predicting primary production than the MCMC since it minimizes total system flow. However, primary production is the only rate that has been measured in all pelagic inverse ecosystem models that we have encountered.

The grazing rates of proto- and metazoans on phytoplankton are likewise constrained by the balance of ΔP, PHYtoDET, and ^{14}C-PP. With ^{14}C-PP measured, both solution schemes accurately predict the grazing terms, with the *in situ* measurements typically falling within the 95% confidence intervals for both the L_2MN and the MCMC. With both schemes, the inverse models tend to slightly underestimate grazing terms (Figs. 1c-f), largely because there are maximal constraints placed on community grazing (see Appendix 1), but PHYtoDET is unconstrained.

Vertical POC flux is much less constrained as a model output since it depends on detrital production and utilization (which are only loosely constrained) as well as other fluxes of energy out of the pelagic ecosystem (particularly respiration). Nonetheless, it is the type of flow that inverse ecosystem models are typically used to infer. The MCMC method does an accurate job of estimating carbon export, with the 95% confidence interval bracketing the actual measurement value for all seven cycles (POC flux was not measured on P0605, Cycle 3). In fact, the MCMC values are all within a single standard deviation of the measured rate (Fig. 1g). The same cannot be said, however, for the L_2MN predictions. For three out of the seven cycles the measured values fall below the 95% confidence intervals of the L_2MN, and for six of the seven cycles the 67% confidence intervals fail to bracket the measurement (Fig. 1h). The L_2MN is thus a poor predictor of vertical carbon flux, consistently overestimating export due to its tendency to shunt energy out of the system as rapidly as possible.

Bacterial production (BP), measured only on the P0704 cruise, was found to be surprisingly low, with BP:^{14}C-PP ratios of 0.04, 0.04, and 0.01 for Cycles 1 through 3, respectively. By minimizing DOC production, the L_2MN solution did an accurate job of predicting bacterial production (Fig. 1i). The MCMC consistently overestimated BP (Fig. 1j), although this overestimate may have resulted holding the DOC compartment in steady state. In an upwelling system, the combination of cold water, high production, and low bacterial biomass likely result in DOC accumulation and advection offshore (see discussion).

Comparison of L_2MN and MCMC: ecosystem parameters – To further compare the L_2MN and MCMC methods, we computed composite ecosystem indices that can be used to compare the different ecosystem states encountered on our cruises. While these indices are difficult to measure in the field, they can be easily calculated from ecosystem models. The differing results provided by the L_2MN and MCMC offer insights into the biases of each solution method.

We calculated GGEs for all heterotrophic compartments (Fig. 2). The MCMC method suggested GGEs of 20-25% for all grazer groups, which is on the low end of the 20-30% range suggested for grazers in the metanalysis of Straile et al. (1997). The L_2MN method, however predicted low GGEs of 10-20% for both protozoan groups, but a high GGE of >35% for mesozooplankton. The bacterial GGEs predicted by the two methods were surprising. The MCMC method predicted high GGEs (20-25%) when bacterial production was not measured on the P0605 cruise and low GGEs (5-10%) when it was measured (Fig. 2d) The GGE solutions from the L2MN showed the

opposite pattern. The MCMC solutions for bacterial GGEs on the P0704 cruise were driven to low values by the extremely low bacterial production measurements, and may be an artifact of our decision to hold DOC in steady state. The L_2MN predicted low GGEs when bacterial production was not measured, thus allowing bacteria to respire most of the carbon they took up (shunting it out of the ecosystem to minimize the L_2 norm). Conversely, high GGE was predicted when bacterial production was measured because of consistently low DOC production in the L_2MN solutions.

To compare the overall utilization of primary production by different ecosystem components, we computed the amount of energy in three alternate pathways: the classical food chain (defined as the direct flow of phytoplankton, both living and detrital, to mesozooplankton), the multivorous food chain (defined as the flow reaching the mesozooplankton that stemmed from protozoan grazing on phytoplankton), and the microbial loop (defined as the sum of bacterial respiration and portion of protozoan respiration supported by bacterial production). The classical food chain was particularly well constrained; although variability of the pathway was incredibly high (ranging from <20% to >140% of ^{14}C-PP), the L_2MN and MCMC were in strong agreement (Fig. 3a). For the multivorous food chain and the microbial loop, however, the two solution methods differed strongly, with the L_2MN consistently predicting less carbon utilization by both pathways. The L_2MN predicted low carbon flow from protozoans to mesozooplankton (Fig. 3b) due to the previously mentioned low gross growth efficiencies of protozoans. Low activity of the microbial loop reflected the minimization of DOC production by phytoplankton and grazers in

the L_2MN (Fig. 3c). We also computed the percentage direct contribution of phytoplankton to vertical POC flux (Fig. 4) to compare the relative importance of sinking cells and grazing processes in carbon export. While the MCMC and L_2MN agreed well on 5 of the 8 cycles, for P0605 Cycles 1, 4, and 5, the L_2MN suggested a significantly larger role for direct phytoplankton sinking than the MCMC.

Effect of steady-state assumption – To test the role of assuming steady state for all compartments in the ecosystem, we set all mass-balance equations equal to zero and again solved the system of equations using the MCMC technique. Figure 5a clearly shows that for ecosystem states when the phytoplankton community was either increasing significantly (P0605 Cycle 4) or decreasing rapidly (P0704 Cycle 1) the steady-state assumption significantly affected the inverse results for many of the flows. In particular, when phytoplankton were declining the SS model underestimated most of the flows, especially the flow of phytoplankton to detritus. The converse was true when the ambient phytoplankton community was increasing the converse was true. Overall, across the 8 cycles, over two thirds of the flows were over or underestimated by the SS model by greater than 7.7%, and 5% of the flows were over/underestimated by more than 35.5% (Fig. 5b).

Inverse ecosystem modeling error sources – Inverse ecosystem modeling errors can arise from three distinct sources: measurement error, solution (underdeterminacy) error, and structural error. While structural error is difficult to assess due to the vast amount of possible model constructions, we addressed the other two sources of error. To calculate the role of measurement error, we computed the

mean MCMC solution for 100 different sets of measurement inputs (randomly selected from normal distributions) for each cycle. We determined the solution error using the MCMC to sample the solution space for the exact measurement values of each cycle. We then computed the coefficients of variation (CV) for each unknown with regard to both the solution and measurement errors.

For the majority (76%) of our ecosystem flows, solution errors were larger than measurement errors (fig. 6a). The exceptions were typically flows that were directly measured or highly correlated with in situ measurements (e.g. mesozooplankton grazing and POC flux were measured at sea, GPP was highly correlated with ^{14}C-PP). With the exception of POC export, flows involving detritus exhibited particularly high solution errors. This was especially the case for flows from detritus to grazers because of our lack of a priori knowledge and experimental measurement of detrital fluxes (Fig. 6b).

DISCUSSION

Spring in the CCE – Venrick (2002) used floristic patterns to divide our study region into a temporally variable coastal region dominated by large phytoplankton and a more stable offshore region with smaller sizes of phytoplankton. If we apply a similar rubric to our studies, three cycles (P0605-2, P0605-3, and P0704-2) cluster with the offshore region while the other five are characteristic of the upwelling-affected coastal region. In addition to significantly lower productivity rates (Table 1), the offshore cycles are much more similar to each other than the coastal cycles. All

three exhibit weak functioning of the classical food chain, but relatively strong multivorous and microbial food webs (Fig. 7). The inshore region shows far more variability. While the strength of the classical food chain varies from 18% to 148% of ^{14}C-PP, it is strongly positively correlated with the multivorous food chain, suggesting that variations in the activity of the mesozooplankton community strongly affect coastal food webs. The microbial loop also exhibits strong variability inshore, varying from 52% to 91% of ^{14}C-PP (compared to 79% to 94% for the offshore region), and its relatively high values throughout the CCE suggest that it is a dominant pathway of carbon flow throughout the region.

Given the apparent importance of mesozooplankton in structuring the coastal region, it is interesting to compare the models' predictions of trophic levels (TL) for this community. Spatial patterns for the mesozooplankton TL were distinctly different on the two cruises (Fig 8). In 2006, the predicted mesozooplankton TL was not strongly correlated with distance from shore. For 2007, however of the prediction of increasing mesozooplankton TL with distance from shore agreed well with cruise measurements made on the copepod *C. pacificus* and the euphausiid *E. superba* (M. Décima, unpublished data). The inverse model also predicts that across the range of ecosystem states sampled direct gravitational sinking of phytoplankton plays a significant, though lesser role in export (varying from 5-35% of total vertical flux in the MCMC model, Fig 4), compared to export of grazing products, a result that agrees well with pigment analyses from sediment traps deployed in the CCE region (M. Stukel, unpublished data).

Inverse ecosystem modeling – Since the pioneering work of Vézina and Platt (1988), inverse ecosystem modeling methods have been frequently used either to compare different ecosystems (e.g. Daniels et al. 2006) or to infer unmeasured ecosystem flows (e.g. Jackson and Eldridge 1992). However, few investigators have utilized field data to assess the efficacy of inverse methods in approximating ecosystem structure. In this study we utilized in situ measurements from two cruises of the CCE LTER program to test the accuracy of both the L_2MN and MCMC solution approaches in predicting cruise measurements and aggregate properties of the ecosystem. With both methods, we used a Monte Carlo technique of randomly varying the input parameters (measurements) for each cycle to generate an ensemble solution that incorporates measurement error. This ensemble solution is distinct from the typical exact solution that assumes perfect field measurements of ecosystem rates; in particular, it averages out some of the biases of the exact L_2MN solution while generating more realistic confidence intervals.

We sequentially withheld individual cruise measurements in order to assess the inverse methods' ability to predict known quantities. Not surprisingly, both methods did a reasonable job of estimating protozoan and mesozooplankton grazing rates, as these flows were well constrained by the field data (Fig. 1c-f). The L_2MN did a much better job of predicting primary production than the MCMC method (Fig. 1a,b); hence it may be a better technique to use when primary production is unmeasured. However, primary production is the only measurement that appears to be included consistently as a measured input for inverse models of pelagic ecosystems. Furthermore, the

MCMC's prediction of primary production would probably have been significantly improved if we had placed a more stringent upper bound on phytoplankton growth rates; the maximum of two doublings per day that we allowed is unrealistically high for the cold water of the CCE.

Model predictions of vertical carbon flux and bacterial production were more interesting, as they are the type of poorly constrained and highly coupled ecosystem flows that inverse models are often used to resolve. The MCMC method was much more accurate at predicting vertical carbon flux than the L_2MN (Figs. 1g,h). Confidence intervals of MCMC solutions consistently bracketed measurement values and solutions were typically less than a standard deviation away from the measured values. In contrast, the L_2MN solutions consistently overestimated POC export. Despite the wide uncertainties it predicted for this flow (average CV for the 7 cycles was 1.98), 95% confidence intervals failed to bracket the true values three out of seven times. This overestimate of POC export by the L_2MN may seem surprising given its tendency to maximize grazer respiration, but it follows logically from the method's minimization of the flows through the system. Rather than allow detritus to be reworked by grazers, the L_2MN exports most detritus directly out of the system.

Bacterial production, as measured on the P0704 cruise by the leucine incorporation technique, was accurately predicted by the L_2MN, but overestimated by the MCMC. This result may be misleading, however, because we lacked measurements of labile DOC and chose to hold DOC concentrations constant. The P0704 cruise took place early in the spring bloom period, when cold nutrient-rich

water led to high phytoplankton growth rates near the Point Conception upwelling center. The combination of high phytoplankton growth with rapid grazing likely led to significant production of DOC, yet measured bacterial production of only 4%, 4%, and 1% of ^{14}C-PP (for P0704 cycles 1-3, respectively) were far below typical marine averages of 10-20% (Ducklow 2000). These low rates may have been due to a combination of low bacterial biomass early in the spring season and cold temperatures that depressed specific growth rates. Regardless of the reason, the combination of high DOC generation and low bacterial production likely led to net accumulation of DOC that was advected away from the upwelling source, as has been shown in other upwelling ecosystems (Alvarez-Salgado et al. 2001; Wetz and Wheeler 2004). If we modify the model to allow for even slight net production of DOC (Figure 9 shows net DOC daily increases of 1% and 2% d^{-1}) the L_2MN and MCMC do similarly well in predicting bacterial production, with the MCMC becoming increasingly accurate as DOC accumulation is increased. Although DOC production was not measured on the cruises, DO^{14}C production rates on springtime CalCOFI cruises have averaged roughly 20% of ^{14}C-PP (R. Goericke, unpublished data) during 24-hour incubations. These are almost certainly an underestimate of production processes as most of the exuded carbon during the incubation will remain unlabeled. While there is some uncertainty about which production processes are assessed by the DO^{14}C method, it likely incorporates mainly DOC production from phytoplankton exudation and viral lysis (both of which are subsumed in our PHYtoDOC term). For the L_2MN solution, phytoplankton DOC production rates were low, ranging from 3.6% to 6.1% of ^{14}C-PP

(mean 4.3%) across our 8 cycles. The MCMC solutions, by contrast, predicted phytoplankton DOC production rates of 8.1% to 39.3% (mean 28.5%), which compare favorably with the measured DO^{14}C production rates on CalCOFI cruises. By this metric, therefore, the MCMC method did a better job of approximating DOC cycling.

Although respiration and GGE were not measured at sea, the distinct differences between the models' apportionment of grazer assimilation into alternate pathways of production, respiration, or excretion allow for a useful comparison of the two solution methods. In a metanalysis of laboratory experiments determining GGEs of flagellates, ciliates, dinoflagellates, and crustaceans, Straile (1997) found little variability across taxa, with all having mean GGEs between 20 and 30%. The only size relationship was a slight (and not statistically significant) decrease in GGE with increasing size. While this agrees well with mean GGE estimates of 24%, 21%, and 19% for heterotrophic nanoflagellates, microzooplankton, and mesozooplankton, respectively, for the MCMC method, the L_2MN predicts distinctly different results of 10-20% GGE for the protozoan taxa and much higher GGEs for the metazoans (Fig. 2).

Many of the biases of the L_2MN have already been diagnosed. In particular, it tends to zero out minor flows (Vézina et al. 2004) and minimize the largest flows in the model. It also often sets biological constraints (e.g. GGE) to either maximum or minimum allowed values and minimizes the production of DOC (Stukel and Landry 2010). The MCMC is a much newer technique, and as such its inherent biases have not been well categorized. By fully sampling the solution space, the MCMC avoids

many of the problems associated with the L_2MN. In particular, rather than choosing unrealistically low or high values for biological constraints (e.g. GGE), the MCMC selects a more likely value near the middle of the allowable ranges (Fig. 2). However, we did identify one bias in the MCMC method that makes the examination of model structure important. When fully sampling the solution space, the MCMC method typically apportions unconstrained flows equally between equivalent compartments. While this may be a reasonable approach, it can lead to biases in the results when different model constructions are used. For instance pathways of carbon flow from nanoflagellates will be altered by the structure of the microplankton community. In our model construction, carbon could flow from nanoflagellates to respiration, DOC, detritus, microzooplankton, or mesozooplankton. If instead we divided the microzooplankton community into heterotrophic flagellates and ciliates, which both graze upon nanoflagellates, the total flow into this combined microzooplankton group would increase at the expense of other outflows from nanoflagellates, due to the greater number of states that can be constructed. Thus when comparing different ecosystems, it is important to maintain similar inverse structures.

Due to the fixed station-based sampling of most oceanographic cruises that do not allow for Lagrangian-based studies, many inverse studies have assumed steady state for their compartments. In fact, these unmeasured mass balance constraints are often assumed to be known exactly, while *in situ* measurements are assigned error terms. Vézina and Pahlow (2003) tested this assumption by comparing L_2MN inverse ecosystem reconstructions of steady-state models to reconstructions of transient states

of a time-varying bloom model. They found that the inverse methods that assumed steady state actually did a better job of evaluating the underlying flows in the bloom model than in the steady-state simulation, and thereby concluded that steady-state assumptions are valid even for periods when the ecosystem components are temporally variable. We chose to readdress this assumption in a different manner, utilizing the measured rate of change of the largest compartment in the model (phytoplankton) to construct a non-steady state (NSS) inverse analysis and then comparing it to an equivalent steady-state (SS) inverse analysis. The differences between the SS and NSS models were significant, with flows often significantly over or underestimated by the SS solution when the natural phytoplankton community was increasing or declining rapidly. Given the biases inherent to the L_2MN, it is likely that the more accurate predictions of the transient states of the bloom model of Vézina and Pahlow (2003) were in fact due to the increased strength of the classical food chain during bloom conditions. As our Fig. 3 shows, the L2MN significantly underestimates flows through the microbial loop and multivorous food webs, which dominate during steady-state conditions. In fact the results of Vézina and Pahlow (2003) can be understood as a simple response of the inverse method to the increasing complexity of the food webs. The L2MN does a good job of estimating the growth phase of the bloom, but becomes less accurate as the bloom reaches its peak and decays and in the steady-state simulations with significantly lower phytoplankton biomass. We suggest that when net biomass changes cannot be measured,

investigators should apply a reasonable error term to their mass balance equations, for instance assuming 95% confidence intervals of ±10% biomass change per day.

CONCLUSION

Investigators have relied on inverse modeling techniques (particularly the L_2MN) to reasonably resolve complex food webs when only a few basic measurements are made. We tested the efficacy of inverse methods across a wide range of ecosystem states within the CCE, and found that they reasonably estimate in situ measurements when measurement errors are taken into account. While an ensemble version of the commonly used L_2MN technique clearly performs better than the newer MCMC method when primary production is not specified as a model input, the MCMC method more accurately depicts pelagic food web flows when primary production is a measured input. In particular, the MCMC method predicted vertical carbon flux, which depends on a number of unmeasured rates; hence the MCMC appears to have more accurately captured the dynamics of the poorly resolved but highly connected detrital pool. This ability to resolve such an under-constrained component of the ecosystem suggests that it may perform well with the highly underdetermined ecosystems often encountered. Nevertheless, results from inverse modeling techniques are highly uncertain, as shown by coefficients of variation that are often greater than 50%. Despite the fact that our simple model, with 10-12 equations constraining only 29 variables, was far more constrained than most inverse models, most of the variability arose from the under-determinacy of the solutions, rather than from measurement uncertainties. We thus suggest that experimental

programs focusing on food web fluxes require an expanded range of experimental measurements, in particular, measurements that constrain the behaviors of the DOC and detrital pools, which play a large role in the model but are very poorly constrained.

ACKNOWLEDGMENTS

This chapter would not have been possible without the cooperative efforts of the many different researchers, students, technicians, and volunteers on the P0605 and P0704 cruises of the California Current Ecosystem (CCE) Long-Term Ecological Research (LTER) program. I am particularly indebted to my co-workers in the Landry Lab (M. Landry, A. Taylor, M. Décima, D. Wick) for providing microzooplankton grazing and microscopy results, the Ohman Lab (M. Ohman, R. Rykaczewski, M. Décima, J. Powell, K. Tsyrklevich, D. Taniguchi) for mesozooplankton biomass and grazing results, the Goericke Lab (R. Goericke, S. Dovel, M. Roadman) for 14C-PP, chlorophyll, and POC data, the Azam Lab (T. Samo) for bacterial production rates, and the Aluwihare Lab (L. Aluwihare, L. Chong) for TOC concentrations. Thorium export measurements were only possible because of willing collaborators from the Benitez-Nelson Lab (C. Benitez-Nelson, K. Maiti, and R. Styles). I am also grateful to the captains and crews of the R.V. Knorr and the R.V. Thompson.

Chapter 3, in full, is currently in preparation for submission: Stukel, M. R., Landry, M. R., Benitez-Nelson, C. R., Goericke, R. "Do inverse models accurately reconstruct food web flows? A comparison of two solution methods using field data

from the California Current Ecosystem." The dissertation author was the primary investigator and author on this paper.

Table 3.1. Measured inputs to the model. μ and m are the phytoplankton specific growth rate and protozoan grazing rates measured by the dilution technique. MesoGr is the mesozooplankton grazing rate as determined by the gut pigment technique. POCFlux is vertical carbon export. BacProd is bacterial production. ΔChl is the in situ rate of change of chlorophyll over the course of the cycle. Bio denotes biomass. Euphotic depth is the depth of integration for biological measurements. *Maximum microzooplankton concentration terms include autotrophic dinoflagellates as they are likely phagotrophic.

		0605-1	0605-2	0605-3	0605-4	0605-5	0704-1	0704-2	0704-3
C-14PP	mgC m^{-2} d^{-1}	4184±1767	563±28	4382±412	1474±251	483±159	1233±815	587±90	2314±910
μ	d^{-1}	0.273±0.060	0.159±0.051	0.243±0.168	0.346±0.068	0.073±0.053	0.293±0.139	0.136±0.032	0.285±0.030
m	d^{-1}	0.125±0.054	0.123±0.063	0.175±0.112	0.154±0.053	0.068±0.042	0.157±0.081	0.166±0.043	0.158±0.048
MesoGr	d^{-1}	0.088±0.046	0.057±0.029	0.112±0.092	0.065±0.007	0.013±0.003	0.475±0.089	0.044±0.008	0.219±0.133
POCFlux	mgC m^{-2} d^{-1}	322±200	72±44	ND	132±49	76±74	83±14	37±11	129±61
BacProd	mgC m^{-2} d^{-1}	ND	ND	ND	ND	ND	53±25	22±12	33±15
ΔChl	d^{-1}	0.070±0.238	-0.004±0.109	0.002±0.589	0.142±0.154	-0.173±0.152	-0.253±0.164	0.014±0.199	-0.069±0.519
PhyBio	mgC m^{-2}	7451±2094	2262±676	7333±2024	3085±629	1653±323	2613±1019	2079±165	2239±333
HnfBio	mgC m^{-2}	631±42	575±32	397±48	406±25	298±11	410±20	457±9	396±16
MicBio*	mgC m^{-2}	1733±1034	128±128	1390±2082	99±228	243±69	262±106	41±48	203±265
MesBio	mgC m^{-2}	1335±532	365±123	1329±408	757±188	243±44	2695±1077	391±87	1715±393
BacBio	mgC m^{-2}	756±263	810±29	489±77	520±45	917±53	539±49	907±54	885±93
POC	mgC m^{-2}	12146±3331	4637±210	10523±3155	5320±694	4845±669	4618±1416	4839±138	6022±752
DOC	mgC m^{-2}	20801±7261	69212±8569	9023±3958	30761±1460	54105±4014	30231±2228	112472±104020	52395±2052
MaxHNFBio	mgC m^{-2}	694	850	554	508	359	463	612	458
MaxMicBio*	mgC m^{-2}	5718	1648	10483	1376	747	2194	653	1259
MaxMesBio	mgC m^{-2}	2120	549	1725	890	280	4095	488	1942
MaxPhyDensity	mgC m^{-3}	431	90.76	822.34	95.15	65.6	116.23	54.66	59.29
MaxHNFDensity	mgC m^{-3}	20	17.82	33.8	21.14	7.14	14.51	10.54	8.85

Table 3.1. Cont.

		0605-1	0605-2	0605-3	0605-4	0605-5	0704-1	0704-2	0704-3
MaxMicDensity	mgC m^{-3}	313	53.3 724.	26	44.44 23.	94 57.	94	39.42	15.59
MaxBacDensity	mgC m^{-3}	29 11	30	13	20	14		14	16
Temp	deg C	11.7±0.4 13.	8±0.2 12.	9±0.3 14.	2±0.2 15.	0±0.2 11.	9±0.2	13.9±0.1	11.8±0.3
Euphotic Depth	m	50	100	25 50	90	50		90	85

Table 3.2. MCMC solutions to the inverse ecosystem model. Fluxes are shown as SOURCEtoSINK, in units of mg C m^{-2} d^{-1}. Compartments are phytoplankton (PHY), heterotrophic nanoflagellates (HNF), microzooplankton (MIC), mesozooplankton (MES), bacteria (BAC), detritus (DET), and dissolved organic carbon (DOC). RES denotes respiration of the living compartments, while MEStoEXT and DETtoEXT are flows from mesozooplankton to higher trophic levels and from detritus that sink out of the euphotic zone, respectively.

	0605 Cycle1	0605 Cycle2	0605 Cycle3	0605 Cycle4	0605 Cycle5	0704 Cycle1	0704 Cycle2	0704 Cycle3
GPP	9089 ± 2306	1296 ± 222	10803 ± 2800	3157 ± 540	1034 ± 275	3094 ± 1188	1362 ± 305	5108 ± 1335
PHYtoRES	3060 ± 1533	438 ± 198	3709 ± 1898	1041 ± 473	356 ± 181	1239 ± 692	528 ± 235	2186 ± 918
PHYtoHNF	956 ± 628	233 ± 132	1365 ± 930	354 ± 161	170 ± 95	198 ± 143	264 ± 108	170 ± 83
PHYtoMIC	724 ± 571	169 ± 120	1350 ± 1485	277 ± 178	263 ± 182	202 ± 164	336 ± 145	752 ± 241
PHYtoMES	1052 ± 574	146 ± 62	1310 ± 819	247 ± 59	77 ± 40	1779 ± 689	96 ± 55	1421 ± 599
PHYtoDET	1294 ± 803	145 ± 103	1877 ± 1507	162 ± 167	270 ± 181	280 ± 369	35 ± 70	824 ± 690
PHYtoDOC	1604 ± 673	233 ± 82	1745 ± 823	598 ± 189	175 ± 78	279 ± 214	150 ± 100	220 ± 162
HNFtoMIC	392 ± 297	76 ± 59	507 ± 359	100 ± 77	55 ± 28	164 ± 112	53 ± 33	78 ± 45
HNFtoMES	313 ± 254	64 ± 52	306 ± 258	88 ± 70	28 ± 15	148 ± 131	65 ± 42	260 ± 178
HNFtoRES	768 ± 311	143 ± 53	967 ± 359	201 ± 74	134 ± 57	351 ± 170	141 ± 54	490 ± 272
HNFtoDET	794 ± 430	166 ± 95	833 ± 394	233 ± 133	148 ± 88	362 ± 238	154 ± 87	419 ± 280
HNFtoDOC	435 ± 193	83 ± 35	530 ± 211	115 ± 48	76 ± 36	179 ± 90	74 ± 30	212 ± 109
MICtoRES	847 ± 377	139 ± 53	1372 ± 863	217 ± 79	169 ± 76	321 ± 170	165 ± 64	577 ± 273
MICtoMES	657 ± 342	116 ± 58	865 ± 444	177 ± 85	110 ± 40	248 ± 145	141 ± 66	388 ± 185
MICtoDET	957 ± 588	164 ± 93	1373 ± 912	272 ± 143	201 ± 120	323 ± 228	195 ± 106	486 ± 276
MICtoDOC	484 ± 240	81 ± 35	752 ± 448	126 ± 51	98 ± 48	161 ± 87	88 ± 36	242 ± 103
MEStoRES	808 ± 306	135 ± 45	997 ± 338	204 ± 68	122 ± 48	727 ± 324	137 ± 53	872 ± 356
MEStoDET	879 ± 400	157 ± 78	861 ± 364	236 ± 112	122 ± 67	972 ± 444	147 ± 80	805 ± 368
MEStoDOC	452 ± 190	77 ± 31	537 ± 200	113 ± 44	68 ± 31	349 ± 142	71 ± 30	351 ± 120
BACtoRES	2623 ± 809	410 ± 92	3524 ± 1316	787 ± 177	384 ± 123	1012 ± 367	401 ± 125	1093 ± 305
BACtoHNF	106 ± 60	57 ± 34	98 ± 56	47 ± 25	47 ± 29	29 ± 20	21 ± 17	34 ± 22

Table 3.2 Cont.

	0605 Cycle1	0605 Cycle2	0605 Cycle3	0605 Cycle4	0605 Cycle5	0704 Cycle1	0704 Cycle2	0704 Cycle3
BACtoMIC	670 ± 338	76 ± 47	871 ± 492	192 ± 78	65 ± 44	73 ± 62	20 ± 18	76 ± 51
DETtoHNF	1613 ± 947	238 ± 169	1603 ± 947	333 ± 251	223 ± 161	954 ± 530	193 ± 142	1219 ± 648
DETtoMIC	1132 ± 956	172 ± 141	1555 ± 1322	220 ± 197	193 ± 160	592 ± 478	168 ± 147	751 ± 535
DETtoMES	605 ± 506	122 ± 109	513 ± 476	162 ± 149	172 ± 122	310 ± 311	135 ± 113	486 ± 435
DETtoDOC	380 ± 381	58 ± 54	774 ± 866	72 ± 67	79 ± 80	100 ± 106	40 ± 39	106 ± 114
DOCtoBAC	3379 ± 1028	537 ± 118	4420 ± 1518	1026 ± 219	497 ± 151	1085 ± 384	432 ± 132	1159 ± 322
DETtoEXT	252 ± 131	56 ± 26	666 ± 1079	124 ± 32	76 ± 40	34 ± 30	16 ± 13	48 ± 57
MEStoEXT	508 ± 231	88 ± 42	655 ± 318	122 ± 53	73 ± 43	450 ± 235	92 ± 55	554 ± 248

Table 3.3. L_2MN solutions to the inverse ecosystem model. Abbreviations are the same as Table 1.

	0605 Cycle1	0605 Cycle2	0605 Cycle3	0605 Cycle4	0605 Cycle5	0704 Cycle1	0704 Cycle2	0704 Cycle3
GPP	5989 ± 1269	834 ± 61	7110 ± 1717	2101 ± 184	732 ± 301	2075 ± 797	952 ± 112	3568 ± 790
PHYtoRES	1505 ± 331	216 ± 19	1810 ± 461	509 ± 48	190 ± 45	529 ± 189	247 ± 27	922 ± 204
PHYtoHNF	934 ± 315	208 ± 58	1522 ± 800	318 ± 71	226 ± 88	232 ± 101	314 ± 59	282 ± 16
PHYtoMIC	927 ± 317	207 ± 59	1523 ± 1245	318 ± 71	276 ± 192	209 ± 108	316 ± 64	763 ± 249
PHYtoMES	1261 ± 498	171 ± 58	1588 ± 929	250 ± 60	83 ± 60	1795 ± 692	91 ± 58	1491 ± 564
PHYtoDET	643 ± 784	45 ± 85	812 ± 1581	158 ± 201	240 ± 364	62 ± 157	7 ± 35	311 ± 548
PHYtoDOC	206 ± 84	23 ± 10	221 ± 157	92 ± 19	19 ± 54	63 ± 89	25 ± 17	97 ± 97
HNFtoMIC	28 ± 32	2 ± 5	65 ± 134	0 ± 2	0 ± 2	50 ± 29	0 ± 0	46 ± 38
HNFtoMES	102 ± 55	30 ± 16	185 ± 183	44 ± 15	39 ± 14	0 ± 2	62 ± 15	36 ± 42
HNFtoRES	818 ± 277	149 ± 36	1092 ± 490	246 ± 60	182 ± 59	274 ± 113	204 ± 55	430 ± 146
HNFtoDET	124 ± 41	25 ± 8	217 ± 116	41 ± 9	34 ± 24	54 ± 34	40 ± 19	69 ± 33
HNFtoDOC	118 ± 39	23 ± 5	172 ± 95	37 ± 8	30 ± 23	43 ± 13	34 ± 6	64 ± 19
MICtoRES	823 ± 277	150 ± 36	1101 ± 717	246 ± 60	194 ± 68	273 ± 115	205 ± 55	644 ± 233
MICtoMES	131 ± 59	31 ± 14	259 ± 263	44 ± 13	55 ± 39	51 ± 29	62 ± 16	115 ± 46
MICtoDET	125 ± 41	25 ± 8	232 ± 219	41 ± 9	42 ± 45	54 ± 36	40 ± 19	107 ± 62
MICtoDOC	119 ± 38	23 ± 5	183 ± 229	37 ± 8	37 ± 34	43 ± 14	34 ± 7	96 ± 31
MEStoRES	723 ± 243	112 ± 24	884 ± 330	171 ± 47	115 ± 31	683 ± 222	120 ± 38	703 ± 223
MEStoDET	183 ± 61	27 ± 6	227 ± 96	42 ± 12	30 ± 14	281 ± 261	31 ± 6	197 ± 115
MEStoDOC	179 ± 60	27 ± 6	221 ± 95	42 ± 12	29 ± 14	198 ± 80	29 ± 8	177 ± 53
BACtoRES	637 ± 163	94 ± 13	835 ± 480	200 ± 25	125 ± 114	275 ± 92	103 ± 18	411 ± 117
BACtoHNF	24 ± 18	5 ± 4	46 ± 45	8 ± 8	4 ± 6	37 ± 27	14 ± 10	51 ± 29
BACtoMIC	19 ± 17	4 ± 4	51 ± 180	8 ± 8	3 ± 11	34 ± 45	14 ± 10	20 ± 32
DETtoHNF	223 ± 238	13 ± 23	124 ± 278	40 ± 57	62 ± 123	163 ± 77	8 ± 10	304 ± 186
DETtoMIC	217 ± 237	13 ± 23	99 ± 264	39 ± 57	56 ± 85	137 ± 70	7 ± 10	126 ± 147

Table 3.3. Cont.

	0605 Cycle1	0605 Cycle2	0605 Cycle3	0605 Cycle4	0605 Cycle5	0704 Cycle1	0704 Cycle2	0704 Cycle3
DETtoMES	299 ± 280	36 ± 32	142 ± 253	78 ± 79	103 ± 62	11 ± 53	74 ± 30	124 ± 212
DETtoDOC	46 ± 87	3 ± 8	63 ± 352	5 ± 16	25 ± 102	11 ± 26	5 ± 7	28 ± 56
DOCtoBAC	675 ± 169	101 ± 14	896 ± 577	214 ± 26	138 ± 157	345 ± 111	128 ± 19	465 ± 124
DETtoEXT	305 ± 117	64 ± 26	1185 ± 1061	126 ± 28	105 ± 252	139 ± 257	35 ± 53	131 ± 252
MEStoEXT	712 ± 243	104 ± 28	870 ± 367	163 ± 47	106 ± 65	676 ± 227	111 ± 42	690 ± 236

Figure 3.1. Model estimation of measured parameters. Each measurement was withheld from a model iteration in order to assess capabilities of predicting in situ measurements. Panels a, c, e, g, i show the MCMC predictions. Panels b, d, f, h, j show the L_2MN predictions. Panels a, b are the predictions of ^{14}C-PP when ^{14}C-PP is not used as a model input. Other measurements are protozoan grazing (c,d), mesozooplankton grazing (e,f), POC export (g,h) and bacterial production (i,j). In situ measurements are on the x-axis and model predictions are on the y-axis. Dotted line is the 1:1 line. Error bars are 95% confidence limits.

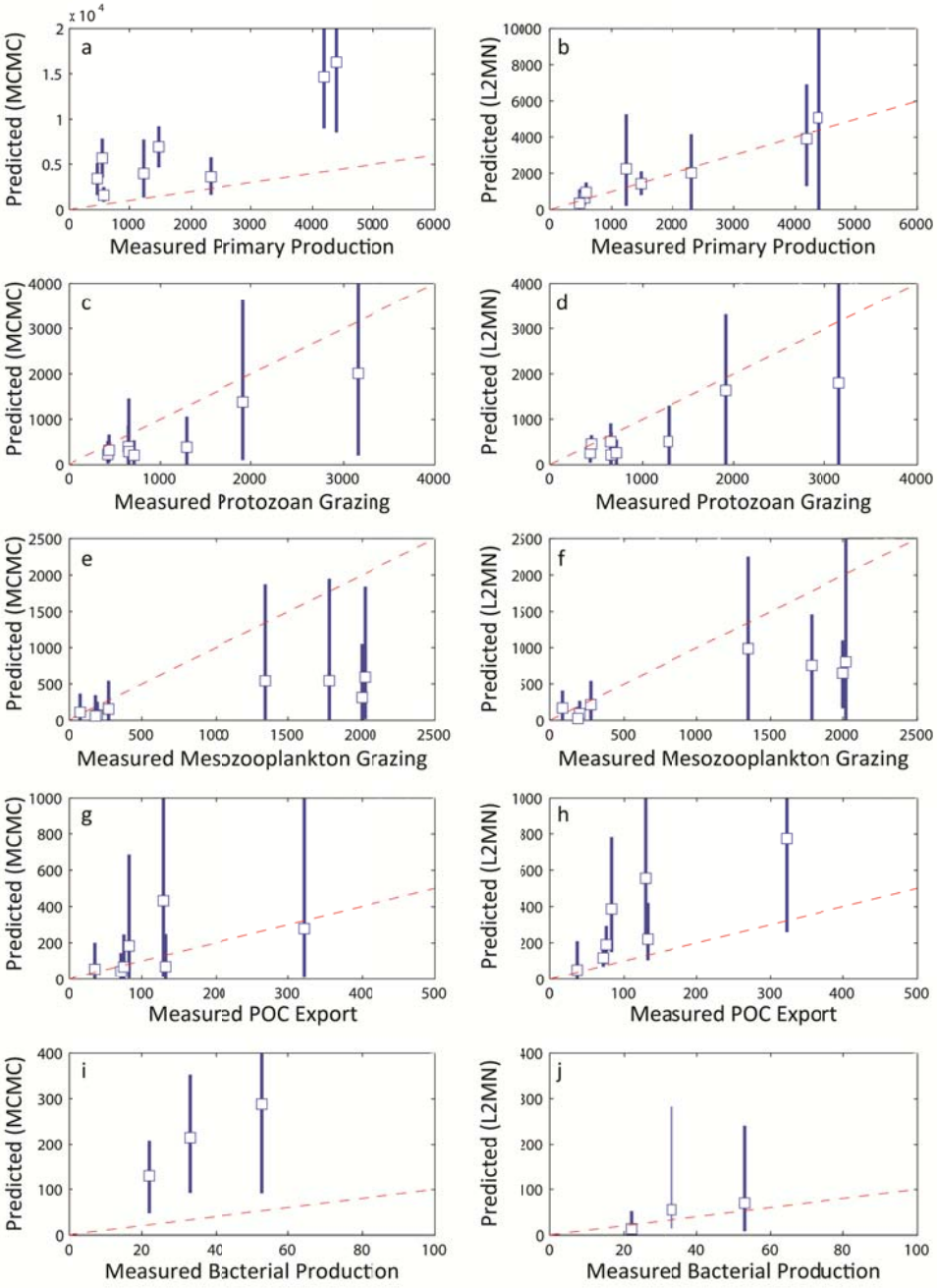
x 10^4
a
Predicted (MCMC)
Measured Primary Production
b
Predicted (L2MN)
Measured Primary Production
c
Predicted (MCMC)
Measured Protozoan Grazing
d
Predicted (L2MN)
Measured Protozoan Grazing
e
Predicted (MCMC)
Measured Mesozooplankton Grazing
f
Predicted (L2MN)
Measured Mesozooplankton Grazing
g
Predicted (MCMC)
Measured POC Export
h
Predicted (L2MN)
Measured POC Export
i
Predicted (MCMC)
Measured Bacterial Production
j
Predicted (L2MN)
Measured Bacterial Production

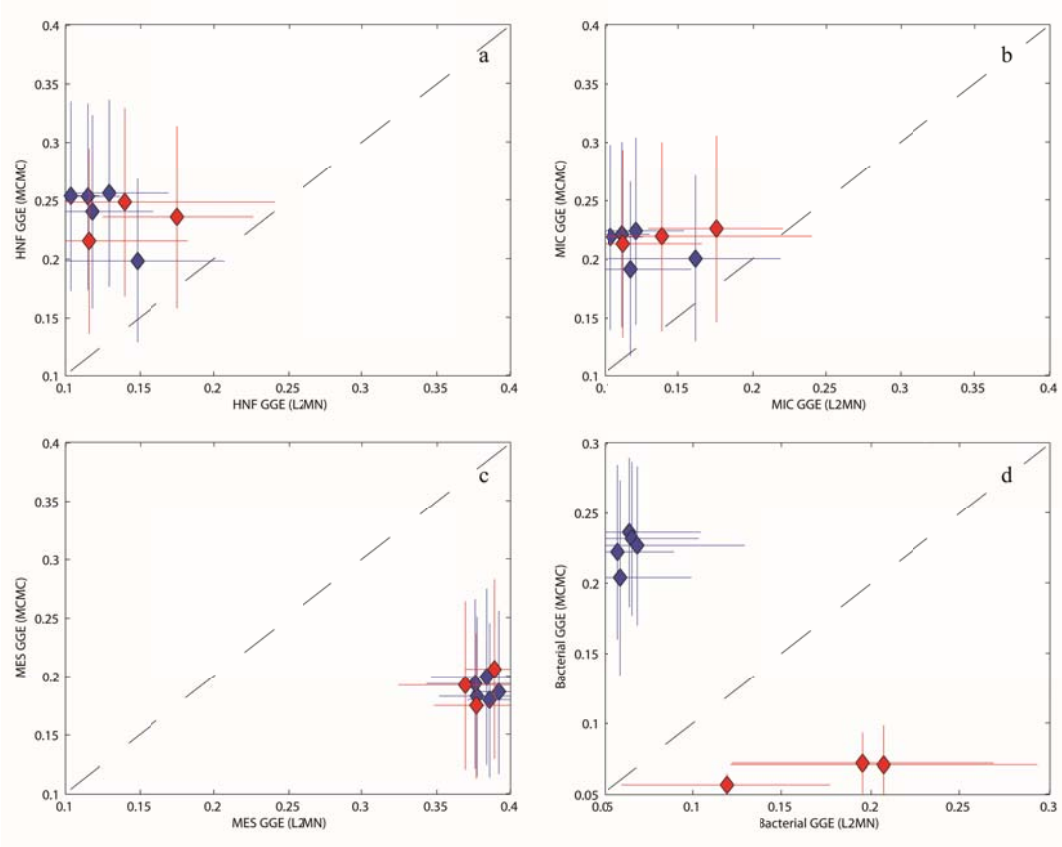

Figure 3.2. Model predictions of gross growth efficiencies of heterotrophic nanoflagellates (a), microzooplankton (b), mesozooplankton (c), and bacteria (d). In panels, L_2MN predictions are on the x-axis and MCMC predictions are on the y-axis. Error bars are ± one standard deviation. Red diamonds are from the P0704 cruise, blue are from the P0605 cruise. Dotted line is the 1:1 line.

Figure 3.3. Comparisons of the relative strengths of the different food web components by the MCMC (y-axis) and L_2MN (x-axis) models. Panel a is the classical food chain defined as the sum of flows reaching the mesozooplankton that derive from phytoplankton without processing by protozoans; these include grazing on living and detrital phytoplankton. Panel b is the multivorous food chain, defined as the flow of carbon to mesozooplankton derived from protozoa. Panel c is the microbial loop, defined as the sum of the respiration of bacteria and the proportion of protozoan respiration that is derived from bacterial production. Flows for all cycles are normalized to ^{14}C-PP. Red diamonds are from the P0704 cruise; blue are from the P0605 cruise. Dotted line is the 1:1 line.

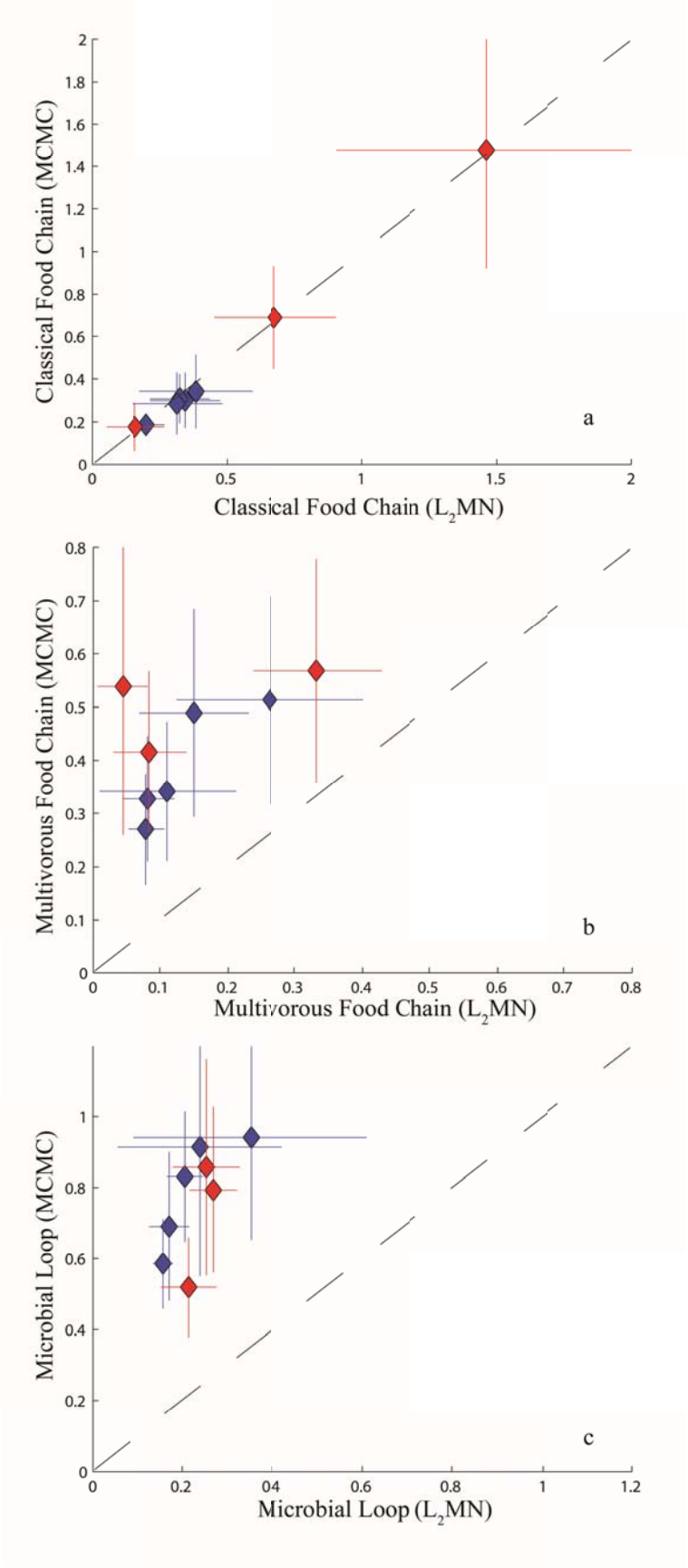
Classical Food Chain (MCMC)
Classical Food Chain (L2MN)
a
Multivorous Food Chain (MCMC)
Multivorous Food Chain (L2MN)
b
Microbial Loop (MCMC)
Microbial Loop (L2MN)
c

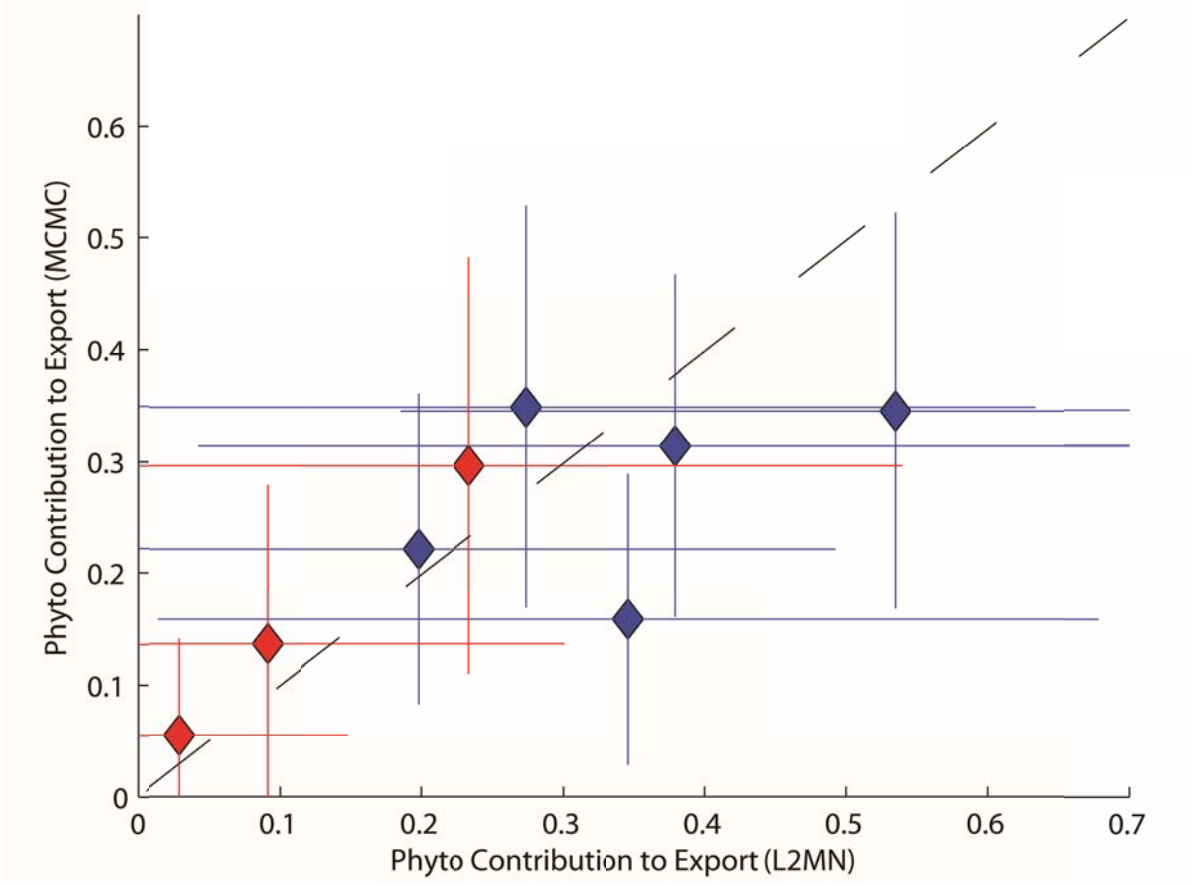

Figure 3.4. Fraction of vertical carbon export derived from gravitational sinking of detrital phytoplankton, as determined by the L_2MN (x-axis) and the MCMC methods (y-axis). Red diamonds are from the P0704 cruise; blue are from the P0605 cruise. Dotted line is the 1:1 line.

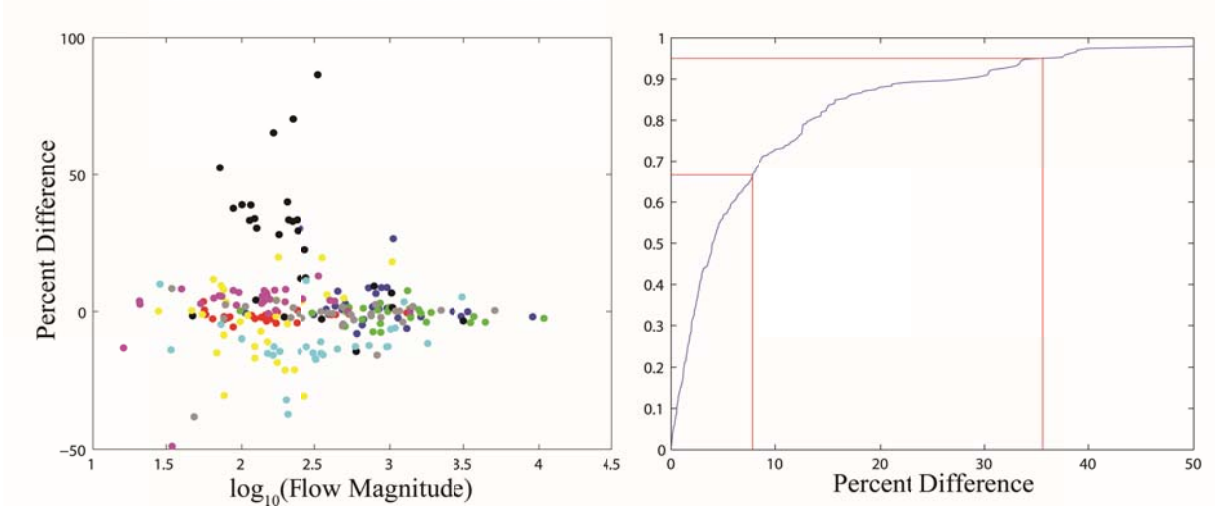

Figure 3.5. Comparison of steady state (SS) and non-steady state (NSS) models. (a) Percent difference between the SS model (in which all compartments were held in steady-state) and the NSS model (in which phytoplankton were assigned their measured rates of change and all other living compartments were assumed to have rates of change of 0±10% biomass d^{-1}). Y-axis is % difference calculated for each flow as $(Flow_{SS}-Flow_{NSS})/Flow_{NSS}$. X-axis is the magnitude of the NSS flow (log mg C m^{-2} d^{-1}). P0605-1 (blue), P0605-2 (red), P0605-3 (green), P0605-4 (black), P0605-5 (yellow), P0704-1 (cyan), P0704-2 (magenta), P0704-3 (gray). Cycles for which phytoplankton were increasing (P0605-4) and decreasing (P0704-1) show the highest percent errors. The flow from phytoplankton to detritus for P0605-4 is is off scale and not shown (3.5 times higher in the SS model than in the NSS model). Panel b shows the cumulative distribution function for percent difference; 67% of the flows were over or underestimated by 7.7%, while 5% were off by more than 35.5%.

Figure 3.6. Comparison of the uncertainties due to under-determinacy of the inverse model and to measurement errors. X-axes represent the coefficients of variation (CV) due to underdeterminacy; y-axes are the CVs due to measurement error. Panel a is color coded for each cycle: P0605-1 (blue), P0605-2 (red), P0605-3 (green), P0605-4 (black), P0605-5 (yellow), P0704-1 (cyan), P0704-2 (magenta), P0704-3 (gray). The flows where measurement errors were more significant than underdeterminacy were typically direct measurements or closely related to in situ measurements, including GPP (x), mesozooplankton grazing (o), phytoplankton to detritus (squares), bacterial respiration (diamonds), bacterial DOC uptake (asterisks), and vertical carbon flux (stars). Panel b shows the same data, but highlighting fluxes to and from detritus. Red is flux from detritus. Blue is flux to detritus. Green is detritus export (vertical POC flux). Dashed lines are the 1:1 line.

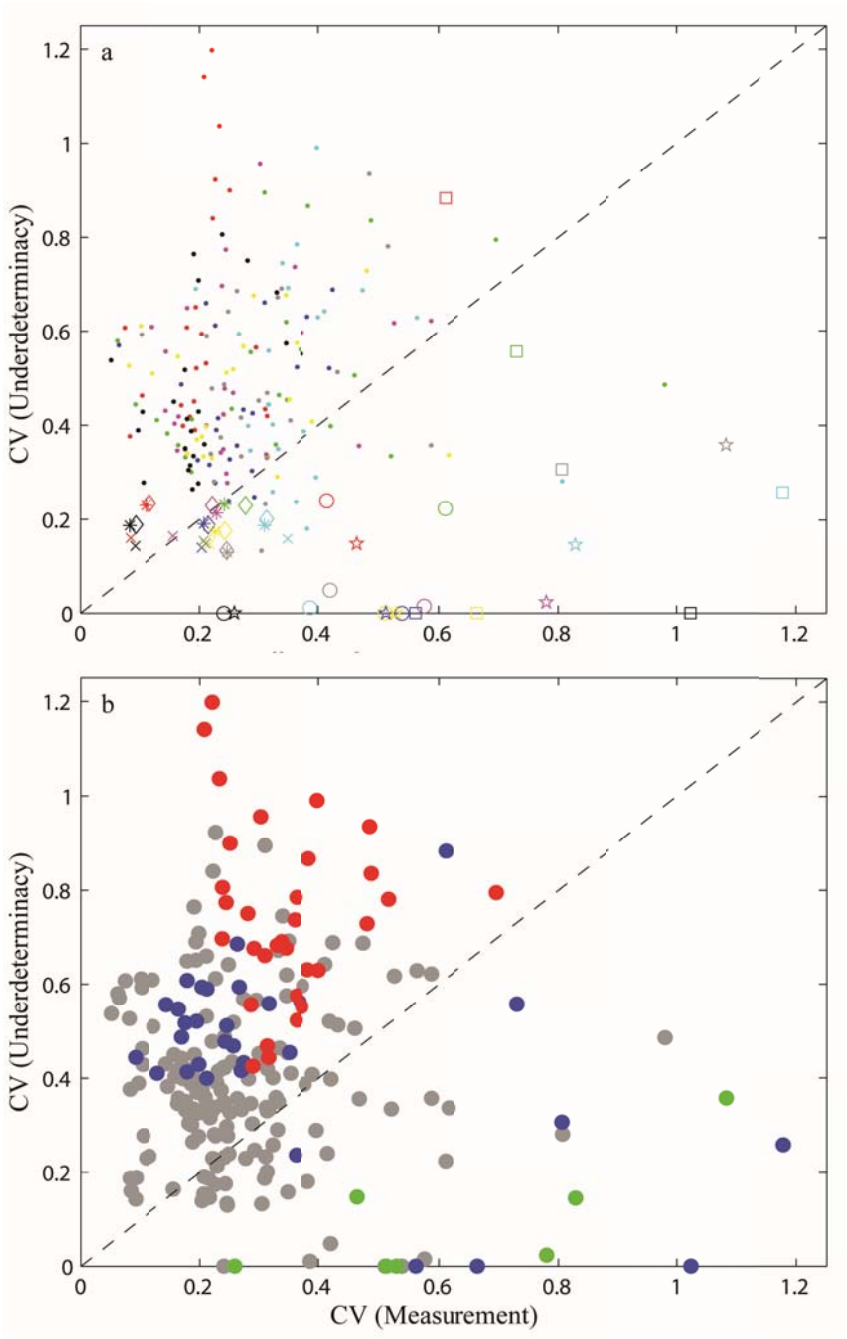
a
b
CV (Underdeterminacy)
CV (Underdeterminacy)
CV (Measurement)
0
0.2
0.4
0.6
0.8
1
1.2

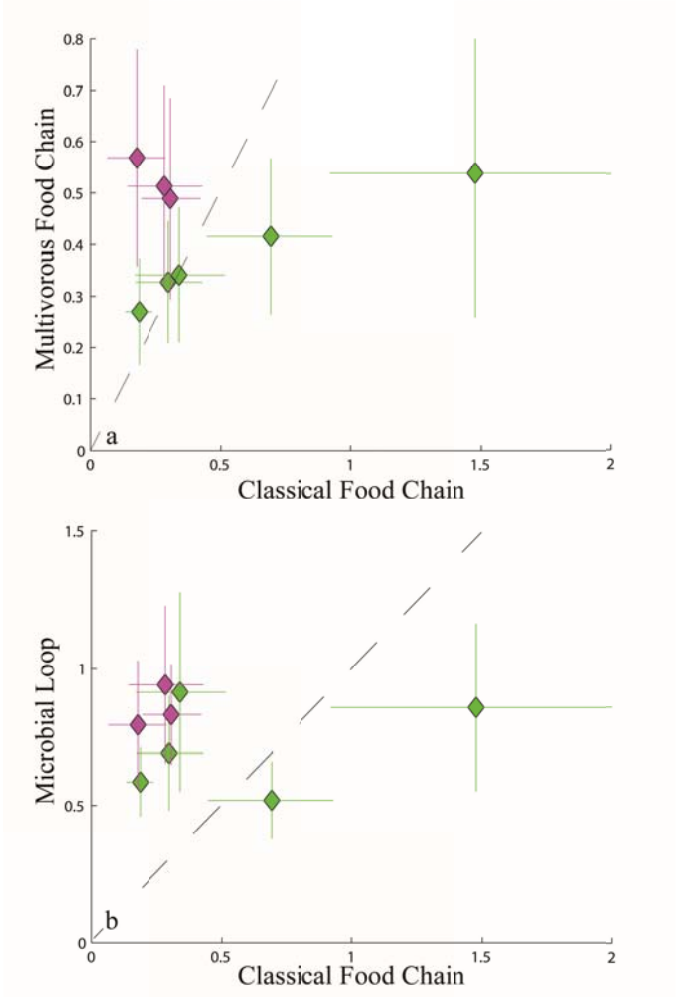

Figure 3.7. Comparison of food webs. Panel a compares the multivorous food chain fluxes (y-axis) to the classical food chain fluxes (x-axis). Panel b compares the microbial loop (y-axis) to the classical food chain (x-axis). All food web fluxes are normalized to ^{14}C-PP. Magenta diamonds are the offshore cycles and green diamonds are the nearshore (upwelling influenced) cycles. Errorbars are ±1 SD. Dashed line is the 1:1 line.

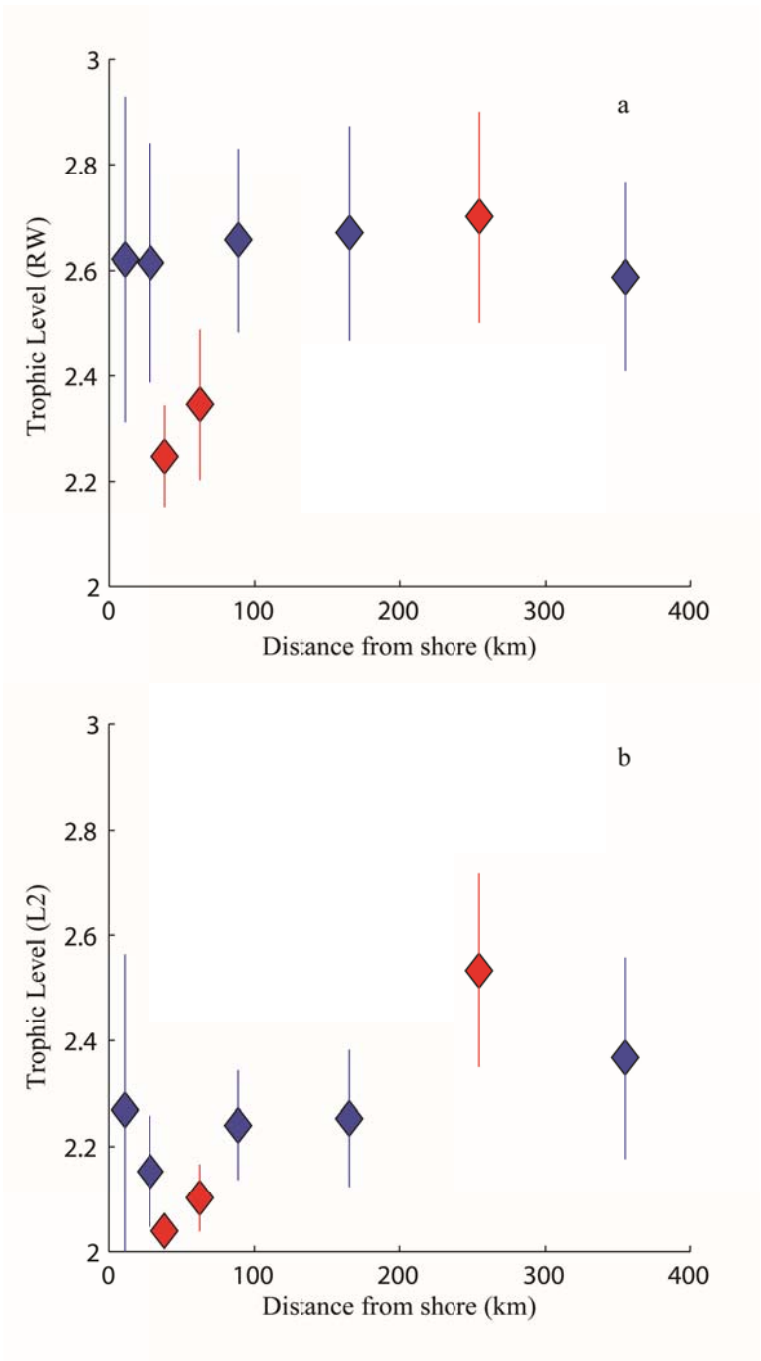

Figure 3.8. Mesozooplankton trophic levels predicted by the MCMC (Panel a) and the L_2MN (panel B) solution approaches. X-axis is the initial distance from shore. Blue diamonds are P0605 and red diamonds are P0704. Errorbars are ±1 SD.

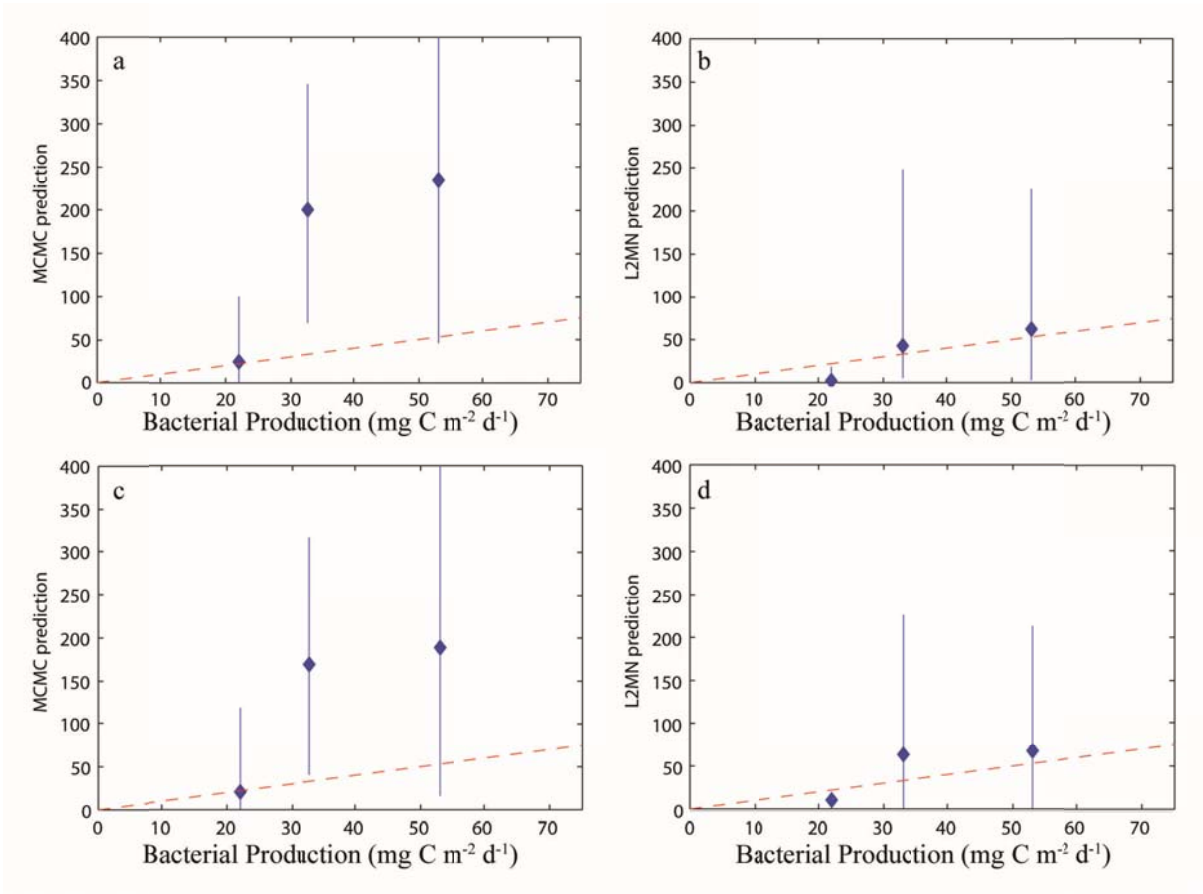

Figure 3.9. Model predictions of bacterial production with assumed DOC accumulation. Figures are comparable to Fig. 1i,j. Panels a,b assume DOC accumulation in the euphotic zone at a rate of 1% d^{-1}; panels c,d assume accumulation rates of 2% d^{-1}. Panels a,c are MCMC predictions, while panels b,d are L_2MN predictions.

APPENDIX 3.1 – Model equalities (Ax=b) and inequalities (Gx≥h)

Equalities:

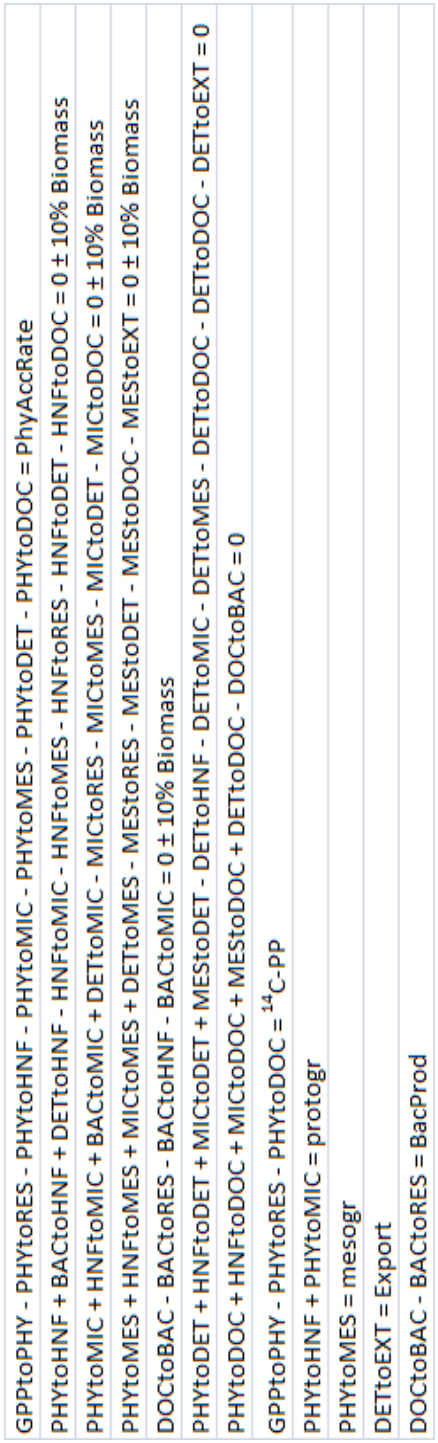

Inequalities:

Rate	Pop	Minimum	Maximum
GGE	HNF	10%[1]	40%[1]
	MIC	10%[1]	40%[1]
	MES*	10%[1]*	40%[1]*
	BAC	5%[2]	30%[2]
BasalResp	MES	$2.314*10^{(\log(9.1)+\log(2)*(T-25)/10}*BioM$ [3]	
Assim. Eff.	HNF	50%[4]	90%[4]
	MIC	50%[4]	90%[4]
	MES	50%[4]	90%[4]
Respiration	PHY	10%	55%[5]
	HNF	20% ingestion[6]	
	MIC	20% ingestion[6]	
	MES	20% ingestion[6]	
	BAC	20% ingestion[6]	
Excretion	DIA	2% NPP[6,7]	55% NPP[6,7]
	AUT	2% NPP[6,7]	55% NPP[6,7]
	CYA	2% NPP[6,7]	55% NPP[6,7]
	HNF	10% ingestion[8]	100% respiration[9]
	MIC	10% ingestion[8]	100% respiration[9]
	MES	10% ingestion[8]	100% respiration[9]
Max Ingestion	HNF		$24*10^{\log(0.6509)+\log(2.8)*(T-20)/10}*BioM$[10]
	MIC		$24*10^{\log(0.2375)+\log(2.8)*(T-20)/10}*BioM$[10]
	MES		$24*10^{\log(0.1816)+\log(2.8)*(T-20)/10}*BioM$[10]
Max Clearance Rate	HNF		$24*10^{\log(203030)+\log(2.8)*(T-20)/10}*BioV$[10]
	MIC		$24*10^{\log(176830)+\log(2.8)*(T-20)/10}*BioV$[10]
	MES		$24*10^{\log(112780)+\log(2.8)*(T-20)/10}*BioV$[10]
GPP	PHY	140%NPP[11]	260%NPP[11]
NPP	PHY		3*PhyBiomass[12]

[1]Straile (1997)

*Because metazooplankton have a basal respiration rate in addition to their activity-dependent metabolic cost, we have implemented a basal metabolic rate that must be paid first, and constrained their GGE such that only 10-40% of the remainder of their

intake can contribute to production. Thus the true GGE of the metazooplankton in our model will range from slightly less than 10% to slightly less than 40%.

[2] Del Georgio and Cole (2000)

[3]Makarieva et al. (2008). An allometric and temperature specific basal metabolic relationship for copepods and krill was used to set a minimum metabolic rate for metazooplankton that is in addition to their ingestion rate specific constraints.

[4] Conover (1966)

[5] Falkowski et al. (1985)

[6]Vézina et al. (2000)

[7]Baines and Pace (1991)

[8] Vézina and Pace (1994)

[9] Vézina and Platt (1988)

[10] Hansen et al. (1997). To ensure that we used maximal clearance and ingestion rates and because grazers are often believed to aggregate at regions of high prey density, the maximum concentrations of prey and predator encountered on each cycle were utilized in setting maximum clearance and ingestion rates. Since epifluorescence microscopy often significantly underestimates ciliate concentrations and all dinoflagellates (both pigmented and aplastidic) are likely phagotrophic, we included autotrohic dinoflagellate biomass in the maximum microzooplankton biomass figures used for calculating clearance and ingestion rates. Biomass was converted to biovolume using conversion factors of 200 and 130 mg C cm^{-3} for heterotrophic nanoflagellates and microzooplankton, respectively (Menden-Deuer and Lessard 2000) and a biomass to biovolume relationship determined for mesozooplankton in the CCE (Lavaniegos and Ohman 2007).

[11]Bender et al. (1999), Laws et al. (2000), Hashimoto et al. (2005)

[12] Production rate based on a specific growth rate of 1.4 d^{-1} or two doublings per day. (Calbet and Landry 2004)

APPENDIX 3.2: L_2 minimum norm (L_2MN) solution method

The typical L_2MN method, as originally implemented by Vézina and Platt (1988), assumes that the measurement and steady-state equations are exact and then calculates the solution that minimizes the L_2 norm. However, as this method tends to zero out particular values and does not generate any confidence intervals, we instead adopted an ensemble L_2MN approach similar to the L_2MN Monte Carlo method used by Stukel et al. (2010). For each model input (measured rates and biomasses and steady-state equalities), we generated a normal distribution from the experimentally determined means (zero for unmeasured steady-state equalities) and variances. Inputs were then chosen randomly from these distributions to allow for simultaneous variation of each input. After inputs were chosen, the L_2MN solution was computed as explained below. For each cycle and numerical experiment we solved the L_2MN for 10,000 independent input parameter sets and determined our L_2MN solution as the mean of these 10,000 sets, while also calculating 95% confidence intervals for all ecosystem flows.

Once the input parameters had been randomly selected, the L_2MN solution was calculated using the algorithm of Vézina and Platt (1988) as implemented in MATLAB by Jackson et al. (2001). This algorithm is designed to find the solution vector that simultaneously solves the system of equations $A\mathbf{x}=b$ and $G\mathbf{x}\geq h$ while minimizing the L_2 norms of $\mathbf{x}$ (and $A\mathbf{x}-b$ if the system of equations cannot be solved exactly). This method begins by using the singular value decomposition (SVD) to decompose the A matrix into the matrices U, L, and V, such that $A=ULV^*$. If k is the

rank of the problem, the first k rows of U and the first k columns of V* were used to find the simplest solution (r_1) that satisfies the equality constraints A**x**=b. The remaining columns of V* then form an orthonormal basis of vectors (V_p) that can be added or subtracted to r_1, while still satisfying the equality Ax=b. V_p is then used to find the solution that minimizes the L_2 norm while satisfying the inequality constraints G**x**≥h, which include constraints requiring that each flow be positive. When the system of equations is solvable (i.e. there are no inconsistencies amongst the equalities and inequalities) a full rank solution can be used (k = size of b), and the residual error will be zero, so the algorithm will minimize the complexity of the solution (minimize the L_2 norm of **x**). Often inconsistencies existed in the data (e.g. when the randomization process led to grazing rate inputs that were higher than the maximum clearance rates or when the difference of growth and grazing was less than the rate of change of the phytoplankton population). In such cases we followed the method of Olsen et al. (2006) and chose the highest rank solution that could generate an answer that satisfied the inequality constraints. When the rank was reduced, the algorithm simultaneously minimized the L_2 norms of **x** and A**x**-b.

APPENDIX 3.3 – The Markov Chain Monte Carlo (MCMC) solution method

The L_2MN solution method selects a single solution vector from among the infinite set of solutions to the under-determined inverse ecosystem problem, but there is no a priori reason to suggest that it selects a solution that accurately depicts the ways in which an ecosystem is constructed. Lacking evidence that any particular cost function can be used to approximate ecosystem structure, Kones et al. (2006; 2009) have suggested fully sampling the allowable solution space and suggest that the most likely ecosystem state may be the mean of all possible ecosystem states.

To calculate such a maximum likelihood solution, we used the MCMC method of Kones et al. (2009). We began with the solution vector from the L_2MN method, and utilized a random combination of the orthonormal basis V_p to generate a new solution that also satisfied the equality constraints. The use of the mirror algorithm (Van Den Meersche et al. 2009) allowed us to ensure that each new solution also satisfied the inequality constraints. It works by computing the planes in an n-dimensional hyperspace that describe the solution space allowed by the inequality constraints. When the line connecting the original solution to the new solution crossed a hyperplane, it was instead reflected by the hyperplane, thus ensuring that all solutions satisfied the inequalities G$\mathbf{x}\geq$h.

When the rank of the problem is full each iteration of the random walk yields a new solution to the problem. However, when the rank of the solution is not full, due to inconsistencies in the system of equations, a residual error (A$\mathbf{x}$-b) exists. In such cases the probability of accepting any new iteration (x_{n+1}) is calculated as:

$$p(\text{Accepting } x_{n+1}) = \frac{e^{\frac{-1}{2}(Ax_{n+1}-b)'W^2(Ax_{n+1}-b)}}{e^{\frac{-1}{2}(Ax_n-b)'W^2(Ax_n-b)}}$$

where W is the weights associated with the equality constraints A**x**=b (the inverse of the standard deviations of the equalities).

After initiating the MCMC algorithm with the L_2MN solution, we used a burn-in period of 20 iterations during which the solutions were not kept, but were simply used to select a randomized starting point for the solution. A long jump length of 2000 was utilized to ensure that each solution vector was independent of the vector preceding it. After the burn-in period, a total of 100 iterations were carried out to characterize the solution space. For each cycle and numerical experiment we ran the MCMC method 100 different times using randomly selected input parameters (as we did for the L_2MN method). This thus generated a total of 10,000 solution vectors that account for both measurement error and under-determinacy error. We calculated the mean of these 10,000 solution vectors as our MCMC solution and also used them to generate confidence intervals for all model outputs.

References

ALVAREZ-SALGADO, X. A., M. D. DOVAL, A. V. BORGES, I. JOINT, M. FRANKIGNOULLE, E. M. S. WOODWARD, and F. G. FIGUEIRAS. 2001. Off-shelf fluxes of labile materials by an upwelling filament in the NW Iberian Upwelling System. Prog. Oceanogr. **51:** 321-337.

BAINES, S. B., and M. L. PACE. 1991. The production of dissolved organic matter by phytoplankton and its importance to bacteria: Patterns across marine and freshwater systems. Limnol. Oceanogr. **36:** 1078-1090.

BENDER, M., J. ORCHARDO, M. L. DICKSON, R. BARBER, and S. LINDLEY. 1999. In vitro O_2 fluxes compared with ^{14}C production and other rate terms during the JGOFS Equatorial Pacific experiment. Deep-Sea Res. I **46:** 637-654.

CALBET, A., and M. R. LANDRY. 2004. Phytoplankton growth, microzooplankton grazing, and carbon cycling in marine systems. Limnol. Oceanogr. **49:** 51-57.

CONOVER, R. J. 1966. Assimilation of organic matter by zooplankton. Limnol. Oceanogr. **11:** 338-345.

DANIELS, R. M., T. L. RICHARDSON, and H. W. DUCKLOW. 2006. Food web structure and biogeochemical processes during oceanic phytoplankton blooms: An inverse model analysis. Deep-Sea Res. II **53:** 532-554.

DEL GEORGIO, P. A., and J. J. COLE. 2000. Bacterial energetics and growth efficiency, p. 289-325. *In* D. L. Kirchman [ed.], Microbial Ecology of the Oceans. Wiley-Liss, Inc.

DUCKLOW, H. 2000. Bacterial Production and Biomass in the Oceans, p. 85-120. *In* D. L. Kirchman [ed.], Microbial Ecology of the Oceans. Wiley-Liss.

FALKOWSKI, P. G., Z. DUBINSKY, and K. WYMAN. 1985. Growth-irradiance relationships in phytoplankton. Limnol. Oceanogr. **30:** 311-321.

HANSEN, P. J., P. K. BJORNSEN, and B. W. HANSEN. 1997. Zooplankton grazing and growth: Scaling within the 2-2,000-mu m body size range. Limnol. Oceanogr. **42:** 687-704.

HASHIMOTO, S., N. HORIMOTO, Y. YAMAGUCHI, T. ISHIMARU, and T. SAINO. 2005. Relationship between net and gross primary production in the Sagami Bay, Japan. Limnol. Oceanogr. **50:** 1830-1835.

JACKSON, G. A., and P. M. ELDRIDGE. 1992. Food web analysis of a planktonic system off Southern California. Prog. Oceanogr. **30:** 223-251.

JACKSON, G. A., N. NIQUIL, A. BURD, and T. L. RICHARDSON. 2001. Ecosystem Modeling Group Software, Inverse model code. Texas A&M Univ. http://oceanz.tamu.edu/~ecomodel/Software/invmodel/invmodel.html.

KONES, J. K., K. SOETAERT, D. VAN OEVELEN, and J. O. OWINO. 2009. Are network indices robust indicators of food web functioning? A Monte Carlo approach. Ecol. Model. **220:** 370-382.

KONES, J. K., K. SOETAERT, D. VAN OEVELEN, J. O. OWINO, and K. MAVUTI. 2006. Gaining insight into food webs reconstructed by the inverse method. J. Mar. Syst. **60:** 153-166.

LANDRY, M. R., and R. P. HASSETT. 1982. Estimating the grazing impact of marine microzooplankton. Mar. Biol. **67:** 283-288.

LANDRY, M. R., M. D. OHMAN, M. R. STUKEL, and K. TSYRKLEVICH. 2009. Lagrangian studies of phytoplankton growth and grazing relationships in a coastal upwelling ecosystem off Southern California. Prog. Oceanogr. **83:** 208-216.

LAVANIEGOS, B. E., and M. D. OHMAN. 2007. Coherence of long-term variations of zooplankton in two sectors of the California Current System. Prog. Oceanogr. **75:** 42-69.

LAWS, E. A., M. R. LANDRY, R. T. BARBER, L. CAMPBELL, M. L. DICKSON, and J. MARRA. 2000. Carbon cycling in primary production bottle incubations: Inferences from grazing experiments and photosynthetic studies using ^{14}C and ^{18}O in the Arabian Sea. Deep-Sea Res. II **47:** 1339-1352.

MAKARIEVA, A. M., V. G. GORSHKOV, B. L. LI, S. L. CHOWN, P. B. REICH, and V. M. GAVRILOV. 2008. Mean mass-specific metabolic rates are strikingly similar across life's major domains: Evidence for life's metabolic optimum. Proc. Natl. Acad. Sci. U. S. A. **105:** 16994-16999.

MENDEN-DEUER, S., and E. J. LESSARD. 2000. Carbon to volume relationships for dinoflagellates, diatoms, and other protist plankton. Limnol. Oceanogr. **45:** 569-579.

OLSEN, Y., S. AGUSTI, T. ANDERSEN, C. M. DUARTE, J. M. GASOL, I. GISMERVIK, A. S. HEISKANEN, E. HOELL, P. KUUPPO, R. LIGNELL, H. REINERTSEN, U. SOMMER, H. STIBOR, T. TAMMINEN, O. VADSTEIN, O. VAQUE, and M. VIDAL. 2006. A

comparative study of responses in planktonic food web structure and function in contrasting European coastal waters exposed to experimental nutrient addition. Limnol. Oceanogr. **51:** 488-503.

SOETAERT, K., and D. VAN OEVELEN. 2009. Modeling food web interactions in benthic deep-sea ecosystems: A practical guide. Oceanography **22:** 128-143.

STRAILE, D. 1997. Gross growth efficiencies of protozoan and metazoan zooplankton and their dependence on food concentration, predator-prey weight ratio, and taxonomic group. Limnol. Oceanogr. **42:** 1375-1385.

STUKEL, M. R., and M. R. LANDRY. 2010. Contribution of picophytoplankton to carbon export in the equatorial Pacific: A re-assessment of food-web flux inferences from inverse models. Limnol. Oceanogr. **55:** 2669-2685.

STUKEL, M. R., M. R. LANDRY, C. R. BENITEZ-NELSON, and R. GOERICKE. submitted. Trophic cycling and carbon export relationships in the California Current Ecosystem. Limnol. Oceanogr.

VAN DEN MEERSCHE, K., K. SOETAERT, and D. VAN OEVELEN. 2009. xSample(): An R function for sampling linear inverse problems. Journal of Statistal Software, Code Snippets **30:** 1-15.

VAN OEVELEN, D., K. VAN DEN MEERSCHE, F. J. R. MEYSMAN, K. SOETAERT, J. J. MIDDELBURG, and A. F. VEZINA. 2010. Quantifying food web flows using linear inverse models. Ecosystems **13:** 32-45.

VENRICK, E. L. 2002. Floral patterns in the California Current System off southern California: 1990-1996. J. Mar. Res. **60:** 171-189.

VÉZINA, A. F., F. BERREVILLE, and S. LOZA. 2004. Inverse reconstructions of ecosystem flows in investigating regime shifts: impact of the choice of objective function. Prog. Oceanogr. **60:** 321-341.

VÉZINA, A. F., and M. L. PACE. 1994. An inverse model analysis of planktonic food webs in experimental lakes. Can. J. Fish. Aquat. Sci. **51:** 2034-2044.

VÉZINA, A. F., and M. PAHLOW. 2003. Reconstruction of ecosystem flows using inverse methods: how well do they work? J. Mar. Syst. **40:** 55-77.

VÉZINA, A. F., and T. PLATT. 1988. Food web dynamics in the ocean .1. Best estimates of flow networks using inverse methods. Mar. Ecol. Prog. Ser. **42:** 269-287.

VEZINA, A. F., C. SAVENKOFF, S. ROY, B. KLEIN, R. RIVKIN, J. C. THERRIAULT, and L. LEGENDRE. 2000. Export of biogenic carbon and structure and dynamics of the pelagic food web in the Gulf of St. Lawrence Part 2. Inverse analysis. Deep-Sea Res. II **47:** 609-635.

WETZ, M. S., and P. A. WHEELER. 2004. Response of bacteria to simulated upwelling phytoplankton blooms. Mar. Ecol. Prog. Ser. **272:** 49-57.

CHAPTER 4

Mesozooplankton contribution to vertical carbon export in a coastal upwelling biome

ABSTRACT

Mesozooplankton can directly impact global biogeochemical cycles by repackaging particulate organic carbon (POC) into dense, rapidly sinking fecal pellets and by undertaking vertical migrations that transport carbon and nutrients to depth. We assessed the contribution of mesozooplankton to vertical flux in the California Current Ecosystem, a productive but spatiotemporally variable coastal upwelling biome, during cruises in April 2007 and October 2008. The use of sediment traps and ^{234}Th disequilibrium measurements allowed us to accurately assess the total passive flux of sinking POC, while pigment analyses and microscopic enumeration of sediment trap samples provided estimates of total fecal carbon transport. Identification of mesozooplankton in paired day-night, vertically-stratified plankton tows allowed calculation of the active transport of carbon by the dominant taxa of vertically migrating mesozooplankton (particularly copepods and euphausiids). Across the nine ecosystem states encountered on the cruises, recognizable fecal pellet mass flux ranged from 3.5 to 135.2 mg C m^{-2} d^{-1} (4 to 119% of total passive flux) at the 100-m depth horizon. Phaeopigment concentrations in sediment traps suggested

that the contribution of herbivorous fecal material may have ranged from 1.3 to 53.6 mg C m^{-2} d^{-1} or from 4.3 to 137 mg C m^{-2} d^{-1}, depending on assumptions about degradation of pigments in mesozooplankton guts. The active transport of carbon by migratory mesozooplankton taxa ranged from 2.4 to 42.8 mg C m^{-2} d^{-1}. Inter-cruise comparisons suggest that fecal pellets contributed a much greater portion of export during the productive spring cruise, when fecal material may have been responsible for 100% source of sinking material, than during the fall cruise. During the fall cruise a gradient was observed with carbon export in productive water parcels driven by a large contribution of fecal pellets, but with vertical flux in less productive regions containing an increasing portion of marine snow and small unidentifiable particles.

INTRODUCTION

The "biological pump," a critical component of global biogeochemical cycles, is responsible for transporting the carbon and nitrogen fixed by phytoplankton in the euphotic zone to the deep ocean. While autotrophs govern the fixation of carbon, however, the flux of carbon to depth is often driven by interactions of multiple trophic levels. The relative importance of phytoplankton production, aggregation processes (Alldredge and Gotschalk 1989; Jackson et al. 2005), mineral ballasting (Armstrong et al. 2002), and mesozooplankton grazing (Buitenhuis et al. 2006) on vertical carbon flux are still hotly debated and are likely regionally and spatially variable. While solid arguments exist supporting the importance of each, the difficulty of directly measuring their effects *in situ* has caused investigators to try to compare contributions based on

models, which may support one theory but do not exclude the others. Clearly, experimental evidence is needed to assess the nature of sinking material.

Within the California Current Ecosystem (CCE), Stukel et al. (submitted) has suggested that the production of fecal material by mesozooplankton is sufficient to account for all variability in vertical carbon flux. Mesozooplankton can mediate biogeochemically-relevant processes in many ways, and thus play crucial roles in the global carbon and nitrogen cycles. By packaging organic matter into dense, rapidly sinking fecal pellets, they can efficiently transport carbon out of the surface ocean on passively sinking particles (Turner 2002). Diel vertically migrating (DVM) mesozooplankton can also actively transport carbon and nitrogen to depth when they feed at the surface at night but descend during the day to respire, excrete, and sometimes die at depth (Longhurst et al. 1990; Steinberg et al. 2000; Al-Mutairi and Landry 2001). At times, mesozooplankton are also able to decrease carbon export rates by exerting top-down pressure on phytoplankton (Goericke 2002; Olli et al. 2007; Landry et al. 2009) and consuming sinking particles (Wilson et al. 2010).

In this study we attempt to directly characterize the importance of mesozooplankton in both active and passive transport of carbon out of the surface ocean during two cruises of the CCE Long-Term Ecological Research (LTER) program in April 2007 and October 2008. We show that across the wide range of environmental conditions sampled identifiable fecal pellets were responsible for 35% of passive carbon export at 100-m depth, although pigment analyses suggested that the total sinking flux of fecal material may have been even higher. We also show that on

average mesozooplankton contribute an additional 19 mg C m^{-2} d^{-1} that is not assessed by typical carbon export measurements (e.g. sediment traps and radionuclide disequilibrium techniques).

METHODS

Cruises and sampling plans – Data for this study come from two cruises of the California Current Ecosystem (CCE) Long-Term Ecological Research (LTER) program conducted during April 2007 (CCE-P0704) and October 2008 (CCE-P0810). During these cruises, water parcels were identified using satellite images of sea surface temperature and chlorophyll, together with Moving Vessel Profiler site surveys, and tagged with a surface drifter drogued at 15-m (Fig. 1). A simultaneously deployed and identically drogued drift array with attached sediment traps (at 1-2 depths) allowed the collection of sinking particulate matter. Paired day-night deployments of a $1m^2$, 202-μm Multiple Opening and Closing Net with an Environmental Sensing System (MOCNESS) collected depth-stratified mesozooplankton samples over the upper 450 m of the water column at the location of the surface drifter. These samples were later enumerated by Zooscan (as described below) and grouped into broad taxononomic and size classes. Oblique bongo tows (0.71-m diameter, 202-μm mesh) were also used twice per day to collect organisms for determination of size-fractionated dry weights and grazing rates of the mesozooplankton community. Size-fractionated dry weights were converted to carbon biomass using the dry weight to carbon relationships of Landry et al. (2001).

^{234}Th export measurements – ^{234}Th deficiency was determined from 4-L samples taken at 8-10 depths per cast of a CTD Niskin rosette, following established small-volume procedures (Benitez-Nelson et al. 2001b; Buesseler et al. 2001; Pike et al. 2005). Immediately after collection, samples were acidified to a pH of ~2 with concentrated HNO_3 and spiked with ^{230}Th (1 mL at 10 dpm mL^{-1}). Four hours later, NH_4OH was added to adjust to a pH of ~9, and 100 μL each of $KMnO_4$ (7.5 g L^{-1}) and $MnCl_2$ (33 g L^{-1}) were added. Samples were shaken and allowed to equilibrate for >8 hours as the Th co-precipitated with MnO_2. Precipitates were vacuum filtered under high-pressure onto 25-mm quartz microfiber filters and mounted into RISO cups. Samples were counted ashore with a low-level RISO beta counter in the Benitez-Nelson lab at the University of South Carolina. After >6 half-lives had passed, they were again counted to establish background beta emission levels. Filtration yields were calculated by Inductively Coupled Plasma Mass Spectrometry (at the WHOI Analytical Facility) after addition of a gravimetrically measured aliquot of ^{229}Th (99.5 dpm) and column chromatography in AG1-X8 100-200 mesh chloride form resin to purify the Th isotopes. Recoveries averaged 86%. ^{238}U was assumed to co-vary with salinity and calculated from the equation: ^{238}U (dpm L^{-1}) = 0.0686•salinity•density (Chen et al. 1986). Deficiency was calculated as the difference between ^{238}U and ^{234}Th. ^{234}Th export was determined using a one-dimension steady-state model ($E = \lambda_{Th} (A_U - A_{Th})$) and trapezoidal vertical integration. Although this steady-state model oversimplifies the complex processes affecting particulate and dissolved Th cycling in

the ocean euphotic zone, it closely matched the ^{234}Th flux results found in sediment traps for 8 out of the 9 cycles assessed (Fig. 2).

^{234}Th export was converted to vertical carbon flux by multiplying by experimentally-determined C:^{234}Th ratios. Particulate samples for the determination of the C:Th ratio were collected using two independent methods, sediment traps and *in situ* pumps. C:Th samples were routinely collected at a depth horizon of 100 m and they were also collected from a depth just below the base of the euphotic zone on the P0810 cruise. Sediment trap C:Th samples were collected as discussed below. *In situ* pump samples were collected using a McLane WTS-LV pump with pre-filters to size-fractionate collected particles. On the P0704 cruise, >20-μm particles were used for calculating the C:^{234}Th ratio; on the P0810 cruise >50-μm particles were used. In each case, 300-L of seawater were filtered through a Nitex filter, which was then rinsed onto a 25-mm quartz microfiber filter. Quartz microfiber filters for the C:^{234}Th ratio were counted on land similarly to the water-column ^{234}Th samples. After background count, filters were combusted in the Costech 4010 elemental combustion analyzer in the SIO Analytical Laboratory. Prior to combustion, filters from the P0810 cruise were acidified to remove inorganic carbon. Filters from the P0704 cruise were not acidified.

Sediment trap deployment and analyses – VERTEX-style drifting sediment traps (Knauer et al. 1979) were deployed at the beginning and recovered at the end of each cycle. Trap arrays consisted of 4-12 particle interceptor traps (PIT) with an inner

diameter of 70-mm and aspect (height:diameter) ratio of 8:1. Each PIT had a baffle on top that consisted of 14 smaller tubes, also with an 8:1 aspect ratio. The tubes in the baffle were tapered at the top, and it was assumed that all particles within the inner diameter of the PIT descended into the trap. The traps were designed to sample settling material accurately by creating a semi-stable boundary layer immediately above the trap, while avoiding mixing and resuspension during recovery. On P0704, 8 PITs were deployed at a depth of 100 m on each cycle. On P0810, 8-12 PITs were deployed at a depth of 100-m and 4-8 PITs were deployed at the base of the euphotic zone, except on Cycle 2, when the euphotic zone was close to 100 m.

Before deployment, each PIT was filled with 2.2 L of a slurry composed of filtered seawater with an additional 50 g L^{-1} NaCl to create a density interface within the tube that prevented mixing with *in situ* water. The traps were fixed with a final concentration of 4% formaldehyde before deployment to minimize decomposition as well as consumption by mesozooplankton grazers (Knauer et al. 1984). Upon recovery, the depth of the salinity interface was determined, and the overlying water was gently removed with a peristaltic pump until only 5 cm of water remained above the surface. The water was then mixed to disrupt large clumps and screened through a 300-μm Nitex filter. Swimmers were removed from the filters under a dissecting scope, and the remaining material was returned to the sample. The tubes were then split with a Folsom splitter, and subsamples were taken for C, N, C:^{234}Th, pigment analyses, and microscopy. Typically, ¼ PIT tube samples were filtered through a pre-combusted GFF, which was either acidified (to assess organic carbon) or not acidified

(for total carbon) prior to combustion in the Costech 4010 elemental combustion analyzer in the SIO Analytical Facility. Entire tubes were typically filtered through quartz microfiber filters for C:^{234}Th analyses as described above. Triplicate subsamples (typically 50 mL) were analyzed for Chl *a* and phaeopigment concentrations using acidification with HCl and a Turner Designs Model 10 fluorometer. Samples for microscopic analysis were stored in dark bottles and analyzed on land as described below.

Microscopic enumeration of sediment trap fecal pellets – On land, sediment trap samples were gently filtered through a 60-μm filter which was then rinsed onto a gridded petri dish. The sample was then analyzed under a dissecting microscope at 25X magnification (Wilson et al. 2008). Recognizable fecal pellets were separated from other sediment trap material. They were then photographed under both bright- and dark-field illumination. Images were analyzed using ImagePro (Media Cybernetics, Inc., ver 6.0), with the bright-field images used to draw outlines around the fecal pellets. Dark-field images were used to determine color of the fecal pellets. Fecal pellets were manually classified into six different shape categories (ovoid, cylindrical, spherical, tabular, amorphous, and ellipsoid) with appropriate length and width relationships used to convert into fecal pellet volumes. For tabular fecal pellets, we assumed that depth was equal to one half of width. Fecal pellets from several of the samples were sorted into broad classes (small, cylindrical, and tabular) and sized and combusted in the CHN analyzer to determine carbon:volume relationships of 0.125 mg C mm^{-3} for ovoids, spheres, and ellipsoids; 0.055 mg C mm^{-3} for cylindrical

and amorphous pellets; and 0.029 mg C mm^{-3} for tabular fecal pellets. Fecal pellets (particularly tabular and cylindrical pellets) were often found broken, likely due to sample processing. When they were clearly recognizable as fecal pellets and the fragment size was apparent, we counted these fragments as individual pellets. While this may inflate the total number of pellets, it likely gave a more accurate measurement of the total fecal pellet mass in the sample.

Mesozooplankton community enumeration – MOCNESS samples were analyzed to determine the concentrations and biomasses of broad taxonomic groups common in the CCE region (copepods, appendicularians, chaetognaths, salps and doliolids, eggs, euphausiids, nauplii, ostracods, polychaetes, pteropods, siphonophores, and others). Mesozooplankton were size-fractionated through a 1-mm filter, then each size-fraction was subsampled with a Folsom splitter until a reasonable amount of material (typically 100-1000 organisms) remained. For night-time samples an additional >5-mm fraction was analyzed to assess more accurately the larger portion of the community. Subsamples were analyzed using ZooScan hardware with ZooProcess and Plankton Identifier software (Gorsky et al. 2010). Following automatic classification of organisms, vignettes were manually checked to ensure correct taxonomic assessment. Length (feret) and area measurements were used to estimate carbon weight of each organism using the relationships in Table 1.

Calculation of active carbon transport - The active transport of carbon by mesozooplankton that feed in the surface at night and respire at depth during the day was calculated for the dominant diel vertically migrating (DVM) taxa in the CCE

region (copepods, euphausiids, chaetognaths, and others - noted to be primarily hyperiid amphipods) by first dividing each taxon into 11 size classes. The day-night biomass difference (integrated to 100-m depth) for each size class was then determined from paired MOCNESS tows. Specific respiration for each size and taxonomic class was computed from the equation:

$$\text{Respiration } \left(\mu\text{L } O_2 \text{ ind}^{-1}\text{hr}^{-1}\right) = e^{a_0 + a_1 \ln(CW) + a_2 T}$$

where CW is carbon weight (mg C) and T is the average temperature (°C) from 100 to 500-m depth. The constants a_0, a_1, and a_2 were assumed to be 0.124, 0.780, and 0.073, respectively, for copepods (Ikeda et al. 2001) and 0.524, 0.8354, and 0.061, respectively, for other metazooplankton (Ikeda 1985). This respiration rate is likely the organisms' standard metabolism, and hence may be an underestimate of their *in situ* metabolism. However, they were unlikely to be feeding at depth, and we believe their standard metabolism to be representative. We assumed that organisms respired at depth for 12 h per day. While we allowed individual size-classes to undergo both normal and reverse DVM, we assumed that bulk taxa (e.g. copepods, euphausiids, etc.) were not undergoing reverse DVM and hence set a minimum active transport rate of 0 for each taxa. The active transport of N was similarly calculated, using size-specific rates of ammonia excretion:

$$\text{Excretion } \left(\mu\text{g N ind}^{-1}\text{hr}^{-1}\right) = e^{a_0 + a_1 \ln(CW) + a_2 T}$$

where CW and T are again carbon weight and average temperature and a_0, a_1, and a_2 are -2.769, 0.711, and 0.071, respectively, for copepods (Ikeda et al. 2001) and -2.1763, 0.8293, and 0.0648, respectively, for other metazooplankton (Ikeda 1985).

Since the dominant euphausiid species in our MOCNESS samples (*Euphausia pacifica, Nematoscelis difficilis,* and *Euphausia gibboides*) are known to be both strong vertical migrators and visual net-avoiders (Brinton 1967), we calculated an adjusted euphausiid active transport rate by assuming that day time vertically-integrated euphausiid biomass (0 to 450 m) should be equal to night time biomass and that net avoidance was constant with depth. When day time tows were deficient in integrated euphausiid biomass relative to paired night time tows, we scaled the day time profile proportionally at all depths so that the integrated biomasses were equal and recalculated respiration at depth. This adjusted active transport rate may be an underestimate, as it does not take into account euphausiids that may migrate deeper than 450 m; thus the true transport rate may lie somewhere between the raw and adjusted rates.

Mesozooplankton gut pigment analyses - Daily rates of mesozooplankton community grazing on phytoplankton were determined from mid-day and mid-night bongo tow samples. The samples were anesthetized with soda water and size-fractionated into size classes of 0.2-0.5, 0.5-1, 1-2, 2-5 and >5 mm. Each size-fraction was divided on a Folsom splitter, with 3/8 being frozen in liquid nitrogen and saved for gut fluorescence analyses. Subsamples of each size class were inspected under a dissecting microscope to remove phytoplankton and detritus, then sonicated in 90% acetone, centrifuged and read for Chl *a*

and phaeopigment concentrations using acidification and a Turner Designs Model 10 fluorometer. As suggested by Conover et al. (1986), phaeopigment estimates were not multiplied by 1.51 (the Chl *a*:phaeopigment ratio). Pigment degradation to non-fluorescent products was further assumed (following Durbin and Campbell 2007) to be included in determination of gut clearance rates, which were estimated using the temperature dependent function K (min^{-1}) = 0.0124 $e^{0.0765\,T\,(°C)}$ of Dam and Peterson (1988), using mean temperature in the depth range of highest chlorophyll where zooplankton were expected to congregate and feed. To determine daily community ingestion rates, the sum of Chl *a* and phaeopigments for all size-classes was averaged between day-night paired tows and multiplied by the gut pigment turnover rate to determine daily community ingestion rates.

RESULTS

Cruise conditions – Nine Lagrangian drift experiments (cycles) were conducted as a part of this study (3 in Apr. 2007, 6 in Oct. 2009, Fig. 2). The P0704 cruise took place during typical spring upwelling conditions in the CCE. It included two inshore cycles (Cycles 1 & 3) near the Point Conception upwelling source with significant surface nitrate concentrations (~5 & 7 μ mol L^{-1}, for Cycles 1 & 3, respectively) and surface chlorophyll concentrations (>1 μg L^{-1}). Both of these cycles featured a large and active mesozooplankton community that impacted phytoplankton with high grazing rates (37.3 and 7.7 mg Chl *a* m^{-2} d^{-1}, respectively) and drove an overall decrease in vertically integrated chlorophyll over the course of the 4-day cycles (Landry et al. 2009). Cycle 2 took place in an offshore anti-cyclonic eddy with

low surface nitrate (<0.1 μM) and chlorophyll (~0.2 μg L^{-1}) concentrations, a distinct deep chlorophyll max at ~70 m, and significantly less mesozooplankton grazing (1.3 mg Chl *a* m^{-2} d^{-1}).

The P0810 cruise took place during a period when typical hydrographic conditions would suggest a more quiescent period. However strong winds from the north beginning on 2 Oct. likely mixed the surface waters near Point Conception stimulating phytoplankton growth during Cycles 3-6. Surface nitrate was relatively low through all cycles (~0.15 – 0.3 μM) except for Cycle 5, which was near the productive side of an upwelling front with surface nitrate concentrations of ~2 μM. Cycles 2 and 6 (which was on the unproductive side of the front) were representative of more oligotrophic conditions, with low surface chlorophyll concentrations of ~0.2 μg L^{-1} and distinct subsurface chlorophyll maxima. While Cycle 1 occurred prior to a wind event (and had a surface chlorophyll concentration of ~0.5 μg L^{-1}), the other three cycles showed increasing surface chlorophyll concentration from north to south (~0.7, 1.0, and 1.4 μg L^{-1} for Cycles 3-5, respectively) suggesting that the community may have been growing as it was advected south. While Cycles 1-3 (like the cycles from P0704) were typically 4 days long, Cycles 4-6 were shortened mini-cycles of 2-day duration.

Carbon export – We measured ^{234}Th concentrations on two or three casts per cycle. With the exception of one anomalous profile on P0810-1, vertical profiles consistently showed ^{234}Th deficiency at the surface and a switch to remineralization

slightly below the base of the euphotic zone (Fig. 3). Repeated profiles showed no strong evidence of increasing deficiency over the two- to four-day experimental cycles. ^{234}Th export rates across the 100-m depth horizon (calculated using a simple one-dimensional steady-state equation) ranged from 460-1980 dpm m^2 d^{-1}, and were highest during the two nearshore cycles from P0704 and P0810-6, and lowest during P0810-1 and P0810-3. These steady-state ^{234}Th export rates closely matched ^{234}Th fluxes determined from sediment traps placed at 100 m (and at the base of the euphotic zone on P0810) with the exception of cycle P0810-4 (Fig. 2). This cycle was located close to the Point Conception upwelling center shortly after a strong wind event moved through the region, and we suspect that upwelling introduced additional ^{234}Th into the surface waters, leading to an underestimation of export by the one-dimensional steady-state equation.

To convert ^{234}Th fluxes to carbon export, we measured the C:^{234}Th ratio on particles collected in two different manners, with sediment traps and with an *in situ* pump deployed at the same depth horizon. While the two methods determined the same broad patterns in C:^{234}Th ratio, including higher C:^{234}Th in surface waters, they disagreed on the magnitude of the ratio (Fig. 4). The *in situ* pump typically underestimated the C:^{234}Th ratio relative to the sediment trap, often by a factor of almost 2. In the absence of an *a priori* reason to trust one method over the other, we used the average C:^{234}Th ratio determined by the two methods to compute our steady-state estimates of carbon export (Table 2).

For the 9 experimental cycles, steady-state carbon export averaged 60 mg C m^{-2} d^{-1} at the 100-m depth horizon. Export was much more variable on the P0704 cruise, for which the onshore cycles had export rates of 83 and 129 mg C m^{-2} d^{-1} (P0704-1 and P0704-3), while the offshore cycle had significantly lower export of only 37 mg C m^{-2} d^{-1}. On P0810, export varied far less and showed no distinct trends with distance from shore, although this may be due to the greater homogeneity experienced during the October cruise. A comparison of export at the 100-m depth horizon to export at the base of the euphotic zone showed significant remineralization, with an average of 46% of carbon remineralized in the 40-50m below the euphotic zone. Our paired sediment traps, by comparison, suggested that only 21% of carbon was remineralized in this depth horizon. Regardless, remineralization was substantial, suggesting that the calculated carbon export for the P0704 cruise (when we only measured export at 100 m) may have underestimated the carbon flux across the base of the euphotic zone.

Sediment trap contents – Sediment trap carbon and nitrogen samples (Table 3) suggested that the C:N ratios on sinking material averaged 6.4 (molC:molN) during the spring cruise, similar to the C:N ratio of particulate organic matter (POM) in the euphotic zone (6.1). While the C:N ratio of the POM in the surface water in the fall was not significantly different, the sinking material was depleted in nitrogen, with average C:N ratios of 10.2 at the base of the euphotic zone and 11.1 at 100 m, suggesting significant reworking of POM as it sank. The magnitude of total pigment flux was highly variable, but phaeopigment flux was consistently an order of magnitude higher than chlorophyll flux (Fig. 5). Pigment fluxes indicate that bulk

phytoplankton sinking rates never exceeded 0.66 m d^{-1} (with an average across all cycles of 0.23 m d^{-1}). This is likely an overestimate as the low Chl:Phaeo ratios suggest that a significant portion of the sediment trap chlorophyll may have sunk undegraded in fecal pellets. Bulk phaeopigment sinking rates ranged from 0.71 to 18.6 m d^{-1} (with an average of 5.0 m d^{-1}). Sediment trap phaeopigment concentrations were strongly correlated with the mass flux of recognizable fecal pellets (Fig. 6), which were presumably the source of the phaeopigments. Pigment fluxes were highest during cycles P0704-1 and P0704-3 when an assemblage of large, active herbivorous mesozooplankton was present.

Two sediment trap samples from each sediment trap deployment and depth were microscopically sorted at 25X magnification to characterize the >60-μm particle size-fraction, which was assumed to represent most of the carbon flux. A qualitative assessment suggested that fecal pellets were the dominant component in most sediment trap samples. For both trap samples of P0704-2, a large number of small zooplankton likely made it through 303-μm mesh screen; we thus believe that organic carbon flux was overestimated on that cycle. On one of two samples from P0704-3 a significant portion of the sample was comprised of marine snow that looked like it contained fragments of degraded fecal pellets and the other sample was primarily fecal pellets. Recognizable fecal pellets were not common in any of the samples from P0810-1, with the surface samples dominated by marine snow aggregates and the deeper samples comprised mainly of small unidentifiable particles. For P0810-2, one of the samples was fecal pellet dominated while the other contained almost nothing

but large fluffy white marine snow. The P0810-3 surface samples contained primarily marine snow while the deep samples contained little material. Overall fecal pellets clearly dominated the flux of particulate material during productive cycles, while the proportion of recognizable material was lower for cycles in the more oligotrophic regions.

Enumeration of recognizable fecal pellets uncovered several distinct patterns. Across all cycles, cylindrical fecal pellets – presumably egested by euphausiids or large copepods – were the most abundant pellet type (Fig. 7) and also typically the dominant source of recognizable fecal pellet carbon (Fig. 8). However, tabular (salp) fecal pellets, while never abundant, were a significant source of POM when present. In particular, one of the two samples from P0704-1 contained enough tabular fecal pellet carbon to represent 125 mg C m^{-2} d^{-1}, which was greater than the total flux of carbon measured in most of the sediment trap deployments. The important, but variable, nature of their contribution to total flux highlights the difficulties in assessing complete budgets of sinking material. Small ovoid fecal pellets (believed to be appendicularian egesta), contributed a consistently small portion of fecal pellet abundance (20% on average) and mass (12%). A strong correlation was found between crustacean abundance and their cylindrical fecal pellets (Fig. 9). In contrast, no statistically significant correlation was found for fecal pellet biomass, likely because biomass variability was driven by large organisms and large fecal pellets that are less accurately sampled. We found no correlations between salps and appendicularians and their respective fecal pellets, likely due to the fact that few of

either taxa were collected in the MOCNESS samples. Mesozooplankton biomass assessed by repeat paired bongo tows was better correlated with recognizable fecal pellets than biomass from MOCNESS tows, perhaps because significantly more bongo tows were made during each cycle. A power law relation between mesozooplankton biomass and fecal pellet mass flux suggested that mass flux increases with roughly the square of mesozooplankton biomass (Fig. 10). We suspect that fecal flux varied directly with mesozooplankton grazing, which would be expected to correlate with the product of mesozooplankton and phytoplankton concentrations (Fig. 10), provided zooplankton ingestion is not saturated.

Active transport by DVM mesozooplankton – While sediment traps and ^{234}Th disequilibrium measurements only measure the flux of organic carbon on passively sinking particles, DVM mesozooplankton also actively transport carbon to depth by feeding in the euphotic zone at night and respiring at depth during the day. Paired day-night MOCNESS tows from the surface to 450 m (with nets typically opening every 50 m) combined with Zooscan analysis of the mesozooplankton community in each net, allowed us to assess the day-night vertical distributions of common mesozooplankton taxa. We focused on four broad taxonomic groups, which were believed to dominate active transport in the CCE region due to both high abundances and strong DVM behavior – copepods (Fig. 11), euphausiids (Fig. 12), chaetognaths (Fig. 13), and our 'other' category (Fig. 14), which was determined to be composed primarily of hyperiid amphipods.

A comparison of the day-night differences in abundance showed consistent deficiency of surface daytime populations relative to nighttime populations, particularly for copepods and euphausiids (Figs. 11 and 12). For most populations, a euphotic zone deficiency in daytime biomass was matched by a subsurface increase, giving us confidence that organisms were actually migrating to depth and that our results were not due to either sampling biases or random variations in patchy populations. However, we did notice that vertically integrated (0 - 450-m) estimates of euphausiid biomass were often significantly higher at night than during the day, suggesting that these visually acute animals were actively avoiding the MOCNESS net during the day. We corrected for this overestimate of euphausiid DVM by scaling up the day time profile by a constant fraction so that daytime biomass equaled nighttime biomass. We also tested for DVM in siphonophores and the combined salps and doliolids taxonomic group, but found no evidence for migratory behavior, largely because these groups were seldom found in the MOCNESS samples.

Mesozooplankton active transport varied from 2.4 to 66.9 mg C m^{-2} d^{-1} and was driven by the DVM of copepods and euphausiids (Table 4, Fig. 15). While copepods were typically responsible for roughly half of active transport, euphausiid active transport was highly variable. Particularly high euphausiid active transport rates of 40.6 and 35.7 mg C m^{-2} d^{-1} (Cycles 0704-3 and 0810-5, respectively) were driven by high abundances of the largest size classes (>7 mm for 0704-3 and >10 mm for 0810-5), which were strong diel migrators whenever present. A positive correlation with surface chlorophyll was found, though it described only 41% of the

variability in active transport. Active carbon transport was a relatively constant fraction of surface nighttime biomass, averaging $9*10^{-6}$ mgC d^{-1} mgC^{-1} (varying from $4*10^{-6}$ to $1.5*10^{-5}$). Active nitrogen transport followed very similar patterns to carbon transport (Table 4), with an average C:N mass ratio of 7.6:1.

DISCUSSION

Export flux measurements – Determining food web control of carbon export requires accurate measurement of vertical POC fluxes, yet methodological uncertainties make these rates difficult to constrain. In an early comparison of the two primary methods of determining flux out of the surface ocean, Buesseler (1991) showed that contemporaneous measurements with sediment traps and ^{234}Th varied significantly. Sediment trap inaccuracy can arise from hydrodynamic biases, swimmer contamination, and solubilization within the trap (Buesseler et al. 2007). Radionuclide disequilibrium techniques suffer from the frequent necessity of assuming steady-state and neglecting vertical and horizontal advective fluxes (Savoye et al. 2006), as well as uncertainties in assessing the variable C:radionuclide ratio (Buesseler et al. 2006).

Despite these difficulties, our paired use of the two techniques yielded similar results, lending credence to the carbon export measurements derived in this study. In particular, the flux of ^{234}Th into our drifting traps agreed well with the steady-state model of ^{234}Th export rates (Fig. 2). On the cycle when the two methods disagreed (P0810-4), the discrepancy was likely due to upwelling near Point Conception after a

strong wind event. The introduction of a modest upwelling term of 0.7 m d^{-1}, combined with the vertical gradient in ^{234}Th of 0.012 dpm L^{-1} m^{-1}, could explain the discrepancy between the steady-state and sediment trap measurements of ^{234}Th flux at the 100-m depth horizon. Nevertheless, without measurements of upwelling, it is impossible to state conclusively why the two methods did not agree. We could also hypothesize the possibility of upwelling affecting cycles P0704-1, P0704-3, and P0810-1, yet find no need to include an upwelling term for these cycles. When determining export rates in an upwelling region, we suggest that it is prudent to either measure upwelling or utilize two different methods of measuring carbon flux.

Unlike the similarity in ^{234}Th flux measurements, a distinct difference was found between the C:234Th ratio as determined by sediment traps and *in situ* pumps (Fig. 4), a result that was also found in the Barents Sea (Coppola et al. 2002). While ^{234}Th export rates in the study varied by a factor of 4, C:^{234}Th ratios varied by a factor of almost 6 and thus had a greater impact on carbon flux rates computed from ^{234}Th disequilibrium. The discrepancy between the two methods of collecting particles is thus a significant issue. In our study, sediment traps predicted significantly higher C:^{234}Th ratios than *in situ* pumps. The *in situ* pump ratio only exceeded the sediment trap ratio on two out of fourteen measurements (neither significant) while the sediment trap ratio was often significantly higher than the pump values. This difference may be a simple result of the oversampling of slowly sinking particles by *in situ* pumps. Slowly sinking particles have greater time to equilibrate with deeper water conditions where POC to total thorium ratios are significantly higher than at the surface, thus

deflating their C:^{234}Th ratio relative to rapidly sinking particles. Despite the attractiveness of this simple explanation for the methodological differences, this pattern has not been found in all studies that compare sediment traps to pumps (e.g. Benitez-Nelson et al. 2001a).

In addition to ^{234}Th methodological issues, sediment traps have their own biases. While we lack the ability to address hydrological or solubilization effects, our microscopic sorting of fecal pellet contents allowed us to assess the impact of swimmer contamination. In general, our method of screening with a 303-μm filter and microscopically sorting the larger size-fraction efficiently removed mesozooplankton from the samples. However, in oligotrophic cycles (particularly P0704-2, but also to a lesser extent in P0810-1, P0810-3, and P0810-6) contamination by small swimmers was a significant issue, suggesting that a smaller mesh size should be used when the mesozooplankton community is dominated by smaller organisms. In P0704-2, swimmers may have comprised over 50% of the sample, suggesting that the sediment traps overestimated carbon flux by a factor of 2 or more. Relative to the steady-state calculation, the sediment traps were actually underestimating ^{234}Th flux, although this result may be misleading as mesozooplankton swimmers were found to have very high C:^{234}Th ratios (data not shown) and hence would not have contributed much thorium to the trap samples.

Contribution of fecal carbon to vertical flux – Ecological relationships have indirectly suggested that fecal pellet flux may drive vertical carbon export in the CCE. Assuming 30% egestion efficiency and no fecal pellet remineralization, Stukel et al.

(submitted) used a simple trophic model to show that mesozooplankton egestion could account for all of the variability in measured vertical carbon flux across three disparate ecosystem states. In Chapter 3, we used inverse ecosystem modeling techniques and concluded that 65%-95% of the vertical flux could be attributed to combined zooplankton grazing processes, with the discrepancy likely resulting from the unrealistic assumption of a completely homogenized detrital pool, which suggested significant and equal recycling of all euphotic zone detritus, regardless of origin. In the present study, we used two different approaches to experimentally assess the contribution of fecal pellets to carbon export: microscopic enumeration of recognizable fecal pellets and pigment analysis of sediment trap samples.

If all-ingested chlorophyll is converted to phaeopigments and none is lost to non-fluorescent particles, then the carbon content of fecal pellets derived from recent herbivory can be calculated as:

$$C_{FP,h} = Ph \times C{:}Chl \times (1 - AE)$$

where, Ph is the phaeopigment concentration, C:Chl is the carbon to chlorophyll ratio of the mesozooplankton prey, and AE is the assimilation efficiency of the mesozooplankton (Downs and Lorenzen 1985). Using this equation and the assimilation efficiencies calculated in Chapter 3, we would conclude that recent mesozooplankton herbivory was responsible for between 1.4% and 42% of vertical carbon flux, with an average across all cycles of 12% (Table 4). This estimate is likely to be very conservative, however, as several studies have shown

mesozooplankton to degrade pigments during digestion (Conover et al. 1986; Lopez et al. 1988; Landry et al. 1994). If we instead assume that mesozooplankton degrade pigments in the same proportion that they utilize prey carbon, we can generate an upper estimate of the amount of carbon-derived from recent herbivory of 4.6% to 106% with an average across all cycles of 36%. While this only represents the fecal flux of herbivorous mesozooplankton, for the P0704 cruise we can extrapolate to the total flux of fecal carbon by utilizing the estimated percentage contribution of phytoplankton to mesozooplankton diets from Chapter 3. With this correction, fecal pellets are responsible for at least 58%, 44%, and 38% of vertical flux for P0704 cycles 1, 2, and 3, respectively, using lower estimates from the Downs and Lorenzen equation (Table 5). If we assume that some of the ingested pigments were assimilated or degraded to non-fluorescing material by the mesozooplankton, fecal flux could easily account for all vertical carbon flux measured at 100 m during the spring. We can also calculate the proportion of flux derived from the gravitational sinking of ungrazed phytoplankton by multiplying the C:Chl ratio by the Chl flux into the sediment traps, although this is likely to be an overestimate as a small proportion of ingested chlorophyll can pass through mesozooplankton guts without conversion to phaeopigments (Downs and Lorenzen 1985). This calculation suggests that phytoplankton were responsible for only 0.2% to 13% of vertical flux, with an average across all cycles of 4%. Considering that chlorophyll flux never exceeded 14% of total pigment flux, it is possible that all pigment flux was derived from fecal pellets. On P0704, gut pigment measurements allowed us to compare phaeopigment

production by mesozooplankton to flux at the 100-m depth horizon. Mesozooplankton grazing was almost an order of magnitude higher than phaeopigment vertical flux (10.6, 9.0, and 2.2x vertical flux, for Cycles 1, 2, and 3, respectively) suggesting significant degradation of fecal pellets in the upper water column.

Direct assessment of the contribution of fecal pellets to vertical flux is complicated by processes that mask the amount of fecal material contained in sediment traps (Turner 2002), including fragmentation of pellets both in the water column and during sample processing and inclusion in marine snow aggregates that mask the fecal origin of the particles. Additionally, small <60-μm pellets, produced by metazooplankton nauplii and microzooplankton (Gowing and Silver 1985), would not have been sampled by our methods, thus indicating that our direct assessment of fecal pellet flux is conservative. Nevertheless, recognizable fecal pellets were found to be a dominant source of carbon flux in the study region. While recognizable fecal pellets represented less than 50% of the mass flux measured in all but two of the sediment trap samples (and significantly less in most), they could account for ~35% of total flux across the 100-m depth horizon in the nine cycles due to their dominant role in vertical flux during higher export periods.

Role of mesozooplankton in vertical carbon flux – Mesozooplankton have been shown to mediate biogeochemical fluxes in many direct and indirect ways. Their fecal pellets are often the dominant recognizable contents in sediment traps (Turner 2002), though the contribution of recognizable fecal pellets to vertical flux is highly variable (Small and Ellis 1992; Gowing et al. 2001; Wilson et al. 2008). In addition to

disintegration processes that often lead to an underestimate of total fecal material using such methods, there is significant variation in fecal pellet carbon:volume ratios, varying from 0.02 to 0.11 mg C m^{-2} (Silver and Gowing 1991; Carroll et al. 1998). While such conversion factors are often calculated for live animals, we calculated conversion factors from the fecal pellets collected in our sediment traps and found that carbon density was higher for smaller classes of particles, decreasing from 0.125 mg C mm^{-3} for small ovoids, spheres, and ellipsoids to 0.055 mg C mm^{-3} for cylindrical pellets and 0.029 mg C mm^{-3} for tabular pellets.

The mesozooplankton role in gravitational particle flux is complicated by the variety of interactions between mesozooplankton and oceanic POM. Mesozooplankton can limit the total production of particles in the surface ocean by exerting grazing pressure on phytoplankton that exceeds growth rate, as observed at nearshore Cycles 1 and 3 during P0704 (Landry et al. 2009). Mesozooplankton also transform sinking material by feeding on particles including their own fecal pellets (Gowing and Wishner 1986) and marine snow aggregates (Wilson et al. 2010). In addition to their role in passive transport, mesozooplankton DVM behavior is believed to play an important role in actively transporting carbon and nitrogen to depth, especially in oligotrophic regions (Longhurst et al. 1990; Steinberg et al. 2000; Al-Mutairi and Landry 2001).

By simultaneously assessing total particle flux (using sediment traps and ^{234}Th), recognizable fecal pellet flux, pigment flux, and active transport of mesozooplankton, we were able to constrain the contribution of mesozooplankton to

carbon export in the CCE during April 2007 and October 2008 (Fig. 16). Across all cycles, the gravitational sinking of ungrazed phytoplankton was only a minor portion of total flux. The contribution of recognizable fecal pellets was much more variable. During the spring cruise, fecal pellets likely comprised the majority of all sinking material. In the fall, however, the contribution of identifiable pellets was significantly less. While total export rates were not significantly different than those in the spring, far fewer fecal pellets were found in the sediment traps. In particular, flux during Cycles 1-3 was dominated by marine snow. The decreased importance of recognizable fecal pellets and phaeopigments in less productive conditions may have been a result of greater residence time of fecal material in the surface layer, allowing increased physical and biological disruption of pellets. Contrary to expectations, the ratio of active to passive carbon export did not increase with distance from shore. Across all cycles active transport comprised 19% of total carbon export across the 100-m depth horizon (varying from 3% to 50%), driven by the DVM of copepods and euphausiids.

While knowledge of mesozooplankton and phytoplankton standing stocks allowed prediction of fecal pellet flux (Fig. 10b), the decreased role of both recognizable and pigmented fecal pellets during the P0810 cruise obscures attempts to predict total sinking flux. The large role of fecal pellets during P0704 compared to P0810, combined with the increased C:N ratio of sinking material on P0810 suggests that different processes may be at work during the spring and fall season. During the spring, a young, actively growing community led to a dominance of export by contemporaneous autochthonous processes. The fall cruise likely sampled an older

community when the proportion of detritus in total POM may have increased. It is possible that slowly sinking particles generated earlier in the season and potentially fragmented and degraded by biological and physical processes may have contributed more to vertical flux than the biological processes assessed during our short experimental cycles.

Acknowledgments

This chapter was made possible by the synergistic efforts of many collaborators working within the CCE LTER Program. I am particularly grateful to members of the Ohman Lab (M. Ohman, J.-B. Romagnon, T. Langland, J. Powell, A. Cawood), Landry Lab (M. Landry, M. Décima), Goericke Lab (R. Goericke, S. Dovel, M. Roadman), and the Benitez-Nelson lab at USC (C. Benitez-Nelson, R. Styles, W. Plessinger, S. Pal). I would like to thank the captains, restechs, and crews of the R. V. Thompson and R. V. Melville who were incredibly helpful at sea.

Chapter 4, in full, is currently in preparation for submission: Stukel, M. R., Landry, M. R., Ohman, M. D., Benitez-Nelson, C. R.. "Mesozooplankton and vertical carbon export in a coastal upwelling biome." The dissertation author was the primary investigator and author on this paper.

Table 4.1. Mesozooplankton length:carbon relationships. For 'Others' we used an equation for hyperiid amphipods, which were noted to be the dominant contributor to the 'other' category.

Taxa	Relationship: C(μg) = fn of length (μm) or volume (μm^3)	Source
Appendicularians 0.49	$*(38.8*(L/1000)^{2.574})^{1.12}$	(Lavaniegos and Ohman 2007)
Chaetognaths 0.22	$1*(L/1000)^{2.580}$	(Gorsky et al. 2010)
Copepods 0.46	$1*(L/1000)^{3.094}$	(Gorsky et al. 2010)
Doliolids 0.51	$*(L/1000)^{2.28}$	(Lavaniegos and Ohman 2007)
Eggs 1.4*	10^{-7}*Volume	(Kiorboe and Sabatini 1995)
Euphausiids 19.0	$32*(L/1000)^{1.484}$	(Gorsky et al. 2010)
Nauplii	$0.1489 * (L/1000)^{2.588}$	(Mauchline et al. 1998)
Ostracods 0.39	$8*17.072*(L/1000)^{2.545}$	(Lavaniegos and Ohman 2007)
Polychaetes 7.5*(L/	$1000)^{1.3848}$	(Lavaniegos and Ohman 2007)
Pteropods	$0.221 * 2.6 * (L/1000)^{2.659}$	(Lavaniegos and Ohman 2007)
Siphonophores 20.4	$7*(L/1000)^{0.834}$	(Lavaniegos and Ohman 2007)
Others 365*	$10^{(-2.314+2.957*\log(L/1000))}$	(Lavaniegos and Ohman 2007)*

Table 4.2. ^{234}Th fluxes and C:^{234}Th ratios.

		Depth (m)	^{234}Th Export (dpm m^{-2} d^{-1})	σ	SedTrap C:Th (mg C dpm^{-1})	σ	McLane C:Th (mg C dpm^{-1})	σ	Carbon Export (mg C m^{-2} d^{-1})
0704-1	**Deep**	100 1	542	108	0.066	0.005	0.042	0.004	83
0704-2	**Deep**	100 1	055	45	0.043	0.010	0.026	0.002	37
0704-3	**Deep**	100 1	978	446	0.087	0.014	0.044	0.012	129
0810-1	**Deep**	100 5	30	732	0.129	0.021	0.033	0.012	43
	Shallow	50 4	78	1128	0.247	0.035	0.095	0.073	82
0810-2	**Deep**	100 1	650	514	0.039	0.002	0.027	0.015	55
0810-3	**Deep**	100 4	56	68	0.050	0.002	0.062	0.065	25
	Shallow	60 7	79	164	0.067	0.013	0.038	-	41
0810-4	**Deep**	100 9	59	669	0.063	0.011	0.048	-	53
	Shallow	50 1	049	180	0.094	0.008	0.066	0.017	84
0810-5	**Deep**	100 1	311	198	0.061	0.008	0.029	-	59
	Shallow	60 1	513	50	0.103	0.013	0.054	0.010	119
0810-6	**Deep**	100 1	904	133	0.036	0.004	0.024	0.001	57
	Shallow	60 1	878	232	0.065	0.020	0.079	-	136

Table 4.3. Sediment trap flux measurements**.** Chl and Phaeopigments are in units of μg Chl *a* equivalents m^{-2} $d^{-1.}$

Cycle	Depth	C_{tot}		C_{org}		N		Chl		Phaeo		FP Mass
	(m)	(mgC m^{-2} d^{-1})	σ	(mgC m^{-2} d^{-1})	σ	(mgN m^{-2} d^{-1})	σ	(μg m^{-2} d^{-1})	σ	(μg m^{-2} d^{-1})	σ	(mgC m^{-2} d^{-1})
P0704-1	100	**173.7**	60.5	**144**	12.7	**22.2**	4.0	**443**	245	**3501**	816	**135.2**
P0704-2	100	**41.4**	10.0	**32**	6.3	**7.6**	1.6	**19**	2	**146**	48	**3.6**
P0704-3	100	**194.5**	50.1	**170**	40.8	**30.0**	8.6	**407**	153	**3449**	701	**53.6**
P0810-1	100 -		-	**74**	10.6	**9.0**	0.8	**47**	19	**529**	133	**4.4**
P0810-1	50 -		-	**112**	34.4	**13.8**	5.7	**17**	7	**337**	128	**6.7**
P0810-2	100 -		-	**69**	12.8	**7.7**	1.3	**-**	-	**-**	-	**7.6**
P0810-3	100 -		-	**78**	6.6	**10.2**	0.9	**12**	-	**217**	-	**5.0**
P0810-3	60 -		-	**120**	12.5	**15.3**	2.8	**31**	20	**331**	235	**22.6**
P0810-4	100 -		-	**149**	36.3	**14.4**	3.9	**266**	97	**2723**	232	**35.4**
P0810-4	50 -		-	**216**	4.4	**25.7**	0.7	**426**	116	**4214**	597	**80.4**
P0810-5	100 -		-	**127**	21.7	**12.4**	1.7	**123**	43	**1141**	76	**14.1**
P0810-5	60 -		-	**128**	27.3	**13.9**	3.8	**251**	43	**1575**	145	**25.9**
P0810-5	100 -		-	**107**	5.0	**8.9**	1.0	**34**	9	**211**	52	**3.5**
P0810-5	60 -		-	**112**	12.3	**10.8**	1.7	**66**	7	**438**	175	**5.1**

Table 4.4. Active transport by diel vertically migrating mesozooplankton. *Indicates adjusted euphausiid active transport value, which takes into account possible day-time net avoidance behavior.

Carbon transport by respiration mg C m^{-2} d^{-1}

	Copepods	Euphausiids	Euphausiids*	Chaetognaths	Others (Hyperiids)	Total	Total*
0704-1	10.0	10.4	5.4	0	0.3	20.6	15.6
0704-2	1.9	1.4	0.6	0.5	0	3.8	3.0
0704-3	1.8	47.5	40.6	0.3	0.1	49.8	42.8
0810-1	16.3	8.0	4.9	0	2.5	26.8	23.7
0810-2	3.4	5.2	4.3	0.8	5.3	14.7	13.8
0810-3	9.0	4.7	3.5	0	4.5	18.2	17.0
0810-4	3.7	0	0	2.6	0	6.3	6.3
0810-5	9.7	55.5	35.7	0.2	1.5	66.9	47.1
0810-6	0	2.4	2.4	0	0	2.4	2.4

Nitrogen transport by excretion mg N m^{-2} d^{-1}

	Copepods	Euphausiids	Euphausiids*	Chaetognaths	Others (Hyperiids)	Total	Total*
0704-1	1.45	1.35	0.70	0	0.04	2.83	2.18
0704-2	0.25	0.18	0.08	0.06	0	0.49	0.39
0704-3	0.29	6.27	5.35	0.05	0.02	6.62	5.70
0810-1	2.18	1.04	0.65	0	0.32	3.55	3.15
0810-2	0.47	0.68	0.57	0.11	0.68	1.94	1.82
0810-3	1.34	0.61	0.45	0	0.58	2.53	2.37
0810-4	0.43	0	0	0.34	0	0.76	0.76
0810-5	1.44	7.18	4.62	0.03	0.20	8.85	6.29
0810-6	0	0.31	0.31	0	0	0.31	0.31

Table 4.5. Contribution of phytoplankton and fecal pellets to vertical flux as assessed from pigment analyses. Carbon export is the average of sediment trap and ^{234}Th-derived carbon export rates (mg C m^{-2} d^{-1}). Phytoplankton biomass was assessed using epifluorescence microscopy. Phy C Flux is calculated as the product of chl flux and C:Chl ratio. AE is the assimilation efficiency of the mesozooplankton (Chapter 3 for P0704 and Conover 1966 for P0810) Herbivorous fecal flux is calculated either assuming no pigment degradation (Downs and Lorenzen 1985) or assuming that pigment is degraded in the same proportion that organic carbon is utilized (Upper). %Phy is the percentage of phytoplankton in the prey of mesozooplankton (Chapter 3) and is used to calculate non-pigmented and hence total fecal flux.

	Depth (m)	C Export	Vert. Int. Phyto Biomass ($mgCm^{-2}$)	Vert. Int. Chl ($mgChlm^{-2}$)	Phy C Flux ($mgCm^{-2}d^{-1}$)	AE	Herb. Fecal Flux (Downs) ($mgCm^{-2}d^{-1}$)	Herb. Fecal Flux (Upper) ($mgCm^{-2}d^{-1}$)	% Phy	Total Fecal Flux (Downs) ($mgCm^{-2}d^{-1}$)	Total Fecal Flux (Upper) ($mgCm^{-2}d^{-1}$)
P0704-1	100	113	2613	67	17.3 0.	61 53.	6	137.0	72%	74.8	191.3
P0704-2	100	34 2079		31	1.3 0.	66 3.	3	9.7	22%	14.9	44.3
P0704-3	100	149	2239	78	11.7 0.	69 31.	4	99.6	56%	56.4	179.1
P0810-1	100	58	748	56	0.6 0.	7 2.	1	7.0			
P0810-1	50	97	748	56	0.2 0.	7 1.	3	4.5			
P0810-2 100		62	609	22							
P0810-3	100	52	644	39	0.2 0.	7 1.	1	3.6			
P0810-3	60	81	644	39	0.5 0.	7 1.	6	5.5			
P0810-4 100		101	2340	68	9.1	0.7	28.1	93.5			
P0810-4	50	150	2340	68	14.6 0.	7 43.	4	144.8			
P0810-5	100	93	961	65	1.8 0.	7 5.	0	16.8			
P0810-5	60	123	961	65	3.7 0.	7 7.	0	23.2			
P0810-6	100	82	396	19	0.7 0.	7 1.	3	4.3			
P0810-6	60	124	396	19	1.4 0.	7 2.	7	8.9			

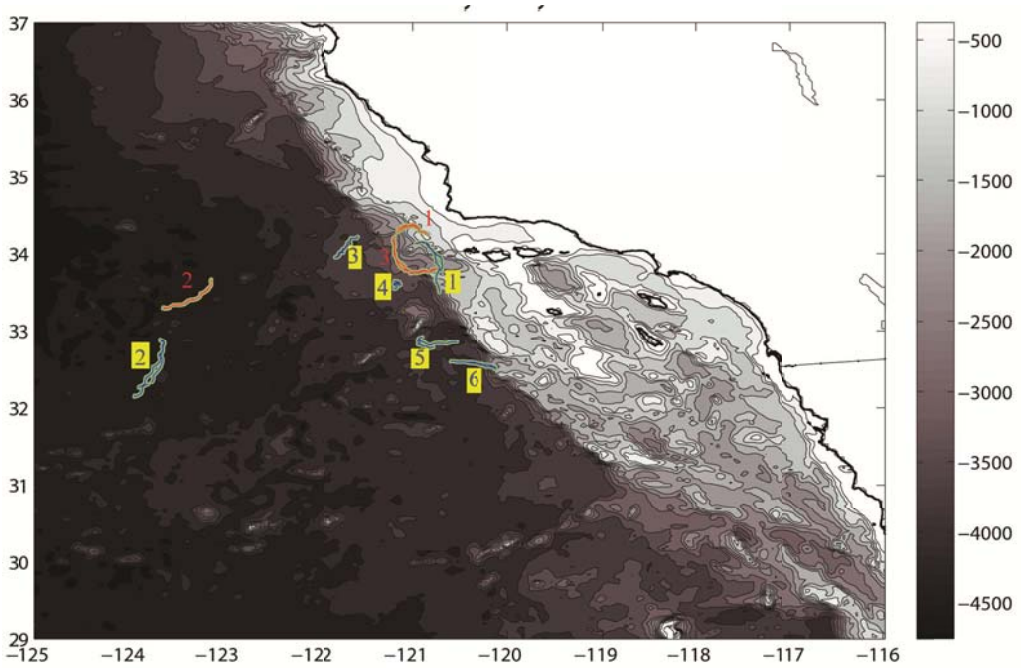

Figure 4.1. Bathymetric map of study region off Pt. Conception, California. Shading shows depth (m). Red traces (highlighted in yellow) show drifter tracks for P0704, while blue show P0810.

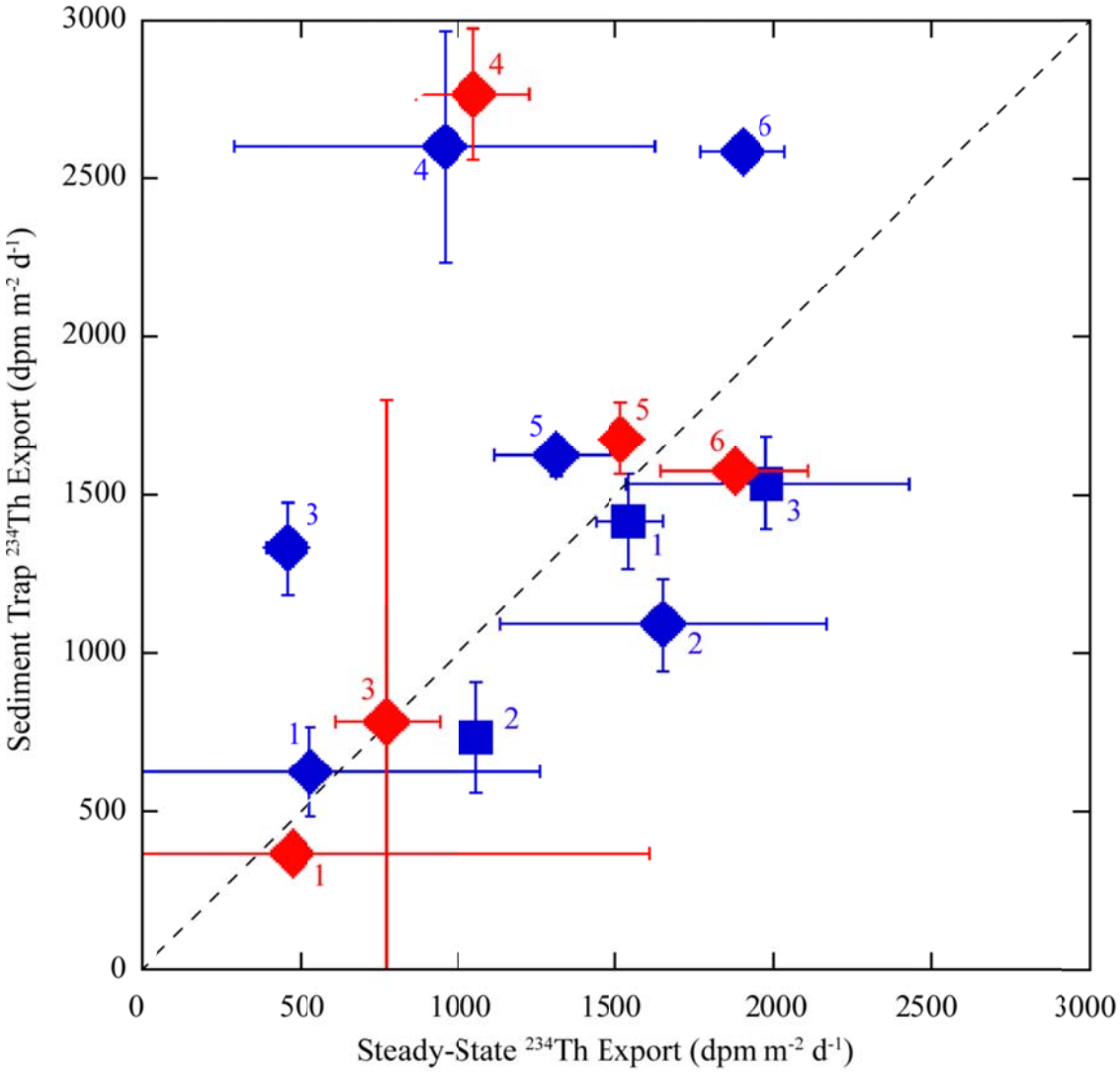

Figure 4.2. Comparison of ^{234}Th export rates as estimated by a ^{238}U-^{234}Th deficiency with a one-dimensional steady-state equation that neglects upwelling (x-axis) and the amount of ^{234}Th collected in contemporaneous sediment traps (y-axis). Blue symbols are at the 100 m depth horizon; red are at the base of the euphotic zone (either 50 or 60-m). Squares are from P0704; diamonds from P0810. Note good agreement for all cycles except P0810-4, when we suspect that strong northerly winds drove upwelling near Point Conception.

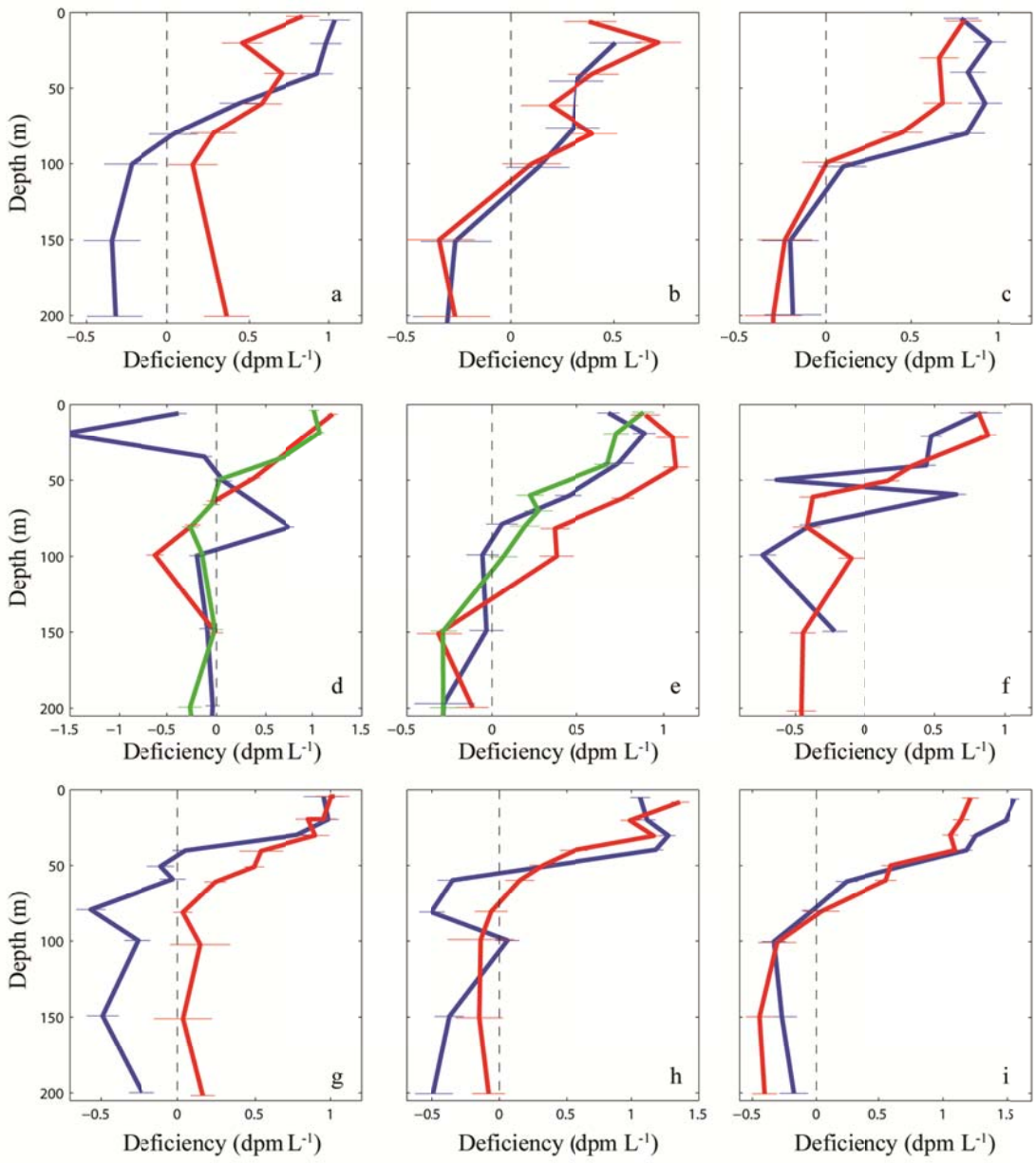

Figure 4.3. ^{234}Th deficiency profiles. X-axis is the deficiency of ^{234}Th relative to ^{238}U. Panels a, b, c, d, e, f, g, h, i are cycle P0704-1, P0704-2, P0704-3, P0810-1, P0810-2, P0810-3, P0810-4, P0810-5, P0810-6, respectively. Blue lines are always the first cast of a cycle, red lines are the second, and when present green lines are the third cast.

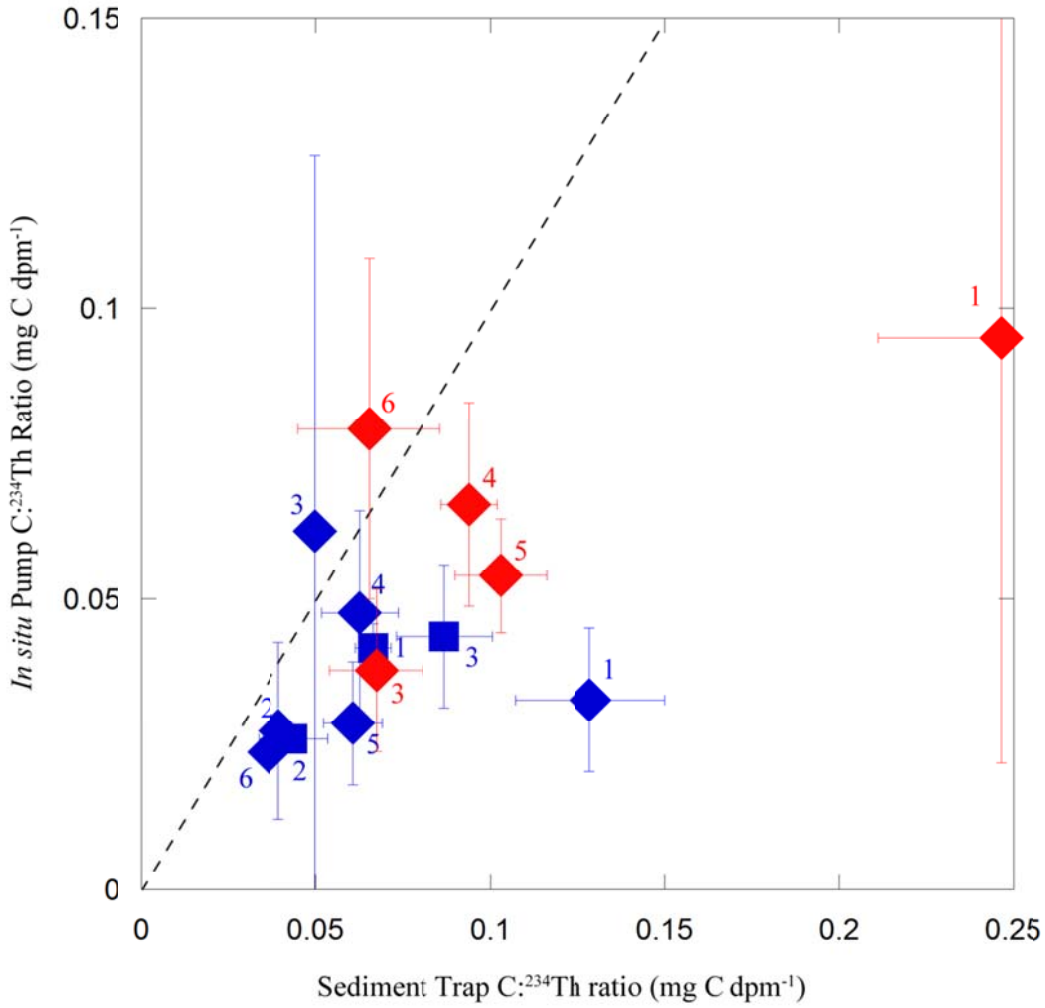

Figure 4.4. C:^{234}Th ratios. X-axis is the C:^{234}Th ratio measured on particles caught in sediment traps, while y-axis is the same ratio measured using *in situ* pumps and size-fractionated particles >20 µm (P0704) or >50-µm (P0810). Blue symbols are at the 100-m depth horizon; red are at the base of the euphotic zone (either 50 or 60 m). Squares are from P0704; diamonds from P0810. Dashed line is the 1:1 line.

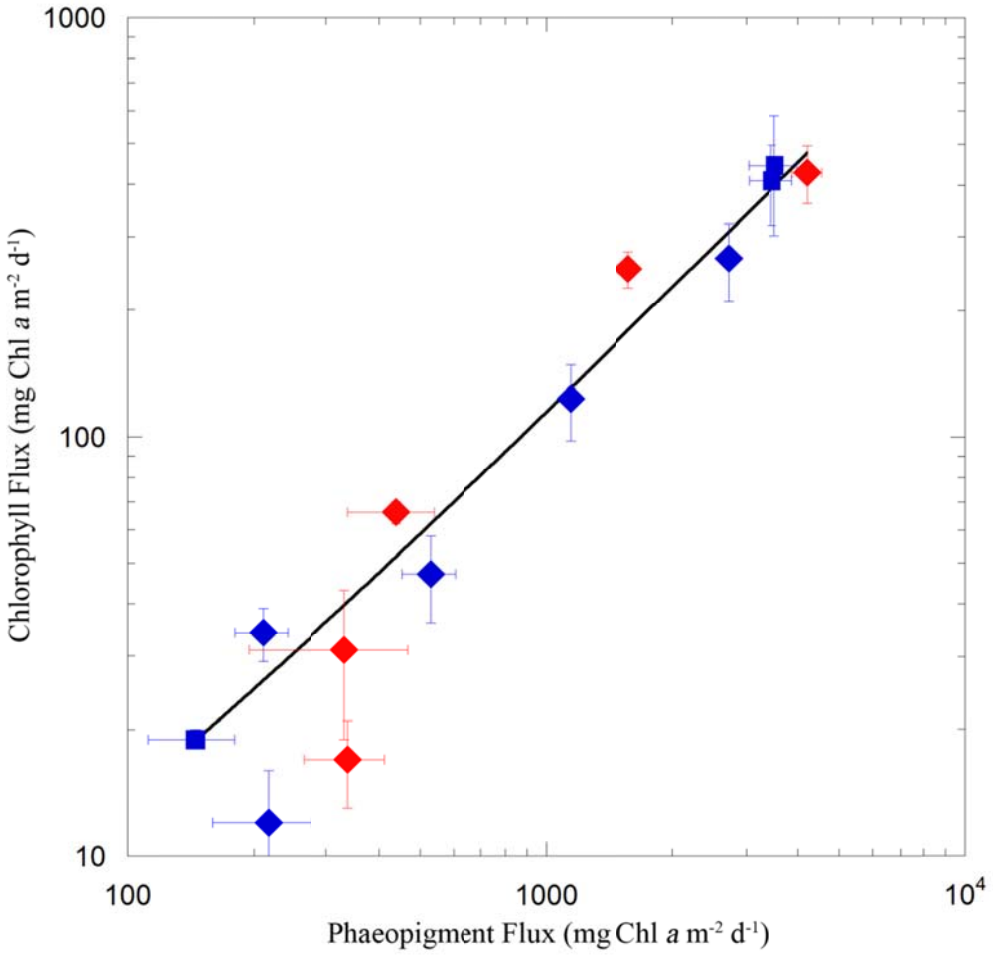

Figure 4.5. Pigment flux. X-axis is phaeopigment flux collected in sediment traps (mg Chl *a* equivalent m^{-2} d^{-1}). Y-axis is Chl *a* flux (mg Chl *a* m^{-2} d^{-1}). Blue symbols are at the 100-m depth horizon; red are at the base of the euphotic zone (either 50 or 60 m). Squares are from P0704; diamonds from P0810. Notice the good agreement for all cycles except P0810-4, when we suspect that strong northerly winds drove upwelling near Point Conception. Shown in black is the regression: Chl = 2.5 + 0.11*Ph with an R^2 of 0.96.

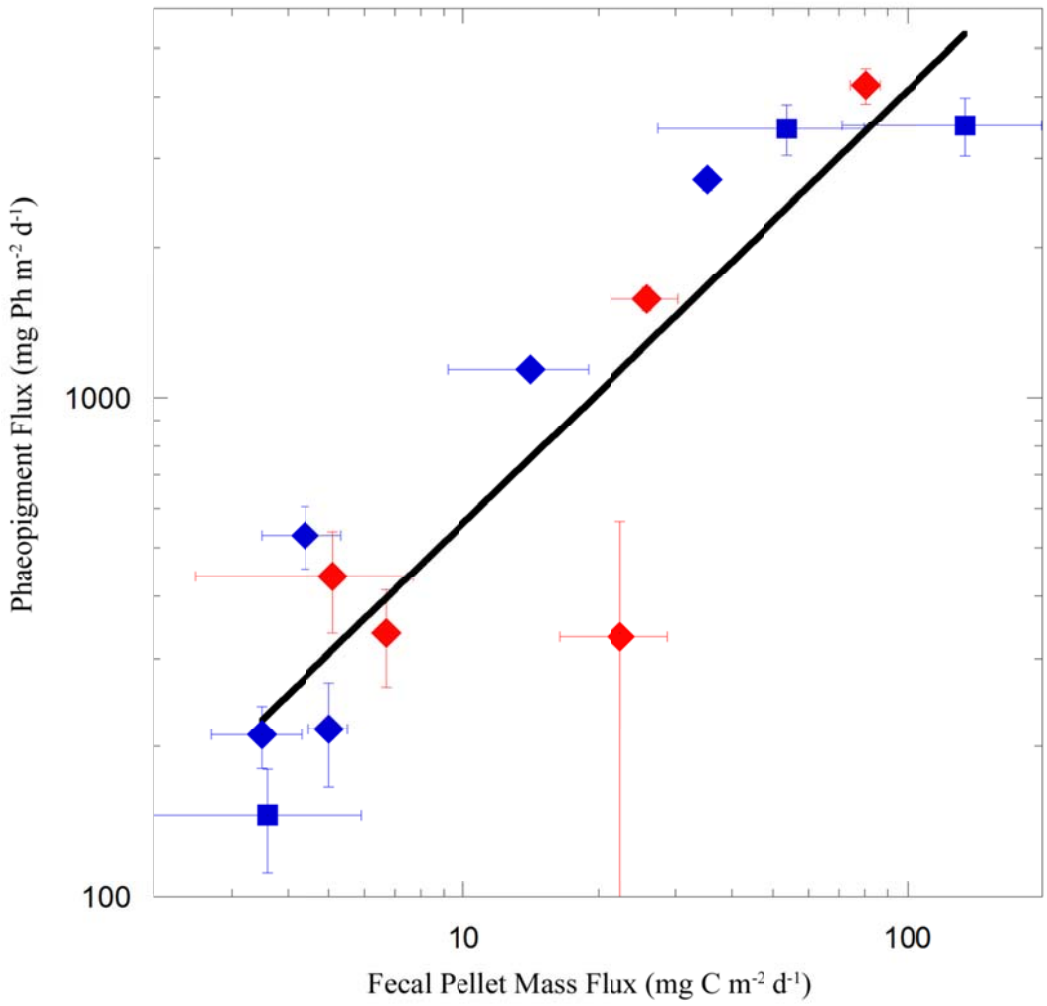

Figure 4.6. Phaeopigment and fecal pellet mass flux. X-axis is the mass flux of recognizable fecal pellets (mg C m^{-2} d^{-1}). Y-axis is phaeopigment (Ph) flux (mg Ph m^{-2} d^{-1}). Blue symbols are at the 100-m depth horizon; red are at the base of the euphotic zone (either 50 or 60 m). Squares are from P0704; diamonds from P0810. Black line shows a power law regression: $Ph = 76 * FP^{0.87}$ with an R^2 of 0.76.

Figure 4.7. Flux of recognizable fecal pellets into sediment traps (10^5 pellets m^{-2} d^{-1}). Dark blue represents ovoid pellets, blue is ellipsoid, teal is spherical, yellow is cylindrical, orange is amorphous, and maroon is tabular pellets. Samples are grouped by cruise, cycle, and depth horizon ('d' denotes 100-m samples, 's' denotes samples from the base of the euphotic zone at either 50 or 60 m). Two samples were enumerated per cycle and depth and are shown next to each other.

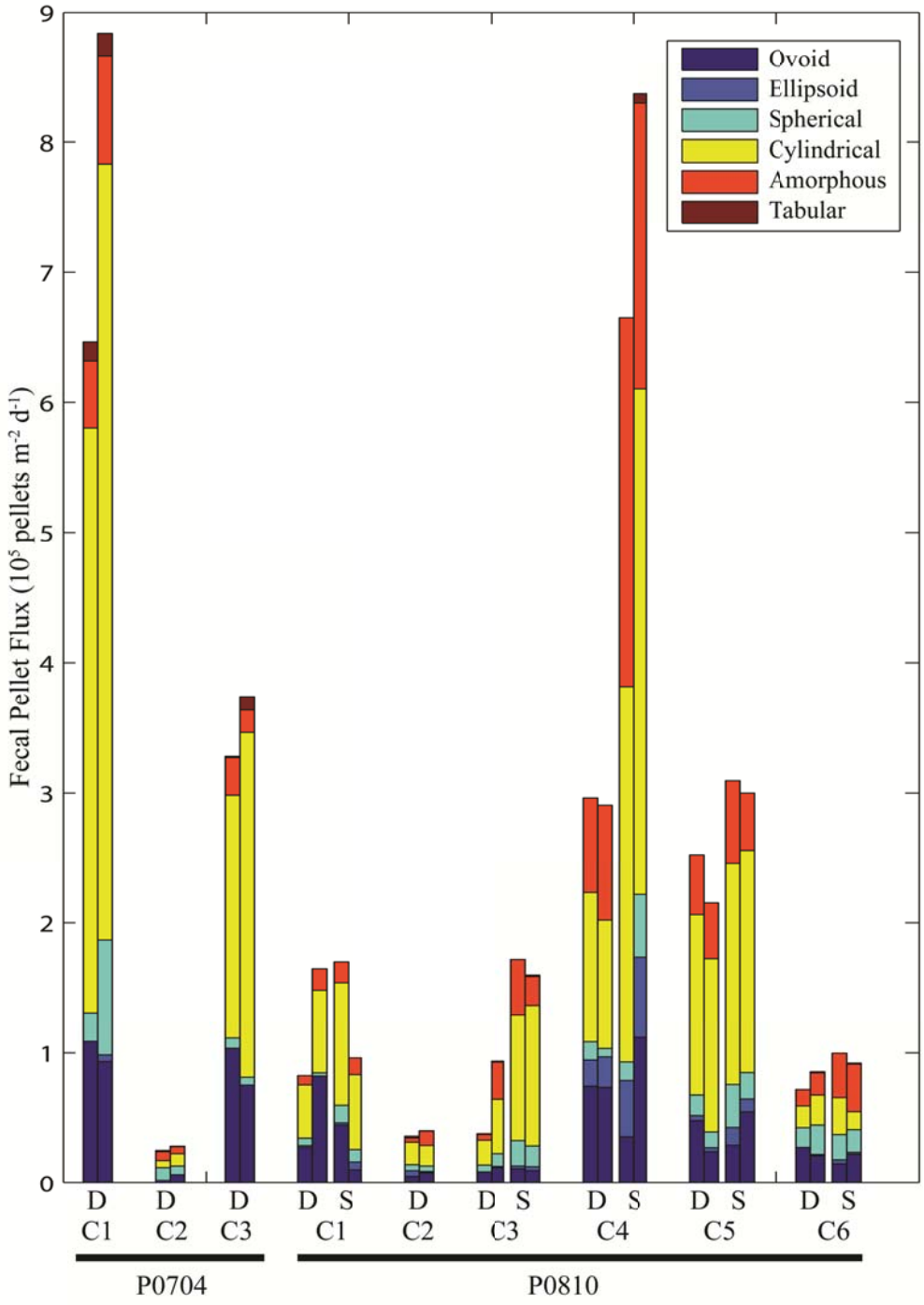
Ovoid
Ellipsoid
Spherical
Cylindrical
Amorphous
Tabular
Fecal Pellet Flux (10^5 pellets m^{-2} d^{-1})
0
1
2
3
4
5
6
7
8
9
D C1
D C2
D C3
D S C1
D C2
D S C3
D S C4
D S C5
D S C6
P0704
P0810

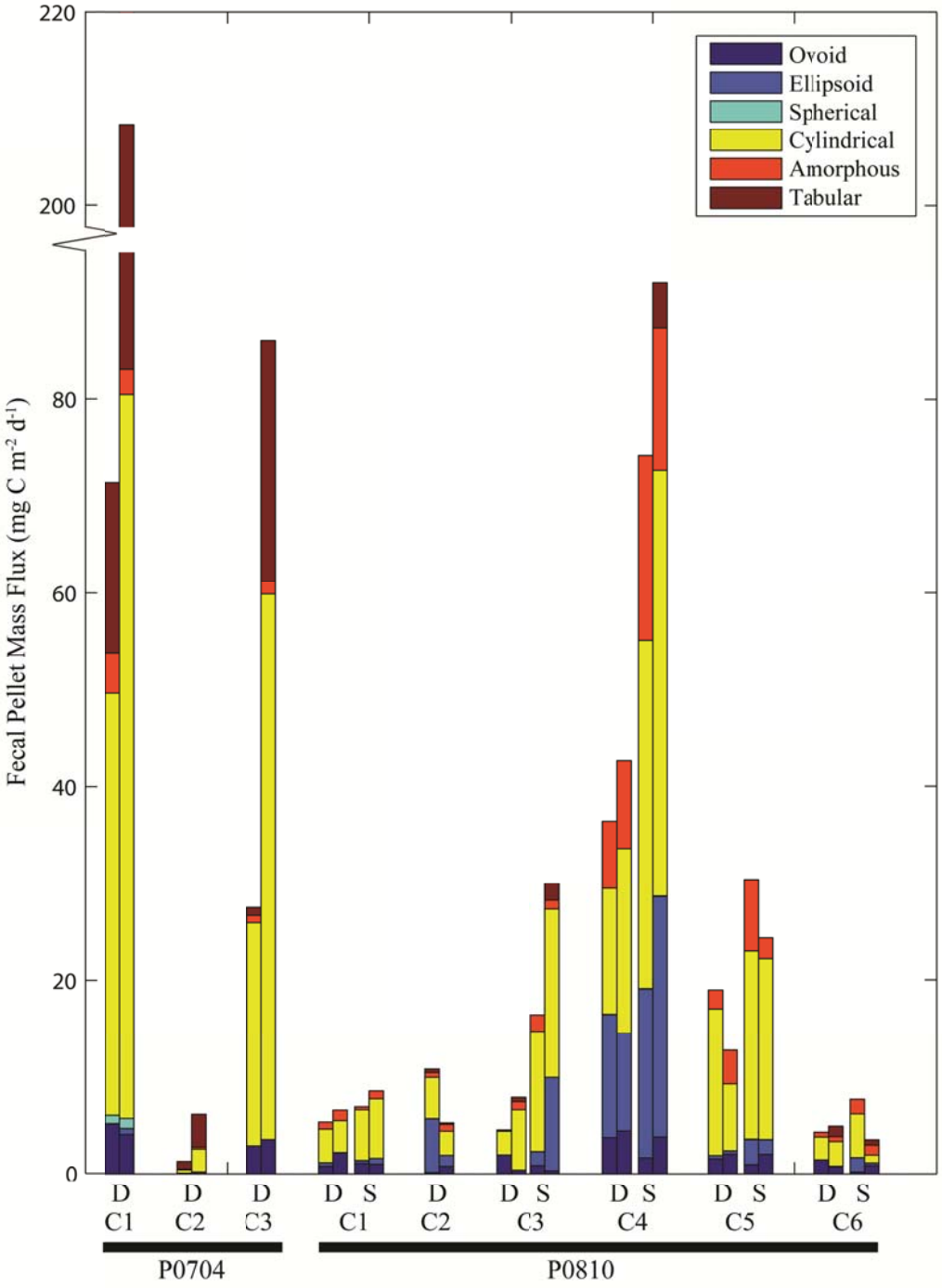

Figure 4.8. Flux of fecal pellet mass into sediment traps (mg C m^{-2} d^{-1}). Symbols and samples are same as in Fig. 7.

Figure 4.9. Relationship between cylindrical fecal pellets and total crustacean abundance. Panel a shows the crustacean abundance (day-night average from MOCNESS tows integrated to 100 m) on the x-axis and cylindrical fecal pellet flux (at 100 m). Panel b shows crustacean biomass and fecal pellet mass flux. Squares are P0704, while diamonds are P0810. Regression line shown in panel a is: FP = -140 + 2.6*CA, with R^2=0.85.

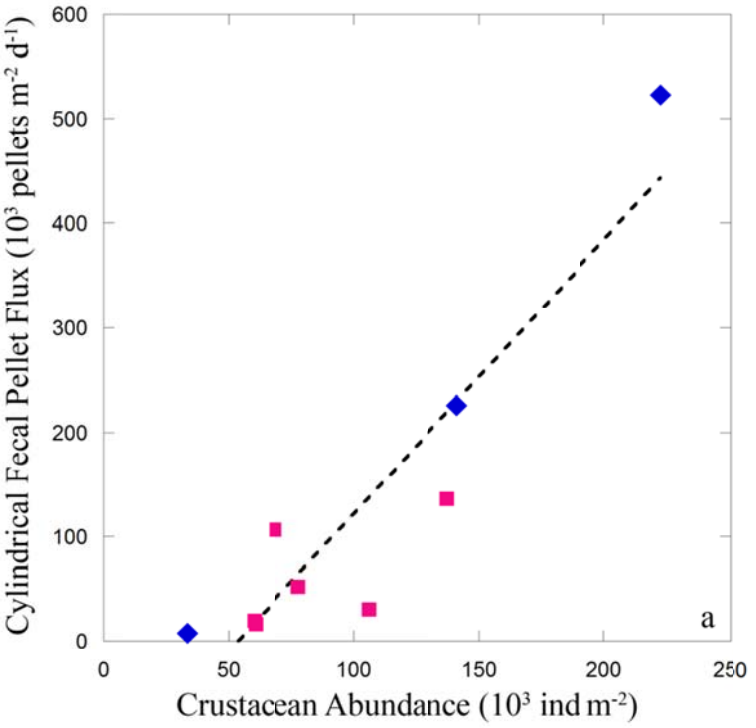
Cylindrical Fecal Pellet Flux (10^3 pellets m^{-2} d^{-1})
600
500
400
300
200
100
0
0
50
100
150
200
250
Crustacean Abundance (10^3 ind m^{-2})
a

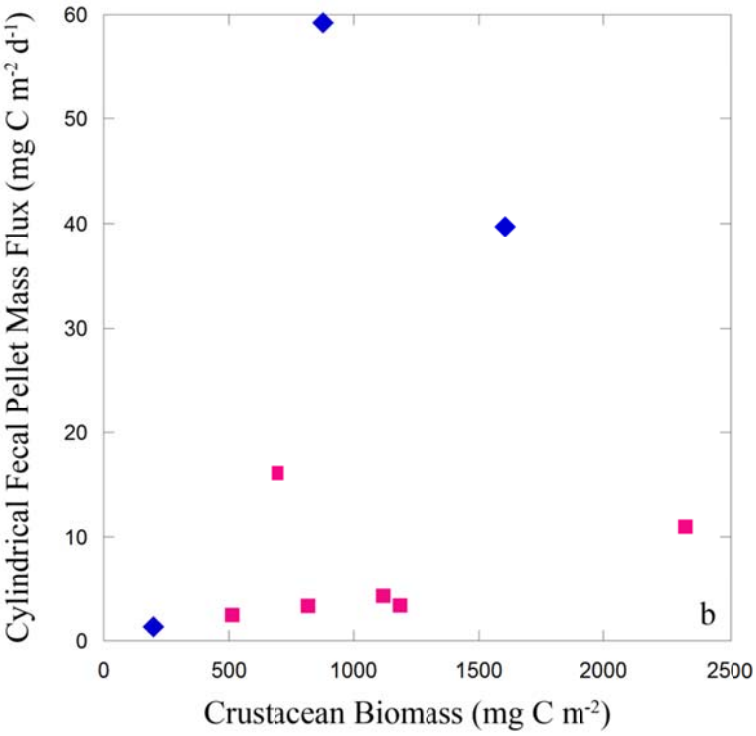
Cylindrical Fecal Pellet Mass Flux (mg C m^{-2} d^{-1})
60
50
40
30
20
10
0
0
500
1000
1500
2000
2500
Crustacean Biomass (mg C m^{-2})
b

Figure 4.10. Relationship between fecal pellet mass flux and mesozooplankton biomass. In panel a, x-axis is mesozooplankton biomass (mg C m^{-2}) as caught in day-night paired bongo tows. Error bars are one standard error around the mean. Y-axis is fecal pellet mass flux (mg C m^{-2} d^{-1}) at 100-m depth with error bars that show the difference between paired measurements. Blue squares are P0704, while red diamonds are P0810. Black line is a power law regression: $FP = 2.4*10^{-5} * Biomass^{1.93}$, with R^2 of 0.95. In panel b, x-axis is the product of mesozooplankton concentration (mg C m^{-3}) and phytoplankton concentration (mg C m^{-3}), with error bars of one standard error. Black line is the regression line: $y = -10.2 + 8.1x$, with R^2 of 0.93.

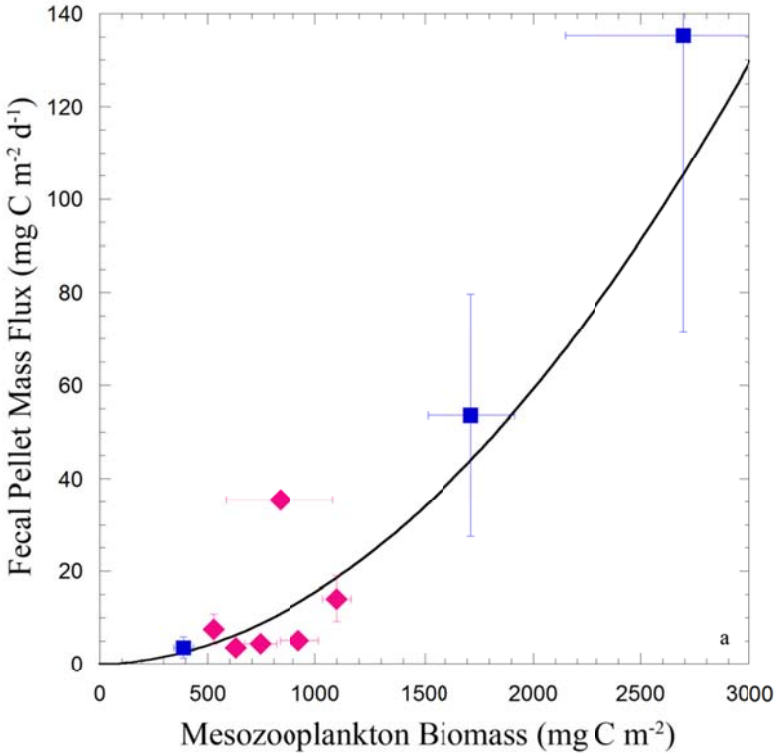
Fecal Pellet Mass Flux (mg C m-2 d-1)
Mesozooplankton Biomass (mg C m-2)
a
0
20
40
60
80
100
120
140
0
500
1000
1500
2000
2500
3000

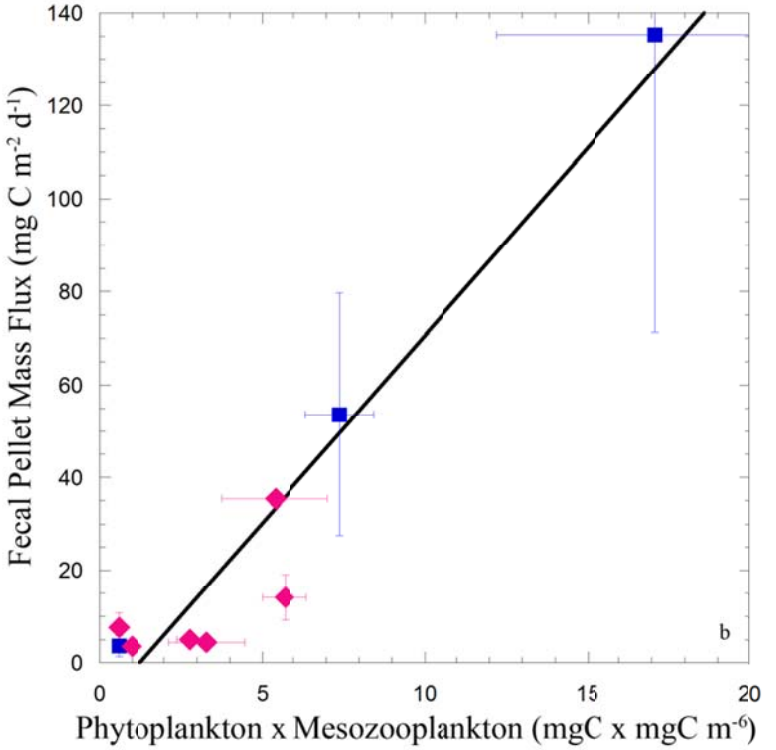
Fecal Pellet Mass Flux (mg C m-2 d-1)
Phytoplankton x Mesozooplankton (mgC x mgC m-6)
b
0
20
40
60
80
100
120
140
0
5
10
15
20

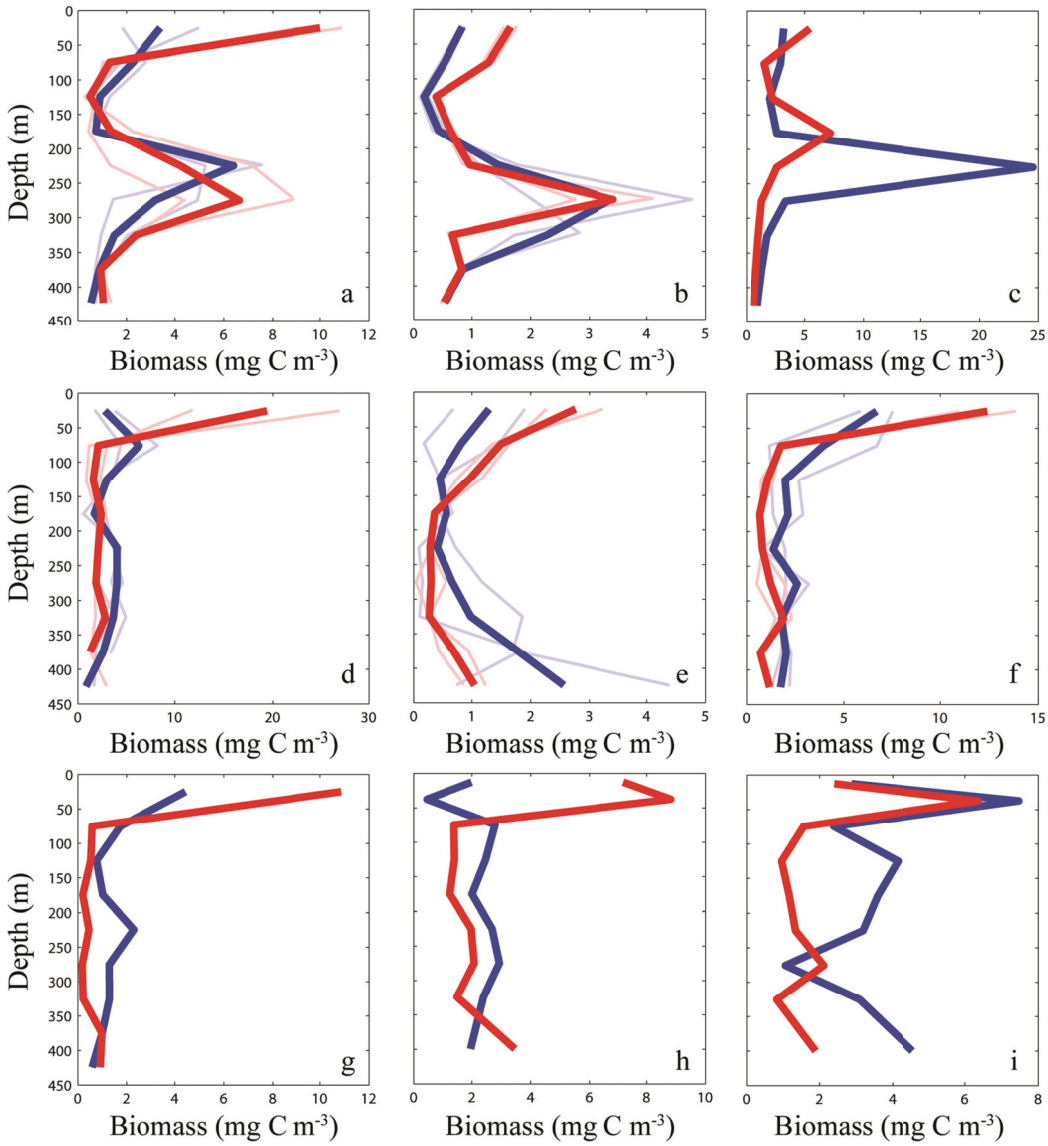

Figure 4.11. Vertical distribution of copepod biomass (mg C m^{-3}). Blue is daytime biomass, red night-time biomass. When two day-night pairs of MOCNESS tows were taken in a cycle, cycle means are shown as the bold line and the light lines show the individual tows. Panels are P0704-1, P0704-2, P0704-3, P0810-1, P0810-2, P0810-3, P0810-4, P0810-5, and P0810-6, for panels a, b, c, d, e, f, g, h, i, respectively.

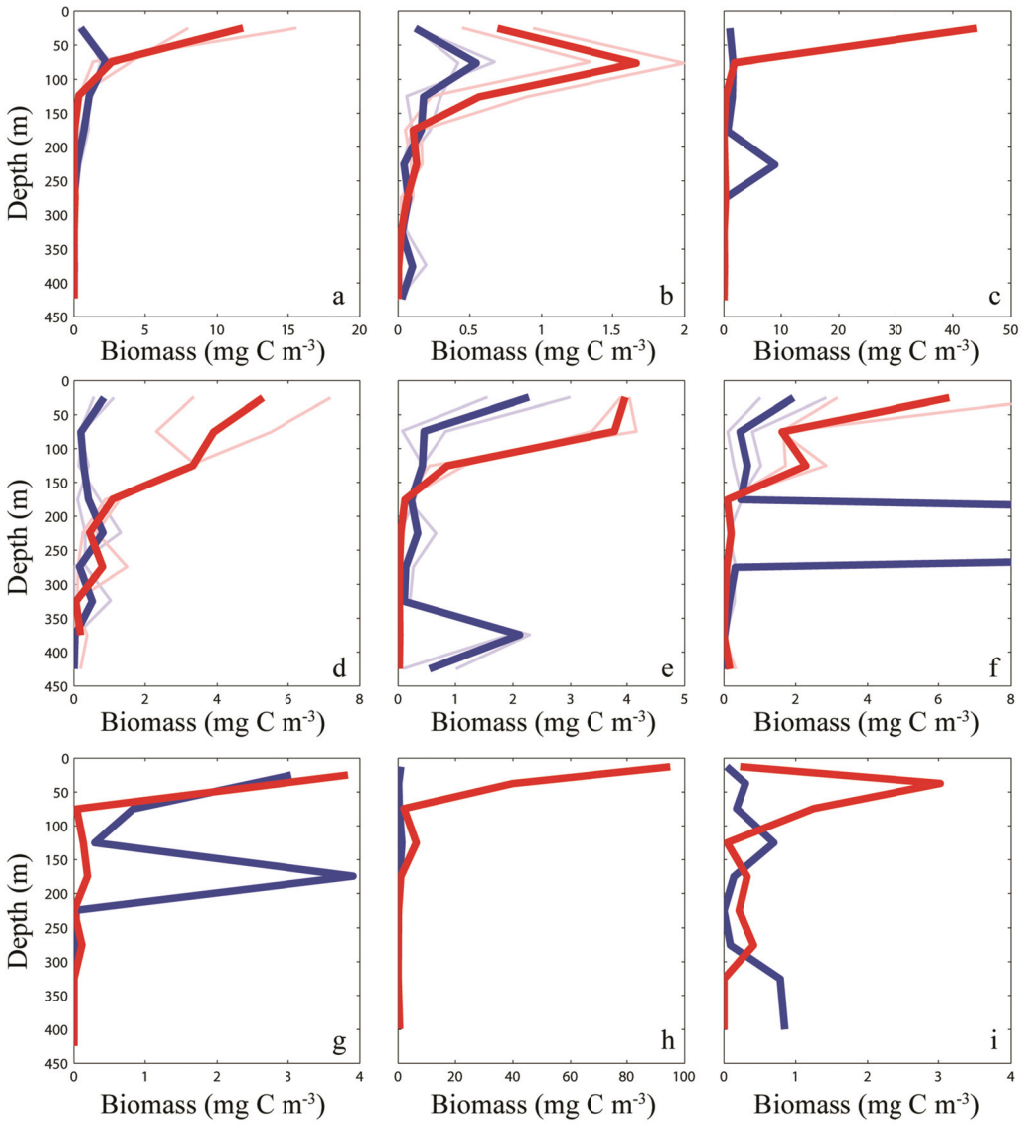

Figure 4.12. Vertical distribution of euphausiid biomass. Panels and lines are the same as Figure 11.

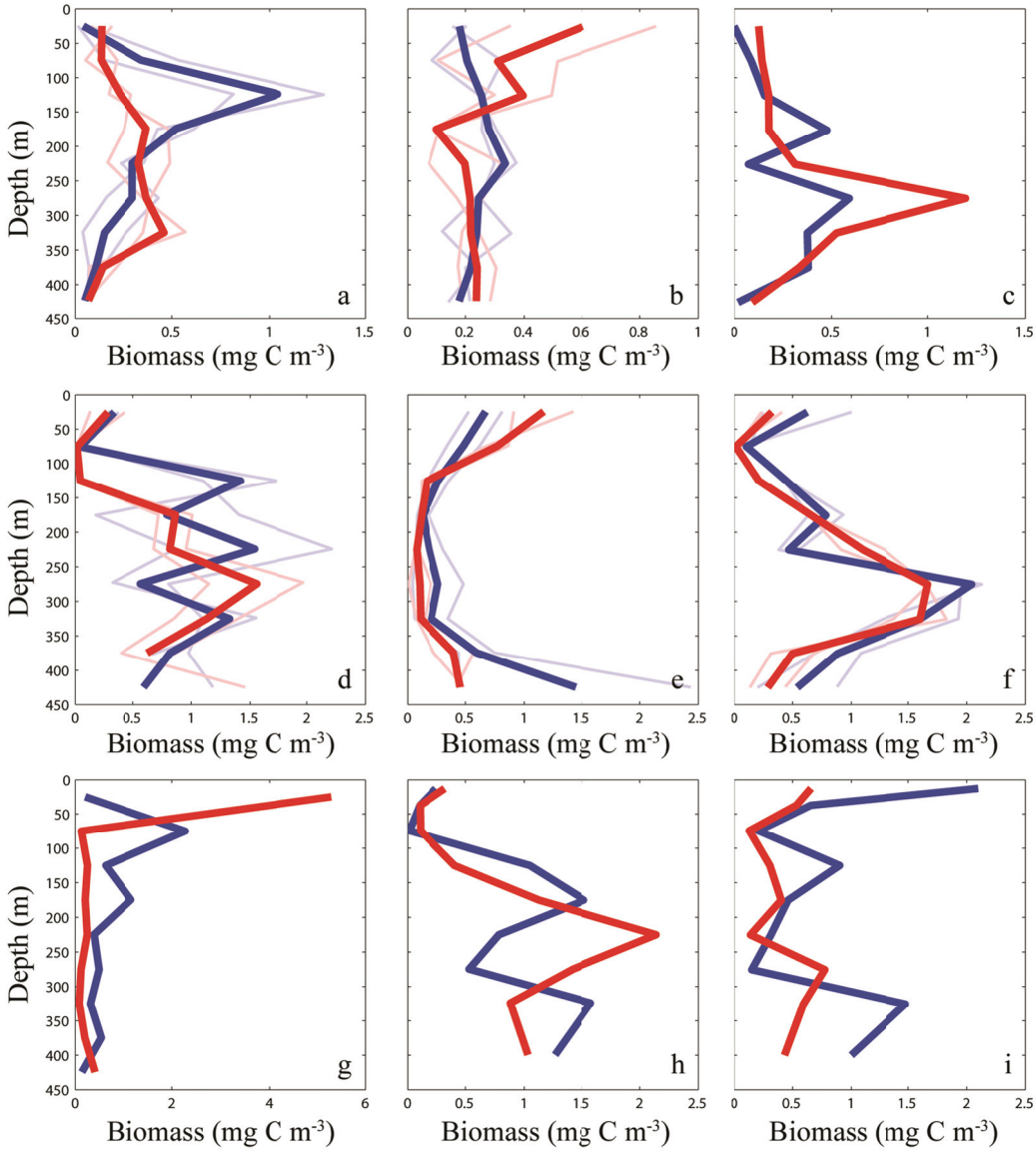

Figure 4.13. Vertical distribution of chaetognath biomass. Panels and lines are the same as Figure 11.

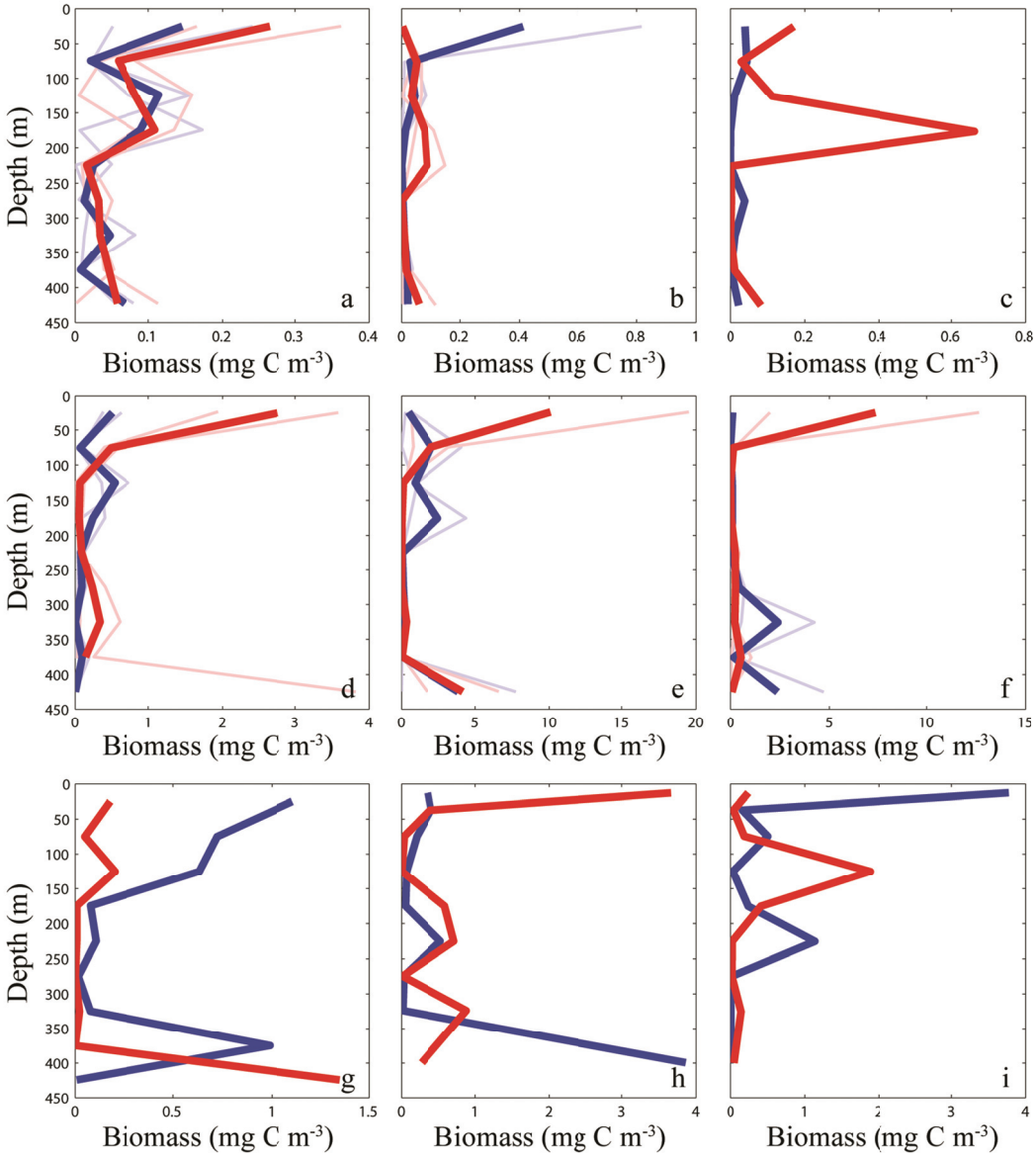

Figure 4.14. Vertical distribution of 'other' biomass. Note that our 'other' category includes all organisms that were not classified as either copepods, chaetognaths, doliolids & salps, eggs, euphausiids, nauplii, ostracods, polychaetes, pteropods or siphonophores. It was primarily composed of hyperiid amphipods. Panels and lines are the same as Figure 11.

Figure 4.15. Active transport of carbon by DVM mesozooplankton. Dark blue is active transport by copepods (mg C m^{-2} d^{-1}) across the 100-m depth horizon. Light blue, yellow, and maroon are active transport by euphausiids, chaetognaths, and 'others', respectively. The 'others' group was composed primarily of hyperiid amphipods. Euphausiid active transport was corrected for net avoidance (see Methods).

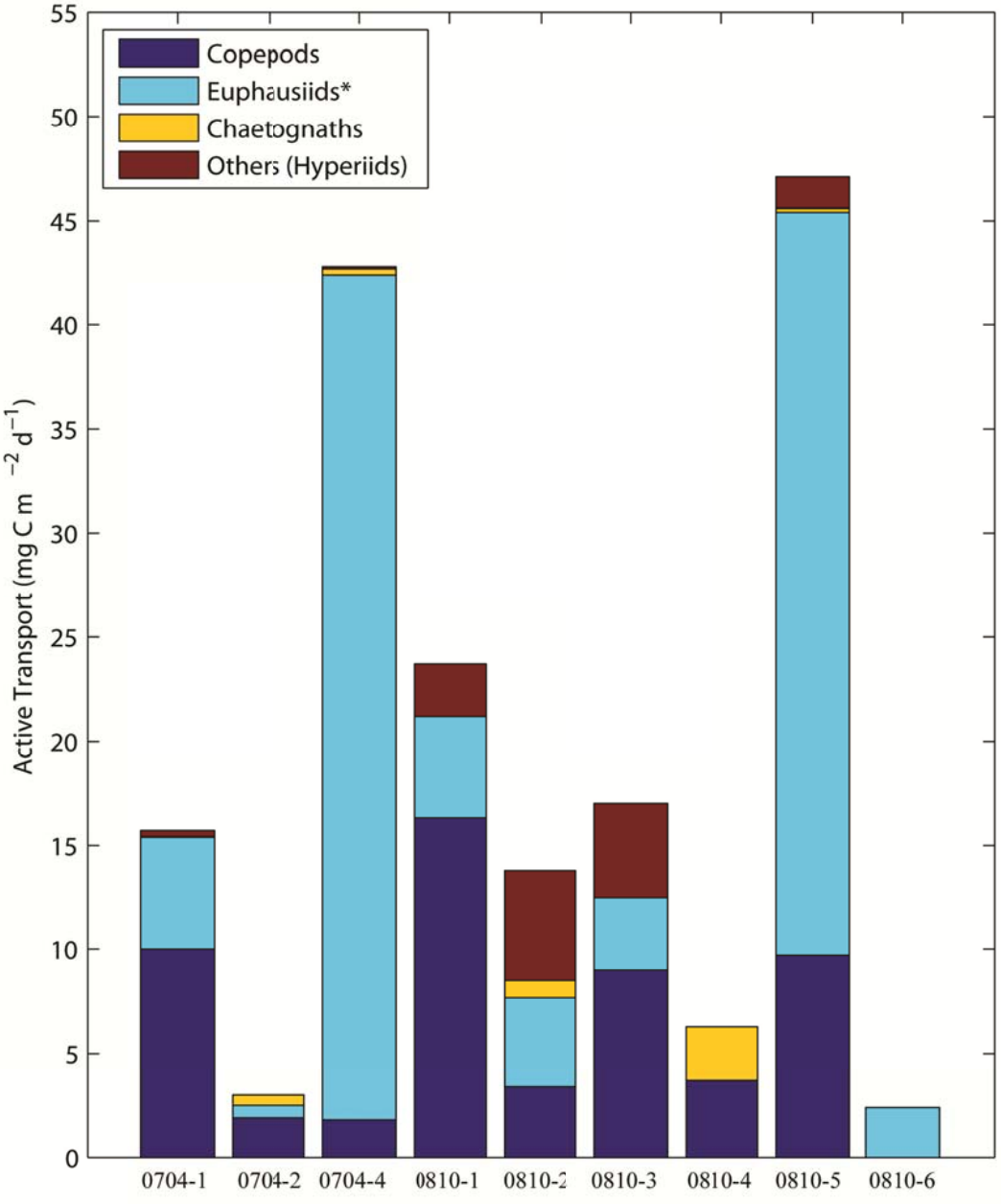
Copepods
Euphausiids*
Chaetognaths
Others (Hyperiids)
Active Transport (mg C m $^{-2}$ d^{-1})
0
5
10
15
20
25
30
35
40
45
50
55
0704-1
0704-2
0704-4
0810-1
0810-2
0810-3
0810-4
0810-5
0810-6

Figure 4.16. Contribution of each flux component to total carbon export. In all panels, green is the flux of sinking phytoplankton, as determined by the product of Chl *a* flux and measured C:Chl ratio, red is active transport by mesozooplankton, and white is unidentified portions of sinking particulate flux. Panels a and b show fecal flux based on phaeopigment flux measurements; brown is herbivorous fecal flux, while blue is other fecal pellet flux as estimated from the proportion of phytoplankton in the diets of mesozooplankton (Chapter 3). Other fecal pellet flux was only estimated for the cycles from P0704. Panel a is an underestimate of fecal pellet flux determined by assuming that total pigment is conserved as it passes through the guts of mesozooplankton. Panel b is a more realistic estimate that assumes that pigment is destroyed in proportion to assimilation efficiency of organic carbon. Panel c is based on microscopic enumeration of identifiable fecal pellets. In all figures, other particulate flux was estimated as the difference between total sinking flux (the average of ^{234}Th derived carbon export and sediment trap measurements) and phytoplankton and fecal flux rates. When the sum of recognizable components exceeded total measured flux, each component was scaled proportionally to accurately portray carbon export rates. Cycles are arranged in order of decreasing vertically integrated chlorophyll concentrations. ‘d’ denotes deep (100-m) samples, while ‘s’ denotes shallow (50 or 60-m samples).

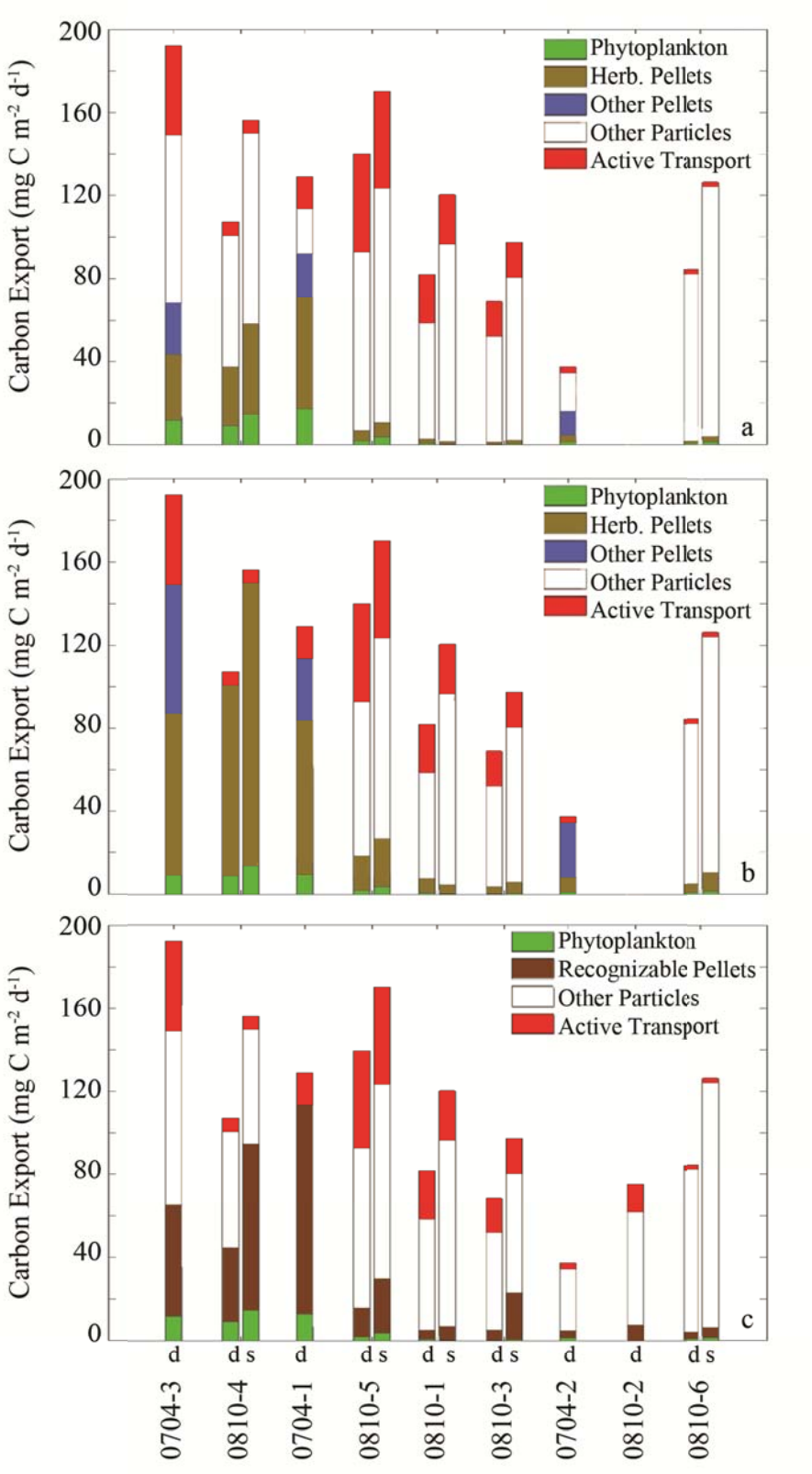
Carbon Export (mg C m-2 d-1)
200
160
120
80
40
0
Phytoplankton
Herb. Pellets
Other Pellets
Other Particles
Active Transport
a
b
Phytoplankton
Recognizable Pellets
Other Particles
Active Transport
c
d
d s
0704-3
0810-4
0704-1
0810-5
0810-1
0810-3
0704-2
0810-2
0810-6

REFERENCES

AL-MUTAIRI, H., and M. R. LANDRY. 2001. Active export of carbon and nitrogen at Station ALOHA by diel migrant zooplankton. Deep-Sea Res. II **48:** 2083-2103.

ALLDREDGE, A. L., and C. C. GOTSCHALK. 1989. Direct observations of the mass flocculation of diatom blooms: characteristics, settling velocities and formation of diatom aggregates. Deep-Sea Res. **36:** 159-171.

ARMSTRONG, R. A., C. LEE, J. I. HEDGES, S. HONJO, and S. G. WAKEHAM. 2002. A new, mechanistic model for organic carbon fluxes in the ocean based on the quantitative association of POC with ballast minerals. Deep-Sea Res. II **49:** 219-236.

BENITEZ-NELSON, C., K. O. BUESSELER, D. M. KARL, and J. ANDREWS. 2001a. A time-series study of particulate matter export in the North Pacific Subtropical Gyre based on Th-234 : U-238 disequilibrium. Deep-Sea Res. I **48:** 2595-2611.

BENITEZ-NELSON, C. R., K. O. BUESSELER, M. R. VAN DER LOEFF, J. ANDREWS, L. BALL, G. CROSSIN, and M. A. CHARETTE. 2001b. Testing a new small-volume technique for determining Th-234 in seawater. J. Radioanal. Nucl. Chem. **248:** 795-799.

BRINTON, E. 1967. Vertical migration and avoidance capability of euphausiids in California Current. Limnol. Oceanogr. **12:** 451-483.

BUESSELER, K. O. 1991. Do upper-ocean sediment traps provide an accurate record of particle flux? Nature **353:** 420-423.

BUESSELER, K. O., A. N. ANTIA, M. CHEN, S. W. FOWLER, W. D. GARDNER, O. GUSTAFSSON, K. HARADA, A. F. MICHAELS, M. R. VAN DER LOEFF'O, M. SARIN, D. K. STEINBERG, and T. TRULL. 2007. An assessment of the use of sediment traps for estimating upper ocean particle fluxes. J. Mar. Res. **65:** 345-416.

BUESSELER, K. O., C. BENITEZ-NELSON, M. R. VAN DER LOEFF, J. ANDREWS, L. BALL, G. CROSSIN, and M. A. CHARETTE. 2001. An intercomparison of small- and large-volume techniques for thorium-234 in seawater. Mar. Chem. **74:** 15-28.

BUESSELER, K. O., C. R. BENITEZ-NELSON, S. B. MORAN, A. BURD, M. CHARETTE, J. K. COCHRAN, L. COPPOLA, N. S. FISHER, S. W. FOWLER, W. GARDNER, L. D. GUO, O. GUSTAFSSON, C. LAMBORG, P. MASQUE, J. C. MIQUEL, U. PASSOW, P.

H. SANTSCHI, N. SAVOYE, G. STEWART, and T. TRULL. 2006. An assessment of particulate organic carbon to thorium-234 ratios in the ocean and their impact on the application of ^{234}Th as a POC flux proxy. Mar. Chem. **100:** 213-233.

BUITENHUIS, E., C. LE QUERE, O. AUMONT, G. BEAUGRAND, A. BUNKER, A. HIRST, T. IKEDA, T. O'BRIEN, S. PIONTKOVSKI, and D. STRAILE. 2006. Biogeochemical fluxes through mesozooplankton. Glob. Biogeochem. Cycle **20:** 18.

CARROLL, M. L., J. C. MIQUEL, and S. W. FOWLER. 1998. Seasonal patterns and depth-specific trends of zooplankton fecal pellet fluxes in the Northwestern Mediterranean Sea. Deep-Sea Res. I **45:** 1303-1318.

CHEN, J. H., R. L. EDWARDS, and G. J. WASSERBURG. 1986. ^{238}U, ^{234}U and ^{232}Th in seawater. Earth Planet. Sci. Lett. **80:** 241-251.

CONOVER, R. J. 1966. Assimilation of organic matter by zooplankton. Limnol. Oceanogr. **11:** 338-345.

CONOVER, R. J., R. DURVASULA, S. ROY, and R. WANG. 1986. Probable loss of chlorophyll-derived pigments during passage through the gut of zooplankton, and some of the consequences. Limnol. Oceanogr. **31:** 878-887.

COPPOLA, L., M. ROY-BARMAN, P. WASSMANN, S. MULSOW, and C. JEANDEL. 2002. Calibration of sediment traps and particulate organic carbon export using ^{234}Th in the Barents Sea. Mar. Chem. **80:** 11-26.

DAM, H. G., and W. T. PETERSON. 1988. The effect of temperature on the gut clearance rate-constant of planktonic copepods. J. Exp. Mar. Biol. Ecol. **123:** 1-14.

DOWNS, J. N., and C. J. LORENZEN. 1985. Carbon : pheopigment ratios of zooplankton fecal pellets as an index of herbivorous feeding. Limnol. Oceanogr. **30:** 1024-1036.

DURBIN, E. G., and R. G. CAMPBELL. 2007. Reassessment of the gut pigment method for estimating in situ zooplankton ingestion. Mar. Ecol. Prog. Ser. **331:** 305-307.

GOERICKE, R. 2002. Top-down control of phytoplankton biomass and community structure in the monsoonal Arabian Sea. Limnol. Oceanogr. **47:** 1307-1323.

GORSKY, G., M. D. OHMAN, M. PICHERAL, S. GASPARINI, L. STEMMANN, J. B. ROMAGNAN, A. CAWOOD, S. PESANT, C. GARCIA-COMAS, and F. PREJGER.

2010. Digital zooplankton image analysis using the ZooScan integrated system. J. Plankton Res. **32:** 285-303.

GOWING, M. M., D. L. GARRISON, H. B. KUNZE, and C. J. WINCHELL. 2001. Biological components of Ross Sea short-term particle fluxes in the austral summer of 1995-1996. Deep-Sea Res. I **48:** 2645-2671.

GOWING, M. M., and M. W. SILVER. 1985. Minipellets - a new and abundant size class of marine fecal pellets. J. Mar. Res. **43:** 395-418.

GOWING, M. M., and K. F. WISHNER. 1986. Trophic relationships of deep-sea calanoid copepods from the benthic boundary layer of the Santa Catalina Basin, California. Deep-Sea Res. **33:** 939-961.

IKEDA, T. 1985. Metabolic rates of epipelagic marine zooplankton as a function of body mass and temperature. Mar. Biol. **85:** 1-11.

IKEDA, T., Y. KANNO, K. OZAKI, and A. SHINADA. 2001. Metabolic rates of epipelagic marine copepods as a function of body mass and temperature. Mar. Biol. **139:** 587-596.

JACKSON, G. A., A. M. WAITE, and P. W. BOYD. 2005. Role of algal aggregation in vertical carbon export during SOIREE and in other low biomass environments. Geophys. Res. Lett. **32:** 4.

KIORBOE, T., and M. SABATINI. 1995. Scaling of fecundity, growth and development in marine planktonic copepods. Mar. Ecol. Prog. Ser. **120:** 285-298.

KNAUER, G. A., D. M. KARL, J. H. MARTIN, and C. N. HUNTER. 1984. *In situ* effects of selected preservatives on total carbon, nitrogen and metals collected in sediment traps. J. Mar. Res. **42:** 445-462.

KNAUER, G. A., J. H. MARTIN, and K. W. BRULAND. 1979. Fluxes of particulate carbon, nitrogen, and phosphorus in the upper water column of the Northeast Pacific. Deep-Sea Res. **26:** 97-108.

LANDRY, M. R., H. AL-MUTAIRI, K. E. SELPH, S. CHRISTENSEN, and S. NUNNERY. 2001. Seasonal patterns of mesozooplankton abundance and biomass at Station ALOHA. Deep-Sea Res. II **48:** 2037-2061.

LANDRY, M. R., C. J. LORENZEN, and W. K. PETERSON. 1994. Mesozooplankton grazing in the Southern California Bight .2. Grazing impact and particulate flux. Mar. Ecol. Prog. Ser. **115:** 73-85.

LANDRY, M. R., M. D. OHMAN, M. R. STUKEL, and K. TSYRKLEVICH. 2009. Lagrangian studies of phytoplankton growth and grazing relationships in a coastal upwelling ecosystem off Southern California. Prog. Oceanogr. **83:** 208-216.

LAVANIEGOS, B. E., and M. D. OHMAN. 2007. Coherence of long-term variations of zooplankton in two sectors of the California Current System. Prog. Oceanogr. **75:** 42-69.

LONGHURST, A. R., A. W. BEDO, W. G. HARRISON, E. J. H. HEAD, and D. D. SAMEOTO. 1990. Vertical flux of respiratory carbon by oceanic diel migrant biota. Deep-Sea Res. **37:** 685-694.

LOPEZ, M. D. G., M. E. HUNTLEY, and P. F. SYKES. 1988. Pigment destruction by *Calanus pacificus*: Impact on the estimation of water column fluxes. J. Plankton Res. **10:** 715-734.

MAUCHLINE, J., J. H. S. BLAXTER, A. J. SOUTHWARD, and P. A. TYLER. 1998. Advances in marine biology - The biology of calanoid copepods - Introduction, p. 1-+. Advances in Marine Biology, Vol 33. Advances in Marine Biology.

OLLI, K., P. WASSMANN, M. REIGSTAD, T. N. RATKOVA, E. ARASHKEVICH, A. PASTERNAK, P. A. MATRAI, J. KNULST, L. TRANVIK, R. KLAIS, and A. JACOBSEN. 2007. The fate of production in the central Arctic Ocean - Top-down regulation by zooplankton expatriates? Prog. Oceanogr. **72:** 84-113.

PIKE, S. M., K. O. BUESSELER, J. ANDREWS, and N. SAVOYE. 2005. Quantification of ^{234}Th recovery in small volume sea water samples by inductively coupled plasma-mass spectrometry. J. Radioanal. Nucl. Chem. **263:** 355-360.

SAVOYE, N., C. BENITEZ-NELSON, A. B. BURD, J. K. COCHRAN, M. CHARETTE, K. O. BUESSELER, G. A. JACKSON, M. ROY-BARMAN, S. SCHMIDT, and M. ELSKENS. 2006. ^{234}Th sorption and export models in the water column: A review. Mar. Chem. **100:** 234-249.

SILVER, M. W., and M. M. GOWING. 1991. The "particle" flux: Origins and biological components. Prog. Oceanogr. **26:** 75-113.

SMALL, L. F., and S. G. ELLIS. 1992. Fecal carbon production by zooplankton in Santa-Monica Basin: The effects of body size and carnivorous feeding. Prog. Oceanogr. **30:** 197-221.

STEINBERG, D. K., C. A. CARLSON, N. R. BATES, S. A. GOLDTHWAIT, L. P. MADIN, and A. F. MICHAELS. 2000. Zooplankton vertical migration and the active transport

of dissolved organic and inorganic carbon in the Sargasso Sea. Deep-Sea Res. I **47:** 137-158.

STUKEL, M. R., M. R. LANDRY, C. R. BENITEZ-NELSON, and R. GOERICKE. submitted. Trophic cycling and carbon export relationships in the California Current Ecosystem. Limnol. Oceanogr.

TURNER, J. T. 2002. Zooplankton fecal pellets, marine snow and sinking phytoplankton blooms. Aquat. Microb. Ecol. **27:** 57-102.

WILSON, S. E., D. K. STEINBERG, and K. O. BUESSELER. 2008. Changes in fecal pellet characteristics with depth as indicators of zooplankton repackaging of particles in the mesopelagic zone of the subtropical and subarctic North Pacific Ocean. Deep-Sea Res. II **55:** 1636-1647.

WILSON, S. E., D. K. STEINBERG, F. L. E. CHU, and J. K. B. BISHOP. 2010. Feeding ecology of mesopelagic zooplankton of the subtropical and subarctic North Pacific Ocean determined with fatty acid biomarkers. Deep-Sea Res. I **57:** 1278-1294.

CONCLUSIONS

Assessing the biological pump – The ecological interactions that influence marine carbon sequestration are diverse and difficult to measure precisely. They involve both direct and indirect trophic interactions with high degrees of spatiotemporal variability, and community dynamics that we are only beginning to understand in the marine realm. All methods have distinct limitations and drawbacks. Direct measurements are costly and time-intensive and often limited by the difficulties in visually discerning components of the mixed detrital pool (e.g. microscopy) or require multiple, and often questionable, assumptions (e.g. pigment analyses). Forward models invariably involve subjective decisions of which processes should be included and poorly constrained parameterizations (Franks 2009), and hence seldomly reject hypotheses. Inverse models, while synthesizing cruise measurements, are always poorly constrained due to the paucity of relevant *in situ* measurements (Kones et al. 2006; Stukel and Landry 2010). Even direct accurate measurements of bulk vertical carbon flux (without assessment of its constituent particles) are difficult to make in the dynamic fluid environment of the ocean (Buesseler 1991).

As a result of my lack of faith in any single method, I have taken more of a pragmatic approach to methodology, utilizing different techniques that seemed to best fit particular questions. In Chapters 1 and 3, I utilized inverse ecosystem modeling techniques to assess the relative contributions of large and small phytoplankton to carbon export and the percentage of vertical flux that was comprised of ungrazed phytoplankton. Chapters 2-4 relied crucially on field measurements of carbon export

(from both sediment traps and ^{234}Th disequilibrium) and the suite of complementary ecosystem measurements made by collaborators in the CCE LTER Program. In Chapter 2, I utilized a simple model of trophic cycling relationships to relate vertical flux to ecological rate measurements and found that the measured variability in carbon export could be explained by processes that lead to mesozooplankton fecal production. While the results of both Chapters 2 & 3 suggested that fecal pellets were the dominant form of sinking material in the CCE region, neither were conclusive demonstrations of that relationship since alternative model structures could have predicted different results. The uncertainty of modeling results led me to look directly at the quantity of fecal pellets in sediment traps in Chapter 4, both by counting identifiable fecal pellets and by using phaeopigments as a tracer of herbivorous fecal material. While individually, each of these methods has its flaws, together they painted a consistent portrait of the biological control of carbon flux in the CCE (at least during the springtime).

Biological control of sinking POC in the CCE – So what can we conclude about the role of plankton in vertical flux of POC? Results from a wide-variety of sources show that during the springtime, at least within the water parcels sampled on the P0605 and P0704 cruises, export of sinking particles was driven by mesozooplankton fecal pellets. A disparate suite of evidence supports this general conclusion. First, phytoplankton net growth rates (growth minus grazing) were closely matched by the water-column accumulation of autotrophs, suggesting a negligible role for massive losses of phytoplankton to direct sinking (Landry et al.

2009; Stukel et al. submitted). Estimates of sinking rates from SETCOL chambers (data not shown) and the insignificant concentration of chlorophyll caught in sediment traps (Chapter 4) both support the view that phytoplankton were not settling out of the water column at any appreciable rate. Estimates of mesozooplankton ingestion (of both phytoplankton and protozoans), combined with reasonable estimates of assimilation efficiency (Stukel et al. submitted and Chapter 3), show that the total flux of POC could have been maintained by mesozooplankton fecal production. Sediment trap analyses from the P0704 cruise also indicate that identifiable fecal pellets were the dominant particle source in sediment traps nearshore, while arguments based on sediment trap pigment contents are consistent with fecal material (herbivorous and nonherbivorous) comprising all or most of the sinking detritus measured on the cruise (Chapter 4).

Results from the P0810 cruise, however, indicate that other processes may have been at work later in the season. For this cruise, high productivity water parcels exhibited a predominance of fecal material in sinking flux while sediment traps from lower productivity regions contained primarily marine snow or particles too small to be identified (Chapter 4). The significantly higher C:N ratios of sinking material on the P0810 cruise further suggested that detritus sank much more slowly in October and that the POC reaching the sediment trap was highly degraded. This combination of factors raises the possibility that processes occuring prior to our arrival at the experimental water parcels may have exerted a large influence on the vertical fluxes measured in our studies.

While this dissertation has specifically focused on the role of mesozooplankton fecal production in carbon export, I do not want to imply that it is the only important factor. We measured $CaCO_3$ in our sediment traps and are certain that biogenic silica was also important as a mineral ballast material. Aggregates were often observed in the sediment traps from October 2008. Mass flocculation and sinking of phytoplankton may occasionally occur as blooms decay and could be an important episodic flux of carbon to depth. We also found evidence (Stukel, unpublished data) for subduction along a front studied on the P0904 cruise (April 2009) that may have contributed a significant flux of carbon out of the ecosystem. However, during the productive spring period in the CCE, it is likely that fecal pellets were the primary source of sinking material in the region. We suggest, therefore, that models attempting to explain patterns of biogeochemical fluxes in the CCE region need to account explicitly for mesozooplankton population dynamics and community grazing; only with the inclusion of mesozooplankton grazing could distinct patterns in efficiency of the biological pump be determined in our studies.

Going forward - Long-term secular changes on multiple fronts – including ocean acidification (Doney et al. 2009) and increased stratification (Sarmiento et al. 2004) – will likely alter marine ecosystem structure and function in the future ocean. In the CCE, long-term trends, possibly related to anthropogenic warming, have already been noted for both phytoplankton (Aksnes and Ohman 2009) and mesozooplankton (Lavaniegos and Ohman 2007; Roemmich and Mcgowan 1995). Anticipating the responses and feedbacks between climate and ocean requires more

than a simple realization that ecosystems will change; it requires a mechanistic understanding of how ecosystem structure drives biogeochemistry (Ducklow et al. 2001). We know that ocean acidification will affect the production of planktonic calcifiers and hence mineral ballasting of sinking POC. We can surmise that increased stratification may decrease nutrient input and new production, with cascading effects on phytoplankton and zooplankton biomass. We can wonder whether a more stratified surface layer will be more conducive to aggregate formation. Yet we do not know which of these processes dominate the flux of organic carbon to depth.

The practical difficulties of distinguising among different export mechanisms, particularly when sinking material is old and degraded (as on our P0810 cruise) has led to a paucity of direct field evidence; instead, mechanisms are typically inferred from correlations (e.g. Klaas and Archer 2002) or built into the structure of models (e.g. Jackson 2001). While these approaches can suggest interesting hypotheses, they invariably lack crucial data necessary to test their veracity, and often lack any *in situ* measurements of carbon flux at all (e.g. Plattner et al. 2005). Going forward, we need a coordinated effort between modelers and experimentalists to generate testable hypotheses that can potentially be used to explicitly and simultaneously test these alternative hypotheses with *in situ* measurements. In particular, characterization of the nature of the euphotic zone detrital pool is necessary using a combination of microscopical (Verity et al. 1996; Verity et al. 2000), optical (Checkley et al. 2008; Gorsky et al. 2000), and chemical analyses, in conjunction with techniques used to assess the varied components of sinking material (Dell'anno et al. 1999; Lundsgaard

1995; Wilson et al. 2008). Also necessary is explicit inclusion of mesozooplankton dynamics within ecosystem-based biogeochemical models (see Buitenhuis et al. 2006; Hood et al. 2006) that are tied to field programs which measure the relevant process rates necessary for model validation.

References

Aksnes, D. L., and M. D. Ohman. 2009. Multi-decadal shoaling of the euphotic zone in the southern sector of the California Current System. Limnol. Oceanogr. **54:** 1272-1281.

Buesseler, K. O. 1991. Do upper-ocean sediment traps provide an accurate record of particle flux? Nature **353:** 420-423.

Buitenhuis, E. and others 2006. Biogeochemical fluxes through mesozooplankton. Glob. Biogeochem. Cycle **20:** 18.

Checkley, D. M., R. E. Davis, A. W. Herman, G. A. Jackson, B. Beanlands, and L. A. Regier. 2008. Assessing plankton and other particles *in situ* with the SOLOPC. Limnol. Oceanogr. **43:** 2123-2136.

Dell'anno, A., M. Fabiano, S. Bompadre, M. Armeni, L. Leone, and R. Danovaro. 1999. Phytopigment and DNA determinations in long-time formalin-preserved trap samples. Mar. Ecol. Prog. Ser. **191:** 71-77.

Doney, S. C., W. M. Balch, V. J. Fabry, and R. A. Feely. 2009. Ocean Acidification: a Critical Emerging Problem for the Ocean Sciences. Oceanography **22:** 16-25.

Ducklow, H. W., D. K. Steinberg, and K. O. Buesseler. 2001. Upper Ocean Carbon Export and the Biological Pump. Oceanography **14:** 50-58.

Franks, P. J. S. 2009. Planktonic ecosystem models: perplexing parameterizations and a failure to fail. J. Plankton Res. **31:** 1299-1306.

Gorsky, G., M. Picheral, and L. Stemmann. 2000. Use of the Underwater Video Profiler for the study of aggregate dynamics in the North Mediterranean. Estuar. Coast. Shelf Sci. **50:** 121-128.

Hood, R. R. and others 2006. Pelagic functional group modeling: Progress, challenges and prospects. Deep-Sea Res. Part II-Top. Stud. Oceanogr. **53:** 459-512.

Jackson, G. A. 2001. Effect of coagulation on a model planktonic food web. Deep-Sea Res. I **48:** 95-123.

Klaas, C., and D. E. Archer. 2002. Association of sinking organic matter with various types of mineral ballast in the deep sea: Implications for the rain ratio. Glob. Biogeochem. Cycle **16:** 14.

Kones, J. K., K. Soetaert, D. Van Oevelen, J. O. Owino, and K. Mavuti. 2006. Gaining insight into food webs reconstructed by the inverse method. J. Mar. Syst. **60:** 153-166.

Landry, M. R., M. D. Ohman, M. R. Stukel, and K. Tsyrklevich. 2009. Lagrangian studies of phytoplankton growth and grazing relationships in a coastal upwelling ecosystem off Southern California. Prog. Oceanogr. **83:** 208-216.

Lavaniegos, B. E., and M. D. Ohman. 2007. Coherence of long-term variations of zooplankton in two sectors of the California Current System. Prog. Oceanogr. **75:** 42-69.

Lundsgaard, C. 1995. Use of a high viscosity medium in studies of aggregates, p. 141-152. *In* S. Floderus, A.-S. Heisakanen, M. Oleson and P. Wassmann [eds.], Sediment trap studies in the Nordic countries 3. Proceedings of the Symposium on Seasonal Dynamics of Planktonic Ecosystem and Sedimentation in Coastal Nordic Waters.

Plattner, G. K., N. Gruber, H. Frenzel, and J. C. Mcwilliams. 2005. Decoupling marine export production from new production. Geophys. Res. Lett. **32:** L11612.

Roemmich, D., and J. Mcgowan. 1995. Climatic warming and the decline of zooplankton in the California Current. Science **267:** 1324-1326.

Sarmiento, J. L. and others 2004. Response of ocean ecosystems to climate warming. Glob. Biogeochem. Cycle **18:** 35.

Stukel, M. R., and M. R. Landry. 2010. Contribution of picophytoplankton to carbon export in the equatorial Pacific: A re-assessment of food-web flux inferences from inverse models. Limnol. Oceanogr. **55:** 2669-2685.

Stukel, M. R., M. R. Landry, C. R. Benitez-Nelson, and R. Goericke. submitted. Trophic cycling and carbon export relationships in the California Current Ecosystem. Limnol. Oceanogr.

Verity, P. G., T. M. Beatty, and S. C. Williams. 1996. Visualization and quantification of plankton and detritus using digital confocal microscopy. Aquat. Microb. Ecol. **10:** 55-67.

Verity, P. G., S. C. Williams, and Y. Hong. 2000. Formation, degradation, and mass : volume ratios of detritus derived from decaying phytoplankton. Mar. Ecol.-Prog. Ser. **207:** 53-68.

Wilson, S. E., D. K. Steinberg, and K. O. Buesseler. 2008. Changes in fecal pellet characteristics with depth as indicators of zooplankton repackaging of particles in the mesopelagic zone of the subtropical and subarctic North Pacific Ocean. Deep-Sea Res. II **55:** 1636-1647.